Exploring the Mechanobiology of Pancreatic Cancer using Tumour Microenvironment Models

Eleonora Peerani

Thesis submitted for the degree of

Doctor of Philosophy

at the Barts and the London School of Medicine and Dentistry,

Queen Mary University of London

August 2020

Centre for Tumour Microenvironment

John Vane Science Centre

Barts Cancer Institute

Queen Mary University of London

EC1M 6BQ

Per Ida, Angelo, Licia e Nunzio

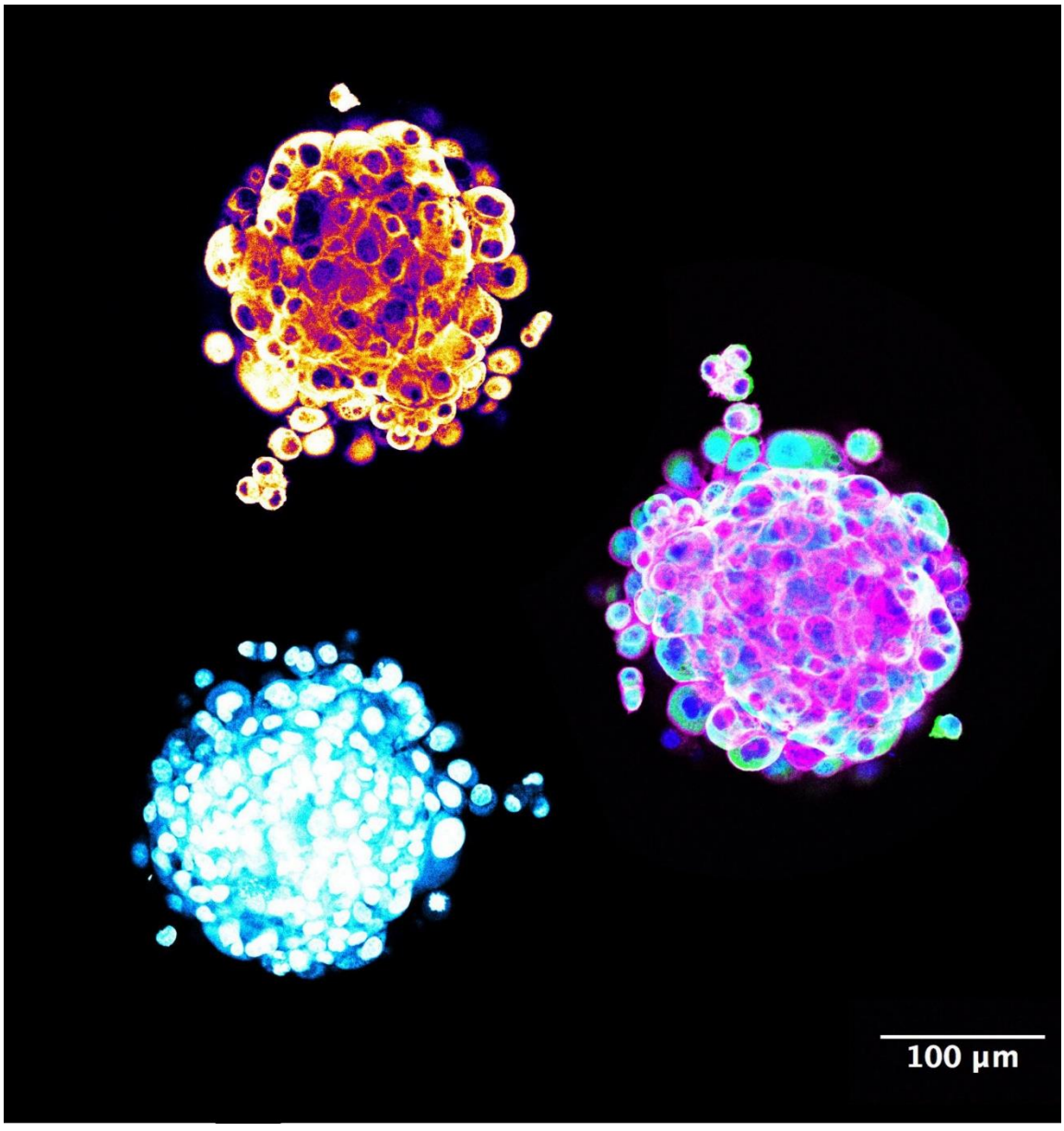

Confocal micrograph of pancreatic tumour spheroids grown in a bioengineered 3D matrix

–

Eleonora Peerani, 2018

Statement of Originality

I, Eleonora Peerani, confirm that the research included within this thesis is my own work or that where it has been carried out in collaboration with, or supported by others, that this is duly acknowledged below, and my contribution indicated. Previously published material is also acknowledged below.

I attest that I have exercised reasonable care to ensure that the work is original, and does not to the best of my knowledge break any UK law, infringe any third party's copyright or other Intellectual Property Right, or contain any confidential material.

I accept that the College has the right to use plagiarism detection software to check the electronic version of the thesis.

I confirm that this thesis has not been previously submitted for the award of a degree by this or any other university.

Signature: _____

Eleonora Peerani

Date: 19 / 08 / 2020

Details of Collaborations and Contributions

The present work would have never been possible without the invaluable help and input of other researchers, students and technicians. Special acknowledgments to:

- Dr Juliana Candido has contributed to antibody dilution optimisation (Chapter3), proliferation analysis (CyQUANT) and primary cell isolation (Chapter 4), *in vivo* work presented in Chapter 4, RNA-seq sample setup and processing (Chapter 5) as well as extensive protocol, experimental and publication planning.
- Dr Eleni Maniati performed all the RNA-seq data bioinformatics analysis presented in Chapter 5.
- Dr Daniela Loessner, Dr Juliana Candido and Dr Laura Lecker synthesised the GelMA polymer batches.
- Niamh Leonard and Shreya Sharma contributed to antibody dilution optimisation and immunohistochemistry staining.
- Dr Stephen Thorpe, Elena Tomas-Bort, Dr Robin Delaine-Smith, Dr Erica DiFederico and Dr William Megone helped with the mechanical characterisation of tissues and hydrogels.
- Dr Beatice Malacrida and Dr Michelle Lockley isolated omental fibroblasts and provided OvCar4 cells respectively
- Colin Pegrum provided murine tissues and helped with animal surgeries.
- Dr David Osuna de la Peña set up Matrigel organoids used as a comparison for RNA-seq in Chapter 5.
- Dr William Megone performed atomic force microscopy on the hydrogels presented in Chapter 6.
- ^{1}H NMR (Chapter 3) was performed by Andrew McCormack and Dr Ferry Melchels.
- Lundrim Bytyqi performed some of the 2D proliferation experiments presented in Chapter 6.

Funding

This work was supported by Barts Cancer Institute (grant codes: CIF1040B, CIF7712B) as well as the following:

- Start-up funding, A/Professor Daniela Loessner
- Two Theme 5 Awards, A/Professor Daniela Loessner
- Organ-on-a-chip Technologies Network Grant, A/Professor Daniela Loessner in collaboration with Dr Aideen Ryan, NUI Galway
- Impetus funding (RNA-sequencing), A/Professor Daniela Loessner

Publications

Peerani E, Candido JB, Loessner D. (2019) **Cell Recovery of Hydrogel-Encapsulated Cells for Molecular Analysis**. Methods in Molecular Biology: Springer.

Peerani E*, Candido JB*, Maniati E, Tomás-Bort E, Sharma S, Kocher H, Wang A, Loessner D. (2021) **The mechano-biological microenvironment of pancreatic ductal adenocarcinoma.** [Manuscript in preparation] * joint first authors

Candido JB, Maiques O, Boxberg M, Peerani E, Tomás-Bort E, Sananes A, Papo N, Magdolen V, Sanz-Moreno V, Loessner D. (2021) **Kallikrein 6 is a potential therapeutic target in pancreatic ductal adenocarcinoma.** [Collaborative manuscript in preparation]

Acknowledgements

My gratitude goes first and foremost to Juliana Candido, for her endless patience and exceptional expertise. Much of this work would not have been completed without her input and for that, I am forever grateful.

Special thanks go to Niamh Leonard, Elena Tomas-Bort, Arantxa Romero-Toledo, Valentine Gauthier, Priyanka Hirani, Beatrice Malacrida, Anissa Lakhani, Reza Roozitalab, and Elliott Puttock. I am deeply indebted with you for your continued support, as much in the lab as outside of it, endless hours of fun and friendships that I am sure will last way beyond my time at Barts. Thank you also to my enthusiastic badminton and football teammates – Elliott, Priyanka, Niamh, Morgan and Valentine, for filling my Thursday evenings with fun, laughter, and a bit of healthy competition.

Goes without saying, many other members of Cancer and Inflammation and Tumour Microenvironment Centres have hugely impacted my time in the lab, including David Osuna de la Pena, Ying Liu, Florian Laforets, Joash Joy, Laura Lecker, Leonie Kohlhammer, Eleni Maniati and Colin Pengrum. Thank you to you, and all the other members of this exceptional Centre!

I extend my gratitude to my collaborators in the School of Engineering and Material Sciences - Stephen Thorpe, Robin Delaine-Smith, Erica Di Federico and William Megone for the endless hours spent calibrating machines together and talking all things data.

I would also like to thank all the technical staff at the Barts Cancer Institute, as well as the Barts Pancreatic and Gynae Tissue Banks, for their continued help and dedication: Shreya, Julfa, Shreya, Linda, George, Nadia and Rory. I need to extend my gratitude to the whole Institute, as I could not possibly mention all of you, although none of this work would have been possible without your excellent support and expertise.

Finally, my gratitude goes to my supervisors A/Professor Daniela Loessner and Professor Fran Balkwill. Not only have they been outstanding mentors, but inspiring examples of successful women in science.

Abstract

The dismal prognosis and treatment options for pancreatic ductal adenocarcinoma (PDAC) have seen little advances over the past decades, making PDAC one of the most lethal malignancies to date. Hydrogel-based *in vitro* modelling of this cancer and its tumour microenvironment (TME) is a promising avenue to bridge the gap between laboratory and clinical data. Current collagen gel-based approaches are limited by varying batch composition, little tuneability and limited mechanical properties, which preclude the accurate recapitulation of key PDAC features, such as matrix stiffness, desmoplasia and drug resistance.

In this study, gelatin methacryloyl (GelMA)-based hydrogels were used for the three-dimensional (3D) multicellular culture of PDAC and stromal cells (myeloid cells and patient-derived fibroblasts). The hydrogel's mechanical properties, architecture and matrix protein expression of embedded cells were characterised and benchmarked against collagen gels and native human tissues. Mechanical testing of fresh human tissues was performed to inform the physical properties of the model. PDAC tissues were significantly stiffer (7.4 ± 0.6 kPa, $p<0.0001$) than normal adjacent tissues (2.2 ± 0.2 kPa), prompting the modelling of these observed biomechanics with the use of GelMA-based hydrogels. Immunofluorescence, flow cytometry, metabolic activity and DNA quantification analyses confirmed the suitability of GelMA hydrogels for 3D PDAC research by showing high viability of embedded cells, spheroid formation ability, expression of cancer-associated markers and proliferation. The simultaneous 3D co-culture of PDAC and stromal cells led to matrix stiffening, increased cell proliferation and increased *in vivo* tumorigenicity via a stiffness-dependant upregulation of IL-6, IL-8, STAT3 and downregulation of ERK. Transcriptomic analyses revealed that 3D GelMA cultures had signatures that correlated with those of cells grown in collagen gels, as well as primary tumour organoids cultured in Matrigel, while showing an upregulation in mechano-transduction pathways. Treatment with the mechano-modulating inhibitor fasudil led to increased chemotherapy efficiency via relaxation of matrix stiffness, downregulation of pro-survival and matrix gene signatures, and reduced IL-6 and IL-8 secretion.

These findings demonstrated that GelMA-based hydrogels are a modular and informative 3D cell culture platform for the investigation of functional, transcriptional and mechanical aspects of the pancreatic TME. The tuneable physical properties of GelMA allowed me to uncover the increased biomechanical functions and to assess treatment responses of PDAC and stromal cells in matrices of physiologically relevant stiffness, which could not be assessed, to this extent, in commonly-used collagen matrices.

Table of Contents

Statement of Originality……3
Details of Collaborations and Contributions……4
Funding……5
Publications……5
Acknowledgements……6
Abstract……7
Table of Contents……8
List of Figures……15
List of Tables……20
Abbreviations……21
Chapter 1 - Project Background and Introduction 24
1.1 Pancreatic Ductal Adenocarcinoma 25
1.1.1 Prevalence and epidemiology 25
1.1.2 Pathophysiology of pancreatic ductal adenocarcinoma 25
1.1.2.1 Pathogenesis of PDAC 26
1.1.2.2 Molecular biology of PDAC 26
1.1.2.3 Molecular subtyping of PDAC 27
1.1.3 The PDAC clinical landscape: challenges and prospects 28
1.1.3.1 Neoadjuvant, adjuvant and palliative treatments 28
1.1.3.2 Targeted therapies 29
1.1.3.3 Stromal targeting therapies 30
1.1.3.4 Immunotherapies 31
1.2 The plastic tumour microenvironment of PDAC 32
1.2.1 The cellular components of the PDAC microenvironment 32
1.2.1.1 Tumour cells 32
1.2.1.2 Stromal cells 33
1.2.1.3 Immune cells 34
1.2.2 The extracellular components of the PDAC microenvironment 36
1.2.2.1 Role of collagens in PDAC 37

1.2.2.2 Role of glycoproteins and proteoglycans in PDAC 38
1.2.2.3 Role of other ECM regulators 39
1.2.2.4 Defining a common matrix signature 39
1.3 The mechanobiology of PDAC 41
1.3.1 Characterisation of PDAC biomechanics 41
1.3.2 Regulators of stiffness 42
1.3.3 Targeting mechanobiology-related processes in PDAC 45
1.4 Pre-clinical models of PDAC 48
1.4.1 Murine models of PDAC 48
1.4.1.1 Xenografts 48
1.4.1.2 Genetically engineered mouse models 49
1.4.2 *In vitro* models of PDAC 50
1.4.2.1 Spheroids 51
1.4.2.2 Explants and decellularised tissue platforms 51
1.4.2.3 Hydrogels 54
1.4.2.4 Microfluidic devices 56
1.5 GelMA hydrogels as a 3D cell culture platform 57
1.5.1 Biophysical properties of GelMA 57
1.5.1.1 Composition and bioactivity 57
1.5.1.2 Stiffness and porosity 59
1.5.1.3 Cell culture in GelMA 60
1.6 Project hypothesis and aims 61
Chapter 2 - Materials and Methods 63
2.1 Patient-derived tissues and cell culture 64
2.1.1 Cell culture and passaging 64
2.1.2 Patient-derived tissues 64
2.1.3 Patient-derived cell isolation 67
2.2 Hydrogel synthesis, characterisation and 3D cell culture 68

2.2.1 GelMA hydrogel synthesis and storage 68
2.2.2 Characterisation of GelMA functionalisation 68
2.2.2.1 TNBS Assay 68
2.2.2.2 Ninhydrin Assay 69
2.2.2.3 Fluoraldehyde Assay 69
2.2.2.4 Nuclear Magnetic Resonance (NMR) 70
2.2.3 GelMA 3D cell culture 70
2.2.4 GelMA-based Collagen hydrogels synthesis and 3D cell culture 71
2.3 *In vitro* treatments and *in vivo* studies 73
2.3.1 MMP- and ROCK- inhibitors: monotherapy studies 73
2.3.2 ROCK inhibitor and Chemotherapy: combinational studies 73
2.3.3 Indirect co-culture: conditioned medium studies 73
2.3.4 Orthotopic xenograft study 74
2.4 Analysis of mechanical properties 75
2.4.1 Flat-end Indentation 75
2.4.2 Unconfined compression 76
2.4.3 Rheometry 76
2.4.4 Atomic Force Microscopy (AFM) 77
2.5 Functional assays 78
2.5.1 IncuCyte proliferation assay 78
2.5.2 IncuCyte scratch-wound assay 78
2.5.3 Transwell invasion assay 78
2.5.4 Viability assay 79
2.5.5 Metabolic activity assay 79
2.5.6 3D proliferation assay 80
2.6 Imaging and image analysis 81
2.6.1 Brightfield microscopy 81
2.6.2 Confocal microscopy 81

2.6.3 Scanning Electron Microscopy (SEM) 82
2.6.4 Sectioning, histology and immunostaining 83
2.6.4.1 Specimen embedding and sectioning 83
2.6.4.2 Haematoxylin and eosin (H&E) 83
2.6.4.3 Masson's trichrome 83
2.6.4.4 Immunohistochemistry (IHC) 84
2.7 Hydrogel digestion, cell retrieval and viability assessment 85
2.7.1 GelMA hydrogel digestion 85
2.8 Gene expression analyses 86
2.8.1 RNA extraction from 3D cell cultures 86
2.8.2 RT-qPCR 86
2.8.3 RNA-sequencing 88
2.9 Protein expression analyses 89
2.9.1 Protein extraction from 3D cultures 89
2.9.2 Flow cytometry 89
2.9.3 Electrophoresis and Western blotting 90
2.9.4 Analysis of secreted factors 92
2.10 Statistical analysis 93
Chapter 3 - Biomechanics and Matrix Proteins of the Tumour Microenvironment 95
3.1 Background 96
3.2 Aim and objectives 97
3.3 Results 98
3.3.1 Tissue stiffness is directly modulated by tumour burden 99
3.3.2 High ECM protein content correlates with tissue stiffness in PDAC 102
3.3.3 A tuneable 3D model mimics tumour stiffness 106
3.3.4 GelMA and collagen hydrogels mimic key architectural features of PDAC tissues 110
3.3.4.1 The nanostructure of GelMA and collagen hydrogels 110

3.3.4.2 Extracellular components of the pancreatic TME 112
3.3.4.3 Cellular components of the pancreatic TME 114
3.4 Conclusions 117
Chapter 4 - GelMA Hydrogels as a 3D Platform to Study Cell Behaviour 120
4.1 Background 121
4.2 Aim and objectives 122
4.3 Results 123
4.3.1 Degree of functionalisation analyses show high GelMA batch consistency . 123
4.3.2 GelMA hydrogels as a 3D platform to study cell behaviour 126
4.3.2.1 GelMA supports cell viability, proliferation and long-term 3D cell culture 126
4.3.2.2 Hydrogel stiffness influences PDAC cell proliferation 129
4.3.3 Optimisation of hydrogel digestion and cell retrieval for downstream analyses 131
4.3.4 UV-induced DNA damage assessment in GelMA cell cultures 136
4.3.5 Investigating the effects of cellular components on the pancreatic TME 139
4.3.5.1 Cancer-associated fibroblasts promote cell proliferation and GelMA hydrogel stiffening 139
4.3.5.2 Co-culture of myeloid and cancer cells contribute to tumour development and metastasis *in vivo* 142
4.3.6 Mimicking the pancreatic TME in GelMA hydrogels using triple cell cultures 146
4.3.6.1 Stromal cells lead to increased cell proliferation in GelMA and collagen hydrogels 146
4.3.6.2 Stromal cells in GelMA result in increased hydrogel stiffness 147
4.3.6.3 Stromal cells lead to increased pro-inflammatory cytokines secretion in GelMA and collagen hydrogels 148
4.3.7 A novel hydrogel-based indirect co-culture system unveils stroma-induced upregulation of pro-survival signals in PDAC cells 150
4.4 Conclusions 153

Chapter 5 - Transcriptomics of PDAC cells in GelMA and Collagen hydrogels. 159

5.1 Background 160

5.2 Aim and objectives 160

5.3 Results 162

5.3.1 Exploratory analysis of differentially expressed genes in GelMA 162

5.3.2 Transcriptome-wide associations with biological pathways 168

5.3.3 Post-translational modifications and matrisome-related gene profiles in GelMA and collagen hydrogels 171

5.3.4 Validation of RNA-seq data in GelMA and collagen hydrogels 174

5.3.5 Secretome-related gene profiles and validation in GelMA and collagen hydrogels 175

5.4 Conclusions 176

Chapter 6 - Targeting the Tumour Microenvironment using *in vitro* Models of PDAC 179

6.1 Background 180

6.2 Aim and objectives 181

6.3 Results 183

6.3.1 Epithelial-mesenchymal transition status and extracellular collagen dictate cell proliferation and treatment response in 2D 183

6.3.2 Inhibition of MMPs, but not ROCK, leads to reduced cell proliferation in 3D 186

6.3.2.1 Effects of GM6001 treatment on PDAC cell proliferation and invasion 186

6.3.2.2 Effects of fasudil treatment on PDAC cell proliferation 190

6.3.3 Inhibition of ROCK, but not of MMPs, lead to cell-mediated stiffness changes in GelMA hydrogels 191

6.3.4 Effects of matrix priming with ROCK inhibitors on chemotherapy efficiency in 3D cell cultures 193

6.3.4.1 Combined treatment of fasudil and chemotherapy lead to reduced cell viability 193

6.3.4.2 Treatment with fasudil, but not chemotherapy, led to reduced matrix stiffness in GelMA 195

6.3.4.3 Effects of ROCK inhibition and chemotherapy on matrisome-related genes and secreted factors 196

6.4 Conclusions 201

Chapter 7 - Discussion and Concluding Remarks 206

7.1 Summary of key findings 207

7.2 Future experiments 210

7.3 Wider research implications and future perspectives 212

7.4 Concluding remarks 217

Chapter 8 - Bibliography 218

Chapter 9 - Appendices 241

9.1 Appendix Chapter 2 242

9.2 Appendix Chapter 5.1 245

9.3 Appendix Chapter 5.2 246

9.4 Appendix Chapter 5.3 248

9.5 Appendix Chapter 6 250

List of Figures

Figure 1.1 Treatment options and associated median survival for PDAC patients……29

Figure 1.2 The role of cancer-associated fibroblasts (CAFs) crosstalk in the PDAC tumour microenvironment…….34

Figure 1.3 Aberrant tissue stiffness and extracellular matrix (ECM) crosslinking promote malignant cell behaviours……..….44

Figure 1.4 Kaplan-Meier survival curves for patients with high and low expression of selected markers…….45

Figure 1.5 Transient administration of stromal targeting agents as a strategy to increase chemotherapy efficiency……47

Figure 1.6 Gelatin methacryloyl (GelMA) hydrogels synthesis and prevalence in peer-reviewed academic publications…….……58

Figure 1.7 Schematic outline of thesis rationale and workflow…….61

Figure 2.1 Schematic representation of cell-laden GelMA hydrogels preparation procedure……...……71

Figure 2.2 Schematic representation of collagen hydrogel preparation procedure……72

Figure 3.1 Schematic representation of patient-derived tissue analysis…….……98

Figure 3.2 Stiffness analysis of fresh human (a-b) PDAC and (c-d) OvCa tumours and respective normal tissues……...…….100

Figure 3.3 Representative haematoxylin and eosin staining of adjacent normal tissues and PDAC tissues post-indentation……...……..101

Figure 3.4 Immunostaining of the matrix proteins in a representative human tumour-adjacent normal and matched PDAC tissue specimen……103

Figure 3.5 Expression of selected matrix proteins and collagen fibre thickness in PDAC compared to tumour-adjacent normal tissues……...……..104

Figure 3.6 Correlation of precise local tissue stiffness and percentage stained area of selected matrix proteins……105
Figure 3.7 Biomechanical characterisation of murine and human tissues, collagen and GelMA hydrogels……107
Figure 3.8 GelMA hydrogels are a tunable and reproducible platform for 3D stiffness modulation, even upon cell incorporation……108
Figure 3.9 Characterisation of the nanostructure of collagen and GelMA hydrogels via scanning electron microscopy……...…109
Figure 3.10 Immunostaining of selected matrix proteins in matched human tumour-adjacent pancreatic and PDAC tissues and in 3D cultures……...……114
Figure 3.11 Immunostaining of selected markers in matched human tumour-adjacent pancreatic and PDAC tissues and 3D cultures……...…115
Figure 4.1 Analysis of GelMA degree of functionalisation via spectrophotometric and ^{1}H NMR…….……..124
Figure 4.2 Cell proliferation and viability of OvCar4 cells in GelMA hydrogels……..…126
Figure 4.3 Spheroid-forming ability of HGSOC and PDAC cell lines in 5% GelMA…...…127
Figure 4.4 Cell proliferation and viability of PDAC cells in GelMA hydrogels……128
Figure 4.5 Brightfield micrographs of PDAC cells in GelMA hydrogels of increasing stiffness……...……129
Figure 4.6 PDAC cell viability and proliferation in GelMA hydrogels……..130
Figure 4.7 Flow cytometry and detection of MIA PaCa-2 cell viability after GelMA hydrogel digestion……..……132
Figure 4.8 General flow cytometry gating strategy for Ca-AM/Et-H1/DAPI staining optimisation……...……..134
Figure 4.9 γH2AX staining reveals limited DNA damage following 10 minutes of UV light exposure……..……136
Figure 4.10 Immunofluorescent detection of γH2AX in GelMA-embedded cells……137

Figure 4.11 Characterisation of cellular fractions of HGSOC ascites fluid and HGSOC and PDAC primary isolated CAFs, by flow cytometry……..……139

Figure 4.12 Immunofluorescence analysis of patient-derived cells confirmed CAF phenotype……...……140

Figure 4.13 CAFs promote cell proliferation in 5% GelMA co-cultures with PDAC cells……..……141

Figure 4.14 Young's modulus measurement of 3% and 5% GelMA BxPC-3 co-cultures with cancer-associated fibroblasts or non-malignant fibroblasts……...……142

Figure 4.15 GelMA hydrogel orthotopic xenograft……...……143

Figure 4.16 Analysis of resected orthotopic xenograft tumorigenic cell population and tumour stiffness…….……...…144

Figure 4.17 PDAC, THP-1 and CAF triple cultures in GelMA and collagen hydrogels...…145

Figure 4.18 Young's of 5% and 7.5% GelMA triple cultures……..…146

Figure 4.19 Secreted interleukin (IL)-6 and IL-8 levels in cell culture supernatants at day 14 of culture in either collagen, 5% or 7.5% GelMA hydrogels……...……147

Figure 4.20 Indirect co-culture experimental setup……...…….150

Figure 4.21 Indirect co-culture of PANC-1 cells with THP-1 cells and CAFs promotes activation of pro-survival pathways via STAT3 phosphorylation……...……152

Figure 5.1 Exploratory clustering and number of differentially expressed genes of PDAC cells grown in Matrigel, collagen, 5% GelMA and 7.5% GelMA matrices…….……..163

Figure 5.2 Volcano plots of p-value and log_2FC for each stiffness (5% and 7.5% GelMA) compared to collagen control……...…….164

Figure 5.3 Overlap of significantly different protein-coding genes and at least two-fold change in 5% and 7.5% GelMA compared to collagen……..……166

Figure 5.4 Number of differentially expressed and strength of correlation between genes of PDAC cells grown in Matrigel versus collagen, 5% GelMA and 7.5% GelMA matrices…..167

Figure 5.5 Analysis of differentially regulated pathways and Gene Set Enrichment Analysis for BxPC-3 and PANC-1 cells in collagen versus 5% and 7.5% GelMA…….……168

Figure 5.6 Expression heatmaps of genes related to proteases, EMT and mechanosensing pathways in BxPC-3 and PANC-1 cells grown in collagen, 5% GelMA and 7.5% GelMA..169

Figure 5.7 Gene Set Enrichment Analysis of Naba's core matrisome and O-linked glycosylation in BxPC-3 and PANC-1 cells in collagen, 5% and 7.5% GelMA hydrogels....171

Figure 5.8 Expression of PDAC matrisome signature and Matrix Index in BxPC-3 and PANC-1 cells in collagen, 5% and 7.5% GelMA hydrogels……..173

Figure 5.9 qRT-PCR validation of RNA-seq data……...…174

Figure 5.10 Expression heatmaps and Gene Set Enrichment Analysis of Naba's matrisome-associated secreted factors and selected cytokines…….……175

Figure 5.11 Schematic representation of cell mechano-transduction mechanisms……..177

Figure 6.1 Effects of epithelial-to-mesenchymal transition status and GM6001, fasudil and gemcitabine/abraxane treatment on the proliferation of PDAC cells in 2D…..……184

Figure 6.2 Effects of GM6001 treatment on PDAC cell proliferation in collagen, 5% and 7.5% GelMA and Transwell cell invasion……..187

Figure 6.3 Effects of GM6001 treatment on gene and protein expression in collagen and 7.5% GelMA hydrogels……189

Figure 6.4 Effects of fasudil treatment on PDAC cell proliferation in collagen and 5% GelMA……190

Figure 6.5 Effects of GM6001 treatment on matrix stiffness as measured by rheometry, confined compression and atomic force microscopy……192

Figure 6.6 Experimental setup of triple culture experiments……..……193

Figure 6.7 Effects of fasudil priming on the efficacy of gemcitabine and abraxane in collagen, 5% and 7.5% GelMA hydrogels…….……...……194

Figure 6.8 Effects of fasudil, gemcitabine and abraxane treatment on the stiffness of collagen, 5% and 7.5% GelMA hydrogels……...….……196

Figure 6.9 Expression heatmaps of selected genes following treatment with fasudil, chemotherapy, for PANC-1 or stromal cells (THP-1 and CAF)……198

Figure 6.10 Effects of treatment with fasudil and chemotherapy on matrix proteins and secreted factors……...…….200

Figure 7.1 Schematic representation of some of the investigated key processes involved during the progression from 2D cultures to 3D cultures and treatment……..……210

List of Tables

Table 1.1 Comparison of selected biomaterials for the 3D cell culture of PDAC cells and pancreatic TME modelling, with associated studies. 52

Table 2.1 Patient information of OvCa and PCa specimens collected throughout the study and their use.. 65

Table 2.2 Table of antibodies used for immunofluorescence. 82

Table 2.3 Secondary antibodies and other immunofluorescent dyes used. 82

Table 2.4 Staining reagents, primary and secondary antibodies used for immunohistochemistry. 85

Table 2.5 Digestion protocol specifications including enzyme names, origin, final concentration and supplier..... 85

Table 2.6 qPCR TaqMan primer details, all Thermo-Fisher Scientific. 87

Table 2.7 qPCR SYBR Green primer details. 87

Table 2.8 Primary and secondary antibodies used for western blotting..... 91

Table 4.1. Digestion protocol specifications including enzyme names, origin, final concentration and representative pictures. 130

Table 4.2. Conditions for flow cytometry and details of calcein-AM (CaAM)/ethidium homodimer-1 (EtH1)/ 4',6-diamidino-2-phenylindole (DAPI) staining of GelMa-retrieved MIA PaCa-2 cells following collagenase I digestion. 133

Table 4.3. Number of tumours, metastases and tumour stiffness of orthotopic xenografts of GelMA hydrogels……...145

Table 6.1. Genotype and phenotype of PDAC cell lines……185

Abbreviations

ADAM	Adamalysin
AF	Alexa-Fluor
AFM	Atomic Force Microscopy
AKT30	Protein kinase B
AMOTL	Angiomotin like-protein
ANGPT	Angiopoietin
ANKRD1	Ankyrin Repeat Domain 1
ANOVA	Analysis of Variance
ATM	Ataxia-Telangiectasia Mutated
ATR	Ataxia-Telangiectasia mutated and Rad3-Related
ATRA	All-Trans-Retinoic Acid
BMP7	Bone Morphogenic Protein 7
BRCA1	Breast Cancer type-1 susceptibility protein
BSA	Bovine Serum Albumin
Ca-AM	Calcein-AM
CAF	Cancer Associated Fibroblast
CCN1	CCN family member 1
CD68	Cluster of Differentiation 68
COL	Collagen (R transcriptomics labelling)
COL1	Collagen type-I
COL1A1	Collagen type-I alpha-1
CSF1R	Colony-Stimulating Factor 1 Receptor
CTLA4	Cytotoxic T Lymphocyte protein 4
CXCL12	C-X-C motif chemokine 12
CXCR4	Chemokine Receptor type 4
DAB	3,3'-diaminobenzidine
DAPI	4',6-diamidino-2-phenylindole
DDR1	Discoidin Receptor 1
DEG	Differentially Expressed Gene
dH_2O	Deionised water
DMEM	Dulbecco's Modified Eagle Medium
DMSO	Dimethyl Sulfoxide
DoF	Degree of Functionalisation
DSBs	Double-Strand Breaks
EDTA	Ethylenediaminetetraacetic acid
EMT	Epithelial-to-Mesenchymal Transition
EpCAM	Epithelial Cell Adhesion Molecule
ERK	Extracellular-signal-Regulated Kinase
Et-H1	Ethidium-Homodimer 1
FAK	Focal Adhesion Kinase
FAP	Fibroblast Activation P
FBS	Foetal Bovine Serum
FC	Fold Change
FDA	US Food and Drug Administration
FDR	False Discovery Rate
FGFR	Fibroblast Growth Factors Receptor
FN1	Fibronectin
FOLFIRINOX	5-fluorouracil, leucovorin, irinotecan and oxaliplatin
GelMA	Gelatin Methacryloyl
GEMM	Genetically Engineered Mouse Models
GPCR	G-protein coupled receptor
GPER	G-Protein-coupled Estrogen Receptor
GSEA	Gene Set Enrichment Analysis
H&E	Haematoxylin and eosin
HA	Hyaluronic Acid
HABP	Hyaluronic Acid-Binding Protein
HD	Homozygous Deletion
HGSOC	High Grade Serous Ovarian Cancer
HIF-1A	Hypoxia Inducible Factor 1
HRP	Horseradish Peroxidase
HUVEC	Human Umbilical Vein Endothelial Cells
IF	Immunofluorescence

IGF-1 (R)	Insulin-like Growth Factor1 (Receptor)
IHC	Immunohistochemistry
IL-	Interleukin
KEGG	Kyoto Encyclopaedia of Genes and Genomes
KPC	LSL-$Kras^{G12D/+}$; LSL-$Trp53^{R172H/+}$; Pdx-1-Cre (mouse model)
KRT19	Cytokeratin 19
LAMC3	Laminin gamma 3
LAP	Lithium Acylphosphinate salt
LGR	Leucine-rich repeat-containing G-protein coupled Receptor 4
LOX	Lysyl Oxidase
LOXL2	Lysyl Oxidase Like 2
LPA	Lysophosphatidic Acid
MA	Methacryloyl (functional group)
MAPK	Mitogen Activated Protein Kinase
MAT	Matrigel (R transcriptomics labelling)
MHC	Major Histocompatibility Complex
MI	Matrix Index
MMP	Matrix Metalloproteinases
MSC	Mesenchymal Stem Cells
MSD	Meso Scale Discovery
MT	Masson's Trichrome
MT1-MMP	Membrane-type MMP
MUC	Mucin
MYL9	Myosin Light chain 9
n/a	not available/applicable
NF	Normal Fibroblast
NF-kB	Nuclear Factor kappa -light-chain-enhancer of activated B cells
O-GlcNAc	*O*-linked β-*N*-acetylglucosamine
ON	Overnight
P/S	Penicillin/Streptomycin
PanIN	Pancreatic Intraepithelial Neoplasia
PBS	Phosphate Buffered Saline
PD-1	Programmed cell Death protein 1
PDAC	Pancreatic Ductal Adenocarcinoma
PDGF	Platelet-Derived Growth Factor
PDX	Patient Derived Xenograft
PEG	Poly(Ethylene Glycol)
PEGPH20	Pegylated recombinant Human PH20 Hyaluronidase
PFA	Paraformaldehyde
PI3K	Phosphoinositide 3-Kinase
PSC	Pluripotent Stem Cells
PSC	Pancreatic Stellate Cells
RAS	MAPK/ERK pathway (aka Ras-Raf-MEK-ERK pathway)
REC	Research Ethics Service
RGD	Arginine, Glycine and Aspartate binding motif
RNA-seq	RNA Sequencing
ROCK	Rho-associated protein kinase
RPKM	Reads Per Kilobase of transcripts, per Million reads
RT	Room Temperature
RTK	Receptor Tyrosine Kinase
RT-qPCR	Reverse Transcription–quantitative Polymerase Chain Reaction
SCID	Severe Combined Immunodeficient (mouse)
SD	Standard Deviation
SDF-1	Stromal Cell-Derived Factor 1
SDS-PAGE	Sodium Dodecyl Sulfate-Polyacrylamide Gel Electrophoresis
SEM	Scanning Electron Microscopy
SEM	Standard Error of the Mean
SERPINA3	Serpin Family member A member 3
SHH	Sonic Hedgehog

SMAD	Mothers Against Decapentaplegic
SPARC	Secreted Protein Acidic and Rich in Cysteine
STAT3	Signal Transducer and Activator of Transcription 3
TAM	Tumour-Associated Macrophages
TAZ	Transcriptional coactivator with PDZ-binding motif
TBST	Tris-Buffered Saline Tween
TCGA	The Cancer Genome Atlas
TGF-α	Transforming Growth Factor-α
TGF-β	Transforming Growth Factor-β
TIMP	Tissue Inhibitor of MMP
TME	Tumour Microenvironment
TNF-α	Tumour Necrosis Factor α
Tregs	Regulatory T cells
UV	Ultra Violet
VCAN	Versican
VEGF	Vascular Endothelial Growth Factor
VIM	Vimentin
vol/vol%	Volume/Volume percentage
WNT	Wingless
wt/vol%	Weight/Volume percentage concentration
YAP	Yes-Associated Protein
ZEB1/2	Zinc finger E-box-binding homeobox proteins 1 and 2
α-SMA	α-Smooth Muscle Actin
γH2AX	Phosphorylated Histone family member X

Chapter 1 - Project Background and Introduction

1.1 Pancreatic Ductal Adenocarcinoma

1.1.1 Prevalence and epidemiology

Pancreatic cancer is a lethal disease with dismal prognosis and a 5-year survival that has changed very little over the past few decades. The median overall survival of patients is only 6 months from diagnosis, with around 9% of patients surviving over 5 years and as little as 1% reaching 10 years [1]. This is in part due to patients presenting with late stage disease, with around 35% baring locally advanced disease and 52% being metastatic, all of which are considered surgically unresectable [2]. This means that despite surgical resection being the best curative treatment, only 10-20% will be eligible for surgery. Moreover, of those patients undergoing surgery, 30% will present early recurrence, or later relapse, with only 3-12% achieving long-term (10 years) survival [2,3]. Because of the overall limited improvement in treatment options and its rising incidence, pancreatic cancer is predicted to become the second leading cause of cancer-related fatalities in the next decade [4]. This prediction reflects the persistence of gaps in our understanding of the mechanisms underpinning pancreatic cancer initiation, progression and metastasis, ultimately leading to a failure in early detection and efficient treatment options. In order to identify and tackle these issues, it is imperative to understand the aetiology and pathophysiology of pancreatic cancer.

1.1.2 Pathophysiology of pancreatic ductal adenocarcinoma

Pancreatic neoplasms are classified according to their histological differentiation (epithelial or non-epithelial) and according to their functional behaviour (benign, pre-malignant or malignant) [5]. Epithelial neoplasms can be exocrine or endocrine depending on the site of initiation, with the exocrine group further divided into ductal and acinar neoplasms [5]. By far the most common type of pancreatic neoplasm, pancreatic ductal adenocarcinoma (PDAC) accounts for over 90% of all pancreatic malignancies, and occurs in the pancreatic ducts which are responsible for transporting pancreatic juices into the duodenum during digestion. The remaining cases include other exocrine tumours (acinar cell, mucinous, serous, etc.) or neuroendocrine tumours (gastrinomas, glucagonoma, insulinoma)[5], which arise in the endocrine pancreatic islets and generally have a far better prognosis than PDAC.

Despite massive advances in oncology, medical imaging and surgery, PDAC-related deaths are projected to more than double from 42 000 (per annum) in 2010 to 88 000 in 2030 in the US alone, only second to lung cancer [4]. Unsurprisingly, PDAC and lung cancer share similar

drawbacks that make them less targetable, in that they are both primarily environmentally caused and detected at late stages. PDAC remains largely unpreventable, with less than 10% of cases having a family history or inherited risk [6], and with risk factors (tobacco, alcohol, obesity, cholesterol, diabetes, etc.) only marginally increasing overall risk by a 1.5 to 2.8 factor in otherwise healthy individuals [7]. Additionally, PDAC is usually detected at a late stage of disease, with advanced stage pancreatic lesions, too late to be surgically resected.

1.1.2.1 Pathogenesis of PDAC

PDAC usually derives from pancreatic intraepithelial neoplasia (PanIN) precursor lesions. PanIN are commonly found in the healthy pancreas, and are characterised by a ductal phenotype, classified as low- or high-grade depending on histological cellular and nuclear dimorphisms, or staged 1 to 3 [8]. During progression however, PanIN lesions increase from an average 16% in healthy individuals to 82% in PDAC patients [9], often located in the head (70%) or tail (6%) of the pancreas [10]. PanIN progression is thought to be slow and hence more prone to being undetected, despite its high prevalence [11], suggesting there is a lack of sensitive and specific early detection methods. Traditionally, PDAC detection is conducted through the measurement of cancer antigen CA19-9 serum levels which, despite being a good marker for monitoring disease state or treatment efficacy, lacks the sensitivity and specificity to be employed as an early detection diagnostic tool [12]. Likewise, the presence of circulating tumour cells carries high prognostic value, but only occurs in a subset of metastatic patients [12]. Hence detection primarily occurs via symptomatic presentation of patients, usually at late-stage disease when very limited treatment options remain viable. In addition to morphological characterisation, genetic mutations driving PDAC carcinogenesis have been well known for many years. In murine models, activation of oncogenic *KRAS* alone is sufficient to drive PanIN formation [13]. Additional driving mutations such as *CDKN2A, TP53* and *SMAD4,* are usually only found in high-grade PanIN and advanced disease stages, while *KRAS* mutations are frequently found, at lower frequencies, even in low-grade lesions [14]. This suggests a progressive and possibly sequential accumulation of oncogenic mutations take place in the pancreas leading to PDAC progression, whose understanding is key in designing early detection strategies.

1.1.2.2 Molecular biology of PDAC

PDAC exhibits altered autocrine and paracrine signalling cascades that, in turn, promote cell proliferation, transformation, migration, invasion and metastasis. For instance, activation of

cell mitogenic self-sustainment, migration and invasion are documented through signalling via receptor tyrosine kinase (RTKs) including epidermal growth factor receptor (EGFR), hepatocyte growth factor receptor (HGFR), fibroblast growth factors receptor (FGFRs), insulin-like growth factor 1 receptors (IGF1Rs) or erbB-2 (ERBB2, HER2), HER3, and their respective growth factors transforming growth factor-α (TGFα), HGF, FGF, IGF [15]. These cascades concur with the activation of pro-survival and anti-apoptotic signals including nuclear factor-κB (NF-κB), AKT30, signal transducer and activator of transcription 3 (STAT3), wingless (WNT), sonic hedgehog (SHH) and NOTCH [16-18]. PDAC also exhibits aberrant metabolism and insensitivity to growth inhibitory pathways, exemplified by abnormal TGFβ signalling. TGFβ directly induces PDAC cell proliferation via SMAD-4-mediated upregulation of WNT7B, which in turn phosphorylates mitogen activated protein kinase (MAPK), tyrosine-protein kinase Src (SRC), and AKT [19]. All of these occur in the context of *KRAS* activation and loss of the tumour suppressor p16 through *CDKN2A* mutations. Activating *KRAS* mutations dominate PDAC pathology which occur in >90% of tumours. Additional mutations inactivating *TP53, CDKN2A* and *SMAD4* are present in 50-80% of tumours, while relatively rarer mutations, such as *TGFBR2, GLI13, MLL3* or *ARID1A,* occur in 10-15% of cases [12]. However, recent advances in high-throughput sequencing have enabled more detailed categorisation of PDAC subtypes based on their mutational landscape [20-23].

1.1.2.3 Molecular subtyping of PDAC

Transcriptome-wide analyses of PDAC tissue samples led Collisson et al. to classify them into three molecular subtypes namely classical, characterised by expression of epithelial and adhesion-related genes; quasi-mesenchymal, expressing mesenchyme-related genes; and exocrine-like, expressing digestive enzymes genes. Survival was best for the classical subtype and worst in quasi-mesenchymal subtype patients [20], however correlations with sensitivity and resistance to current therapy regimens, including gemcitabine and nab-paclitaxel or FOLFIRINOX, are not known. Following this, Bailey et al. proposed four alternative subtypes based on whole exome sequencing and copy number variation [21]. Genomic stability or instability were further suggested as stratification criteria by Waddell et al. suggesting unstable subtypes might be more susceptible to DNA-damage inducing therapeutics compared to stable counterparts [22]. As the role of tumour microenvironment (TME) became evident in later years, Moffitt et al. included PDAC stroma in their classification, proposing an "activated" vs "normal" PDAC stroma subtypes, with the latter correlated with better prognosis [23]. Since then, single cell RNA-sequencing (scRNA-seq) and high content digital

imaging advances have led to extensive characterisation and classification of PDAC in the context of its TME [18]. Therefore, future studies should continue linking molecular and histomorphology data to infer prognostic relationships.

1.1.3 The PDAC clinical landscape: challenges and prospects

For the majority of patients, symptom presentation remains the most common form of detection. However, PDAC symptoms, including fatigue, jaundice, nausea and abdominal pain, are largely unspecific, and occasionally totally absent, often resulting in delayed diagnosis [12]. Additionally, since symptoms arise very late during PanIN progression to metastatic PDAC, most patients remain largely inoperable. Another staggering reason for PDAC's dismal prognosis is the absence of highly efficient treatments and low response rate to available therapies. Prophylactic treatments include anti-inflammatory drugs, such as aspirin, which appears highly controversial, especially in gastric cancers [24].

1.1.3.1 Neoadjuvant, adjuvant and palliative treatments

To date, the best potentially curative option remains surgical resection, which is performed with a Whipple procedure since 1935 and consists in the removal of the head of the pancreas as well as duodenum and bile duct, or by distal pancreatectomy and spleen removal [12]. The surgery is highly invasive and regardless of its success, 90% of patients will relapse after resection [25,26]. This could be associated with a lack of adequate staging options, inadequate neoadjuvant treatment or radiological staging, and differences in tumour aggressiveness leading to undetected metastases. Recent advancements in the field of radiology, sophisticated imaging and sequencing techniques, as well as neoadjuvant treatments, can help surgeons to select patients who will benefit from surgery or from different therapy options [2]. Current neoadjuvant therapy options include chemotherapy, chemo-radiotherapy and targeted therapies [2].

For unresectable tumours, the main palliative treatment option remains chemotherapy (Figure 1.1). Since 1997, gemcitabine has been the first-line of treatment for newly-diagnosed PDAC cases [27]. In 2013, new evidence showed that gemcitabine conferred a significant increase in survival if administered in combination with a nanoparticle albumin-bound version of paclitaxel (nab-paclitaxel) [28], which is used to date. Around the same time, a combinational therapy of 5-fluorouracil, leucovorin, irinotecan and oxaliplatin named FOLFIRINOX was being tested [29]. Both treatment lines had similar 1-year survival rates,

with FOLFIRINOX being slightly less tolerated, especially in older patients [30,31]. Both treatment options are still in use today, as both neoadjuvant (prior to surgery), adjuvant (after surgery) or palliative (unresectable) regime options, the latter yielding the least responses [32,33].

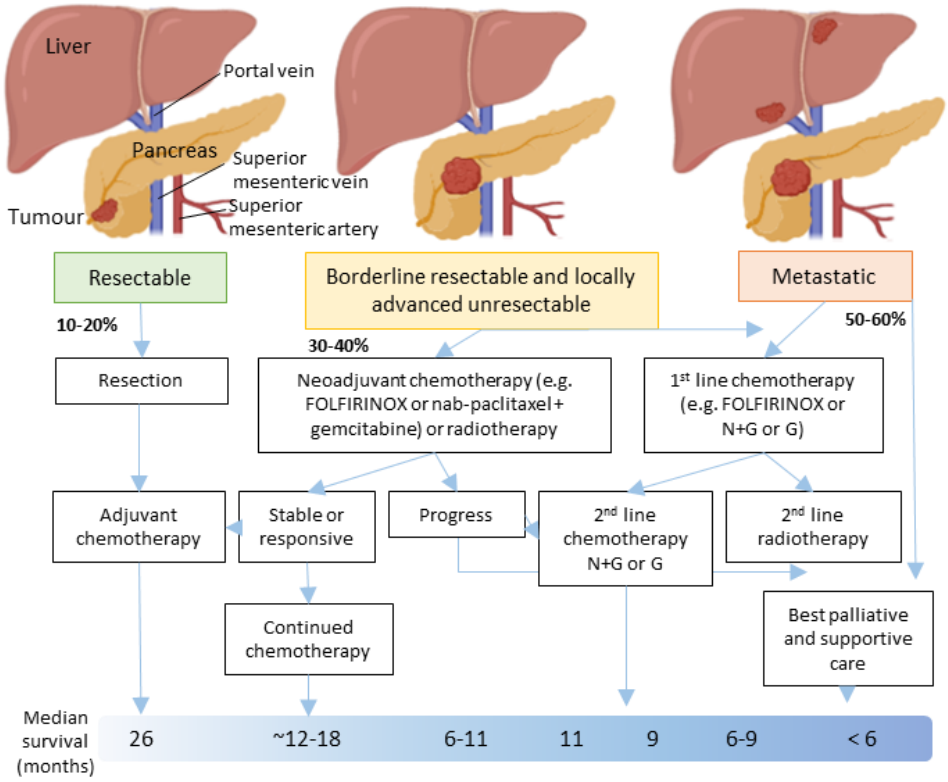

Figure 1.1 Treatment options and associated median survival for PDAC patients. Patients are stratified according to tumour stage (resectable, borderline resectable and locally advanced unresectable, metastatic). FOLFIRINOX= folinic acid, fluorouracil, irinotecan and oxaliplatin; N= nab-paclitaxel; G= gemcitabine. Adapted from Neoptolemos et al. 2018.

1.1.3.2 Targeted therapies

Several targeted therapies have been evaluated as single agent or in combination with chemotherapy with, unfortunately, most agents failing to improve survival significantly [26]. These include anti-angiogenic compounds, such as sunitinib, sorafenib and axitinib or vascular endothelial growth factor (VEGF) inhibitors bevacizumab and aflibercept [34-37]. Their failure could be attributed to the hypo-vascular nature of PDAC, which makes anti-angiogenic agents largely ineffective. Agents targeting other key signalling cascades, such as the phosphoinositide 3-kinase (PI3K) inhibitor rigosertib [38], the multi-kinase targeting masitinib [39] and the anti-IGF1 antibodies ganitumab and cixutumumab [40], have also been ineffective in combination with gemcitabine. The only agent, currently approved, with statistically significant, although marginal, patient survival improvement is erlotinib. Erlotinib pharmacologically inhibits EGFR, which is upstream of GTPase KRAS [26]. As *KRAS*

activating mutation is highly present in PDAC patients, erlotinib is postulated to have only a minimal effect in this cancer type. In fact, randomised trials have reported a mere ~2 weeks improvement in survival with combinational erlotinib treatment over gemcitabine alone [41]. Similarly, inhibitors of the JAK/STAT pathway, such as ruxolitinib, failed in clinical trials at phase II despite significantly improving survival in patients with systematic inflammation [42]. These failures could be partially explained by advanced disease state at diagnosis, lack of patient stratification guidelines but most importantly by the high molecular heterogeneity of PDAC, as well as the highly stromal and fibrotic nature of these tumours, promoting tissue stiffness, reducing drug delivery, half-life and altering metabolism.

1.1.3.3 Stromal targeting therapies

The pancreatic TME has gained significant interest in the last decades, due to its ability to shape and influence cancer cell behaviour and determining treatment response. This comprises both cellular and extracellular elements which will be discussed in detail in Section 1.2. In the effort of exploiting the stroma to enhance drug accumulation, secreted protein acidic and rich in cysteine (SPARC) protein was used as a prognostic biomarker. SPARC is produced by fibroblasts and is known to bind to albumin, thereby potentially enriching the concentration of nab-paclitaxel directly at the tumour site [43]. However, no association was found between stromal SPARC levels and overall survival [43]. Increased desmoplasia and tissue stiffness in PDAC are the result of high extracellular matrix (ECM) deposition, hypo-vascularisation and increased intra-tumoral pressure. Therefore administration of ECM-modulating treatments, such as the pegylated recombinant hyaluronidase PEGPH20, were aimed at targeting ECM molecules, hyaluronic acid (HA) in this case, intending to decrease tumoral fibrosis, interstitial fluid pressure and normalise vasculature [44,45]. Successful implementation in mice, prompted PEGPH20 use in combination with gem/nab-paclitaxel or FOLFIRINOX in clinical trials (NCT01839487, NCT01959139). Although phase I and II clinical studies showed promising results in patients with high tumour HA content when treated with PEGPH20 and gem/nab-paclitaxel (survival of 9.2 vs 4.3 months) [46], phase III failed to reach primary endpoint of overall survival and was terminated [47]. Earlier in 2019, the PEGPH20 and FOLFIRINOX arm had also been discontinued due to high treatment-related adverse events [47]. This suggested ECM targeting alone is not sufficient and that the cancer cell-stroma interplay might be more complex than previously thought. Importantly, although stroma is a physical barrier to drug delivery, it may also act as a protective barrier for the containment of migrating and proliferating cells. A separate study showed that genetical depletion of stromal fibroblasts lead to increased tumour aggressiveness and

decreased survival [48]. Similar results were observed targeting myofibroblast growth and collagen deposition via the SHH pathway inhibitor IPI-926 which, despite decreasing stromal content and normalising vasculature, accelerated tumour metastasis [49], underlining the dichotomy between the cancer-supporting and restraining roles of the PDAC stroma. A better understanding of the complex interactions between tumour, stroma and their contribution to tissue architecture may pave the way to novel therapeutic strategies.

1.1.3.4 Immunotherapies

One of the "hallmarks of cancer" is the ability of cancer cells to suppress and modulate the immune response either directly or via alterations to other TME components [50]. Immunosuppression mechanisms include activation of regulatory T cells (Tregs), myeloid-derived suppressor cells (MDSCs), inhibition of effector T cells, antigen-presenting cells (APCs) and modulation of macrophage populations within the tumour [26,51]. Tumour and stromal derived ECM molecules can also create a barrier leading to immune cell exclusion, such is the proposed role for matrix molecules such as HA, fibronectin (FN1) and versican (VCAN) in PDAC [45,52]. Immune response baseline status is predictive of survival in pancreatic cancer, therefore manipulation of immunological features of PDAC could have direct clinical effects [53]. Among the most popular, are inhibitors of proteins involved in T cell modulation, also termed checkpoint blockade molecules, such as programmed cell death protein 1 (PD-1) or cytotoxic T lymphocyte protein 4 (CTLA4), targeted by nivolumab and pembrolizumab or ipilimumab respectively [54]. However, PDAC's cell plasticity, poor immunogenicity and low antigenicity, have so far proven refractory to these agents in monotherapy [55], despite being successful in many other solid tumours. This is likely due to the highly desmoplastic and unique PDAC stroma, that limits T cell abundance and function. Other immunotherapy approaches include cancer vaccines using tumour-specific antigens of which, the GTPase RAS peptide (vaccine TG01/GM-CSF) in combination with gemcitabine is currently in clinical testing with encouraging preliminary results [56].

Despite no clear breakthrough of immunotherapies in this disease yet, they hold great potential for the future of treatment as our understanding of the immune response regulatory network and molecular makeup in PDAC increase. The key will be to be able to translate our molecular understanding into clinical significance by identifying which patients are more likely to benefit from each treatment strategy. This requires interdisciplinary collaboration from basic research to trial design and results integration from a genetic, stromal and immunologic point of view.

1.2 The plastic tumour microenvironment of PDAC

Tumours encompass much more than just masses of malignant cells, they interact, produce and recruit a number of additional non-transformed cells and molecules which make up their TME. The non-malignant components of the TME have a plastic and often tumour-sustaining or -promoting role at each step of carcinogenesis [57]. The physiological and pathological relevance of the stroma began to be recognised in the 1960s when the term "extracellular matrix" was first coined however, a deep understanding of its involvement in shaping the "hallmarks of cancer" was not described until the late 2000s [50,57]. Elucidating the bilateral interactions between tumour and its surrounding stroma is of vital importance in PDAC since it exhibits an unusually desmoplastic microenvironment, whereby up to 80-90% of the total tumour mass is made up by stromal components [58-60].

1.2.1 The cellular components of the PDAC microenvironment

1.2.1.1 Tumour cells

Mounting evidence is increasing our understanding of the complex interplay between tumour and non-malignant cells however, the specific role of tumour cells in initiating and modifying their surrounding is still not well characterised. Aggressive PDAC cells display increased proliferating, invading, migrating behaviours at the tumour edge or "invasive front". This behaviour is termed tumour-budding and is an independent adverse prognostic factor [61,62]. These budding cells present genetic signatures and behaviours very similar to cells undergoing epithelial-to-mesenchymal transition (EMT), such as reduced E-cadherin expression, loss of β-catenin expression on the cell surface, overexpression of N-cadherin, Snail and zinc finger E-box-binding homeobox proteins 1 and 2 (ZEB1/2) [62]. Other stromal components have been shown to express E-cadherin suppressors (such as ZEB1) [62], highlighting the establishment of a permissive microenvironment surrounding tumour cells. Numerous reports also link EMT to features of cancer stem cells, such as signalling through WNT, which links development of tumour buds and the promotion of stem cell-like phenotypes [21,63].

Increased understanding of cancer cell behaviours in combination with improved host-related and tumour-related biomarkers may eventually lead to better patient stratification. Although conventional histology is usually sufficient to determine disease state, a number of molecules can be useful both as *in vitro* cancer markers or to distinguish metastatic PDAC

cells in neighbouring tissues. PDAC cells usually overexpress cytokeratins including CK19, CK7, CK18 as well as mucins (MUC1, MUC4, MUC5AC) and the diagnostic CA19-9 and CA125 markers [5].

1.2.1.2 Stromal cells

Stromal cells in PDAC comprise fibroblasts, endothelial cells, and immune cells. The most abundant cell type in PDAC tissues are cancer-associated fibroblasts (CAFs), of which pancreatic stellate cells (PSCs) are the predominant subtype, alongside tissue-resident fibroblasts and mesenchymal stem cells, which can all be recruited by the tumour and contribute to increased desmoplasia [64,65]. Well known markers of CAFs include α-smooth muscle actin (α-SMA), stromal cell-derived factor-1α (SDF-1), fibroblast activation protein (FAP), and fibroblast specific protein-1 (FSP-1) [66] (Figure 1.2). They are activated by a number of growth factors including of TGF-β, SHH, tumour necrosis factor α (TNF-α), platelet-derived growth factor (PDGF), and interleukin (IL)-1, -6, and -10 [66] (Figure 1.2). In turn, they secrete a number of pro-survival and pro-tumorigenic stimuli, namely through TGF-β signalling, IGF and EGF secretion [66]. CAFs can also induce desmoplasia namely through the secretion of ECM molecules including collagen types I and III, fibronectin, proteoglycans, hyaluronan and glycosaminoglycans, leading to increased interstitial pressure, stiffness and hypoxia [67]. Additionally, they can contribute to a number of pro-tumorigenic processes including the induction of EMT, as well as cancer cell invasion, metastasis and chemoresistance [64] (Figure 1.2).

Although desmoplasia is known to confer aggressiveness by supporting cancer cell proliferation and dampening immunity [44,68], many recent studies have started to shed light on the protective role of stroma, whereby the genetic or therapeutic ablation of CAFs led to the development of undifferentiated and highly metastatic tumours [48,49]. This is exemplified in the clinical failure of CAF secretome-targeting strategies such as SPARC or PEGPH20 therapies. This dual pro-tumorigenic and restraining function of CAFs is also attributable to a high intra- and inter-tumoral heterogeneity as described by several transcriptomic, phenotypic and functional studies [18,69]. Puleo et al. recently proposed a classification of PDAC samples by incorporating both the canonical tumour subtypes (basal-like, classical) [23] as well as four distinct stromal components (structural vascularised, activated, inflammatory and immune), in an attempt to better represent observed heterogeneities [70]. Interestingly, stroma-activated phenotypes were characterised by higher CAF content, lower immune cell

infiltrate and showed worse prognosis compared to other subtypes [70]. This highlights the complexity between the cellular microenvironment, or more specifically the interactions between the immune and stromal cell compartments.

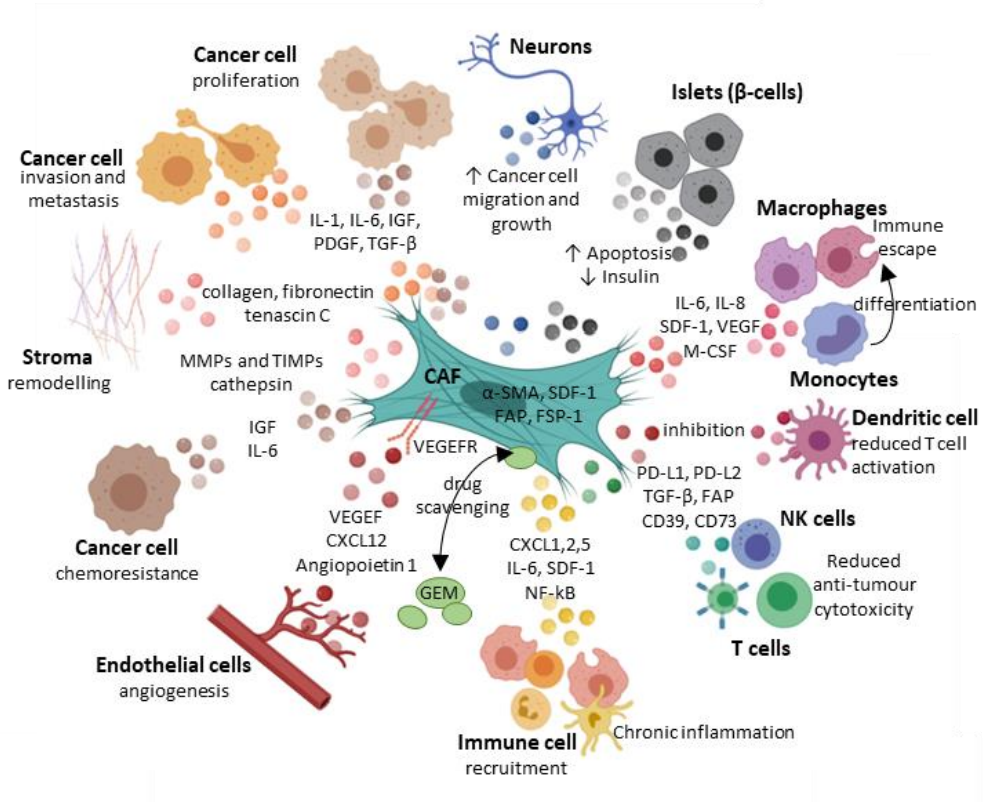

Figure 1.2 The role of cancer-associated fibroblasts (CAFs) crosstalk in the PDAC tumour microenvironment. Shown are some of the key stromal processes orchestrated by CAFs. CAFs promote cancer cell proliferation, invasion, metastasis and chemoresistance, as well as stromal remodelling and matrix deposition involved in cell migration and hampering drug delivery. CAFs also mediate tumour angiogenesis, migration along neurons and affect the physiological exocrine functions of the pancreas. They also play an important role in shaping the immune microenvironment towards a pro-tumorigenic and immunosuppressive milieu by affecting the function and recruitment of various immune cells. α-SMA= alpha smooth muscle actin; CXCL= chemokine (C-X-C motif) ligand; FAP= fibroblast activation protein; FSP= fibroblast-specific protein; GEM= gemcitabine; M-CSF= macrophage colony-stimulating factor; IL= interleukin; IGF= insulin-like growth factor; MMP= matrix metalloproteinases; PDGF= platelet-derived growth factor; PDL-1= programmed death ligand; SDF-1 = stromal cell-derived factor 1; TGF-β= transforming growth factor beta; TIMP= tissue inhibitor of metalloproteinases; VEGF= vascular endothelial growth factor; VEGFR= vascular endothelial growth factor receptor. Adapted from Sun et al., 2018; Monteran et al., 2019; Kleef et al., 2016.

1.2.1.3 Immune cells

PDAC exhibits an immunosuppressive landscape from early on in tumorigenesis [71]. The presence of immunosuppressive leukocytes ultimately contributes to the lack of tumour infiltrating lymphocytes (TILs) and leads to the early immune escape of tumour cells, namely immune excluded or immune-quiescent microenvironments [71]. Significant mechanisms of immune evasion include the expression of cell surface proteins PD-1 ligand (PD-L1), CTLA4 and colony-stimulating factor 1 receptor (CSF1R). In addition, immunosuppressive

chemokines secretion (such as CXC motif chemokine 12) and cytokines (IL-1, IL-6, IL-10 TGFβ, TNF) further induce an immunosuppressive microenvironment. PD-L1 and CTLA4 are defined as checkpoint inhibitors, conferring inhibitory signals to prevent immune cell activation, and correlate with worse prognosis when expressed in the TME of PDAC [72]. CSF1R is primarily found on myeloid cells where it's involved in recruitment and differentiation [51]. Its functional contribution to tumour size, maintenance and survival has already been established in murine models for the squamous subtype [51]. Hence why many therapeutic strategies are targeted at reprogramming immune cells through checkpoint proteins, such as CTLA4 and PD-1, to induce activation [71].

With regards to innate immunity, macrophages constitute the predominant subtype of the TME [73], and their infiltration has been correlated with poor prognosis in PDAC [72,74]. The role of tumour associated macrophages (TAMs) in assisting tumour development, progression and metastasis as well as conferring resistance to chemotherapy and radiotherapy, has been elucidated in a number of pre-clinical models [51,75]. This is because TAMs are seemingly a significant feature of the TME and themselves contribute to immune cell suppression and sustain tumour progression. For example, TAMs upregulate IL10 and IL13 to limit the immune response [51]. TAMs have recently been shown to support a pro-tumour microenvironment via a feedback regulatory loop mechanism through Siglec-1 engagement, upregulation of CCL8 and M-CSF [51,73]. Further to this, TAMs have also recently been seen to upregulate surface receptors such as CD24 as an immune escape mechanism, whose blockade showed to limit immune escape. A number of therapeutic interventions to re-educate or limit the recruitment of macrophages are currently being tested [76]. One such example is targeting macrophages through CSF1R inhibition, whose signalling is involved in differentiation of myeloid progenitors into monocytes, macrophages, dendritic cells or osteoclasts. Therapeutic ablation of macrophages through CSF1R inhibition in murine models has led to tumour regression, increased cell death, T-cell activation independent of PD-1 inhibition, and downregulation of squamous subtype-associated genes [51].

Most PDAC patients develop an immunosuppressive TME that impedes effector T cell infiltration, despite T cells being abundant in the stroma of primary PDAC and correlating with increased survival [72,77]. $CD8^+$ T-cells are activated by interacting with antigens presented on major histocompatibility complex (MHC) class I molecules of antigen-presenting cells. Low expression of MHC class I molecules on PDAC cells can inhibit T-cell activation in PDAC [78]. Additionally, engagement of checkpoint blockade receptors inhibit activation of T

cells, even in highly infiltrated tumours. Other immunosuppressive mechanisms include the recruitment of Tregs and TAMs with an alternative polarisation, together with myeloid-derived suppressor cells, which block the anti-tumour activities of effector $CD4^+$ and $CD8^+$ T-cells [77]. The immune quiescence of these tumours, combined with low or suppressed adaptive immunity activation, results in scarce invasion of cytotoxic T lymphocytes into the TME, low immunoediting, low mutational burden and hence higher resistance to checkpoint immunotherapies [79]. Reduced effector $CD8^+$ T-cells and increased $CD4^+$ $Foxp3^+$ Tregs levels have also been validated histologically in resected PDAC samples [74,80].

1.2.2 The extracellular components of the PDAC microenvironment

Tumour-stroma interactions prompt continuous remodelling and deposition of the dense pancreatic ECM. In turn, the matrix provides a number of biochemical and mechanical stimuli which guide cells' survival and behaviours including pro-fibrotic stimuli, immunosuppressive signals and architectural support. The influence of biomechanics during PDAC progression will be discussed in detail in the next Section (1.3 The mechanobiology of PDAC). While genetic alterations in tumour cells are the initiating and driving event, cancer progression involves a dynamic ECM which modulates virtually all functional aspects of tumour and tumour-associated stromal cells [81]. In fact, the ECM is postulated to play a role and modulate all hallmarks of cancer [81]. Unsurprisingly, increased ECM remodelling is associated with increased risk for malignant transformation in pancreatic cells [82]. Because of the dually sustaining and restraining roles of this dense matrix [17,48], an intimate understanding of the feedback between ECM and tumour is required for the development of successful prevention and treatment strategies.

The bulk of the ECM is made up of fibrous proteins and molecules, mainly heavily cross-linked and highly aligned collagen type I, which is largely produced by activated CAFs [58]. Pancreatic CAFs are also responsible for the deposition of other main ECM components, including other collagens, fibronectin (FN1), laminins, hyaluronic acid (HA), and versican (VCAN) [52,83]. Tumour cells and TAMs are also, although to a lesser extent, contributing to ECM deposition and fibrillar collagen formation [84]. At the interface between cancer cells and stroma sits the basement membrane, a cancer cell-derived macro-structure that is disrupted during PDAC progression, exposing cancer cells to the surrounding matrix, promoting EMT, migration and subsequent tumour spread to adjacent vessels and tissues [85].

With the advent of high throughput "omic" techniques, it has now been possible to characterise pancreas, PanIN and PDAC-specific sets of commonly expressed ECM molecules and their cellular origin [86,87], named the matrisome. While similar analyses had been conducted for the study of matrisomes in colon [88], prostate [89], ovarian and breast cancers [90], Tian et al. were the first to characterise the PDAC matrisome using integrated proteomic approaches [87]. Collagens, glycoproteins and proteoglycans are the three categories constituting the "core matrisome" [91], and their contribution to PDAC initiation and progression will be the focus of the next sections.

1.2.2.1 Role of collagens in PDAC

The most abundant and studied proteins of the PDAC ECM are collagens. To date, 28 types have been characterised [92], of which collagen I, II and V are the most common type located in the interstitial space, while IV, XV and laminin are predominant in the basement membrane [93]. Through disruption of the basement membrane, PDAC cells are exposed to increased levels of interstitial collagens, which have known pro-survival and tumorigenic affects [93,94]. Importantly, the majority of the desmoplastic reaction in PDAC is attributed to increased crosslinking and production of collagen type I [93-95]. Hence increased levels of collagen type I deposition in PDAC have been associated with poor prognosis and reduced overall survival [95]. On the other hand, basement membrane collagens, such as collagen type XV, are known to hinder EMT and invasive cell features [96], and their expression is reduced or lost during tumour progression. In fact, overexpression of collagen XV can inhibit the migratory and invasive phenotype of PDAC cells in matrices otherwise rich in collagen I [96]. However, the role of matrix proteins in disease is not always as clear cut. Laminin and collagen IV for instance, are amongst the predominant components of the basal membrane, and while low laminin levels are associated with decreased survival [97], high levels of collagen IV expression in PDAC stroma are known to promote cell proliferation and invasion [98]. Additionally, collagen IV can also be produced by tumours themselves as a protective mechanism against low nutrient-induced apoptosis [98]. Therefore, even within the same structure, ECM molecules may have contrasting effects and influence on PDAC pathogenesis.

The main mechanism by which collagens regulate PDAC pathobiology is through signalling via integrin receptors on the surface of malignant cells [98]. Integrins are transmembrane heterodimeric glycoproteins with an α- and β-subunit, whose different combinations confer binding specificity to different collagens [98]. Integrin α1β1 for instance, binds weakly to

collagen I but has a high affinity for collagen IV [99]. Contrariwise, integrin α2β1 binds weakly to collagen IV and strongly to both collagen I and V [99]. The binding of collagen I or V to α2β1 integrin receptors on PDAC cells has been shown to promote proliferation, migration, adhesion and prevent apoptosis of the latter [98,100]. Conversely, knockdown of β1 integrins in PDAC cells led to reduced adhesion to collagen but also resulted in hampered tumour growth and metastasis after implantation in an orthotopic mouse model [101].

The binding of collagen to integrin receptors leads to the activation of downstream signalling pathways which, in turn, are able to activate or inhibit different gene programs. For instance, migration of PANC-1 cells, a commonly used PDAC cell line, along collagen I is mediated by focal adhesion kinase (FAK) pathway activation downstream of collagen I- α2β1 integrin binding [102]. FAK activation leads to the phosphorylation of β-catenin, activation of WNT signalling and loss of E-cadherin [103]. Activation of FAK also leads to N-cadherin overexpression which, together with E-cadherin loss, results in the loss of cell adhesion and increased migration, all hallmarks of EMT [102,104]. In addition to integrins, collagens can also bind and signal through dimeric transmembrane receptor tyrosine kinases (RTKs), such as discoidin receptor 1 (DDR1), which is overexpressed in PDAC [104]. DDR1-collagen I binding leads to FAK pathway activation, N-cadherin expression as well as production of matrix metalloproteinases (MMPs) 2 and 9, proteases involved in ECM degradation [104,105]. Hence, the ECM's composition and collagens balance are capable of directing cell phenotype via induction of programs such as EMT.

1.2.2.2 Role of glycoproteins and proteoglycans in PDAC

Glycoproteins and proteoglycans are composed of core proteins that undergo post-translational glycosylation, which affects their conformation and cell signalling function [106]. In cancer cells, these proteins commonly undergo aberrant glycosylation which results in structural and functional changes [106]. An example are N- and O-linked glycosylation and the expression of core proteins periostin, fibulin 1, galectin 1, which are upregulated in PDAC [106-108]. A common glycoprotein with important implications in PDAC pathobiology is fibronectin (FN1). FN1 binds to integrin receptors (α5β1) and, similarly to collagen, can signal through the FAK pathway [103]. Importantly, FN1 retains collagen-binding sites making their structural and signalling role highly interlinked [109]. Aside its cooperative effects, FN1 supports PDAC cell proliferation [110], and can self-sustain its own production and overall ECM synthesis by CAFs by binding and releasing active TGFβ [111]. Fibronectin is also known to mediate resistance to radiotherapy by promoting PDAC cell invasion through the basal

membrane, an event which is nullified by either α5β1 blocking antibodies or fibronectin depletion [112]. Similarly, vitronectin is a major glycoprotein that binds to α5β3 integrins and collagens, promoting PDAC cell proliferation via IL-8 secretion [113].

Amongst the major PDAC proteoglycans lumican has been associated with markedly increased survival [114]. PDAC cells exposure to lumican in the ECM forces them into a quiescent state via G0/G1 cell cycle arrest, as well as inducing EGFR internalisation and hence inhibiting AKT and MAPK signalling [114]. Additionally, proteoglycans often bind to hyaluronic acid (HA), a non-sulfated glycosaminoglycan whose expression is highly abundant in the PDAC ECM [45]. Its importance is also highlighted by its ability to bind to CD44 thereby promoting tumour cell survival, proliferation and invasion [115,116]. Unsurprisingly, HA has been one of the main targets of PDAC stromal therapies with the use of PEGPH20 or other angiotensin inhibitors [44-47,117]. Versican (VCAN) is another proteoglycan known to bind to HA [118]. VCAN is present in the interstitial ECM space of normal tissues [119], but its expression dramatically increases in disease, so much that it has been described as a key component in a matrix signature common to many solid tumours, including PDAC [120]. VCAN's role in PDAC is not well characterised, however recent work suggests that its production is driven by both epithelial and stromal cells, and its accumulation correlates with CD8+ T cell exclusion [52].

1.2.2.3 Role of other ECM regulators

Additional categories of the matrisome include ECM-affiliated proteins, ECM regulators and secreted factors. These include mucins, such as MUC5AC, MUC1 and MUC16, which are highly upregulated in PDAC compared to normal pancreas [121]. ECM regulators include proteolytic and remodelling enzymes such as MMPs, adamalysins (ADAMs and ADAMTSs) as well as their inhibitors, tissue inhibitors of MMPs (TIMPs) and serine protease inhibitors (serpins), amongst many others. The role of MMPs in shaping the PDAC ECM will be discussed in more detail later (Section 1.3.2). Secreted factors include a plethora of cytokines and growth factors, many of which are implicated in PDAC, such as WNTs members, TNF-α, TGF-β, nodal and many more [63,111,122].

1.2.2.4 Defining a common matrix signature

With the advent of quantitative mass spectroscopy proteomic approaches, as well as transcriptomics in recent years, a number of different studies have started to systematically

examine and characterise the composition and dynamics of the ECM during cancer initiation and progression [87,120]. Using both human samples or murine models, it is now possible to screen the tumour proteome and ECM in search of common matrix denominators [120], assess their contribution to treatment response [123], correlation with overall survival [87,120], as well as their cells of origin [87]. One such example is the matrix index (MI), a 22-gene matrisome signature predictive of disease level and tissue stiffness [120]. Although originally characterised in high grade serous ovarian cancer (HGSOC), high MI correlated with shorter overall survival in 12 other solid tumour types, including PDAC [120]. Unsurprisingly, this signature includes some of the described collagens (COL11A1, COL1A1), glycoproteins (FN1) and proteoglycans (VCAN) which have prognostic value in PDAC [52,95,124]. This suggested selected host matrix molecules and stiffness might be eliciting a common response in human cancers. The role of stiffness and biomechanical processes in regulating PDAC tumorigenesis will be the focus of the next section.

1.3 The mechanobiology of PDAC

Besides biochemical signalling, the ECM also retains mechanical properties that provide important physical cues to cells influencing, in turn, intracellular signalling cascades. The ECM comprises the bulk of the stroma and is responsible for increased interstitial tissue pressure, stiff mechanics and physicochemical cues that promote proliferation, survival and metastasis [85,125]. The simultaneous compression of blood and lymphatic vessels leads to increased intratumoural pressure, reduced blood supply and hypoxia, which further promotes tumour growth, metastasis, resistance to treatment, as well as hampering drug delivery [126]. Several prognostic indexes have now suggested the combination of physical, genetic and histochemical tumour properties for the stratification of patients, such as the matrix index [120], or the activated stroma index [127].

1.3.1 Characterisation of PDAC biomechanics

Measured tumour stiffness often varies between different regions of the same sample, between different patients and even based on the technique and analysis conducted. The majority of reports have so far employed atomic force microscopy (AFM) for the nanoscale assessment of local stiffness in murine healthy and diseased samples [17,128]. The Young's modulus describes the elastic properties of a tissue and is a measure of its stiffness. Rice et al. reported an increase in the Young's modulus in murine models of PDAC progression from 1 kPa in C (Pdx1-Cre) mice (normal pancreas) to 2 kPa in KC PanIN mice (Pdx1-Cre; LSL-Kras$^{G12D/+}$) up to 4 kPa in mice representing a malignant phenotype , KPC (Pdx-1 Cre, LSL-Kras$^{G12D/+}$, LSL-Trp53$^{R172H/+}$) [128]. Collagen I amounts as well as collagen fibre thickness also progressively increased from normal pancreas (2.8 μm), to PanIN, to PDAC (3.7 μm) [128]. Similarly, Laklai et al. reported the stiffness of KPC tumours to be between 0.2 – 6 kPa [17]. Additionally, Nguyen et al. described a strong association between human PDAC cell stiffness and their invasive potential through upregulation of the mechanoregulating genes vimentin, actin and laminin A [129]. More recently, Rubiano et al. described the stiffness of fresh, unfixed, resected human PDAC samples by unconfined compression, allowing to sample larger areas of tissue (1-3 mm) [130]. Their results indicated that both pancreatitis (2.15 ± 0.41 kPa) and PDAC tissues (5.46 ± 3.18 kPa) exhibit a higher Young's modulus compared to normal pancreatic tissues (1.06 ± 0.25 kPa).

1.3.2 Regulators of stiffness

By providing mechanical cues, ECM stiffness can directly alter the behaviour and function of PDAC cells. Stiff collagen matrices for instance, are known to alter vimentin and E-cadherin expression in the malignant cells, contributing to EMT via nuclear translocation of β-catenin [128]. Stiff tumours show a markedly higher number of crosslinked collagen fibres [17,128], which have been associated with enhanced MMP activity, a proxy for increased matrix digestion, migratory and invasive phenotypes [131]. Equally, therapeutic abrogation of PDAC cell contractility resulted in reduced MMP activity, suggesting that malignant cells also play a direct role in influencing the mechanics of the ECM [131]. ECM stiffening in PDAC is mainly achieved through collagen fibre crosslinking by lysyl oxidase (LOX), an extracellular copper-dependant enzyme [132,133] (Figure 1.3). Additionally, LOX is involved in metastasis, hampers drug delivery and its expression is increased under hypoxia [133]. Conversely, *in vivo* targeting of LOX via neutralising antibodies in KPC mice resulted in decreased proliferation and improved survival [133]. Some of these observed effects are likely due to LOX effects beyond that of collagen crosslinking, as LOX inhibition also led to overall reduced desmoplasia and blood vessel normalisation [133-135]. Consistently with these findings, increased collagen fibre count, thickness and stromal stiffness are associated with shorter patient survival [17] (Figure 1.4).

In addition to LOX, tissue transglutaminase 2 (TG2) is also responsible for the crosslinking of collagen I fibres [136]. TG2 is induced by TGFβ and its expression dramatically increases during PDAC progression [136]. PDAC cells express and secrete TG2 in the surrounding ECM, where it crosslinks collagen fibres while also inducing collagen I production by other malignant cells and CAFs, creating a positive feedback loop [136]. Additionally, CAFs can induce desmoplasia via the secretion of other ECM molecules, collagens I and III, FN1, proteoglycans, and glycosaminoglycans [67]. Increased ECM crosslinking can intracellularly activate yes-associated protein (YAP) and its PDZ-binding transcriptional coactivator (TAZ), which translocate to the nucleus enhancing proliferation [136] and EMT programs [137,138] (Figure 1.3). Concordantly, YAP/TAZ nuclear localisation significantly increases in response to substrate stiffness [137,139], while strikingly all the gene signatures associated with increased ECM stiffness are also related to YAP/TAZ signalling [140]. This suggests YAP/TAZ act as a pivotal centre in the mechanotransduction of physical ECM properties. Additionally, recent work found that receptor tyrosine kinase (RTK)–Ras oncogenes ability to reprogram normal cells into cancer precursors requires mechanical signals and increased force transmission between transformed cells and the ECM [139]. This process leads to the build-up of cytoskeletal

tension and stiffening which lead to the activation and nuclear translocation of YAP/TAZ. The group identified Rac1 as a mediator of oncogenic mechanosignalling, sufficient and required for epithelial cells to be sensitised and responsive to stiffness [139].

Since over 80% of patients with advanced disease show high collagen deposition, PDAC cells have developed a number of mechanisms that allow them to overcome this fibrotic barrier during metastasis [95]. MMPs are the main class of enzymes involved in ECM degradation and matrix remodelling and one of the mechanisms underlying cell dissemination and metastasis [141]. There are 23 human MMPs each with a specific, sometimes overlapping, proteolytic activity and specificity within the ECM [141]. These include enzymes with collagenolytic activity (collagenases) such as MMP1, MMP8, MM13, gelatinases (MMP2, MMP9) and membrane-type (MMP14 or MT1-MMP). Collagenases specifically degrade collagen into denatured fragments, constituents of gelatin, which gets further degraded by gelatinases, both of which are expressed in high amounts in PDAC [142]. Other classes include matrilysins (such as MMP7), which promote invasion [143], stromelysins (such as MMP3), involved in tumorigenesis, and their tissue inhibitors (TIMP1-4) [142]. The prevalent PDAC membrane-bound MMP is membrane type 1-MMP (MT1-MMP or MMP14) [142,144], which is upregulated during EMT and, in turn, also promotes it through the release of latent TGF-β [145]. Collagen I has been shown to induce the expression of MT1-MMP suggesting, once more, that collagens are capable of directly regulating the expression of proteases involved in their remodelling [144] (Figure 1.3).

TIMPs are a family of secreted enzymes with the ability to inhibit various zinc-dependant endopeptidases, including MMPs. TIMP1 inhibits most secreted MMPs, and is highly expressed in PDAC, especially in response to treatment, where it contributes to drug resistance [146,147]. Importantly, TIMP1 expression is induced by increased tissue stiffness [147]. TIMP2 has a dual role in that it is required for the activation of MT1-MMP, whilst also acts as a potent inhibitor of MMP2 [146]. TIMP3 is known to inhibit all MMPs and members of the ADAMs and ADAMTSs families, each with different specificity. TIMP3 is often downregulated in PDAC, with associated poor prognosis [148]. Therefore, the course of ECM remodelling in disease is orchestrated by a delicate balance between MMPs and TIMPs secretion into the TME [131,147].

An additional mechanism whereby cells remodel the ECM is through regulation of Rho-associated protein kinase (ROCK) signalling. ROCK is a family of serine/threonine kinases that are the core regulators of actomyosin cytoskeletal arrangement, therefore controlling cellular contractile forces generation [149]. By regulating actomyosin contractility they are also

responsible for ECM remodelling and overall tissue contractility [149]. Crosstalk between ECM regulatory pathways is highlighted in PDAC, where ROCK1/2 can promote the expression of MMP10 and MMP13 to enhance local cell invasion via collagen degradation [150]. In murine models, inhibition of ROCK activity resulted in reduced ECM degradation and increased survival [150]. In humans, high ROCK expression is associated with significantly lower survival (Figure 1.4). Strikingly, ROCK activation alone was sufficient to significantly increase tissue stiffness and promote collagen deposition [151]. These responses were mediated by the activation of β-catenin. Inhibition of factors for actomyosin contractility, downstream of ROCK (such as LIM kinases or myosin ATPase), was sufficient to reverse ROCK activation effects [151]. Additionally, inhibition of FAK, which also signals through β-catenin upon integrin activation, or LOX, also decreased tissue tension [151] (Figure 1.3).

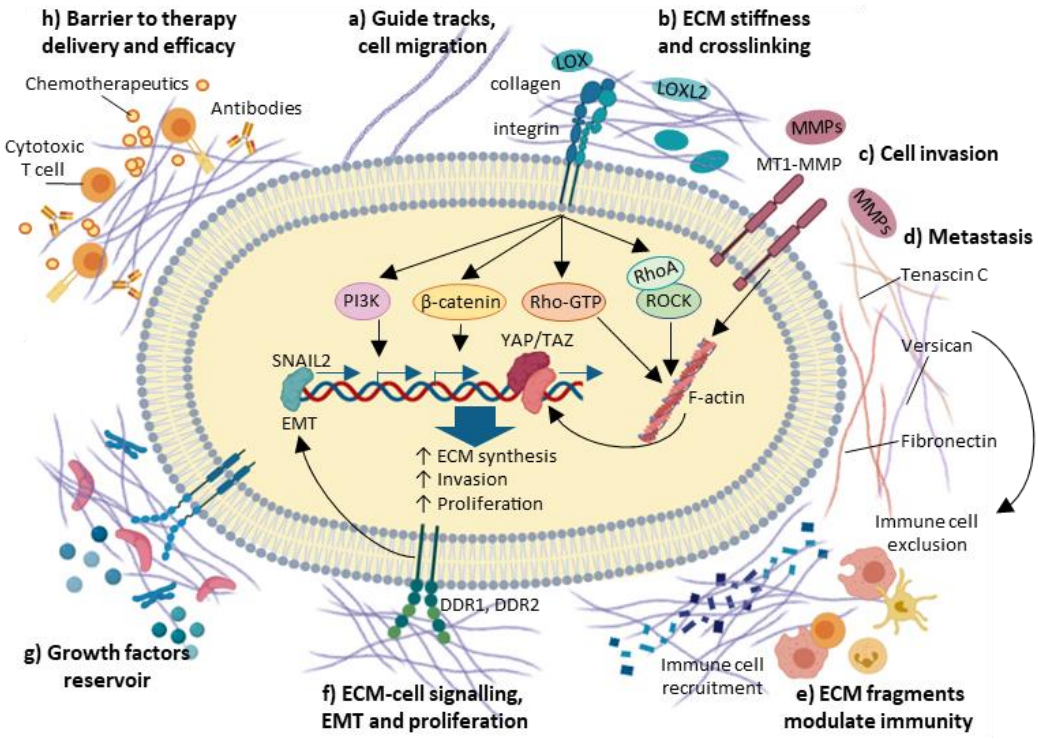

Figure 1.3 Aberrant tissue stiffness and extracellular matrix (ECM) crosslinking promote malignant cell behaviours. Increased ECM crosslinking contributes to a number of pathogenic mechanisms: **a)** ECM fibres acts as guiding tracks for cell migration. **b)** Increased ECM stiffness can signal through integrins whose downstream effectors can, in turn, promote further ECM synthesis, ECM crosslinking, F-actin polymerisation, cell invasion and proliferation. Extracellular collagen crosslinking is mediated by enzymes such as lysyl oxidase (LOX) and LOX-like 2 (LOXL2). **c)** Proteolytic enzymes such as matrix metalloproteinases (MMPs) are responsible for ECM remodelling and can signal through membrane-type MMPs (MT1-MMP) to stimulate cell invasion. **d)** The ECM provides proliferative and pro-metastatic signals as well as forming a pro-survival niche at the metastatic sites. **e)** Generation of ECM fragments can trigger aberrant immune responses as well as guiding cell migration. **f)** Increased cell-ECM signalling through, for instance, discoidin domain-containing receptor 1 and 2 (DDR1, DDR2) leads to transcriptional activation, and expression of MMP and epithelial–mesenchymal transition (EMT) markers. **g)** EMT, proliferation or angiogenesis can be triggered by growth factors, sequestered in the crosslinked ECM and released via proteolytic cleavage. **h)** The ECM acts as a barrier preventing immune cell infiltration and hindering the delivery and efficacy of treatments. PI3K= phosphoinositide 3-kinases; ROCK= Rho-associated kinases; YAP/TAZ= yes-associated protein, transcriptional coactivator with PDZ-binding motif. Adapted from Bonnans et al., 2014; Tang et al., 2013.

Tumour cells are not the sole contributors to tissue stiffness. CAFs are known to secrete abundant ECM components including collagens, FN1, MMPs and TIMPs [59]. As opposed to epithelial cells, matrix remodelling is an essential physiological function of fibroblasts, and is therefore sustained in both normal and diseased tissues [152]. However early mutations, such as the loss of *Timp*, are sufficient for the conversion to CAF phenotype, and induce cancer cell motility and tumour progression by unleashing MMP activity in the stroma [153]. CAFs can also control matrix remodelling via ROCK-dependant actomyosin contractility [154], and therefore its targeting could have concomitant effects on tumour cells and their TME [154,155]. Similarly to cancer cells, CAFs can also regulate actomyosin contractility via the activation of the YAP/TAZ axis [156]. In turn, ECM stiffness can further activate YAP, leading to a positive feedback loop that stabilises YAP activation, a CAF-activated phenotype and induces further tissue stiffening [156]. Finally, fibroblasts are known to respond to matrix composition and stiffness via the activation of TGF-β signalling which, in turn, confers them their activated, contractile, CAF phenotype [157,158].

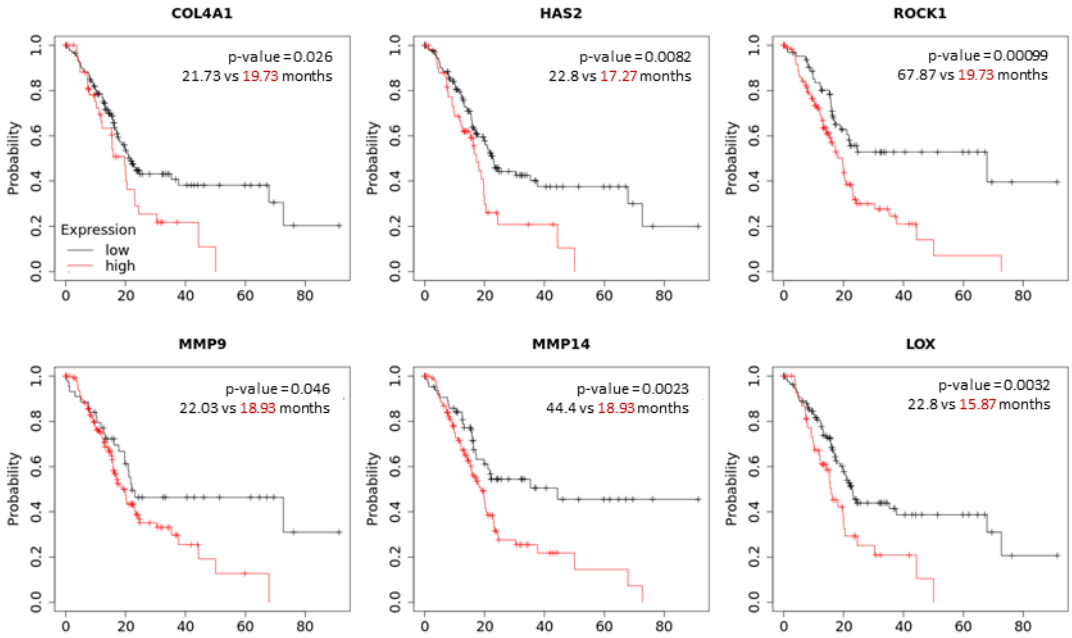

Figure 1.4 Kaplan-Meier survival curves for patients with high (red) and low (black) expression of collagen IV, hyaluronic acid (HAS2), Rho-kinase 1 (ROCK1), matrix metalloproteinases 9 and 14 (MMP9, MMP14), lysyl oxidase (LOX). Curves were calculated from public RNA-seq databases (mRNA data from Gene Expression Omnibus, European Genome-Phenome Archive and The Cancer Genome Atlas) for a total of 177 PDAC patients and plotted via Kaplan-Meyer plotter. p-values and mean survival (months) are indicated for each graph.

1.3.3 Targeting mechanobiology-related processes in PDAC

Regarding the alterations in TGF-β signalling, all-trans-retinoic acid (ATRA) has been suggested as a therapeutic intervention in PDAC due to its ability to hinder CAF mechanical

activation of TGF-β [158], hence preventing perpetuation of fibrosis. In KPC mice, administration of ATRA in combination with gemcitabine resulted in enhanced drug response, increased tumour necrosis, reduced ECM deposition and fibrosis [159]. The ongoing phase IB study STAR_PAC in PDAC is currently repurposing ATRA alongside gemcitabine and nab-paclitaxel as a stromal targeting agent (NCT03307148) [160].

Regarding MMP targeting in PDAC, only two phase III trials have been published [161,162]. The first one adding marimastat, a broad-band MMP inhibitor (targets MMP1, MMP2, MM7, MMP9 and MT1-MMP) to gemcitabine, showed the MMP inhibitor could be well-tolerated, but did not lead to any response or survival benefits in PDAC patients [161]. The second trial combined BAY 12-9566 or tanomastat, another broad-spectrum inhibitor of MMP2, MMP3, MMP9, which was well tolerated alone but led to a lower median survival compared to the gemcitabine arm (3.74 months versus 6.59 months) [162]. However, disappointing clinical trials results through MMP inhibition do not imply that MMPs do not contribute to PDAC progression. The lack of clinical benefits may likely be due to inclusion at advanced stage disease, as well as broad spectrum inhibitors lacking the efficacy and specificity to block such a multifaceted pathway [163]. Inhibitor unspecificity may also be blocking potential tumour inhibitory effects of MMPs, as exemplified by MMP9 deficiency which, on a *Kras(G12D)* background enhances tumour progression and invasion [164], explaining the failure of the tanomastat trial [162].

Two recent studies by Cortes et al. also identified G-protein-coupled estrogen receptor (GPER) as key regulator in PDAC cancer-stroma sensing, regulating tissue stiffness, hypoxia and desmoplasia [134,135]. In this regard, they suggested the repurposing of tamoxifen, a widely used estrogen receptor antagonist in breast cancer, to act as a GPER antagonist in order to normalise the PDAC TME [134]. Treatment with tamoxifen led to lower matrix crosslinking, lower tissue stiffness, increased vascularisation via the downregulation of hypoxia inducible factor 1 (HIF-1A) and increased tumour apoptosis [134], suggesting tamoxifen may be employed as a potential stromal-targeting therapy. Despite the promising results of the study, it remains to be seen whether tamoxifen may give any benefits to PDAC patients in clinical scenarios, where the stroma acts as both a restraining and supporting entity.

More recently, Vennin et al. showed that transient ROCK tissue priming (i.e. targeting the tumour mechanics via ROCK inhibitors) prior to chemotherapy, was efficient in releasing tissue tension, sensitising PDAC cells to treatment and increasing treatment efficiency [155]

(Figure 1.5). Importantly, mechanical priming with the ROCK inhibitor fasudil improved chemotherapy efficiency in both primary and secondary tumour sites and disrupted the movement of metastatic cells [155]. This study also demonstrated that stratified patient-derived tumours had a graded response to priming, suggesting tissue manipulation prior to chemotherapy may have clinical relevance [155]. In addition, CAF treatment with fasudil led to a normalisation of matrix production via suppression of collagen and TIMP secretion, while also stimulating MMP1 and collagenase activity [165]. This may have interesting therapeutic implications in PDAC, which is highly metastatic and notoriously untargetable by long-term matrix ablating treatments (such as PEGPH20) (Figure 1.5). To date, there are no reported uses of fasudil for the treatment of cancer in the clinic, therefore future phase I clinical trials will have to determine the safety and efficiency of transient ROCK tissue priming in combination with gemcitabine and nab-paclitaxel.

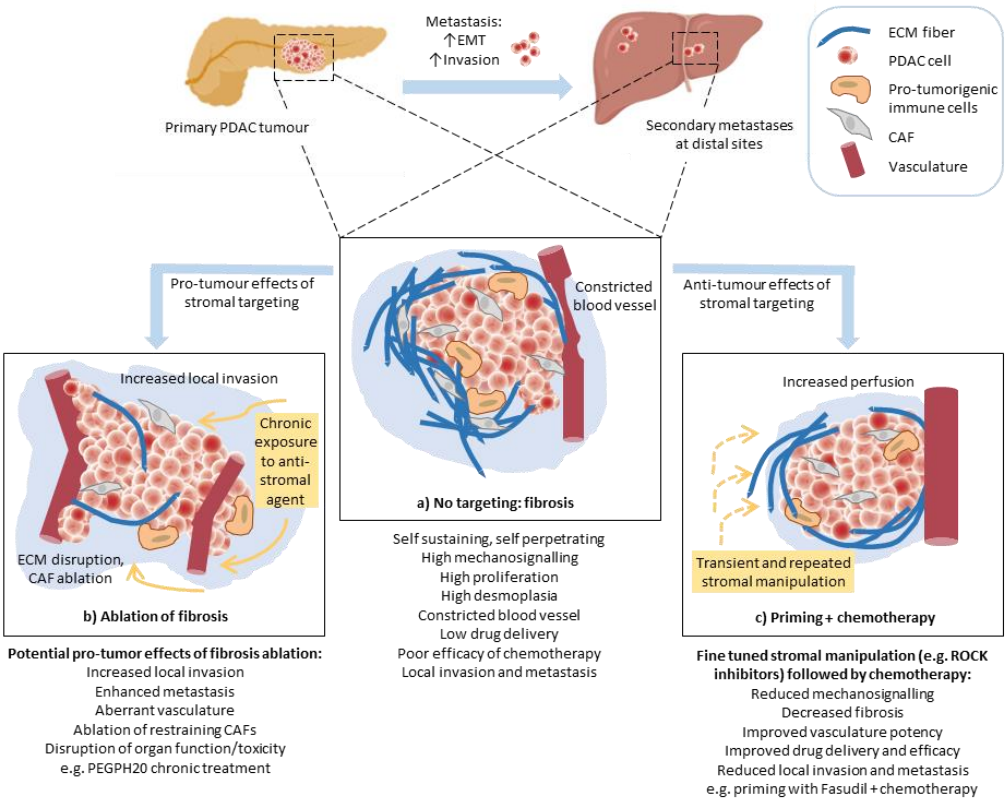

Figure 1.5 Transient administration of stromal targeting agents ("priming") as a strategy to increase chemotherapy efficiency while re-equilibrating tissue stiffness, decrease fibrosis and reduce metastasis. a) No targeting leads to self-sustained perpetration of fibrosis, desmoplasia and metastatic potential. **b)** Ablation of CAF and/or key ECM components via chronic anti-stromal agent targeting increases local invasion due to the dual restraining and promoting role of the PDAC stroma. **c)** Transient stromal targeting allows to temporarily release tissue tension and pressure, increasing the efficiency of chemotherapeutics, re-establishing stromal balance in both primary and secondary sites. Adapted from Vennin et al., 2017.

1.4 Pre-clinical models of PDAC

The establishment of the first pancreatic cancer cell line dates back to 1963 (CaPa), and it was followed, over a decade after, by the establishment of PANC-1 (1975), MIA PaCa-2 (1977), Capan-1 (1977), AsPC-1 (1982), Capan-2 (1986) and BxPC-3 (1986), which are amongst the most popular, and currently used, cell lines in PDAC research [166]. Aside from the obvious lack of heterogeneity and mutational instability, one of the major disadvantages of the use of established cell lines is the lack of stromal and extracellular cues that constitute the majority of the PDAC tumour under physiological conditions. On the other hand, the use of well-characterised murine strains allowed recapitulation of the *in vivo* architectural and immune physiologies, but constituted a much more laborious, expensive, and complex system to analyse. Attempts to characterise tissue function and architecture *ex vivo* date back as far as 1912, when Alexis Carrel described the first attempts at prolonging the life of tissues outside of the organism, and is considered one of the first ever recorded attempts of three-dimensional (3D) cell culture [167]. Since then, many novel approaches for the 3D culture of cells have been developed in an attempt to bridge the gap between the simplicity of established cell lines and the complexity of murine models. Because of their rheological properties, similar to those of human tissues, ease of handling, and ability to recreate 3D environments in a defined and controllable manner, hydrogels have been at the forefront of 3D cell culture research for many decades [168].

1.4.1 Murine models of PDAC

1.4.1.1 Xenografts

One approach to study tumour development *in vivo* is the implant of immortalised cell lines into severe combined immunodeficient (SCID) mice thereby creating a xenograft model. Implantation can be made either subcutaneously or orthotopically onto the pancreas, after which tumour cells are capable of synthetizing and recruiting their own stroma [169]. Xenografts therefore have some predictive value while showing more genetic and stromal diversity than cells grown in monolayers [170,171]. However, one of the main limitations of cell line xenografts is their limited ability of predicting clinical outcomes to therapeutic interventions. Because of the immunocompromised nature of SCID mice, the tumours often develop free from selective pressures and immune cell infiltrates normally present in PDAC [172]. This makes them less useful compared to other models in the context of tumour evolution or immunotherapies. Lastly, cell-line xenografts are limited by the availability and

heterogeneity of established cell lines and therefore fail to represent the high phenotypic and genetic heterogeneity observed in patients [172]. These shortcomings are highlighted in studies that have assessed the predictive value of xenografts and their associated clinical outcome [171]. An assessment by the NCI showed that over several decades, there was very little correlation between data obtained from xenografts and their clinical efficacy [171]. Examples include the EGFR inhibitor centuximab, providing 85% regression in xenografts [173], which then failed in phase III clinical trials [174], similarly to endostatin [175], or thiazolidinediones [176].

Patient-derived xenografts (PDX) address some of these limitations by transplanting directly a piece of human tumour tissue after resection or expanded primary cells into mice [172]. Resected tumours advantageously carry surrounding stroma and ECM which are maintained after transplantation. Hence, PDXs retain morphological, genetical composition and metastatic potential of the original tumour [177]. Importantly, PDXs can better replicate responses observed in the clinic compared to cell-line xenografts, possibly owing to their increased stromal content [177,178]. Their transcriptomics analysis can predict sensitivity to anticancer drugs opening up the possibility of personalised medicine [179]. Amongst the main drawbacks of these models is the difficulty of establishment and engraftment, which also negatively correlates with patient survival probably owning to the inherent aggressiveness of the tumour. PDX establishment can take up to 6 months [180], longer, in many cases, than the median patient survival after diagnosis, which limits its applications as a personalised diagnostic tool. The other limiting factor is the availability and size of tissue that can be devoted to research, as well as the very small proportion of patients that can undergo surgical resection in the first place (Figure 1.1) [181]. Lastly, although better than cell line xenografts, PDXs still do not fully replicate the stromal, morphological and immunological landscape of the host [172].

1.4.1.2 Genetically engineered mouse models

Genetically engineered mouse models (GEMM) are created via the introduction of specific genetic mutations in order to recapitulate the genetic landscape of human PDAC. This was first achieved with the activation of *KRAS* in the murine pancreas, which led to PanIN ductal lesions capable of evolving into PDAC [182]. However, the most popular and characterised GEMM in PDAC research is the KPC mouse, with an activating oncogenic mutation in *KRAS*, mutation in the tumour suppressor *Trp53*, driven by a pancreas specific (Pdx1) Cre (Pdx-1 Cre, LSL-$Kras^{G12D/+}$, LSL-$Trp53^{R172H/+}$) [183]. This model is able to recapitulate many features of human disease including tumour evolution and genetic landscape. Additionally, GEMMs also exhibit the same symptoms that define the human disease, such as loss of

weight and appetite (cachexia), and eventually, pain [184]. KPC mice retain the dense tumour stroma that is responsible for decreased anticancer drug delivery [44,45,58] and resistance to therapeutic treatment, as seen in humans [185]. GEMMs have also increased our understanding of the dual restraining and tumorigenic role of the tumour stroma [48,49] and of mechanics of the TME during PDAC progression [17,128]. Moreover, they retain an immune system, making them the only murine model in which to begin to investigate immunotherapeutic treatments.

While GEMMs and KPC models represented fundamental innovations for pre-clinical PDAC research, their main disadvantage resides in that they are time consuming and very expensive [169]. Additionally, significant genetic differences between mice and humans can lead to the formation of mutations not seen in human PDAC, as well as higher occurrence of unwanted mutations (such as BRCA1 which, in mice, is on the same chromosome as p53) [186]. This was exemplified with the clinical failure of the hedgehog pathway inhibitors, which had initially given promising results in KPC [185]. In order to overcome these drawbacks, a plethora of 3D cell culture approaches and substrates have emerged in recent years, in an attempt to make tumour modelling, drug discovery and testing, faster, more accessible and controllable.

1.4.2 *In vitro* models of PDAC

Traditional cell culture has been based on the ability to grow, expand and passage cells by seeding them on glass or plastic surfaces. Despite advances in the production of suitable tissue-culture plastic substrates and media, traditional cell culture in monolayers fails to recapitulate key elements of the TME, leading to poorly translatable results [187] and limited potential as personalised medicine tools [188]. An obvious limitation is the lack of multicellularity and immunity, which are pivotal elements for the assessment of therapeutic efficiency. Another key element is the inherent stiffness of plastic/glass surfaces, which have a Young's modulus in the region of 3 GPa (or 3 x 10^6 kPa), incredibly higher than the recorded stiffness of PDAC tissues (100 Pa to 10 kPa) [130]. Reduced cell-to-cell contact, induced apicobasal polarity, lack of multiple cell types, reduced matrix deposition, lack of diffusion gradients and hypoxia are among other factors responsible for an increased sensitivity to drugs and reduced translation potential [189]. Importantly, because of all the above reasons, 2D culture favours the propagation of immortalised and established cell lines, whereas the culture of primary human PDAC cells still remains challenging [190]. Efforts to narrow the gap between *in vitro* drug testing and clinical outcomes has prompted the development of a number of 3D approaches, whereby the combined use of tumour and

stromal components with a matrix or scaffold has allowed researchers to begin to understand and recapitulate the TME [191]. These *in vitro* TME models allow the incorporation of multiple cell types, cell-matrix interactions, stiffness modulation, formation of morphological and functional structures, overcoming some of the limitations imposed by 2D cultures and beginning to reflect patient heterogeneity and clinical responses [139,192-194]. These will be discussed in more detail in the following sections.

1.4.2.1 Spheroids

A recent review from our group screened publications related to 3D culture methods for PDAC research [195]. From this, spheroids emerged as the most popular 3D method, accounting for 42% of publications regarding 3D cell culture of PDAC, followed by organoids (33%), scaffolds (16%) and microfluidics (9%) in 2019 [195]. Spheroids represent the oldest form of *in vitro* 3D culture, dating back as far as 1906 with the invention of the hanging-drop technique [196]. They are also one of the simplest techniques, as spheroid formation only involves either the plating of cells in ultra-low attachment plates or the use of the hanging-drop technique, whereby the lack of direct contact between cells and a surface allows them to form multicellular aggregates [193]. Because of their 3D architecture and limited oxygen diffusion, the core of the spheroid can become hypoxic and resistant to treatment, providing a significant improvement from 2D cultures for drug testing [197]. This model allows the inclusion of multiple cell types, such as PDAC cells and CAFs, leading to the formation of a desmoplastic-like stroma, tumour-like architecture and cell morphology [193]. However, the lack of ECM limits the cell seeding numbers, passaging and length for which these cultures can be kept [193]. Lastly, as a high proportion of seeded cells die due to anoikis, there is a strong clonal selection which prevents an accurate recreation of the PDAC TME and associated treatment responses. This has led to the development of a number of different biomaterials, matrices and substrates that allow the incorporation of cells while mimicking the tumour architecture more closely (Table 1.1).

1.4.2.2 Explants and decellularised tissue platforms

The direct use of tissues after resection (explants), taken as whole tissue or slices, provides the most faithful representation of local tissue architecture, ECM and cellular composition. These can be used for the subsequent seeding of additional cancer cells, perfused with autochthonous patient serum, and used for the assessment of personalised treatment response [198]. However, in the majority of cases, specialised imaging is required and is the only readout technique [198,199].

Table 1.1 Comparison of selected biomaterials for the 3D cell culture of PDAC cells and pancreatic TME modelling, with associated studies.

Abbreviations: iPSC= induced Pluripotent Stem Cells, PSC= pancreatic stellate cell, RGD= Arginine, Glycine and Aspartate binding motif, MSC= Mesenchymal Stem Cells, HUVECs= Human Umbilical Vein Endothelial Cells.

Matrix	TME elements recapitulated	Cells	Advantages	Disadvantages	References
Tissues					
Explants	Cellular and extracellular structures and composition	PANC-1, AsPC-1, Capan-1	Personalised medicine uses, authentic cellular and ECM arrangement and function	Short lived, hard to maintain *ex vivo*, limited tissue availability, loss of function *ex vivo*, low reproducibility	[198,199]
Decellularised tissues	ECM structure and composition	Human induced pluripotent stem cells (iPSC)-derived organoids	Conserved ECM topography, composition, and biochemical cues	Partial matrix and structure loss during decellularisation, lack of complex cellular structures	[200]
Natural materials					
Matrigel	3D pancreatic organoid structures and basic stroma composition (CAFs)	Murine tumour-derived cells and CAFs	Matrix supports cell differentiation and 3D organoid formation, allows interaction with stromal cells, implantable	Undefined composition, batch-to-batch variability, murine origins, limited stiffness range, no limited shape control	[201,202]
Collagen	Main ECM constituent, predominant in PDAC, fibrillar structure, biochemical cues	BxPC-3, PANC-1, MIA PaCa-2,	Clinical and physiological relevance of collagen, lower batch variation than Matrigel, implantable	Murine origins, requires chemical crosslinking, limited stiffness range, induction of multiple cancer pathways	[131,144,203,204]
Hyaluronan	Hyaluronic acid structure and crosslinking, inclusion of stromal cells	MIA PaCa-2, PANC-1, AsPC-1, FC1245, murine PSCs and human CAFs	Hyaluronan plays an important role in PDAC treatment response, clinically relevant, wide range of sizes and chemical modifications	Requires adhesive ligands (such as RGDs) for cell adhesion, limited stiffness range	[205,206]
Fibrin	3D network and architectural support	PDX-derived PDAC organoids	On demand gelation and degradation via thrombin, controlled crosslinking with no added chemicals	Not a major component of the PDAC TME, limited stiffness range	[207]
Alginate	3D network and architectural support	PDX-derived PDAC organoids	Two step cell encapsulation and easy cell recovery, can be mixed with other hydrogels	Not a component of the PDAC TME, requires adhesive ligands (such as RGDs) for cell adhesion, limited stiffness range	[207]

Semi-synthetic materials					
Gelatin (methacrylated)	Porous structure, biochemical cues, tunable stiffness, inclusion of stromal cells	BxPC-3, Capan-2, MIA PaCa-2, PANC-1, patient-derived CAFs, monocytes	Allows cell attachment, MMP-cleavable, controllable mechanics (wide range), suitable for bioprinting, relevant component of the TME, transparent, high shape control, implantable	Requires photo-polymerisation (UV or visible light)	Peerani et al. (*in preparation*)
Hyaluronan (methacrylated)	Fibrillar 3D structure, biochemical cues	COLO-357, Human MSCs	Clinically relevant, biodegradable, easy crosslinking, improved mechanical properties	Reduced bioactivity, requires radical photo-polymerisation	[208,209]
Self-assembling peptides	Inclusion of stromal cells, can incorporate ECM molecules	Primary PDAC cells, PSCs, macrophages	Controllable cell encapsulation, bioactivity, can be gelled in solutions containing ECM components	Limited shape control, costly, limited scalability, limited stiffness control	Osuna de la Peña et al. (*in preparation*)
Synthetic materials					
Poly(ethylene glycol) (PEG)	Porous 3D structure	COLO-357, PANC-1	Direct inclusion of cell adhesion ligands (e.g. RGD), wide stiffness range, transparent, controllable size/shape, implantable, high reproducibility	Non-degradable backbone with little bioactivity, mainly inert	[210-212]
Poly(ethylene glycol) diacrylate (PEGDA)	Porous 3D structure	MIA PaCa-2	Direct inclusion of cell adhesion ligands (e.g. RGD), wide stiffness range, transparent, controllable size/shape	Inert, generally very stiff for biological applications and brittle	[213]
Poly(lactic-co-glycolic acid) (PLGA)	Porous 3D structure	PANC-1	Biodegradable, transparent, controllable size/shape, implantable, can be used as drug eluting compound	Direct degradation limits its applications, increased hydrophobicity	[214]
Polycaprolactone (PCL)	Supporting biomaterial, drug delivery	No PDAC studies to date	Can enable controlled drug release, biocompatible, implantable, suitable for bioprinting	Limited cell adhesion, inert	[215,216]
Polyacrylamide (PAM)	Controllable stiffness	AsPC-1, BxPC-3, Suit2-007	Allows spatial patterning and multiple ligand conjugation, wide stiffness range, high reproducibility	No biological cues, inert	[128]
Polydimethylsiloxane (PDMS)	Resistant, supporting structure	AsPC-1, Capan-2, MIA PaCa-2, PANC-1, PDX-derived cells	Used for microfluidics design, can be micropatterned to achieve defined shapes, direct cell migration, adhesion, function and control fluid flow.	2-dimensional, stiff substrate, no biological function, prevents cell attachment	[217,218]
Hybrid approaches					
Microfluidics (various hydrogel compositions)	Inclusion of stroma, flow (perfusion) and blood vessels	AsPC-3, BxPC-3, MIA PaCa-2, PANC-1, patient-derived PSCs, CAFs, HUVECs	Incorporation of multiple cell types interacting physiologically, possible cell separation for subsequent analyses, formation of complex vascular and ECM networks	Hard to assess contribution of individual cell components, limited scalability, require longer culture time	[192,219-222]

Once resected, tissues are prone to quick degradation and necrosis, which temporally limits the use of these explants as well as requiring culture condition optimisation. Each section or tumour piece will only provide a local snapshot, which might not be representative of the tumour behaviour as a bulk. Additionally, the scarcity of patients which undergo surgery, the limited availability of tissue, and its short-lived nature (hours to few days) make this model low throughput and poorly scalable [199].

In the context of cancer, decellularised tissue platforms are resected tumours which undergo several detergent washes in order to remove all original cellular components, while maintaining an intact ECM composition [223] and architecture. Decellularisation of pancreatic tissues has been reported in a number of organs from human [224], rat [200] and porcine [225] origin. Because of the lack of cellular components, these platforms can usually be kept for longer than tissue explants [199]and allow the response of individual cell types to matrix stimuli. Despite recent improvements, it is still unclear whether the decellularisation process at all affects the ECM structure, composition, biomechanics or function. Additionally, in order to be used as a 3D model, cells are often seeded on top of the tissue, resulting in a rather two-dimensional model unless significant invasion and remodelling occur. Interestingly, a few groups have lyophilised tissues after decellularization and subsequently hydrated them to form hydrogels, whose composition retained the same molecules present in native ECMs, while giving them more controllable and modular hydrogel properties [223,224].

1.4.2.3 Hydrogels

Because of their rheology, similar to that of human tissues, hydrogels are the most common formulation of both natural and synthetic biomaterials for 3D cell culture. Culture methods that allow the growth of single cells or the prolonged culture of spheroids with physiological stiffness are crucial in modelling cancer initiation, functions and treatment response. Matrigel is the most widespread gelling biomaterial for 3D cell and organoid culture. It consists of a mixture of basement membrane proteins derived from Engelbreth-Holm-Swarm murine sarcoma, with the ability of forming a gelling phase above 10°C [201]. When cultured in Matrigel and the appropriate supplements, cells with stem-like properties can differentiate and proliferate to form structures reminiscent of their tissue of origin, named organoids [207,223]. Organoids have traditionally been used to study human development, they have however, huge potential in the study of disease, TME modelling and pre-clinical drug screening [226,227]. Despite this, the murine origins of Matrigel, batch-to-bath variation, and low stiffness

constitute the main drawbacks of its use in truly recapitulating biochemical and physical aspects of the TME [226].

Collagen type I hydrogels are the main alternative to Matrigel, due to the high collagen content in both healthy and diseased tissues, especially in highly desmoplastic cancers such as PDAC [95]. Commercially available collagen is usually of bovine or rodent origin (cowhide or rat tail), and provided at much lower concentrations than Matrigel. To ensure stability at 37°C and hydrogel formation, collagen requires chemical crosslinking, thanks to which collagen gels have a wider stiffness range and better tunability compared to Matrigel [228]. This has allowed the investigation of morphological and EMT phenotypes of PDAC cells in matrices with different stiffness [203]. In addition, rat tail collagen forms disorganised fibrillar structures reminiscent of those formed in vivo [228]. Another key advantage of collagen gels is the retention of MMP-cleavable sequences, which make the study of cell migration and invasion possible. This prompted a number of different studies and the discovery of MT1-MMP as mediator of PDAC cell invasion and chemo-resistance [131,144,204]. Nevertheless, the biomechanical properties of collagen gels are still limited compared to physiological conditions and so is their tuneability [228].

Alternative biomaterials with natural origins include hyaluronic acid, fibrin, alginate, dextran and chitosan-based hydrogels. The main limitations of these hydrogels are the lack of cell adhesion motifs, the lack of physiological relevance to the PDAC TME, and their poor mechanical tunability [228]. For this reason, important components of the TME, such as HA, have been chemically crosslinked to either synthetic, or semi-synthetic biomaterials in order to provide more stable and controllable networks for long term studies [228]. Semi-synthetic hydrogels combine both a naturally derived elements (such as gelatin, collagen, hyaluronic acid) and a chemical modification to increase the resulting hydrogel's crosslinking, stiffness, and stability. Examples include gelatin methacryloyl (GelMA) [229], thiolated gelatin-HA [209], or poly(ethylene glycol) diacrylate-HA (PEGDA-HA) [213] which have improved mechanical properties compared to their unfunctionalized counterparts, while retaining cell adhesion and cleavable motifs. Lastly, hydrogels can be derived from synthetic biomaterials including poly(ethylene glycol) (PEG), PEGDA, poly(lactic-co-glycolic acid) (PLGA), polycaprolactone (PCL) and polyacrylamide to name a few, most of which have been used for the 3D culture of PDAC cells (Table 1.1). Because of their intrinsic inertness, PEG and its derivatives grant no cell attachment or cell-mediated matrix cleavage. However, this can be easily solved via the addition of custom functional groups such as RGD (Arginine,

Glycine, and Aspartate cell binding motifs) or the on-demand incorporation of multiple ECM molecules [210,212]. Finally, synthetic and semi-synthetic biomaterials can achieve a much greater range of stiffness and viscosity compared to naturally-derived hydrogels, hence opening the possibility for bioprinting of 3D structures [230-233].

1.4.2.4 Microfluidic devices

Also known as 'organ-on-a-chip', microfluidic devices aim to recapitulate complex 3D microenvironments on a synthetic chip, with the addition of perfused microchannels which allow the flow of nutrients, cells or therapeutics, mimicking the human circulatory system. This perfusion system can allow continuous supply of nutrients and oxygen as well as the removal of waste and side products from the culture [192]. The main limitations of these devices are that they require high initial optimisation, long-term culture, and their endpoint analysis is usually restricted to imaging. Because of this, microfluidic devices currently remain quite expensive and poorly scalable. In PDAC research, the majority of microfluidic devices have been created through soft lithography of PDMS (Table 1.1), and loaded with cancer cells, CAFs, or HUVECs, usually encapsulated in either collagen type I, HA or Matrigel hydrogels [192,220,221]. Importantly, cells in the devices showed an ability to remodel the ECM [192], and higher resistance to chemotherapeutics compared to traditional spheroid cultures [219]. Porous PDMS membranes have also been used for the separation of different cell types within the device, while allowing cell migration and vasculature-like network development using endothelial cells [194,220]. The use of such complex 3D systems holds great promise in the field of PDAC research as they allow the progressive addition and modulation of a number of TME parameters including cell types and numbers, matrix substrate, vascularisation and mechanics.

1.5 GelMA hydrogels as a 3D cell culture platform

Hydrogels are a network of hydrophilic polymers that crosslink and swell in water (hydro) thereby capturing many times their original weight [234]. Physicochemical properties of hydrogels depend on a number of factors including their polymer composition, method used for crosslinking, polymerisation process, and concentration. Because of this versatility, they can provide different combinations of properties for any intended use and application [228]. For the purpose of cancer modelling, hydrogels based on naturally occurring biopolymers are preferred, as they are biocompatible, have low immunogenicity and can retain cell-responsive motifs. Contrariwise, synthetic materials provide a great deal of tuneability in terms of their mechanical, physical and structural properties, with virtually no batch-to-batch variation but they lack cell-instructive features [235]. In this project, I employed a semi-synthetic hydrogel named gelatin methacryloyl (GelMA). GelMA combines the advantages of natural biomaterials thanks to its gelatinous derivation as well as the chemically active functionalisation groups (methacrylamide and methacrylate groups) that confer the hydrogel's reproducible and controllable physicochemical properties. Once synthesised, the GelMA polymer undergoes radical photo-polymerisation to form a crosslinked hydrogel, a reaction which requires high wavelength UV light exposure in the presence of a photoinitiator (Figure 1.6 a). GelMA is also referred to as gelatin methacrylate, methacrylated gelatin, methacrylamide modified gelatin, or gelatin methacrylamide in the literature by different groups (Figure 1.6 b). Since its first characterisation in 2000 by Van Den Bulke and colleagues [236], the use of GelMA has rapidly increased in popularity as a tissue engineering biomaterial and, more recently, as a cancer model platform (Figure 1.6 b).

1.5.1 Biophysical properties of GelMA

1.5.1.1 Composition and bioactivity

Gelatin is comprised of partially hydrolysed collagen, mainly type I, and as such is the most abundant protein in the human body [237]. Because of its partially denatured composition, gelatin has a higher solubility and much lower batch-to-batch structural variations compared to commercial collagen [238]. In fact, gelatin is neither immunogenic nor antigenic [239,240], making GelMA a suitable platform for the inclusion of immune cells. Importantly, the retention of collagen binding sites as well as cell attachment RGD sequences [241] make it an ideal matrix for the study of tumour-ECM interactions in a collagen-rich tumour such as PDAC or

ovarian cancer. Because of these inherent structural and functional similarities to GelMA, collagen type I gels have been used as a control matrix throughout this study.

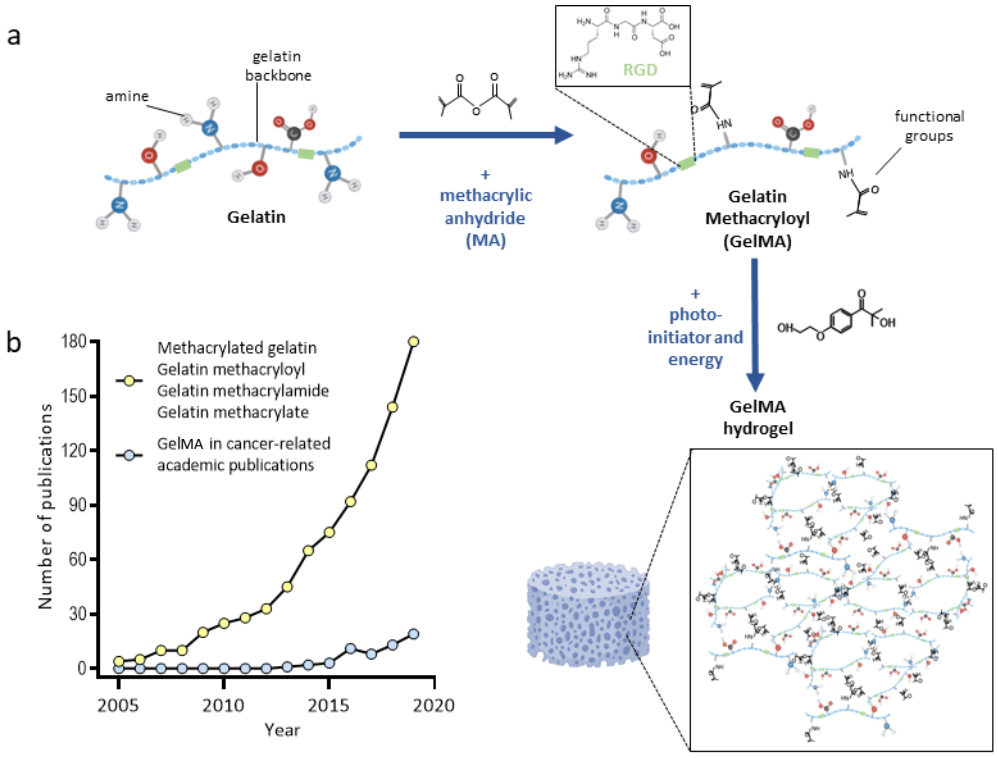

Figure 1.6 Gelatin methacryloyl (GelMA) hydrogels synthesis and prevalence in peer-reviewed academic publications. a) Gelatin reacts with methacrylic anhydride (MA) forming gelatin functionalised with methacryloyl functional groups (GelMA). This substitution occurs on primary amines, therefore the RGD domains (green segments), along the gelatin backbone, are retained. Next, free radicals are generated by the addition of the photo-initiator, initiating polymerisation of the methacryloyl functional groups, and resulting in a crosslinked hydrogel. **b)** Number of academic GelMA-related publications, by year. The increasing popularity of this semi-synthetic biomaterial is accompanied by the growing number of relevant publications each year. GelMA hydrogels have only recently been used for biomedical applications in cancer (2014 onwards), underlying the novelty of this model. To my knowledge, no publications have yet used GelMA for pancreatic cancer research. Search terms: gelatin methacrylate, gelatin methacryloyl, gelatin methacrylamide, or methacrylated gelatin, as used by different research groups to refer to GelMA. Data obtained on www.scopus.com by screening terms in publications' titles, abstracts and keywords as of June 2020. RGD= RGD= Arginine, Glycine and Aspartate binding motif.

In solution, gelatin has the ability to form crosslinked hydrogels at low temperatures [236]. With the introduction of methacryloyl groups (MA) onto the gelatin (Gel) amino acids, gelatin solutions can crosslink in a controllable manner with the assistance of a photoinitiator and exposure to light, through the photo-polymerisation of the functional side groups [236]. This allows the operator to control the temporal aspect of the reaction as well as parameters including neutral pH, room temperature and concentration, without compromising the stability of the crosslinked product [229]. These adjustments make GelMA hydrogels particularly suitable as a cell culture model, as they allow the fine-tuning of different synthesis parameters to match the requirements of various cell types. Owing to its stability, GelMA can be moulded and micropatterned in a variety of shapes, sizes and volumes to suit the

intended application. Additionally, its transparency allows for easy imaging of 3D structures, even by simple brightfield microscopy. More recently, groups have begun to optimise conditions for GelMA hydrogel's applications in 3D bioprinting [238].

Generally, less than 5% wt/wt of the gelatin amino acid residues will be modified by MA during GelMA synthesis [236]. This implies that the majority (>95%) of the functional amino acid residues present on the gelatin backbone (including RGD motifs and MMP-cleavable sites) will be retained in the resulting GelMA hydrogel. Moreover, the RGD motifs do not contain amine groups capable of reacting with MA, therefore they are unaffected during GelMA synthesis, granting good cell adhesive properties in these hydrogels [241-243] (Figure 1.6 a). Additionally, the enzymatic degradation of GelMA hydrogels *in vitro* by collagenases (type I and type II, or MMP1 and MMP8) is significantly faster compared to other enzymatic approaches, underlining the retention of MMP-sensitive sites in crosslinked GelMA hydrogels [244,245]. This will be discussed further in Chapter 4.

1.5.1.2 Stiffness and porosity

A number of different parameters allow tuning of the physical properties of GelMA hydrogels. Firstly, the degree of functionalisation (DoF) or amount of MA substitutions onto the gelatin amine groups, can determine the amount of crosslinking, and hence stiffness, of the resulting hydrogels [242,246]. In this regard, reports have shown that the compressive modulus (E, kPa), or stiffness of GelMA, is directly proportional to its DoF (2.0 ± 0.18 KPa (for low DoF), 3.2 ± 0.18 KPa (medium DoF), and 4.5 ± 0.33 KPa (high DoF) [246]. In order to ensure reproducibility, all the batches utilised in this study were synthetized with similar, high, DoFs. The concentration and nature of the photoinitiator, the UV exposure time and its wavelength, are among the other parameters that allow simple and precise tuning of the physical properties of GelMA hydrogels [229]. For instance, longer UV exposure, shorter UV wavelength or higher photoinitiator concentration, all result in hydrogels with a higher compressive modulus, E. Once again, these parameters were optimised and then left unchanged for the duration of this study in order to return comparable and reproducible results. E is also directly proportional to the initial concentration (% wt/vol) of GelMA polymer. For instance, reports have found E values of 2, 10 and 20 kPa for 5, 10, 15% wt/vol GelMA respectively (with an unchanged medium DoF) [242]. This simple adjustment allows to achieve hydrogels of equal composition and different stiffness, which will be employed throughout this study. The range of stiffness achieved with these semi-synthetic hydrogels (1-30 kPa) is much higher than that achievable with un-functionalised natural gelatin or

collagen, and therefore represent a good strategy for the investigation of stiffness-associated processes and modelling of physiological human tissue rigidities.

The porosity of a material also dictates the ability of cells to adhere, migrate, proliferate and invade into a matrix. Once again, GelMA's DoF or its storage (i.e. freeze-dried) can be altered to achieve hydrogels with controlled porosity [246]. For instance, a simple change in GelMA DoF (low, medium, high) resulted in GelMA hydrogels with decreasing pore sizes (50, 30 and 25 μm respectively) [246]. Biomaterials with a pore size of 25-35 μm are conducive of cell proliferation and migration, to be favoured for cell culture applications [246,247].

1.5.1.3 Cell culture in GelMA

Migration, viability and proliferation of different cell lines within GelMA hydrogels have been widely studied and extensively described [229]. Cells can be suspended in the GelMA aqueous solution prior to crosslinking in order to form cell-laden 3D hydrogels (Figure 2.1). Pioneering studies successfully implemented GelMA hydrogels as 2D and 3D cell culture systems [248], with high viability [229,235], thanks to their high biocompatibility, bioactivity through cell-responsive motifs and controllable biomechanics. Evidence of cell matrix remodelling, migration and spreading within the hydrogels has also been extensively reported [232,242,249]. Although its first characterisation dates back to over 20 years ago [236], GelMA's implementation as a 3D cell culture system dates back to the early 2010s and was predominantly confined to the field of tissue engineering and regenerative medicine [230,231,238,250,251]. A few groups have now employed GelMA in the field of cancer research, including studies on ovarian [235,252], glioblastoma [253,254], breast [255,256], prostate [257,258] and colon cancer (Loessner, Ryan, unpublished). Thus far, there have been no reported uses of GelMA for the culture of PDAC cells.

1.6 Project hypothesis and aims

The purpose of this work is to exploit the tuneability of gelatin methacryloyl (GelMA) hydrogels as a pre-clinical model of PDAC in order to investigate the effects of different tumour microenvironment components and its biomechanics. The present body of work aims to characterise the biomechanics of human tissues in order to recapitulate tissue dynamics, and to establish a hydrogel-based model system in which stiffness can be controlled, measured, and predicted. In an effort to mimic physiological conditions, multiple cell types including cancer, stromal and immune cells, will be incorporated in the model, and their behavioural and molecular profiles will be assessed. Wherever possible, patient-derived cells will be employed in order to strengthen the translational and clinical relevance of the model. The characterisation and validation of such platform requires an interdisciplinary approach whereby the material sciences and engineering hydrogel design considerations meet the functional, molecular and -omics analyses of the cultured cells. Additionally, findings will be benchmarked and compared against another popular 3D cell culture system, namely collagen type I gels. I hypothesise that this GelMA-based model will not only allow the investigation of stiffness-related cell behaviours and gene signatures, but also allow the investigation of stromal and biomechanics-targeting combination therapy regimes, in the attempt to bridge the gap between laboratory and clinical efficacy (Figure 1.7).

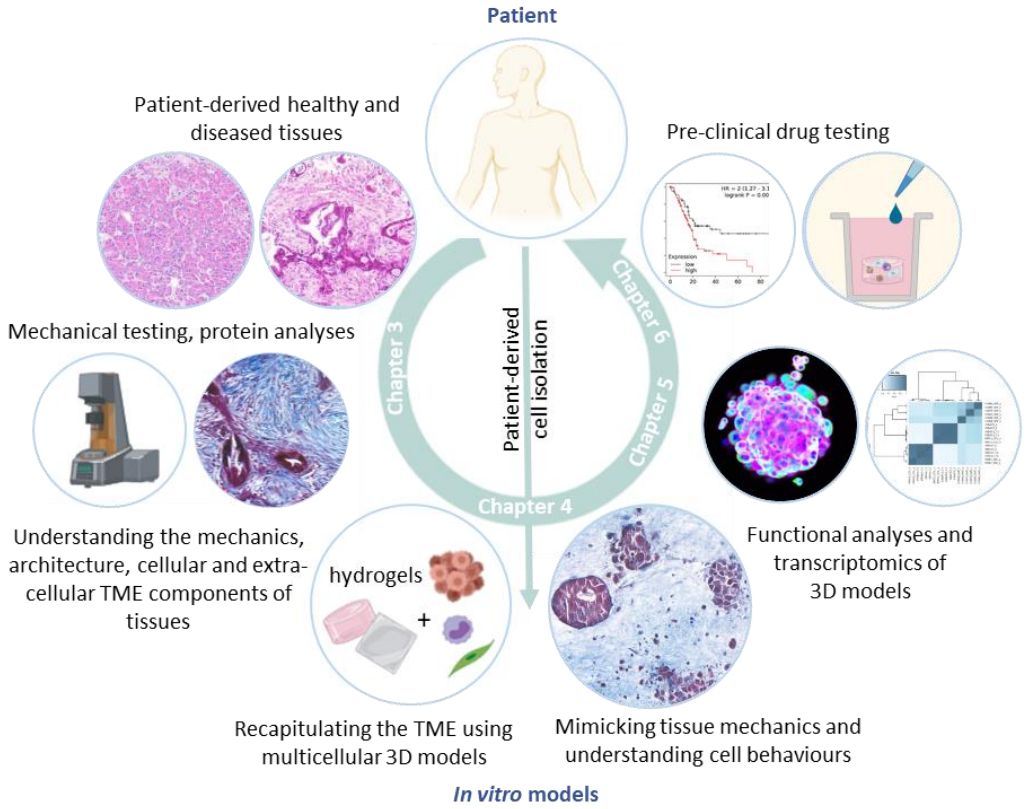

Figure 1.7 Schematic outline of thesis rationale and workflow.

The overarching hypothesis of the presented work will be investigated with the following proposed aims:

1. Describe differences in stiffness between tumour-bearing and tumour-naïve tissues and assess direct correlations with matrix production, in order to recapitulate physiological tissue properties using GelMA hydrogels and collagen type I controls.
2. Characterise GelMA hydrogels and assess their potential as a 3D PDAC cell culture system, by investigating various cancer cell functions in hydrogels with different biomechanical properties. Concomitantly, increase the complexity of the model, by adding multiple cellular components of the TME, and study their effect on stiffness and *in vivo* tumorigenicity.
3. Explore the transcriptional profile of PDAC cells in GelMA hydrogels of increasing stiffness and collagen control gels, in order to uncover associations with mechanobiology and other matrix signatures.
4. Test the translational value of this 3D PDAC model by targeting pathways and processes important in the mechanobiology of PDAC.

Fresh tissues from pancreatic cancer patients were used wherever possible. Due to the limited availability of patient-derived material, ovarian cancer tissues and ascites were also used for characterisation and cell isolation as indicated in Table 2.1. The high grade serous ovarian cancer (HGSOC) cell line OvCar-4 was used as a proof of concept in the initial stages of GelMA hydrogels optimisation and treatment assessment, due to the work previously conducted by my group [229,249,252], and expertise in my Centre [123,259,260]. Similarly to PDAC, HGSOC is a peritoneal cancer characterised by poor prognosis and survival, as patients often present at a late stage, after disease spread [261]. Importantly, both PDAC and HGSOC present complex TMEs, the understanding of which may have therapeutic implications. Therefore the engineering of pre-clinical 3D cell culture platforms for both solid tumours is particularly relevant.

Chapter 2 - Materials and Methods

2.1 Patient-derived tissues and cell culture

2.1.1 Cell culture and passaging

All assays were carried out using PDAC cells BxPC-3, Capan-2, MIAPaCa-2 and PANC-1 (ATCC, CRL1687, CRL1420, CRL1469), the THP-1 (ATCC TIB202) monocytic cell line, and HGSOC cells OvCar-4 (gift from Lockley Lab) as stated in each experiment. Cells were cultured at 37°C and 5% CO_2 in high glucose Dulbecco's Modified Eagle Medium (DMEM, Gibco), supplemented with 10% foetal bovine serum (FBS) (Gibco) and 1% penicillin/streptomycin (P/S) (Thermo Fisher Scientific). Cells were passaged with either 0.5%/0.2% (v/v) trypsin/ Ethylenediaminetetraacetic acid (EDTA) (Sigma-Aldrich) or TrypLE (Thermo-Fisher Scientific) and used for a maximum of 20 passages. Cell viability was routinely checked after passaging and kept above 90%. Mycoplasma tests were conducted monthly to ensure cells were contamination-free.

2.1.2 Patient-derived tissues

Patient-derived tissues were collected through the Barts Pancreas Tissue Bank for PDAC tissues (REC: 18/SC/0630), or the Barts Gynae Tissue Bank ethics for OvCa tissues and ascites (REC: 15/EE/0151) with full written informed consent between 2017 and 2019. Tissue samples were either used for primary cell isolation and cell culture or left in Dulbecco's phosphate buffered saline (PBS) (Sigma-Aldrich at 4°C for mechanical testing (usually carried out within 24 hours from surgery). Samples from patients that had received chemo- or radiation therapy prior to surgery were labelled accordingly. 'Adjacent normal' tissue was only available from surgeries accompanying other conditions such as cancer (matched samples), or other peritoneal disorders.

Table 2.1 Patient information of OvCa and PCa specimens collected throughout the study and their use. Samples highlighted in blue were from patients who had undergone chemotherapy treatment.

Experimental group	Patient number	Anonymised ID	Received	Diagnosis	Analysis
Ascites	1	PT0634	19/07/2018	Bilateral ovarian serous borderline tumours with focal microinvasion and micropapillary proliferation.	CAF isolation for 3D cultures
	2	PT0849	26/04/2019	HGSOC, tubo-ovarian type. FIGO 4a	CAF isolation for 3D cultures
	3	PT0928	07/08/2019	HGSOC, tubo-ovarian type. FIGO 3c	CAF isolation for 3D cultures, SEM
Ovarian cancer tissue	4	PT0873	21/05/2019	Carcinosarcoma with heterologous differentiation.	Mechanical testing, H&E
HGSOC tissue	5	PT0685	19/09/2018	Interval debulking surgery; HGSOC of left tubal origin showing near total response to chemotherapy; CRS 3/3.	Mechanical testing, H&E
	6	PT0601	21/09/2018	Interval debulking surgery; right tubo-ovarian HGSOC with widespread peritoneal metastasis; CRS 2/3.	Mechanical testing, H&E
Normal ovary tissue	7	PT0674	04/09/2018	Left ovary normal.	NF isolation for 3D cultures
	8	PT0672	11/09/2018	Normal ovary.	Mechanical testing, H&E
	9	PT0677	20/09/2018	Normal ovary.	Mechanical testing, H&E
	10	PT0701	25/10/2018	Normal right ovary.	Mechanical testing, H&E
	11	PT0715	02/11/2018	Normal left ovary.	Mechanical testing, H&E
	12	PT0719	09/11/2018	Normal ovary.	Mechanical testing, H&E
Diseased omental tissue	13	SGH002	08/11/2019	HGSOC primary debulking surgery, stage 3c	CAF isolation for 3D cultures, IF
	14	G518	13/01/2020	Clear cell adenocarcinoma of the ovary, stage 1a	CAF isolation for 3D cultures
	15	G522	30/01/2020	Mucinous adenocarcinoma of the ovary, stage 1c	CAF isolation for 3D cultures

Experimental group	Patient number	Anonymised ID	Received	Diagnosis	Analysis
PDAC tissue	16	B01 P0556A AA01	04/09/2018	PDAC	CAF isolation for 3D cultures
	17	B01 PO570B AA08	18/09/2018	PDAC	CAF isolation for 3D cultures
	18	B01 P0611B AA06	26/11/2018	Pancreatic adenosquamous carcinoma	H&E, IHC
	19	B01 P0655A AA05	05/02/2019	PDAC	Mechanical testing, H&E
	20	B01 P0664B AA04	11/03/2019	PDAC	Mechanical testing, H&E, IHC
	21	B01 P0706B AA05	28/05/2019	PDAC	Mechanical testing, H&E, IHC
	22	B01 P0728A AA05	04/06/2019	PDAC	Mechanical testing, H&E, IHC
	23	B01 P0781B AA05	31/10/2019	PDAC	Mechanical testing, H&E
	24	B01 P0791B AA01	13/12/2019	PDAC	H&E, IHC
Pancreatic cancer tissue	25	B01 P0540B AA04	10/08/2018	Cholangiocarcinoma	H&E, IHC
	26	B01 P0742B AA06	23/07/2019	Ampulla adenocarcinoma	Mechanical testing, H&E
Tumour-adjacent tissue	25	B01 P0540B EE04	10/08/2018	Adjacent to diseased 'normal' tissue, matched sample	H&E, IHC
	17	B01 PO570B EE05	18/09/2018	Adjacent to diseased 'normal' tissue, matched sample	NF isolation for 3D co-culture studies
	18	B01 P0611B EE06	26/11/2018	Adjacent to diseased 'normal' tissue, matched sample	H&E, IHC
	19	B01 P0655A EE05	05/02/2019	Adjacent to diseased 'normal' tissue, matched sample	Mechanical testing, H&E
	20	B01 P0664B EE05	11/03/2019	Adjacent to diseased 'normal' tissue, matched sample	Mechanical testing, H&E, IHC
	22	B01 P0728A EE05	04/06/2019	Adjacent to diseased 'normal' tissue, matched sample	Mechanical testing, H&E, IHC
	26	B01 P0742B EE06	23/07/2019	Adjacent to diseased 'normal' tissue, matched sample	Mechanical testing, H&E
	24	B01 P0791B EE06	13/12/2019	PDAC	H&E, IHC

HGSOC=High-grade Serous Ovarian Cancer tissues; CAF=Cancer-Associated Fibroblasts; NF=Normal Fibroblasts; FIGO=International Federation of Gynaecology and Obstetrics staging; SEM= Scanning Electron Microscope; PDAC= Pancreatic Ductal Adenocarcinoma; H&E= Haematoxylin & Eosin CRS=Chemotherapy Response Score; IF=immunofluorescence

2.1.3 Patient-derived cell isolation

Normal fibroblasts (NF) and cancer-associated fibroblasts (CAFs) were isolated from normal or diseased tissues respectively. Briefly, tissue was sectioned with a sterile blade (Corning) and placed in a 50 ml tube in 0.05% Collagenase V in Roswell Park Memorial Institute (RPMI) medium. The tube was placed at 37°C/100 rpm in a Brunswick Innova 40 shaker (Eppendorf) for 1-3 hours. The tube was then centrifuged, cell were washed once in DMEM/F12 medium, and then plated in T25 cell culture flasks (Corning) in complete supplemented DMEM.

Cell composition of ascites fluid was characterised by Dr Juliana Candido via flow cytometry. CAFs were also isolated from ascites following filtering through a 70 μm mesh and centrifugation at 1500 rpm for 10 min. The resulting pellet was treated for 10 minutes with Red Blood Cell Lysis Buffer (Thermo Fisher Scientific) at room temperature (RT) and then washed in PBS. Following 5 minutes of centrifugation, cells were resuspended in 20% FBS/DMEM and plated in T75 cell culture flasks at 0.3 x 10^6 cells/ml.

Following isolation, fibroblast's phenotype was characterised via flow cytometry (FC) and immunofluorescence (IF) as indicated in the above Table 2.1. Patient-derived NF or CAFs were initially incorporated in collagen and GelMA hydrogels, for 14 days of culture in a 2:1, 4:1 and 1:4 ratio (cancer cells : CAFs) and a final cell density of 3.5 x 10^5 cells/ml. For triple culture and indirect co-culture experiments (see section *In vitro* treatment studies), cells were incorporated in either a 2:2:1 or 1:2:2 ratio (cancer cells : THP-1 : CAFs).

2.2 Hydrogel synthesis, characterisation and 3D cell culture

2.2.1 GelMA hydrogel synthesis and storage

GelMA batch synthesis was performed by Dr Daniela Loessner, Dr Juliana Candido and Dr Laura Lecker as previously described [229]. The resulting liquid was freeze-dried in a Labconco 4.5 Plus benchtop freeze-drier (Labconco) over 4-5 days under sterile conditions. Lyophilisation yielded a fluffy white foam, which was kept at -80 °C to -20°C for long-term storage.

2.2.2 Characterisation of GelMA functionalisation

2.2.2.1 TNBS Assay

The TNBS assay was used to quantify the amount of free amino groups on the gelatine backbone (qualitative measurement of amines, sulfhydryls, hydrazides and quantitative measurement of ε-amino groups). A high degree of gelatine functionalisation (GelMA with high degree of functionalisation) would result in a low amount of free amino groups. TNBS (also known as Picrylsulfonic acid) is used in this assay as it reacts with primary amines or hydrazine groups to give an orange-coloured derivate, quantifiable via an absorbance measurement.

For this, GelMA foam and un-functionalised gelatin (Sigma-Aldrich) were dissolved in 0.1 M sodium bicarbonate (Sigma-Aldrich) at 500 µg/ml concentration. A standard dilution of GelMA and gelatine ranging from 0 to 500 µg/ml was prepared and pipetted in a 96-well plate (Costar). 0.01% TNBS/0.1 M sodium bicarbonate was added in a 1:2 ratio onto each well (final volume 255 µl) and incubated for 5 minutes at RT and subsequently for 2 hours at 37°C in the dark. The absorbance of the samples at 335nm was read on a BMG Labtech FLUOstar Optima Microplate reader (Labtech) against the serial dilution of gelatin. To calculate the degree of functionalisation (DoF), regression lines were calculated for each GelMA batch m_{GelMA} and compared to the gelatine solution regression line m using the equation:

$$DoF = \left(1 - \frac{m_{GelMA}}{m}\right) 100$$

2.2.2.2 Ninhydrin Assay

Gelatin and GelMA foam were dissolved at a 35 mg/ml concentration in MilliQ water (Merck-Millipore) and warmed up to 40ºC - 50ºC until fully dissolved. Different dilutions of the gelatin solution (0-80%) were prepared in MilliQ water (Merck-Millipore) to obtain a standard curve. A 0.5 M citric acid (Sigma-Aldrich) solution was prepared, adjusted to pH 5.5 and then added to two parts of glycerol (Sigma-Aldrich) in a 1:2 ratio. Ninhydrin (2,2-dihydroxyindane-1,3-dione) (Sigma-Aldrich) was then added to the citric acid/glycerol solution at a 2.5 mg/ml concentration. 50 µl of GelMA or gelatine standard were added to an Eppendorf tube in duplicates, following which, 0.950 ml of ninhydrin solution were added. 50 µl of water were used as blanks. The Eppendorf tubes were then placed in a boiling water bath (Grant Instruments), protected from light for 13 minutes and then left to cool at RT for 1 hour. Ninhydrin reacts with free primary and secondary amine groups to produce a purple colour solution. Next, 250 µl of sample were pipetted from each Eppendorf in triplicates into a 96-well plate (Costar) and absorbance was read at 570 nm emission on a BMG Labtech FLUOstar Optima Microplate reader (Labtech). The degree of functionalisation was calculated by finding the gradient of the gelatine solution regression line m and the average absorbance of the sample $\bar{A}$ and using the equation:

$$DoF = \left(1 - \frac{\bar{A}}{m}\right)100$$

2.2.2.3 Fluoraldehyde Assay

Fluoraldehyde (Thermo Scientific) can be used for the detection of primary amines as its active compound, o-phthalaldehyde, becomes fluorescent linearly with the presence of the latter. For this, GelMA foam was dissolved at 0.5 mg/ml alongside gelatine (1 mg/ml) in PBS (Thermo Fisher) at 37 ºC until fully dissolved. A serial dilution of gelatine ranging from 0.02 to 1 mg/ml was prepared in PBS (Thermo Fisher). Next, 500 µl of GelMA or gelatine serial dilutions were mixed in a 1:1 ratio with fluoraldehyde (Thermo Fisher). Fluorescence was measured with emission 450 nm and excitation wavelength of 360 nm using a BMG Labtech FLUOstar Omega Microplate reader (Labtech). The degree of functionalisation was calculated by finding the gradient of the gelatine regression line m and the average absorbance of the sample $\bar{A}$ with the following equation:

$$DoF = \left(\left(0.5 - \frac{\bar{A}}{m}\right)/0.5\right)100$$

2.2.2.4 Nuclear Magnetic Resonance (NMR)

Proton nuclear magnetic resonance (^{1}H NMR) was also used to measure the degree of methacrylic anhydride (MA) onto the gelatin backbone, by comparing the NMR spectra of gelatin to the one of functionalised gelatin (GelMA). ^{1}H NMR was performed by Andrew McCormack at the Heriot-Watt University in Edinburgh. Briefly, GelMA samples and gelatin were separately dissolved at around 50 mg/mL in deuterium oxide, and the chemical shift of each sample was measured [242,262]. This method looks at the lysine methylene proton existing on the carbon atom that joins the amino group (which then gets functionalised with methacrylic anhydride, MA). This proton gives a peak around 3 parts per million (ppm). This peak was highest on gelatin NMR spectra and decreased in GelMA congruently with MA addition, indicating the amino groups were now connected to methacryloyl groups. Annotating the spectra allows to quantify the area under each NMR peak (λ), which can be used to calculate the degree of functionalisation. The DoF can be calculated as follows:

$$DoF = \left[1 - \left(\frac{\lambda\ of\ lysine\ methylene\ proton\ of\ GelMA}{\lambda\ of\ lysisne\ methylene\ proton\ of\ gelatin}\right)\right] \times 100\%$$

To help normalise the intensities of signals between runs, the λ of aromatic moieties in each spectra was made constant ≃100, as this peak doesn't change during the reaction, and can therefore be used for calibration.

2.2.3 GelMA 3D cell culture

GelMA hydrogels were prepared by dissolving dried GelMA foam in PBS at 3%, 5%, 7.5% or 10% wt/vol for 1 hour at 37°C. A 10 mg/ml stock of photo-initiator was prepared by dissolving 2-Hydroxy-4'-(2-hydroxyethoxy)-2-methylpropiophenone (Irgacure D-2959, Sigma-Aldrich) in PBS at 70°C for 10 minutes and then sterilised using a 0.2 μm syringe filter unit (Millipore). The photo-initiator solution was added into the dissolved GelMA (final photo-initiator concentration: 0.5% vol/vol). Next, cells were harvested and pelleted at the desired concentration (3.5 x 10^5 cells/ml unless otherwise stated) prior to mixing with the GelMA/photo-initiator mixture to establish the GelMA precursor solution (this step was omitted when obtaining acellular hydrogels) (Figure 2.1a). The precursor solution was casted into sterilised custom-made Teflon moulds (Queensland University of Technology) and sealed with glass slides (VWR). The precursor solution was crosslinked in a CL-1000 Ultraviolet Crosslinker (UVP) at 365 nm for 10 minutes (Figure 2.1b), after which the hydrogel was removed from the mould by lifting the glass slide. Note that for 3% wt/vol hydrogels a 12 minutes UV crosslinking time was used instead, to allow full crosslinking. The

resulting hydrogels were cut in equal sized 4 mm x 4 mm x 2 mm constructs using sterile PMMA cutting guides (Queensland University of Technology) and scalpel (Swann-Morton) (Figure 2.1c). Each hydrogel was placed free-floating in a separate well of a 24-well plate (Costar) in supplemented 10%-FBS/1%-P/S/DMEM (Figure 2.1d). The latter was replaced after 2 hours to ensure photo-initiator removal and subsequently replaced twice per week. The resulting cultures were labelled 'monocultures' when only containing one cell type and 'co-/triple-culture' when NFs, CAFs, THP-1 were added to the cancer cells. Cell-containing GelMA cultures were kept for 14 days, unless otherwise noted.

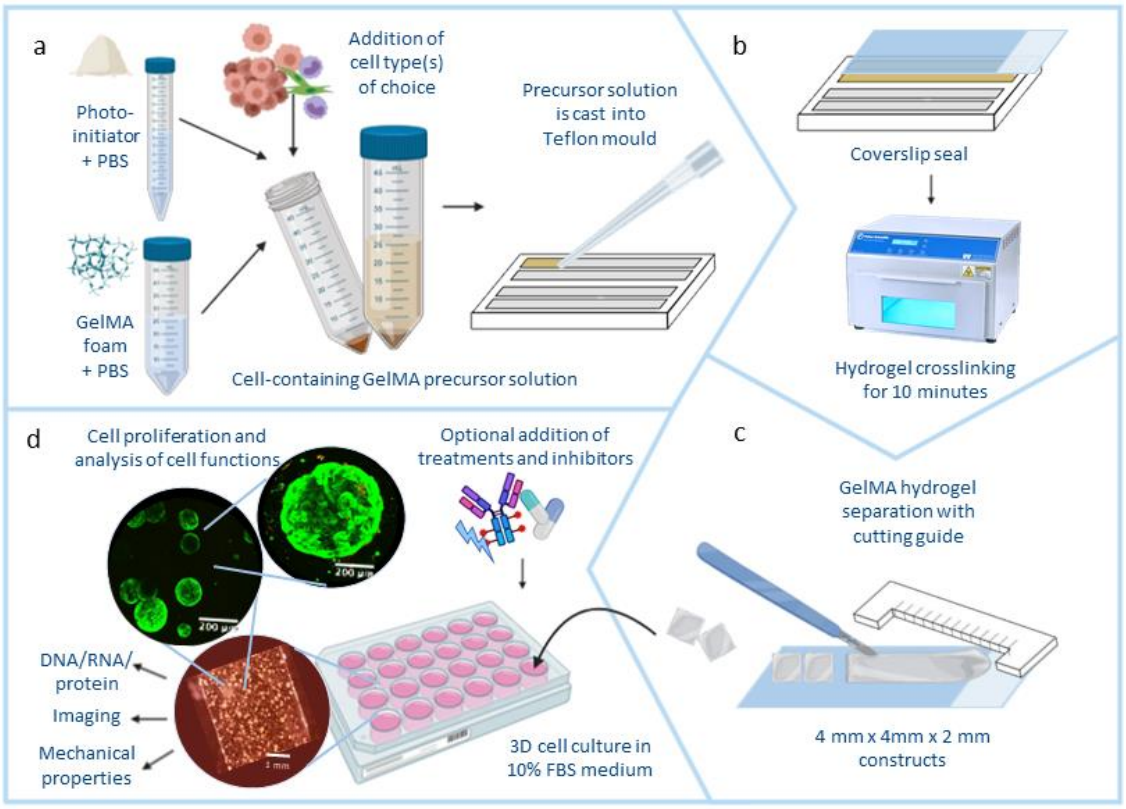

Figure 2.1 Schematic representation of cell-laden GelMA hydrogels preparation procedure. (a-b) The cell-containing precursor solution (comprising GelMA foam, PBS and diluted photo-initiator) was casted into a customised Teflon mould, covered with a glass slide, and polymerised via photo-crosslinking (10 minutes at 365nm UV light). **(c)** Hydrogels were cut to obtain identical-sized constructs, using a scalpel and cutting guide. **(d)** Constructs are transferred into a multi-well plate with appropriate cell culture medium, in which the hydrogels are free-floating, allowing formation of multicellular spheroids over time (green: live cells; red: dead cells).

2.2.4 Collagen hydrogels synthesis and 3D cell culture

Collagen mixture (1mg/ml) was obtained by mixing 1:3 of rat-tail Collagen type-I (Thermo Fisher), 10:10 10X DMEM (Sigma), 1:58 1M sodium hydroxide (Acros Organics), 1:19 sterile water (Sigma), and 1:2 of cells in DMEM (Gibco) at the desired concentration (3.5 x 10^5 cells/ml unless otherwise stated). Cell-free media alone was added for the formation of

acellular hydrogels. Modified concentrations to the above mixture ratios were made to obtain 4, 6, and 8 mg/ml hydrogels during optimisation phase. The optimal collagen mixture volume for plating and hydrogel formation was found to be 100 µL (+10% excess). This was added directly into each well of a 96-wells plate (Costar), and incubated at 37°C for 30 minutes to set (Figure 2.2). Once set, 100 µL of cell culture media were added into each well and incubated overnight at 37°C/5%CO_2. The following day hydrogels were scooped out of the well with the aid of a sterile metal spatula (Sigma Aldrich) and placed individually into a 24-wells plate, free-floating in 10%FBS/1%P-S/DMEM. Cell-containing collagen hydrogels were handled and treated the same as their GelMA counterparts, with media change twice per week and culturing over 14 days, unless otherwise noted. For treatment experiments, gels were made in a minimum of sextuplicate per treatment group to allow for proliferation, imaging, mechanical properties and other analyses.

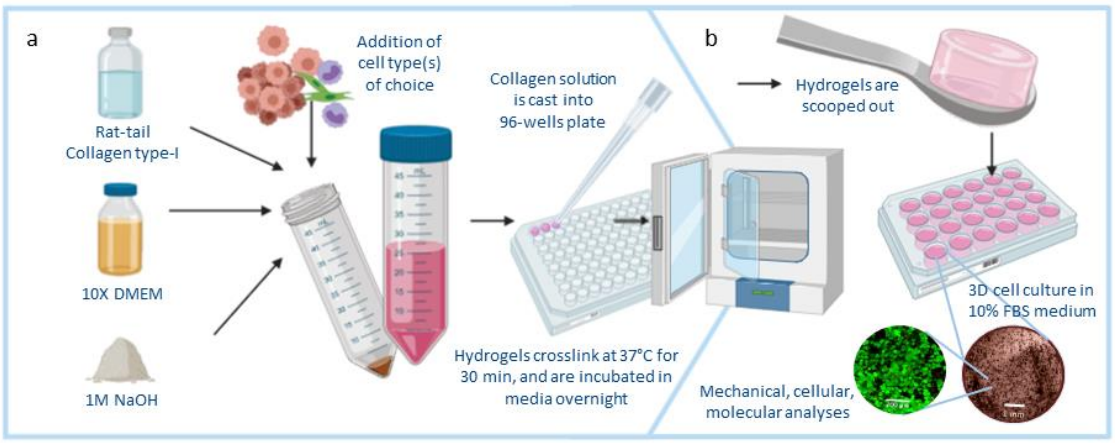

Figure 2.2 Schematic representation of collagen hydrogel preparation procedure. (a) After passaging, cells at the desired concentration were added to rat-tail collagen type-I and crosslinked in 10X DMEM and 1M NaOH. The mixture was then casted directly into a 96-wells plate and left to crosslink at 37°C for 30 minutes. Following media addition, the hydrogels were left in the plate overnight. **(b)** Set hydrogels were scooped out using a metal spatula and placed free-floating in 24-wells plates.

2.3 *In vitro* treatments and *in vivo* studies

2.3.1 MMP and ROCK inhibitors: monotherapy studies

Collagen, 5% and 7.5% GelMA hydrogels were synthesised as previously described incorporating either the PDAC cell lines BxPC-3, Capan-2, MIAPaCa-2 and PANC-1 or the HGSOC cell line OvCar-4 as monocultures. Hydrogels were treated with either the broad-band MMP inhibitor ilomastat (20 μM, GM6001, targeting MMP-1, -2, -3, -8, -9) (Merck), the ROCK inhibitor fasudil (10 μM, Tocris) or the GM6001 negative control peptide in dimethyl sulfoxide (DMSO) (20 μM, Merck). The treatments were dissolved directly into 10%FBS/1%P-S/DMEM. Treatment started on day 1 post-cell-encapsulation and replaced every 72 hours for 14 days of culture. Experiments were conducted in four technical replicates and three biological repeats.

2.3.2 ROCK inhibitor and chemotherapy: combinational studies

BxPC-3 or PANC-1 cancer cells, patient-derived CAFs and THP-1 triple cultures (in a 1:1:2 and 1:2:2 ratio) were incorporated in either collagen, 5% or 7.5% GelMA hydrogels as previously described. Appropriate monoculture controls (PDAC only) and stroma (CAFs and THP-1s) controls were also set up. CAFs isolated from patients 2, 3, 14 and 15 were used for these experiments (see Table 2.1). Hydrogels were cultured in complete 10%FBS/1%P-S/DMEM cell culture media. On day 7, cultures were treated with 10 μM fasudil (Tocris) in complete media or media alone as control. Cultures were subsequently treated on day 10 with 100 nM gemcitabine and 100 nM nab-paclitaxel (abraxane) in complete media (used fresh, both were a kind donations of the St Bartholomew's Hospital, UK) or media alone. Experiments were conducted in four technical replicates and three biological repeats.

2.3.3 Indirect co-culture: conditioned medium studies

3D indirect co-culture experiments were set up to study the effect of stromal-cells secreted-factors (THP-1s and CAFs) on PDAC pro-survival cell signalling pathways and vice versa, via indirect stimulation. For this, either PANC-1 cells or THP-1 and CAF cells (stroma) were embedded in collagen, 5% and 7.5% GelMA hydrogels. CAFs isolated from patients 13 and 14 were used for these experiments (see Table 2.1). Next, 6 hydrogels were placed in each well of a 12-well plate (Corning) in 1 ml of supplemented media, either as monocultures

(either 6 PANC-1 hydrogels or 6 stroma hydrogels) or as indirect co-cultures (3 PANC-1 and 3 stroma hydrogels in the same well). Plates were incubated for 72 hours, after which PANC-1 and stroma hydrogels were separated using an inverted microscope (Thermo-Fisher Scientific) for subsequent protein extraction and analysis.

2.3.4 Orthotopic xenograft study

All animal *in vivo* work was performed by Dr Juliana Candido with the help of Colin Pengrum in the Biological Services Unit of the Barts Cancer Institute. All experiments were conducted in compliance with UK Code of Practice for the housing and care of animals bred, supplied or used for scientific purposes and approved by the Institute. 5% GelMA hydrogels were made as previously described with BxPC-3 or PANC-1 cells +/- THP-1 monocytes in a 1:2 ratio and cultured for 14 days. One hydrogel was implanted into the flank of severe combined immune deficiency spontaneous mutation (NOD/SCID) mice, with 6 mice used per condition. Animal appearance and weight was recorded weekly and once tumours reached a palpable size, after 10-14 weeks, animals were sacrificed. Presence of ascites and metastases was noted, GelMA hydrogels, tumour and liver tissues were surgically removed, and the latter were taken histological and immunohistochemical analysis.

2.4 Analysis of mechanical properties

2.4.1 Flat-end Indentation

Indentation testing was performed on fresh, unfixed patient-derived and murine ovarian and pancreatic tissues, (see patients 4-6; 8-12 for OvCa tissues and 19-23 and 26 for PDAC tissues in Table 2.1). Fresh mice whole ovaries and pancreas were provided by Colin Pengrum, from adult female mice with a $Pax8^{--}$, Cre^{--} background. Wherever possible, specimens were tested within 24 hours from surgery. Samples were kept at 4°C in PBS until tested and were allowed to reach ambient temperature prior to testing. If the sample did not present with flat, parallel surfaces at resection, the sample was sliced using a scalpel (Swann-Morton).

Indentation testing was performed on an Instron ElectroPuls E1000 machine (Instron) equipped with a 10N load cell with a 0.1 mN resolution and a metal flat-end cylindrical indenter (Øi: 1-4 mm) as previously described [263]. Samples were hydrated in PBS during testing to prevent drying out. Sample height was recorded as the plate to sample top displacement prior to indentation. A preload of 0.2 mN was applied. Specimen diameter (Øs) was measured with a digital calliper to ensure Øs:Øi was kept ≥ 3:1 for testing accuracy. The specimen thickness (Ts) to indenter diameter (Øi) ratio (x) was kept $1:1 \leq x \leq 2:1$, as this minimises modulus calculation bias [263]. Immediately prior to testing, green tissue dye (Thermo-Fisher Scientific) was applied to the indenter metal head in order to mark the exact position of indentation points on the specimen. This was later used to correlate stiffness with matrix protein expression via immunohistochemistry. Testing was conducted with a displacement control mode protocol with a compression phase (20% or 30%) at a 1% s^{-1}, displacement-hold (600 seconds) and unloading (to 0% specimen strain at 1% s^{-1}). For big samples (> 4 mm), multiple indentation tests were performed in distinct areas (up to 4). Following testing, the samples were fixed in 10% formalin (Sigma-Aldrich) and sent for embedding, sectioning and immunohistochemical analysis.

Data from flat-end indentation testing were processed in MATLAB R2019 (MathWorks) using the code provided in 9.1 Appendix Chapter 2. Tissue moduli (E) was calculated from the resulting experimental data load-displacement curve using a corrected mathematical model [263]. This also allowed comparison with stiffness data obtained via unconfined compression.

Shortly, the reduced modulus (E_r) is related to the indenter contact area $A=\pi a^2$ and the elastic contact stiffness dP/dw as follows:

$$Er = \frac{1}{\beta} \times \frac{dP}{dw} \times \frac{1}{2} \times \frac{\sqrt{\pi}}{\sqrt{a}}$$

where constant β is assumed to be 1 for flat-ended indenters, the equation can be simplified to:

$$Er = \frac{m\sqrt{\pi}}{2\sqrt{A}}$$

where m is the slope of the force-displacement curve [N/mm] calculated on MATLAB. Next, the elastic modulus (E)[MPa] was calculated as follows:

$$E = E_r(1 - v^2)$$

where v is the Poisson's ratio and it's assumed to be 0.5 as tissues behave as incompressible materials.

2.4.2 Unconfined compression

Unconfined compression was used for the bulk testing of both acellular and cell-laden GelMA hydrogels. For the latter, hydrogels were cultured for 14 days prior to testing, unless otherwise stated. Varying polymer concentrations (3-10% wt/vol) were tested. Compression testing was performed on an Instron 3342 machine (Instron) equipped with a 10N load cell as previously described [263]. Natural logarithms of the recorded stress and strain values were used to obtain a load-displacement curve for each sample. The Young's modulus (E) was calculated as follows:

$$E = \frac{stress}{strain} = \frac{\left(\frac{force}{area}\right)}{\left(\frac{expanion}{length}\right)}$$

Sample height was recorded on the machine prior to testing, while the surface area of the hydrogels was measured from pictures via ImageJ (NIH) and found to be between 9-16 mm^2. The slope of the stress strain curve at 15-20% strain was taken as the compressive modulus (E)[kPa]. Samples were tested in a minimum of quadruplicates per test group.

2.4.3 Rheometry

Rheometry testing was used for the bulk testing of both acellular and cell-laden collagen hydrogels. For the latter, hydrogels were cultured for 14 days prior to testing, unless otherwise stated. Rheometry was used as collagen hydrogels present irregular surface geometries and were too soft to be tested by either indentation or compression. Testing was

performed on a DHR3 Rheometer (TA Instruments) equipped with an 8 mm plate geometry, and analysis was conducted using TRIS®DHR3 software. Before testing, samples were left equilibrating for three minutes to allow them to reach room temperature and mechanical equilibrium. Loss modulus was averaged in sweep frequency testing between 0 and 0.2Hz while storage modulus was taken in amplitude sweep at 5.9-6.3 rad and converted to compressive modulus (E) as follows:

$$E = 2G(1 + v)$$

where G is the measured shear modulus and v is the Poisson's ratio, assumed to be 0.5 in incompressible materials. Samples were tested in triplicates for each test group.

2.4.4 Atomic Force Microscopy (AFM)

Rheometry testing was used to measure at a nano-scale the stiffness of acellular and cell-laden GelMA hydrogels with and without GM6001 (Merck) treatment (regime is detailed in MMP and ROCK inhibitors: monotherapy studies). AFM testing was performed and analysed by Dr William Megone. Interfacial AFM was performed using an NT-MDT Ntegra Atomic Force Microscope (NT-MDT Spectrum Instruments). ORC 8 – 10 Contact AFM tips (Bruker) were used, with spring constants of ~0.05 N/m. Before testing, the tips were plasma oxidised and calibrated (nA to nm conversion) by indenting a silicon wafer before testing the hydrogel interfaces. Each sample was indented on three separate 1x1μm areas, in which 100 indents were performed. The time for each curve was set at 1 s. The indentation depth was kept between 500 – 1000 nm depending on the sample. Acellular hydrogels were used as calibration, allowing the precise detection of 'spheroids' and cell cluster' areas within cell-laden hydrogels. A minimum of three samples for each condition were tested.

2.5 Functional assays

2.5.1 IncuCyte proliferation assay

The kinetic proliferation assay was performed on the IncuCyte ZOOM (Essen Bioscience) using 96-well plates (Corning) and analysed on the IncuCyte ZOOM software (Essen Bioscience). Prior to cell seeding, 96-wells plates (Corning) were coated with 10 μg/μl of either poly-L-lysine (Sigma) or rat-tail collagen type-I (Gibco) and incubated overnight at 4°C. 24 hours prior to the assay set up, cells were washed and subsequently starved with 1%FBS/1%P-S/DMEM. Cells were then detached and counted as previously described (see Cell culture and passaging). Cells were seeded at a 5 x 10^3 cells/well density (except Capan-2 cells which were seeded at 10 x 10^3 cells/well) and imaged over 7 days in complete medium or medium with the addition of either 20 μM of GM6001 (Merck), 10 μM fasudil (Tocris), or 100 nm of both gemcitabine and abraxane (used fresh, kindly donated by the St Bartholomew's Hospital). A minimum of 5 wells was used for each cell line and treatment condition. Image analysis, confluency (%) assessment, and growth data was obtained via the IncuCyte Zoom (Essen Bioscience).

2.5.2 IncuCyte scratch-wound assay

Scratch-wound and cell migration assays were performed using the IncuCyte Zoom (Essen Bioscience) in conjunction with 96-well Image Lock plates (Essen Bioscience). Plates were coated and cells seeded as described in the previous paragraph at a 1 x 10^5 cells/well density (except Capan-2 cells which were seeded at 1.2 10^5 cells/well) and incubated at 37°C overnight to allow cell adhesion onto the plate. The scratches were generated using a IncuCyte Wound Maker (Essen Bioscience), after which wells were washed in PBS (Sigma-Aldrich) once, prior to the addition of treatments as detailed above, or control media alone. Wells were imaged for up to 5 days, with minimum of 5 wells was used for each cell line and treatment condition. Image analysis, wound confluency (%), wound width (μm), and cell migration data was obtained via the IncuCyte Zoom (Essen Bioscience) cell migration software.

2.5.3 Transwell invasion assay

Invasion assays were performed in 24-well multi-well cell culture inserts (Merck) with 8 μm pores as previously described [264]. Briefly, 10% FBS/DMEM was placed in the lower chamber

to act as a chemoattractant. 8 μm pore-sized transwell permeable supports were coated with either 60 μl of Matrigel (Corning) or rat-tail collagen type I (Gibco). Cells were seeded in 350 μL at a 1 x 10^5 cell concentration in serum-free medium containing 0.1% (w/v) bovine serum albumin (BSA)(Sigma Aldrich) and 20 μM GM6001 (Merck). This was pipetted directly into the top chamber of the transwell. Control inserts at the same cell seeding density and containing 350 μL of serum-free medium with 0.1% (w/v) BSA with 20 μM GM6001 control peptide (20 μM) were also set up. Wells containing cells in media with no FBS in the top chamber and no chemoattractant FBS in the bottom chamber were used as controls for random invasion of cell from the top chamber to the bottom (none of which was observed). Transwells were incubated at 37°C/5%CO_2 for 48 hours, after which cells remaining on the upper surface of the insert were removed using a cotton bud. To quantify the number of cells that migrated or invaded to the bottom of the insert, inserts were fixed with 100% ice-cold methanol (Sigma-Aldrich), stained with 1% (w/v) crystal violet (Fluka)/ 20% (v/v) methanol and the stain was extracted using 10% (v/v) acetic acid (Sigma-Aldrich). Absorbance was read at 595 nm. Invasion assays were performed in three biological and technical replicates for each cell line.

2.5.4 Viability assay

Cell viability in GelMA and collagen hydrogels was visually assessed using a Live/Dead Viability/cytotoxicity kit for mammalian cells (Life Technologies). Briefly, media was diffused of the hydrogels by placing them in PBS for 30 minutes at 37°C. The kit comprises of two dyes, calcein-AM (Ca-AM) and ethidium-homodimer 1 (EtH1). Live cells are stained based on their cytoplasmic esterase activity, which hydrolyses calceinacetoxymethyl (2 μM) into fluorescent Ca-AM (green). Dead cells are stained based on their membrane permeability, which allows EtH1 (4 μM, red) to bind to DNA. Cells were then imaged by confocal microscopy on a Zeiss Laser Scanning Microscope LSM710 (Zeiss).

2.5.5 Metabolic activity assay

Hydrogels in triplicates (minimum) were collected at day 1 and endpoint (day 14 unless otherwise specified) for this analysis, from at least 3 biological replicates. Cell metabolic activity was used as a proxy for viability and assessed via AlamarBlue® assay (ThermoFisher Scientific) using cell-laden GelMA and collagen hydrogels as previously described [229]. 3D cell cultures were incubated with 4% (vol/vol) Alamar Blue reagent in phenol-red-free DMEM (Gibco) and left in a humidified incubator, in the dark, for 6 hours. Cell-free hydrogels

and/or cell culture medium only, served as controls. Supernatant's fluorescence was measured by spectrophotometry (POLARStar OPTIMA plate reader, BMG Labtech) in a black 96-well-plate with clear bottom (Nunc, Thermo-Fisher Scientific) using an excitation wavelength of 544nm and emission of 590nm. Hydrogels were then incubated in PBS at 37°C until they lost the blue coloration and were then stored at -80°C for successive DNA content quantification. The fluorescence values of media-only controls was subtracted from all the samples during analysis.

2.5.6 3D proliferation assay

PBE buffer was made as follows: 20mM Na_2HPO_4 (Merck), 30mM NaH2PO4 in H2O (Merck), 5mM Na_2EDTA (AJAX Chemical), adjusted to pH 7.1 and autoclaved at 121°C for 15 min. Hydrogels were collected at day 1 and endpoint (day 14 unless otherwise specified) for this analysis, from at least 3 biological and technical replicates. Proliferation in 3D cultures was evaluated via DNA content quantification using a CyQUANT cell proliferation assay kit (Invitrogen). Following metabolic activity quantification as described above, hydrogels were stored at -80°C for >24 hours. Hydrogels were then digested in 300 µl of 0.5 mg/ml proteinase K (Invitrogen)/PBE buffer at 65°C overnight. 50 µl of each sample was added to a black 96-well plate with clear bottom (Corning) in duplicates. Samples were treated with 1.4 U/ml RNAseA (Invitrogen) dissolved in cell lysis buffer (Invitrogen), 180 nM sodium chloride (Sigma-Aldrich) and 1mM EDTA (Ambion) for 1 hour at ambient temperature. 1x CyQUANT® dye solution (Invitrogen) was diluted in cell lysis buffer and added to the plate. Fluorescence was measured after 5 minutes via spectrophotometry using an excitation wavelength of 485 nm and emission 520 nm on a BMG Labtech FLUOstar Optima Microplate reader (Labtech). A λDNA standard (0-2000 ng/ml) was used to convert fluorescence values into DNA content.

2.6 Imaging and image analysis

2.6.1 Brightfield microscopy

Brightfield imaging was performed on cell-laden GelMA and collagen hydrogels at multiple time points with an EVOS XL Core Cell-Imaging-System (Thermo-Fisher Scientific). Where necessary, image analysis was performed on ImageJ (NIH).

2.6.2 Confocal microscopy

For immunofluorescent (IF) analysis of 3D cultures, hydrogels were permeabilised with 0.2% Triton X-100 (Sigma-Aldrich) for 1 hour at room temperature, washed with 0.1 M glycine/PBS (Thermo-Fisher Scientific). Primary antibodies were diluted in 2% BSA (Sigma-Aldrich) in PBS and incubated overnight at 4°C. After washing, the hydrogels were incubated with secondary antibodies in 2% BSA/PBS, phalloidin (0.3 U/ml, Invitrogen) and 4′,6-diamidino-2-phenylindole (DAPI) (2.5 μg/ml, Invitrogen) for 1 hour at RT. Fluorescence microscopy was performed on a Zeiss Laser Scanning Microscope LSM710 (Zeiss). z-Stacks were acquired with 10 μm slice thickness for a minimum of 10 sections.

For cells grown in monolayer, 20 x 10^3 cells were plated on round sterile coverslips (VWR) in a 24-well plate (Corning) and placed in a humidified incubator overnight to allow cell adhesion. Coverslips were then rinsed in PBS for 5 minutes and subsequently fixed in 4% paraformaldehyde (PFA)(Sigma-Aldrich) for 10 minutes. Following two PBS washes, the coverslips were permeabilised with 0.1% Triton (Sigma-Aldrich)/PBS for 5 minutes and then washed twice again in PBS. Coverslips were blocked for 90 minutes in 2% BSA/5% goat serum/ 0.3 M glycine/ 0.1% Triton/PBS after which primary antibodies were added in blocking buffer overnight at 4°C. Washing, secondary antibody staining, addition of DAPI and imaging was performed as described above. Coverslips were mounted onto glass slides (VWR) with ProLong Gold antifade reagent (Invitrogen) prior to imaging.

Table 2.2 Table of antibodies used for immunofluorescence. mAb=monoclonal antibody; pAb=polyclonal antibody

Antibody	Dilution	Species	Clonality	Cat. number	Supplier
αSMA	1:70	Rabbit	pAb	ab5694	Abcam
FN	1:100	Rabbit	pAb	ab2413	Abcam
KRT19	1:200	Rabbit	EP1580Y	ab52625	Abcam
p-γH2A.X (Ser139)	1:500	Mouse	JBW301	05-636	Merck
VIM	1:100	Mouse	mAb	M0720	Dako

Table 2.3 Secondary antibodies and other immunofluorescent dyes used.

Secondary antibody/dye	Dilution	Species	Cat. no	Supplier
Anti-rabbit AlexaFluor 488	1:1000	Goat	A-11008	Thermos-Fisher Scientific
Anti-mouse AlexaFluor 488	1:1000	Goat	A-11001	Thermos-Fisher Scientific
Anti-rabbit AlexaFluor 568	1:1000	Goat	A-11035	Thermos-Fisher Scientific
Anti-mouse AlexaFluor 568	1:1000	Goat	A-11004	Thermos-Fisher Scientific
Anti-rabbit AlexaFluor 633	1:1000	Goat	A-21070	Thermos-Fisher Scientific
Anti-mouse AlexaFluor 633	1:1000	Goat	A-21050	Thermos-Fisher Scientific
Phalloidin AlexaFluor 647	1:300 (0.3 U/ml)		A22287	Thermos-Fisher Scientific
DAPI	1:10 000 (1 μg/ml)		D1306	Thermos-Fisher Scientific
Calcein-AM	1:2000 (2 μM)		L3224	Thermos-Fisher Scientific
Et-H1	1:500 (4 μM)		L3224	Thermos-Fisher Scientific

2.6.3 Scanning Electron Microscopy (SEM)

Scanning Electron Microscopy (SEM) was performed on both GelMA and collagen cell-laden hydrogels in order to visualise their nano-structure and cell-matrix interaction patterns. Imaging was performed with the help of Russell Bailey (lead technician, Nanovision Lab, Queen Mary University of London). Hydrogels were prepared as previously described with a 3.5 x 10^3 cells/ml initial cell density (both as monocultures and PANC-1, THP-1, CAF triple cultures) and cultured in both 5% GelMA and collagen hydrogels for 14 days. Samples were fixed for >24 h with 4% PFA at room temperature. To dehydrate the hydrogels, these were immersed in sequential ethanol solutions of increasing concentration (25%, 50%, 70%, 80%, 90%, 95%, 100%), twice in each solution for 5 min. Samples were then dried in a K850 critical point dryer (Quorum Technologies). Specimens were placed in a 'Mini' sputter coater (Quorum Technologies) for gold coating (current of 20 mA, resulting in 10nm gold film thickness). Samples were imaged on an Inspect F50 microscope (FEI). SEM micrographs fibres thickness was quantified via ImageJ (NIH) from 4 distinct gels.

2.6.4 Sectioning, histology and immunostaining

2.6.4.1 Specimen embedding and sectioning

Primary PDAC and HGSOC tumours, GelMA and collagen hydrogels were fixed in 4% PFA for >24 h, placed in 70% ethanol and sent for paraffin embedding and sectioning by the Barts Cancer Institute Pathology unit. Samples were sliced into 7 μm sections on a microtome, mounted onto glass slides and deparaffinised with xylene, 100% ethanol and 70% ethanol solutions (10 min each). The sections were then rehydrated with distilled water. After deparaffinising, slides were used for either haematoxylin and eosin (H&E) staining, Masson's trichrome staining, immunohistochemistry (IHC) staining, or IF staining as described above.

2.6.4.2 Haematoxylin and eosin (H&E)

H&E staining was performed in order to visualise cell nuclei, cytoplasm and ECM with Mayer's haematoxylin for 5 min and eosin Y (Sigma-Aldrich) for 10 min by the Barts Cancer Institute Pathology unit.

2.6.4.3 Masson's trichrome

Masson's trichrome staining kit (all Sigma) was used in order to visualise collagen fibres (blue), keratins and muscle fibres (red) and nuclei (black) in both tissues and hydrogels. Briefly, after deparaffinising, slides were submerged in warm (60°C) Bouin's solution, followed by Weigert's solutions A and B and the working Weigert's Iron Haematoxylin solution for five minutes. Next, the slides were washed in tap water prior to incubation in the Biebrich Scarlet/Acid Fuchsin Solution for 15 minutes. Following another wash in deionised water, the slides were incubated in phosphomolybic/phosphotungstic acid for 15 min and then aniline blue solution for 10 min. Following washing in deionised water slides were incubated in 1% acetic acid for 5 min. Slide dehydration was performed with two subsequent washes in 95% ethanol and 100% ethanol (Thermo-Fisher Scientific), xylene (Thermo-Fisher Scientific) and mounted in DPX (Sigma-Aldrich) with a coverslip (VWR). Definiens Tissue Studio software (Definiens AG) was used with a modified protocol for the analysis and quantification of stained areas (blue) over total area. Fibres and fibre bundle thickness was measured using CaseViewer (3DHISTECH) for 4 matched patient tissues in 3 random fields of view and 5 spots each.

2.6.4.4 Immunohistochemistry (IHC)

10x Tris-buffered saline (TBS) was made as follows: 1.5M NaCl (Sigma-Aldrich), 200mM Trizma base (Sigma-Aldrich) in deionised H_2O (dH2O), pH adjusted to 7.6 with >20 ml hydrochloric acid (Thermo-Fisher Scientific). TBST was made by dilution TBS 1:10 in dH2O with 0.05 % v/v Tween 20 (Sigma-Aldrich). The staining shown and antibody dilution optimisations were performed in part by Dr Juliana Candido, Shreya Sharma or Niamh Leonard. Heat-induced antigen retrieval was performed at 95°C for 20 min in a water bath in sodium citrate buffer (pH 6) unmasking solution (Vector Laboratories). Endogenous horseradish peroxidase (HRP) activity was blocked with 0.6% hydrogen peroxide (Thermo-Fisher Scientific) in methanol for 20 minutes. Primary antibody (Table 2.4) was diluted in antibody diluent (Zytomed Systems) and incubated at room temperature for 1 h or overnight at 4°C, followed by 3 washes in TBST and incubation with HRP-conjugated secondary (Invitrogen) for 1 h at room temperature. Meanwhile, Vectastain ABC HRP solution (Vector Laboratories) was prepared according to manufacturer's instructions and, after 3 washes in TBST, was incubated onto the slides for 1 h. Brown colour development was achieved with a 3,3'-diaminobenzidine (DAB)–based Super Sensitive Polymer-HRP IHC detection system (Biogenex). Mayer's haematoxylin (Sigma-Aldrich) served as counterstain. Sections where subsequently dehydrated in 100% ethanol and two xylene incubations of 5 minutes each. Sections were sealed with DPX mountant (Sigma-Aldrich) and imaged on a Pannoramic 250 Flash III scanner (3DHISTECH). Positive and negative control tissues were stained for all antibodies during the optimisation phase. Definiens Tissue Studio software (Definiens AG) was used for the analysis and quantification of stained areas (brown) over total area. Expression of the protein of interest was quantified as (%) staining as follows:

$$\%\ Stained\ area = \left(\frac{IHC\ marker\ area\ (brown)}{total\ tissue\ area}\right) \times 100$$

In collagen and GelMA hydrogels, the staining was further quantified by selecting 8 spheroids or cell aggregates at random for each hydrogel. Percentage (%) of staining was therefore quantified in proximity of cell clusters to avoid noise and quantification of the staining coming from the hydrogel (which often stained brown, as in the case of COL-1 and FN1). A modified protocol was optimised on Definiens (Definiens AG) for the quantification of collagen fibres (blue) on Masson's Trichrome staining.

Table 2.4 Staining reagents, primary and secondary antibodies used for immunohistochemistry.

Antibody	Dilution	Species	Clonality	Cat. number	Supplier
Biotinylated HABP	1:100	Stain		385911	Merck
CD68	1:50	Mouse	PG-M1	ab783	Abcam
COL-1	1:3000	Rabbit	EPR7785	ab138492	Abcam
FN1	1:500	Rabbit	pAb	F3648	Sigma-Aldrich
KRT19	1:400	Rabbit	EP1580Y	ab52625	Abcam
VCAN	1:250	Rabbit	pAb	HPA004726	Sigma-Aldrich
αSMA	1:200	Rabbit	pAb	ab5694	Abcam
Biotinylated anti-rabbit IgG	1:200	Goat		BA-1000	Vector Lab
Biotinylated anti-mouse IgG	1:200	Horse		BA-2000	Vector Lab

2.7 Hydrogel digestion, cell retrieval and viability assessment

2.7.1 GelMA hydrogel digestion

GelMA hydrogel digestion for retrieval of cells with a high viability had not been previously optimised. Five approaches were used to digest cell-laden GelMA-based hydrogels (Table 2.5). Their efficiency in hydrogel degradation, and viability of recovered cells was assessed via flow cytometry. We published this method in Methods in Molecular Biology, 2019 [235].

Table 2.5 Digestion protocol specifications including enzyme names, origin, final concentration and supplier.

Condition label	Name, origin, diluent	Working concentration	Catalogue number
1	Trypsin/EDTA	0.5%/0.2%	Sigma-Aldrich 59418C
2	Collagenase I from *Clostridium histolyticum* in serum-free DMEM	1 mg/ml	Life Technologies 17018029
3	Collagenase V from *Clostridium histolyticum* in Hank's Salt Balanced Solution	1 mg/ml	Sigma-Aldrich C9263
4	Dispase II from *Bacillus polymyxa* in PBS	2.5 U/ml	Stem Cell Technologies 7913
5	Collagenase XI from *Clostridium histolyticum* and Dispase II from *Bacillus polymyxa* in DMEM (10% FBS, 1% P/S)	0.125 mg/ml 0.625 U/ml	Sigma-Aldrich C9407; Stem Cell Technologies 7913

GelMA hydrogels were incubated with the above solutions until digestion was complete (20-40 min) and then taken for flow cytometry staining as described in the "flow cytometry" section below.

2.8 Gene expression analyses

2.8.1 RNA extraction from 3D cell cultures

Gene expression was assessed by reverse transcription–quantitative polymerase chain reaction (RT-qPCR). Cells were either detached from monolayers for 2D expression analysis or cultured for 14 days in either GelMA or collagen hydrogels as previously detailed. Six hydrogels were pulled for this analysis into one gentleMACS orange tube (Miltenyi Biotec) containing 600 µL of TRIzol Reagent (Invitrogen). Hydrogels were disrupted with a gentleMACS Dissociator tissue homogeniser (Miltenyi Biotec) using an RNA program for 84 seconds. Tubes were then spun at 1000 g for 3 minutes to collect homogenised hydrogel at the bottom of the tube. This procedure was repeated three times, after which the homogenised solution was moved to a RNAse-free tube (Ambion). Chloroform (Sigma-Aldrich) was added as 1/5 of the TRIzol volume, vortexed, and centrifuged at 16 000 g for 15 minutes to allow RNA separation. The aqueous fraction was moved to a fresh tube (Ambion) and mixed with equal amounts of isopropanol (Sigma-Aldrich) in order to precipitate the RNA. Following centrifugation at 16 000 g for 30 min, further precipitation was achieved by sequential washes with 70% ethanol/water and 100% ethanol, with 16 000 g for 5 min centrifugation step following each. Samples were left to air-dry for > 30 min and dissolved in RNAse-free water (Ambion). RNA quality and concentration were measured on a Nanodrop 2000 spectrometer (Thermo-Fisher Scientific).

2.8.2 RT-qPCR

RNA amounts were normalised to 500-1000 ng of total RNA and reversed transcribed with a High-Capacity cDNA Reverse Transcription kit (Thermo-Fisher Scientific) on a T100 thermal cycler (Biorad) following manufacturer's instructions. Briefly, temperature was held at 25°C for 10 min, then raised to 37°C for 2 h to allow reverse transcriptase activity and lastly at 85°C for 5 min to ensure enzyme denaturing. The resulting cDNA solutions were diluted 1:40 and stored at −20 °C. For qPCR, a total 10 µL reactions were prepared by mixing 4 µL of cDNA to 0.5 µL of gene-specific primers (Thermo-Fisher Scientific, see Table 2.6), 0.5 µL of *HPRT1* housekeeping probe (Thermo-Fisher Scientific) and 5 µL of TaqMan 2x Master Mix (Thermo-Fisher Scientific) in a minimum of duplicates in a PCR 96-well plate (Thermo-Fisher Scientific). Plates were sealed with PCR film (Thermo-Fisher Scientific) and run on a StepOnePlus Real-Time PCR System (Thermo-Fisher Scientific). The thermal cycling conditions used were two hold phases at 50°C and 90°C for 2 and 10 min respectively,

a 15 seconds denaturation step at 95°C, a primer annealing and extension phase at 60°C for 1 minute, repeated for 40 cycles. Alternatively, qPCR was carried out using the SYBR Green method. For this, cDNA solutions were diluted to 5 ng/μL for storing. A total 10 μL reaction was prepared in 384-well PCR plates (Thermo-Fisher Scientific), by adding 2 μL of cDNA to 5 μL of PerfeCTa SYBR Green FastMix Low Rox (Quanta Biosciences), 2.8 μL of RNase-free water (Invitrogen), 0.2 μL of gene-specific primers and run on a QuantStudio 7 system (Applied Biosystems) (see Table 2.7). *RPS13* was used as housekeeping gene internal control. Results were interpreted using the Ct method with expression normalised to housekeeping gene. Relative expression was calculated as follows:

$$Expression = 2^{(Ct(housekeeping) - Ct(GOI))}$$

where GOI is the target gene of interest and housekeeping refers to *HPRT1* or *RPS13*.

Table 2.6 qPCR TaqMan primer details, all Thermo-Fisher Scientific.

Target gene	Exons targeted	Amplicon length (bp)	Fluorophore and quencher
COL11A1	Hs01097664_m1	56	FAM-MGB
COL1A1	Hs00164004_m1	66	FAM-MGB
CTSB	Hs00947439_m1	99	FAM-MGB
FN1	Hs01549976_m1	81	FAM-MGB
HPRT1	Hs02800695_m1	82	VIC-MGB
MMP9	Hs00957562_m1	67	FAM-MGB
TGFBI	Hs00932747_m1	63	FAM-MGB
VCAN	Hs00171642_m1	72	FAM-MGB
VIM	Hs00958111_m1	65	FAM-MGB
YAP1	Hs00371735_m1	64	FAM-MGB

Table 2.7 qPCR SYBR Green primer details.

Target gene	Forward primer	Reverse primer	Amplicon length (bp)
CDH1	CCCACCACGTACAAGGGTC	CTGGGGTATTGGGGGCATC	94
MMP2	GTGAAGTATGGGAACGCCGA	AGAAGCCGTACTTGCCATCC	154
MMP3	CACTCACAGACCTGACTCGG	CATCCACGCCTGAAGGAAGA	20
MMP9	TTCTGCCCGGACCAAGGATA	ACATAGGGTACATGAGCGCC	109
RPS13	TCGGCTTTACCCTATCGACGCAG	ACGTACTTGTGCAACACCATGTGA	153
TIMP1	GGGGATGCCGCTGACATCCG	CTCGCTGCGGTTGTGGGACC	87
VIM	GACAATGCGTCTCTGGCACGTCTT	TCCTCCGCCTCCTGCAGGTTCTT	236

2.8.3 RNA-sequencing

RNA-sequencing (RNA-seq) sample preparation, RNA extraction optimisation and quality controls were performed with Dr Juliana Candido. For transcriptomics analysis, RNA was extracted from BxPC-3 and PANC-1 cells cultured in collagen, 5% GelMA and 7.5% GelMA for 7 days with an initial cell seeding density of 7 x 10^5 cells/ml. As an additional comparison, primary PDAC cells (from patients 12556, 12560 and 12975) were grown as organoids in Matrigel basement membrane matrix (BD Biosciences) by Dr David Osuna de la Peña. Hydrogels were formed by mixing 25 000 cells with 100 µL of Matrigel, stabilised for 10 minutes, and cultured for 7 days in DMEM/F12 (Gibco) supplemented with 2% B27 (Gibco), 20 ng/mL FGF-2 (PeproTech UK) and 2 mM L-glutamine (Gibco).

RNA extraction was performed as described above, with 6 hydrogels pulled for each condition, in duplicates for each stiffness/cell line (for a total of 6 conditions + 3 Matrigel organoids conditions). After removal of the aqueous phase, RNA clean-up was performed using a RNeasy Mini kit (Qiagen) following the manufacturer's instructions and stored at −80 °C prior to processing. As an additional quality control, the RNA Integrity Number (RIN) was measured using a High-Sensitivity D1000 Screen Tape system (Agilent) and run on a 4200 TapeStation (Agilent). RNA with RIN<8 was excluded from sequencing. Total RNA (100 ng) in water was prepared in fully skirted 96-well plate (Thermo-Fisher Scientific), sealed with film (Thermo-Fisher Scientific) and sent on dry ice for poly-A capture sequencing by the Oxford Genomics Centre (Oxford, UK). RNAseq bioinformatics data analysis and graphing was entirely performed by Dr Eleni Maniati.

2.9 Protein expression analyses

2.9.1 Protein extraction from 3D cultures

Protein extraction from GelMA hydrogels for downstream immunoblotting analysis had not been previously optimised. For this, digestion with 0.3 mg/ml Liberase (Roche) was attempted, as this enzyme is routinely used for tissue dissociation and is posed to increase the quality and reproducibility of dissociation compared to *Clostridium histolyticum's* traditional collagenase. This method was efficiently used for protein extraction from cell-containing collagen and GelMA hydrogels, at day 14 of culture unless otherwise stated. Hydrogels were incubated for 30 minutes in PBS at 37°C to allow medium and FBS to diffuse out of the hydrogel (as these have been found to give false positive results during protein quantification). Six to eight hydrogels per condition were pulled into one vial (Eppendorf) containing 1 ml of 0.3 mg/ml Liberase (Roche) dissolved in serum-free DMEM (Gibco). Vials were placed on a heated 37°C Brunswick Innova 40 shaker (Eppendorf) at 100 rpm for 20 min. After 10 min the content of the vials was pipetted vigorously with a P1000 (Gilson) to speed the digestion process with mechanical disruption. (Complete) Radio-Immunoprecipitation Assay (RIPA) buffer was prepared as follows: 10 ml RIPA buffer (Thermo-Fisher Scientific) one tablet of protease inhibitor cocktail I (Roche), and 1% phosphatase inhibitor cocktail II (Sigma-Aldrich). After digestion, vials were centrifuged at 4°C for 5 minutes at 16 000 g, resuspended in 30 µl of complete RIPA buffer (Thermo-Fisher Scientific), vortexed and incubated on ice for 15 minutes. The centrifugation step was repeated, the clear aqueous phase was collected in a fresh tube (Eppendorf) and samples were aliquoted and frozen at -80°C.

2.9.2 Flow cytometry

Flow cytometry buffer was prepared as follows: 2.5% wt/vol BSA (Sigma-Aldrich), 2 mM EDTA (Ambion) in PBS (Sigma-Aldrich), adjusted to pH 7.2. Characterisation of cell viability was conducted following cell retrieval from GelMA hydrogels to establish the efficiency of hydrogel digestion. Following retrieval, cells were centrifuged, resuspended in flow cytometry buffer (2.5% BSA/2mM EDTA/PBS), stained with Ca-AM (50 µM) for viable cells and DAPI (1 µg/ml) and EtH1 (20µM) for dead cells. Appropriate fluorescence minus one controls were used, as well as unstained and stained 2D-culture live and dead cells as positive and negative controls. A condition with 50:50 live:dead cells was created by mixing GelMA-recovered cells with ethanol killed cells in a 1:1 ratio. Flow cytometry data was

acquired on LSR Fortessa I Cell Analyser (BDBIoscience). Data analysis was performed in FlowJo version 10.0.8 (Treestar Inc.). A detailed protocol can be found in our publication [235].

Flow cytometry was also used for the characterisation of patient-derived fibroblasts after isolation from tissues and ascites. For this, cells were detached from the plate, resuspended in 0.5 ml of flow cytometry buffer, stained with 1:20 α-SMA (APC, Biolegend), 1:20 FAP (PE, Biolegend), 1:100 EpCAM (AF488, Thermo Fisher Scientific) in flow cytometry buffer and incubated for 20 min in the dark. After washing, 1:450 Fixable Viability Dye (Biologend) in PBS was added and incubated for 25 minutes. After washing, cells were resuspended in 4% paraformaldehyde for 10 minutes at RT, washed twice in flow cytometry buffer and acquired on LSR Fortessa I Cell Analyser (BDBIoscience) the following day.

2.9.3 Electrophoresis and Western blotting

Protein concentration was determined with a Pierce BCA protein assay kit (Thermo-Fisher Scientific) following manufacturer's instructions. Samples were normalised to 18 µg unless otherwise stated, to which were added 5 µl of NuPAGE LDS Sample buffer (Invitrogen), 2 µl of NuPAGE Sample Reducing Agent (Invitrogen) and adjusted to a final volume of 20 µl. Samples were denatured at 90 °C for 10 min. 3-(N-morpholino)propanesulfonic acid (MOPS) running buffer was prepared as follows: 50ml NuPAGE® MOPS sodium dodecyl sulphate (SDS) running buffer (20x) (Thermo-Fisher Scientific) in 950 ml of dH_2O, 0.25% NuPAGE antioxidant (Thermo-Fisher Scientific). Protein separation was performed via SDS-PAG Electrophoresis with 4-12% NuPAGE Bis-Tris precast gels (10- or 15-well, Invitrogen) in MOPS running buffer with 0.25% NuPAGE antioxidant (Thermo-Fisher Scientific) at 100 V for 1.5 h. Next, transfer buffer was prepared as follows: 50ml NuPAGE® transfer buffer (20x) (Thermo-Fisher Scientific), 200 ml methanol (Thermo-Fisher Scientific) in 750ml of dH_2O. A this point a GelCode Blue Safe Protein Stain (Thermo-Fisher Scientific) was performed on the gel or, alternatively, proteins were blotted onto a polyvinylidene fluoride membrane by wet transfer in 20% methanol/NuPAGE Transfer Buffer (Invitrogen) at 60V for 2 h. Membranes were blocked in 5% wt/vol non-fat dry milk (Marvel)/TBST for 1 h at room temperature and incubated with primary antibodies overnight unless otherwise stated (see Table 2.8). Polyvinylpyrolidine (PVP) was prepared by mixing 5% wt/vol Polyvinylpyrolidine (Sigma-Aldrich) in 1x TBST. Phospho-antibodies were diluted in 5% (PVP)(Sigma-Aldrich)/TBST while 5% milk (Marvel)/TBST was used for all other antibodies. Membranes were then washed in TBST, three times for 5 min each and incubated

with HRP-linked species-specific secondary antibody for 1 h at room temperature. ECL Prime Western Blotting detection reagent (GE Healthcare) was incubated with the membrane for 1 min prior to chemiluminescent detection on an Amersham Imager 600 (GE Healthcare) and analysed by densitometry on ImageJ (NIH).

Table 2.8 Primary and secondary antibodies used for western blotting.

Antigen	Dilution and incubation	Diluent	Species	Molecular weight (kDa)	Cat. number	Supplier
CDH1	1:1000, 1 h RT	Milk	Mouse	97	610182	BD Biosciences
GAPDH	1:5000, 1 h RT	Milk	Rabbit	37	D16H11	Cell Signaling
KRT19	1:1000, 1 h RT	Milk	Rabbit	44	ab52625	Abcam
p-γH2A.X (Ser139)	1:500, ON 4°C	Milk	Mouse	14	05-636	Merck
p44/42 MAPK (Erk1/2)	1:1000, 1 h RT	PVP	Rabbit	42/44	4695	Cell Signaling
p-p44/42 MAPK (Erk1/2) (Tyr202/204)	1:1000, ON 4°C	PVP	Mouse	42/44	9106	Cell Signaling
p-STAT3 (Tyr705)	1:1000, ON 4°C	PVP	Rabbit	79/86	9145	Cell Signaling
STAT3	1:1000, 1 h RT	PVP	Mouse	79/86	9139	Cell Signaling
TUBA1A	1:5000, 1 h RT	Milk	Rabbit	50	11H10	Cell Signaling
VCL	1:2000, 1 h RT	Milk	Mouse	117	SAB4200080	Sigma-Aldrich
VIM	1:1000, 1 h RT	Milk	Rabbit	54	ab92547	Abcam
HRP-linked anti-rabbit IgG	Primary dependant, 1:5000	Primary dependant	Goat		7074	Cell Signaling
HRP-linked anti-mouse IgG	Primary dependant, 1:5000	Primary dependant	Horse		7076	Cell Signaling

ON=overnight; RT=room temperature; PVP=5% polyvinylpyrolidine/TBST; Milk=5% milk/TBST

2.9.4 Analysis of secreted factors

GelMA and collagen-cultured cell-secreted chemokines were analysed through the novel electrochemiluminescent multiplex immunoassay platform Meso Scale Discovery (MSD). This MSD V-Plex human Cytokine kit (MesoScaleDiscovery) was used to measure the levels of 30 human cytokines in single samples, IFN-γ, IL-1α, IL-1β, IL-2, IL-4, IL-5, IL-6, IL-7, IL-8, IL-10. A total of 40 conditions were run on this assay, including supernatant from BxPC-3 and PANC-1 cells cultured in collagen, 5% and 7.5% GelMA and triple culture hydrogels as detailed below.

PANC-1 cells were grown either as monoculture or as triple culture in a 1:2:2 ratio with patient-derived CAFs and THP-1 for 14 days in either collagen, 5% or 7.5% GelMA. CAFs used for this experiment had been isolated from patient 3 (see Table 2.1). Appropriate monoculture controls were also included. Hydrogels were treated +/- fasudil (10 μM, Tocris) on day 7 and +/- gemcitabine/abraxane (100 nm each, donation from St Bartholomew's Hospital) as detailed in ROCK inhibitor and Chemotherapy: combinational studies. On day 14 of culture, supernatant was pulled for each condition into a single tube (Eppendorf), centrifuged at 1000 g for 5 min to remove cellular residuals and stored at -80°C. The MSD Cytokine kit (Meso Scale Discovery) was run in duplicates for each condition by Dr Juliana Candido, as per manufacturer's instructions. Plates were read on a MSD plate reader model 1250 (Meso Scale Discovery), in three separate batches. In order to account for inter-batch variability, values were normalized to controls present on each respective plate to generate a 'fold change' score compared to the controls.

2.10 Statistical analysis

All images, including micrographs, immunofluorescence, immunoblots, etc., were processed and analysed using ImageJ (NIH, US) with the exception of immunohistochemistry staining which were processed using Definiens Tissue Studio software (Definiens AG). Output files from flat-end indentation testing were processed in MATLAB R2019 (MathWorks). RNAseq analysis was performed by Dr Eleni Maniati in R 3.5.2 (R Foundation). All other numerical data were analysed and plotted on Prism v8.3 (GraphPad).

A Shapiro-Wilk test was used to check for data's normality. Significance was tested with a two-samples t-test (for normally-distributed data) or Mann-Whitney U test (for non-parametric data) and presented as mean ± standard deviation (SD), unless otherwise stated. Analysis of variance (ANOVA) with Bonferroni correction and Tuckey post-hoc analysis was used for comparisons amongst multiple groups, Kruskal-Wallis one-way ANOVA was used for non-parametric dataset comparisons. The statistical test conducted is explicitly stated in the caption of the corresponding graphs. Significance was conventionally reported as $p \leq 0.05$ (*), $p \leq 0.01$ (**), $p \leq 0.001$ (***).

Chapter 3 - Biomechanics and Matrix Proteins of the Tumour Microenvironment

3.1 Background

A high ECM content, stiffness and desmoplasia have been associated with poorer prognosis across a number of solid tumours, including PDAC and HGSOC [130,259]. In the pancreas, increased ECM remodelling and cross-linking result in progressive tissue stiffening concordant with disease progression from normal tissues (1 kPa) to PanIN (2 kPa) and PDAC (4 kPa) [128]. Pancreatic cancers are in fact, amongst the stiffest solid tumours [128], and this is reflected in the presence of a highly desmoplastic stroma. This increased matrix stiffness is documented to stimulate a number of pro-survival signalling pathways and cell behaviours including EMT [128], cell invasion [129], and treatment response [134,265]. Despite its established role in promoting tumorigenesis, the stiffness of patient-derived, fresh tumour tissues has not been extensively characterised in the organs of origin in either PDAC or HGSOC. Thus far, only two groups have investigated the effect of PDAC tissue stiffness on disease progression on murine[128] and human[130] specimens. Work performed in our Centre has previously shown a positive correlation between tissue stiffness and extent of disease in a multi-layered tumour microenvironment (TME) analysis of the omental metastases of HGSOC [123,259]. Therefore, I firstly aimed to characterise the biomechanics of diseased pancreas and ovary tissues and compare them to their healthy counterparts.

Recent work in HGSOC [259] began to shed some light into a common matrix signature (the 'matrix index') that is associated with poor prognosis and increased matrix stiffness. Although it was first characterised in HGSOC, this matrix signature was found to be a common denominator in a number of solid tumours including PDAC. Fibronectin (FN1), versican (VCAN) and collagen type-I alpha-1 (COL1A1) are part of this signature. Therefore, in addition to mechanical characterisation, I began investigating the ECM landscape and matrix proteins involved in increased tissue fibrosis and stiffness which, in PDAC, are poorly characterised.

Lastly, I sought to show that recapitulation of the measured stiffness could be achieved through the use of modular 3D cell culture platforms. For this purpose, I began characterising the mechanical properties of hydrogels commonly used for 3D cell culture (namely collagen type-I hydrogels) and that of semi-synthetic hydrogels, gelatin methacryloyl (GelMA). A simple adjustment in the initial GelMA polymer concentration (%wt/vol), and crosslinking time during hydrogel synthesis, resulted in a range of stiffness which was measured using unconfined compression and predicted with a simple mathematical model. I

hereby describe a thorough characterisation of the mechanical properties of GelMA hydrogels and how they can be exploited to model tissue stiffness *in vitro*. Matrix protein expression in these matrices was also investigated. This chapter provides the biomechanical framework in which the functional and transcriptomics characterisation of GelMA-embedded cells were later conducted.

3.2 Aim and objectives

In this Chapter, differences in stiffness between tumour-bearing and tumour-naïve tissues, as well as any direct correlations with matrix production, will be characterised and quantified. The biomechanics of human tissues will then be recapitulated using different 3D cell culture hydrogel models.

I will investigate:

- Alterations in tissue stiffness during disease progression in PDAC and HGSOC
- Involvement of matrix proteins in the modulation of stiffness
- Whether tissue stiffness can be mimicked and maintained in different 3D models
- Whether matrix production can be replicated upon cell culture in 3D models.

3.3 Results

3.3.1 Tissue stiffness is directly modulated by tumour burden

Flat-end indentation testing was conducted in order to quantify the mechanical properties of human tumour tissues and compare them to tumour-naïve tissues. Young's modulus (E) describes the stiffness of a given material and is defined by the relationship between stress (the force per unit area applied during indentation) and strain (the directional deformation of the specimen) during unidirectional deformation. Tissue modulus was measured on 5 normal and 3 diseased human ovary specimens as well as 4 matched (diseased and adjacent normal, total 8) and 2 diseased human pancreas samples. I hypothesised that tumour burden would impact the biomechanics of a sample at a whole-tissue level.

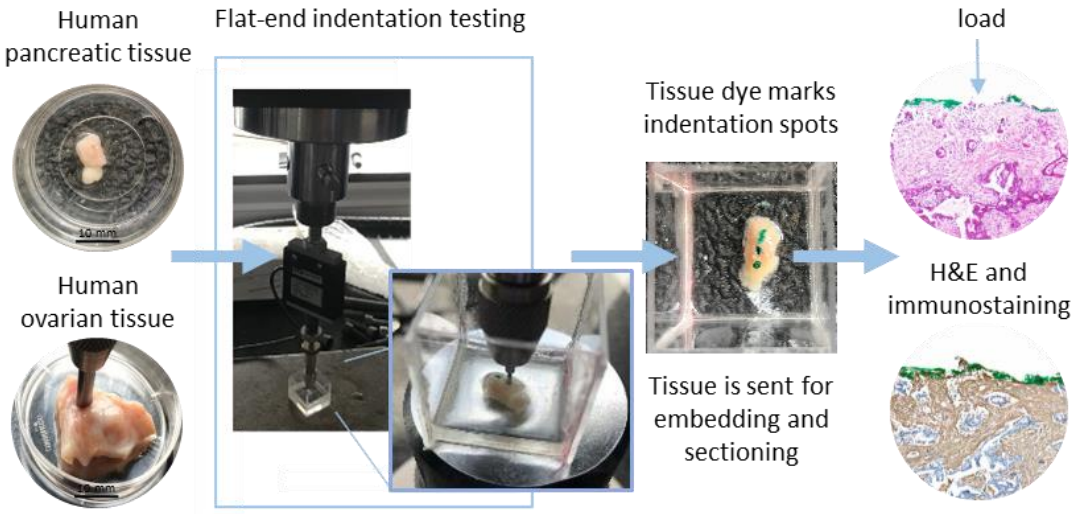

Figure 3.1 Schematic representation of patient-derived tissue analysis. Macroscopic images of human pancreas specimen and human ovary specimen (both non-diseased). Samples were taken for indentation testing in order to assess their mechanical properties. The setup included an Instron 5967 machine with a stage, sample holder, mobile 10N load cell and metallic indenter head. Green tissue dye was applied onto the indenter head just before testing. The sample was fully submerged in PBS during this procedure. The tissue dye marked the indentation spots after testing, therefore the sample could be fixed and taken for embedding ad sectioning, vertically along the indentation axis.

A 10 N load cell equipped with a flat, rigid cylindrical indenter head was used to measure tissue modulus of fresh, unfixed and fully-hydrated samples. The strain range was set at 20-30% with a 1% per second rate, meaning the sample was compressed to a maximum of 30% of its initial height in order to preserve tissue integrity. The deep modulus, defined as the modulus reached in the 10-30% strain region, was used for this analysis and graphed. Relaxation of the tissues was also measured. This is defined as the percentage recovery that the sample achieves after deformation, along the axis on which such deformation happened. For all analysed tissues, relaxation was near or >100% indicating the tissues exhibit a highly

viscoelastic behaviour. A green tissue dye was used on the indenter head during this process, allowing to exactly locate the indentation sports once the tissue had been sectioned. This allowed to perform direct correlation analyses between local tissue stiffness and protein expression as shown in Figure 3.1.

Mechanical testing of PDAC and tumour-adjacent normal tissues revealed a significant increase in Young's modulus in tumour compared to normal tissues (Figure 3.2). After indentation, histological analysis was performed to ensure the specimen either showed a normal pancreas structure or the typical PDAC features (Figure 3.3). The Young's modulus (10-20% strain) of histologically normal tissues was found to be 2.2 ± 0.2 kPa (n=4, mean ± SEM) while the modulus of tumour tissues was 7.4 ± 0.6 kPa (n=6), indicating a significant increase in tissue stiffness (Figure 3.2 a). Additionally, when plotted on a single histogram, the frequency of PDAC and normal tissues stiffness values produced two distinct peaks (Figure 3.2 b), indicating a separation in the value distributions. In the ovaries, the Young's modulus (20-30% strain) did not significantly differ in diseased tissues (8.52 ± 1.13 kPa, n=3) compared to healthy samples (8.85 ± 1.71 kPa, n=5), and this was reflected in the stiffness value frequency distribution plot, where the two peaks overlap with no clear separation (Figure 3.2 c-d).

It is worth mentioning that all "normal" and "healthy" ovary tissues had been removed during surgeries aimed at reducing the risk of some other gynaecological disorders, such as endometriosis in the case of oophorectomy. Bearing of another disease may have, per se, affected the stiffness of the "normal" ovaries due to local inflammation or abnormal function. For the analysis of ovarian tissues, five normal ovaries, one ovarian cancer and two high grade serous tissues were analysed. All HGSOC samples were from patients that had previously undergone chemotherapy which, in turn, would have affected the quality of the resected tissue, tumour, and its biomechanics. This might help explain why very little difference is seen in healthy versus diseased ovaries. Similarly, all matched "normal" pancreatic tissues were taken from patients with pancreatic cancers in a different site of the pancreas, but they underwent accurate histological characterisation following mechanical testing to ensure they could be classified as such. Our group did not have access to healthy pancreas as collection was not covered by the "Barts Pancreatic Tissue Bank" ethics.

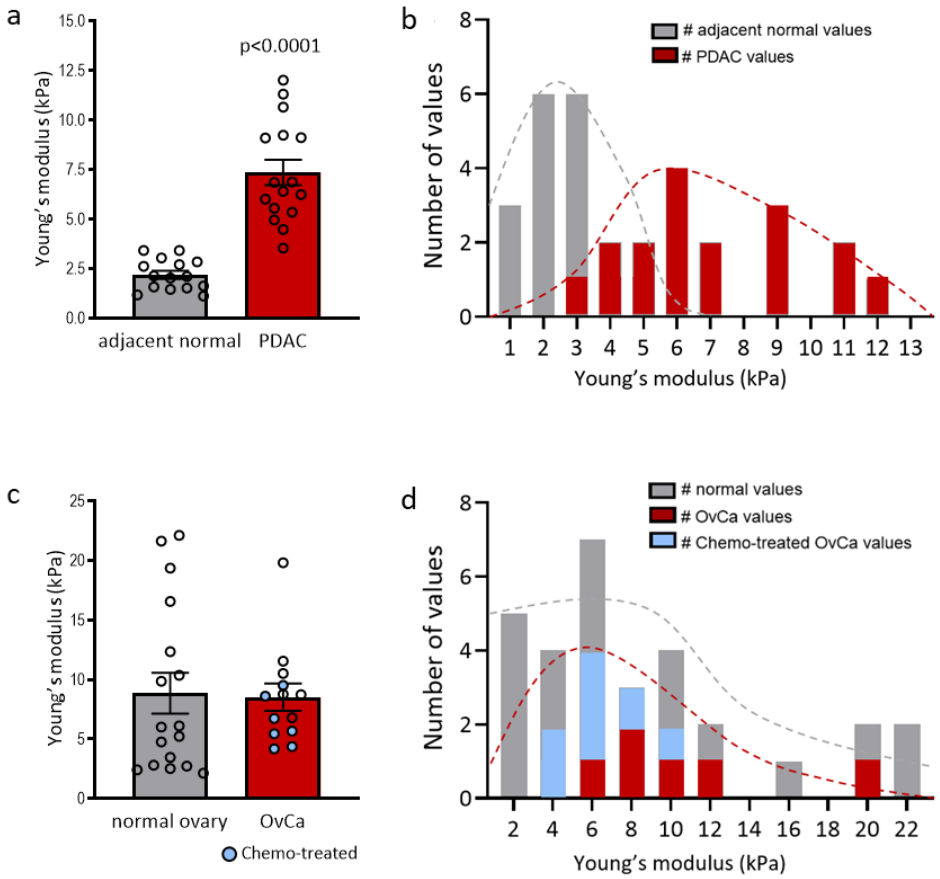

Figure 3.2 Stiffness analysis of fresh human (a-b) PDAC and (c-d) OvCa tumours and respective normal tissues. (a) Young's modulus of adjacent normal tissues (2.2 ± 0.2 kPa) and matched PDAC tissues (7.4 ± 0.6 kPa), n= 4 adjacent normal tissue and n=6 PDAC specimens, t-test <0.0001; **(b)** Pancreatic tissues stiffness values frequency histogram with distribution overlay reveals normal distribution of the two datasets with separated peaks, 4.86 kPa ± 3.23 kPa, 2 bin width (grey=number of adjacent tissue stiffness values, red=number of PDAC stiffness values); **(c)** Young's modulus of normal ovaries (8.85 ± 1.71 kPa) and non-matched OvCa tissues (8.52 ± 1.13 kPa), n=5 normal ovaries, n=2 HGSOC chemo-treated samples , n=1 OvCa treatment-naive sample, Mann-Whitney U test p=0.53; **(d)** Ovarian tissues stiffness values frequency histogram with distribution overlay reveals non-normal distribution of the datasets with no clear peak separation, 8.71 ± 5.88 kPa, 2 bin width (grey=number of normal ovary stiffness values, red=number OvCa stiffness values)

The use of green dye on the indenter head allowed to precisely locate the indentation spots from each tissue sections (Figure 3.3 a-b). Haematoxylin and eosin (H&E) micrographs (Figure 3.3 c, purple circles) showed the structure of normal pancreas with the typical acinar cell morphology. On the right (Figure 3.3 c, blue circles), the typical histomorphology of PDAC showed small to medium-sized irregular glands dispersed in a dense, desmoplastic stroma, consisting of ECM proteins, stromal and inflammatory cells (Figure 3.10, Figure 3.11) [5]. Neoplastic regions were characterised by a loss of the triangular acinar cell morphology. The irregular PDAC tumour glands resembled disorganised ducts and were morphologically extremely heterogeneous within and between patients. Other histological features that contribute to the grading and staging of PDAC include variability in cell size, shape and number (pleomorphism), nuclei (polymorphous) and mitotic state [5].

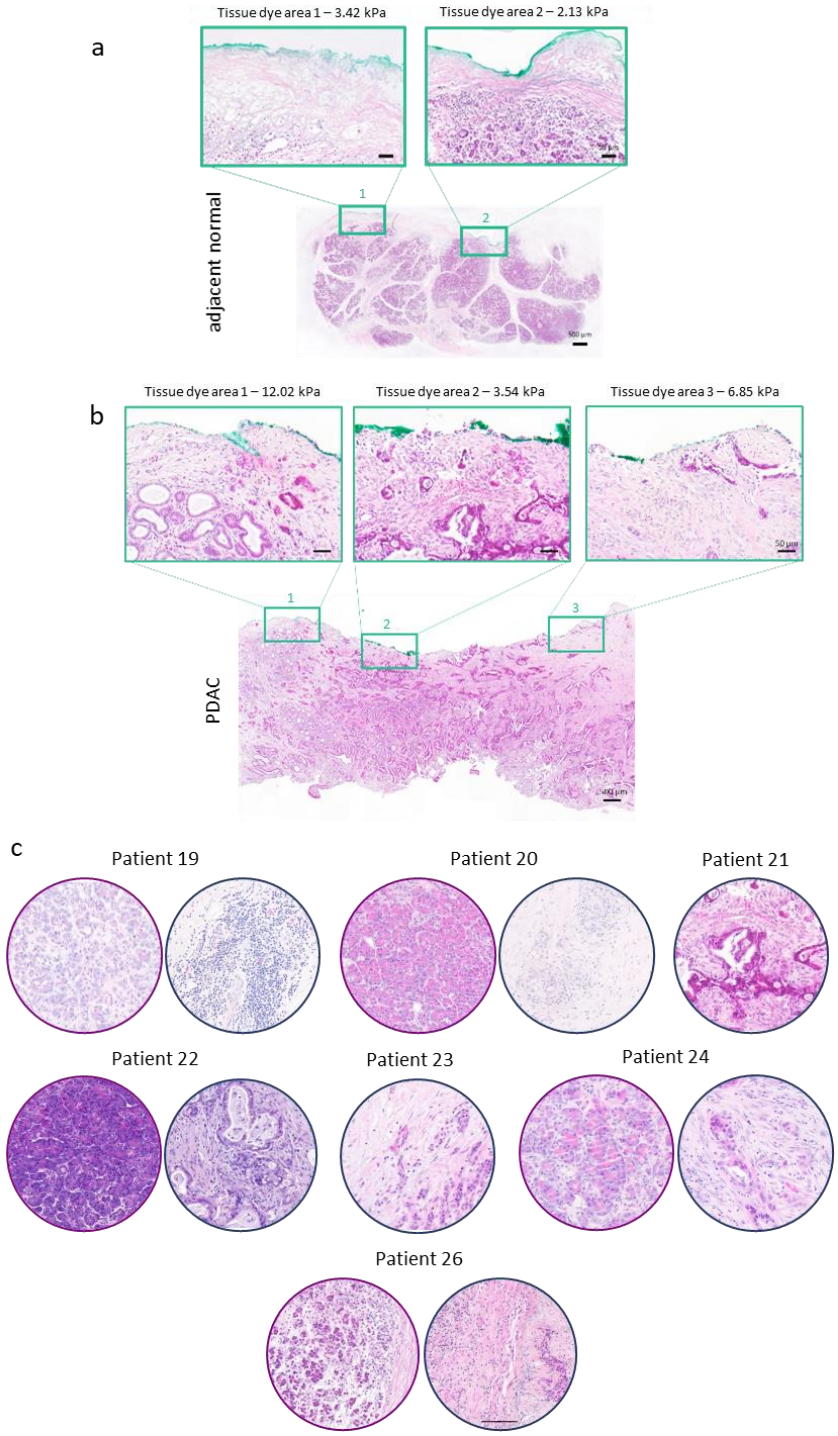

Figure 3.3 Representative haematoxylin and eosin (H&E) staining of (a) adjacent normal tissues and (b) PDAC tissues post-indentation. Green tissue dye marked the exact indentation spots, to which its specific Young's modulus value could be assigned. H&E micrographs depict a distinct desmoplastic reaction and altered structural features in diseased pancreas compared to its normal counterpart. Scale bars, 500 μm, inserts 50 μm; **(c)** Representative H&E staining of adjacent normal (purple circles) and diseased (blue circles) tissues from patients 19-26 (see Table 2.1). Scale bar applies to all, 50 μm.

To summarise, pancreatic tissue Young's moduli were significantly increased in tumour tissues compared to "adjacent normal" tissues. Such difference was not observed in the ovarian specimens when comparing "normal" ovaries to HGSOC ovaries; however, the latter group had a sample size which was too small to infer any significant differences.

3.3.2 High ECM protein content correlates with tissue stiffness in PDAC

In PDAC, increased desmoplasia, fibrosis and stiffness, accompanied by a loss of defined architectural features, such as the typical acinar cell structures, was already evident when looking at the H&E staining (Figure 3.3). For further characterisation, I submitted normal and PDAC samples for immunohistochemical (IHC) analysis after mechanical testing. Following on from the work of Pearce et al. [259], I sought to investigate and quantify the expression of proteins that are linked with poor overall survival and may be part of a common matrix response in solid tumours. In particular, I was interested in determining any potential correlations between matrix protein expression and tissue stiffness, which has not been done in PDAC.

IHC analysis was performed for FN1, VCAN, COL1 as well as Masson's Trichrome (MT) on post-indentation samples. The overall amount of chromogen (% area), brown in the case of IHC and blue representing all collagens from MT staining, was quantified using the Definiens Tissue Studio software (Definiens). Whole tissue analysis on serial sections was used for this analysis. All the investigated matrix proteins were upregulated in PDAC tissues compared to tumour-adjacent normal tissues from the same patient (Figure 3.4), indicating that tumour cells play a role in increased stiffness as well as ECM production. Distal "normal" specimens taken from diseased patients still retained a typical pancreas histology with clear acinar cell morphology and limited intracellular matrix secretion. MT stains blue all collagens and some fibrous connective tissues, while pink or red represent the cytoplasm, keratins and muscle fibres. Darker brown/black features represent cell nuclei. High amounts of disorganised "blue staining" in PDAC samples was indicative of increased tissue fibrosis and deregulated collagens and matrix production.

Despite the limited sample number, Definiens quantification of staining revealed a significant increase in the production of FN1 ($p=0.018$), VCAN ($p<0.0001$), COL1 ($p=0.031$) and overall collagens/connective tissue ($p=0.022$) in PDAC samples compared to matched tumour-adjacent normal samples (Figure 3.5). Collagen fibres and bundles thickness was quantified using CaseViewer (3DHISTECH) on the MT micrographs. Thickness analysis revealed an increase in collagen and connective tissue fibre diameter in PDAC tissues compared to tumour-adjacent normal (Figure 3.5 b). Diameter of fibres in PDAC tissues were over >4 times larger than adjacent tissues, suggesting single fibres might be merging together to form bigger bundles, contributing to crosslinking, fibrosis and tissue stiffening.

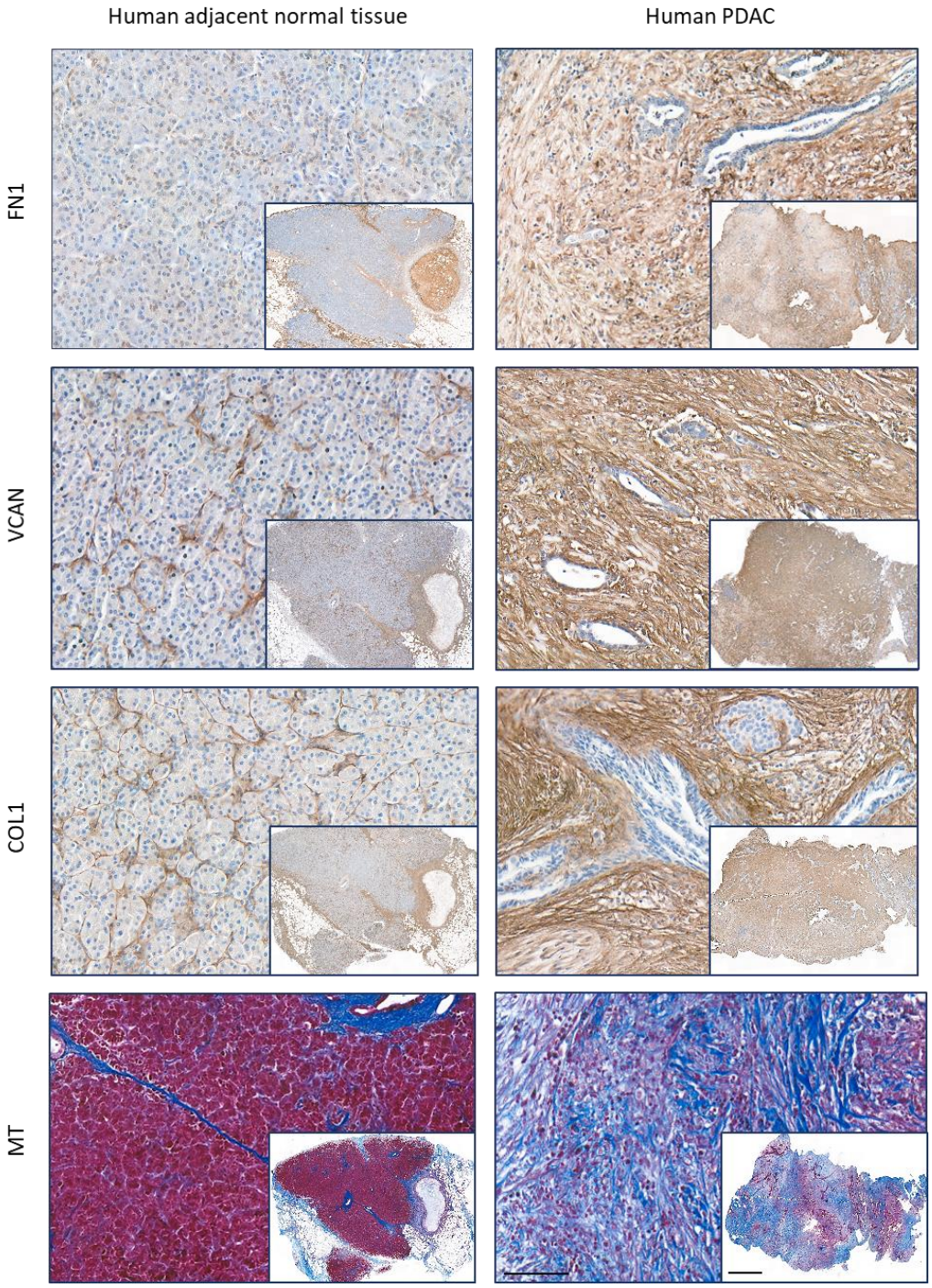

Figure 3.4 Immunostaining of the matrix proteins fibronectin (FN1), versican (VCAN), collagen-I (COL1) and Masson's Trichrome (MT) staining in a representative human tumour-adjacent normal (left) and matched PDAC tissue specimen (right). For FN1, VCAN and COL1, positive cells are visualised with DAB staining (brown chromogen). MT micrographs (bottom row) stain blue for collagens and some fibrous connective tissue, black for nuclei and pink/red for cytoplasm, keratins and muscle fibers. Normal pancreas (left) retained an orderly architecture with a typical acinar cell structure accompanied by overall low FN1, VCAN, COL1 and total collagens staining. PDAC tissues (right) presented with a fibrotic architecture, no clear exocrine cell structures and an overall increase in tumour-associated matrix production. Representative micrographs from patient 21 (see Table 2.1) are shown. Scale bars apply to all 100 μm, inserts 1000 μm.

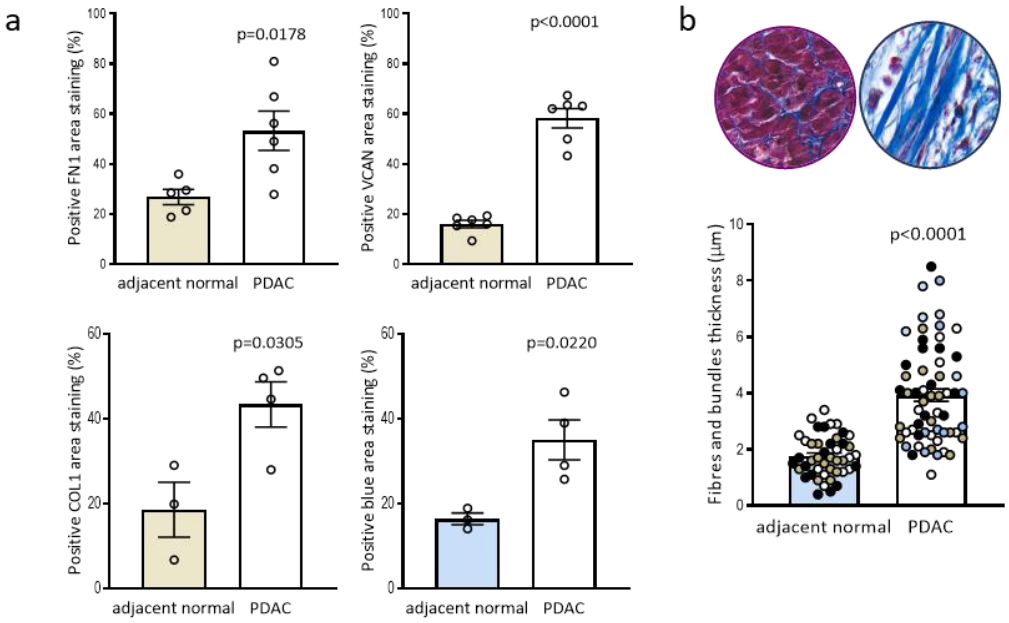

Figure 3.5 Expression of fibronectin (FN1), versican (VCAN), collagen-I (COL1), total collagen content (MT) and collagen fibre thickness is higher in PDAC compared to tumour-adjacent normal tissues. (a) Definiens Tissue Studio quantification of FN1, VCAN, COL1 and MT staining (representative micrographs shown in Figure 3.4). Each dot represents a different patient. For this analysis, stained percentage of total tissue area was calculated as follows: Positive protein area stained (%) = area IHC marker stained (μm^2)/total tissue area (μm^2). Mann-Whitney U-test, FN1 p=0.0178, VCAN p<0.0001, COL1 p=0.0305, total collagens p=0.0220. **(b)** Thickness quantification of collagen fibres and bundles in MT micrographs (blue staining), insert diameter 500 µm for scale. For this, three fields of view were taken per tissue at 63x magnification with five random areas quantified in each. Each colour represents a patient: black=patient 18, blue=patient 21, white= patient 22, brown=patient 24. Fibres in PDAC tissues were significantly thicker (3.93 ± 0.23 µm, n=60) compared to those in adjacent normal tissues (1.76 ± 0.11 µm, n=45), Mann-Whitney U-test p<0.0001.

I therefore hypothesised that fibre disorganisation, thickness and increased matrix production may be directly responsible for the observed increased tissue moduli. In order to investigate this further, I measured the percentage area stained from the regions immediately below the green tissue dye and matched it with the tissue stiffness, to unveil potential correlations between local matrix production and local stiffness (Figure 3.6 a). The analysis was performed on stained tissues from patients 20, 21, 22 (see Table 2.1), with 1-3 indentation points identifiable with green tissue dye in each sample. Of the three analysed proteins, VCAN expression showed the highest correlation with local stiffness (R^2=0.812, p<0.0001), followed by FN1 (R^2=0.634, p<0.001) and COL1 (R^2=0.613, p=0.0172; Figure 3.6 b). When taken alone (Figure 3.6 c), tumour samples showed lower correlation with stiffness (lower R^2), and showed a positive significant correlation only in the case of VCAN and COL1 (despite lower p-values). Unfortunately, only a few specimens fitted the criteria for this analysis (n=3 patients), hence a larger sample cohort would be needed to ascertain the robustness of these results. In the case of tumour tissue analysis (Figure 3.6 c), a larger

sample pool would potentially allow to detect much higher interpatient variability, greatly affecting the outcome of the analysis.

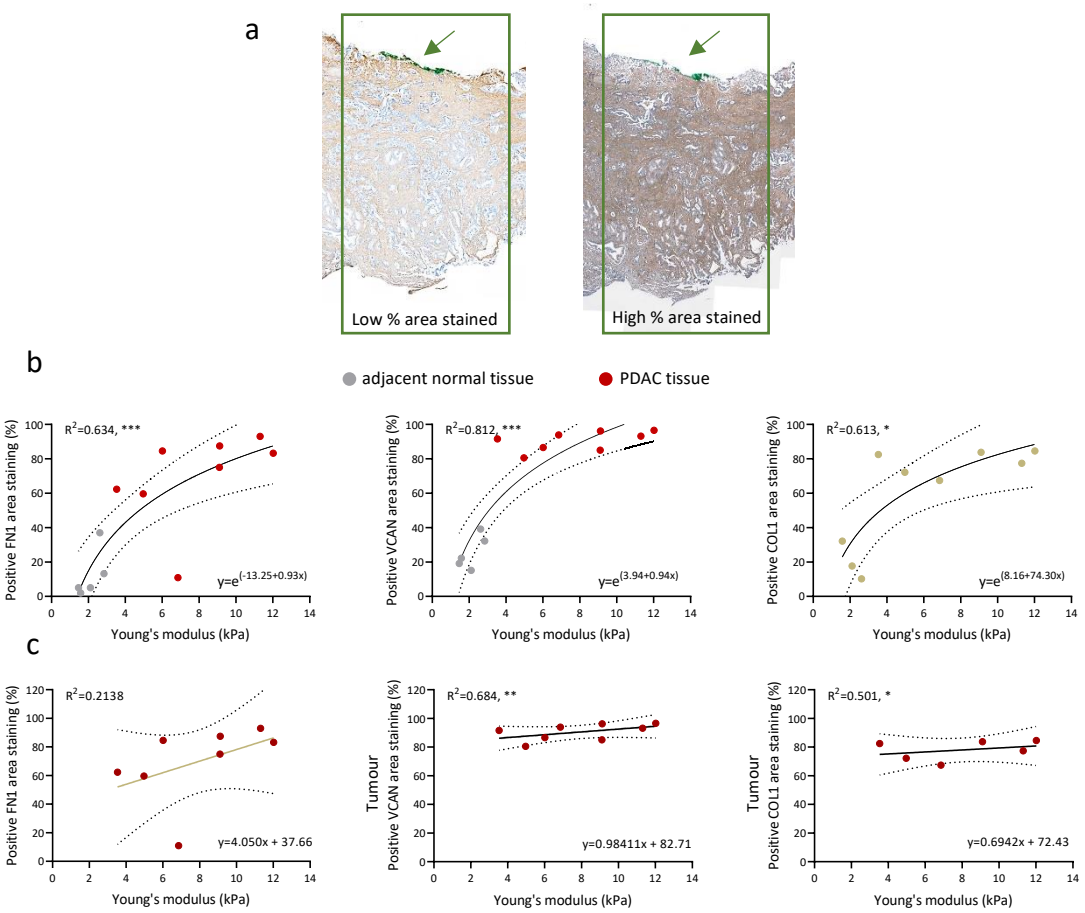

Figure 3.6 Correlation of precise local tissue stiffness and percentage stained area of FN1, VCAN and COL1 immediately below indentation location. (a) Green tissue dye (arrow) marked the exact location where mechanical testing (indentation) was performed. Green box (width 1 mm for scale) indicates the area, immediately below the testing area, which was used for staining analysis. Positive percentage area stained was calculated with the Definiens Tissue Studio software (Definiens). Representative micrographs show a low (left) and high (right) positive area staining of two different proteins (FN1 and VCAN) on the same tissue region (3.53 kPa); **(b)** XY plots of tissue stiffness (x-axis) and (%) positive area stained (y-axis) for FN1, VCAN and COL1. Semi-log curve fitting with 95% confidence band is shown, with line equation reported on the bottom right of each graph. Tissues from patients 20, 21, 22 (see Table 2.1) were used for this analysis. Spearman correlation, R^2 on graph, p=0.0011 (FN1), p<0.001 (VCAN), p=0.017 (COL1). (c) XY plots of tissue stiffness (x-axis) and (%) positive area stained (y-axis) for FN1, VCAN and COL1. Linear fitting with 95% confidence band shown for tumour tissues only, p=0.25 (FN1), p=0.019 (VCAN), p=0.053 (COL1).

In summary, correlations between matrix protein expression and tissue stiffness both at a whole-tissue level and subsequently at a local level were shown in this section. Expression of FN1, VCAN, COL1 as well as total collagens were significantly increased in PDAC tissues compared to tumour-adjacent normal tissues. Analysis of Masson's trichrome-stained collagen fibres revealed an increase in fibre size and bundle formation in diseased tissues. Finally, FN1, VCAN and COL1 were directly involved in matrix stiffening, as Young's modulus positively correlated with percentage area stained for the tested matrix proteins in the exact area of testing.

3.3.3 A tuneable 3D model mimics tumour stiffness

After characterising the stiffness of human tissues, I sought to investigate the mechanical properties of their murine tissue equivalents, as an additional comparison. Whole-tissue healthy ovaries and pancreas from female mice with Pax8-; Cre-p; p53 f/f; PTEN f/f; BrCa2 f/wt background were used for this. Following this characterisation, the range and biomechanics of human tissues was recapitulated with the use of 3D models. The elastic modulus of commonly-used collagen type-I gels, as well as that of semi-synthetic gelatin methacryloyl (GelMA) hydrogels, was assessed and compared to human data. GelMA allows precise tuning of the resulting hydrogel's mechanical properties through adjustment of the initial GelMA polymer concentration and crosslinking time. I was therefore able to establish a simple mathematical equation allowing the prediction of GelMA hydrogel stiffness based on the initial concentration (% wt/vol) and crosslinking time (min) used.

The tissue modulus of murine tissues was characterised via flat-end indentation of fresh, unfixed samples, the same technique used for human samples. For GelMA hydrogels, Young's modulus was calculated from whole-hydrogel compression data on an Instron E1000 machine and adjusted to be comparable to data obtained via indentation, as previously reported [263]. Because collagen gels presented irregular topographies, and were too soft to be tested via either indentation or compression, their Young's modulus was measured via rheometry on a Discovery Hybrid Rheometer (TA Instruments).

Despite providing a molecular, immunological and architecturally complex microenvironment, murine tissues were extremely soft compared to healthy human equivalents (Figure 3.7 a) and were therefore not a viable option for the recapitulation of human tissue stiffness. Collagen gels presented as soft matrices (1 mg/ml = 1.26 ± 0.04 kPa) even at increased concentrations (8 mg/ml collagen = 1.44 ± 0.085 kPa; Figure 3.7 d). Other standard matrices, such as 4.4, 8, and 17 mg/mL Matrigel have a stiffness of approximately 20, 70, and 300 Pa, respectively [266]. The stiffness range achieved with GelMA hydrogels was much greater (1.1 ± 0.5 kPa to 17 ± 2.35 kPa) and was tuneable by simply altering the initial GelMA polymer concentration (3–10% wt/vol). Based on experimental Young's modulus measurements, I optimised an equation which allowed the prediction of GelMA hydrogel stiffness based on UV crosslinking time and initial polymer concentration (Figure 3.7 b, d blue bars, 3% = 1.1 kPa, 5% = 3.4 kPa, 7.5% = 8.6 kPa, 10% = 16.6 kPa):

$$E = E_{max}\left(\frac{C}{100}\right)^{n}\left(1 - e^{-(t-A)/\tau}\right) \qquad \text{with } 3 \leq C \leq 20 \text{ and } 5 \leq t \leq 30$$

where the compressive modulus (E, kPa) of GelMA hydrogels was calculated based on GelMA polymer concentration (C, % wt/vol) and UV crosslinking time (t, min), with E_{max} corresponding to 7995, n=2.28, A=4.2 and τ =11.5. The modulus of cell-free GelMA hydrogels matched the prediction (Figure 3.7 d). Similarly to the human tissues, hydrogels exhibit highly viscoelastic properties reflected in high relaxation (~100%) values. Lastly, the stiffness of human tumour-adjacent normal and PDAC tissue samples closely resembled that of 5-7.5% GelMA hydrogels, hence why these conditions were chosen for treatment studies presented in Chapter 6. Collagen gels were used throughout this study as a soft matrix control as well as for their popularity and prominence as 3D cell culture system in the literature

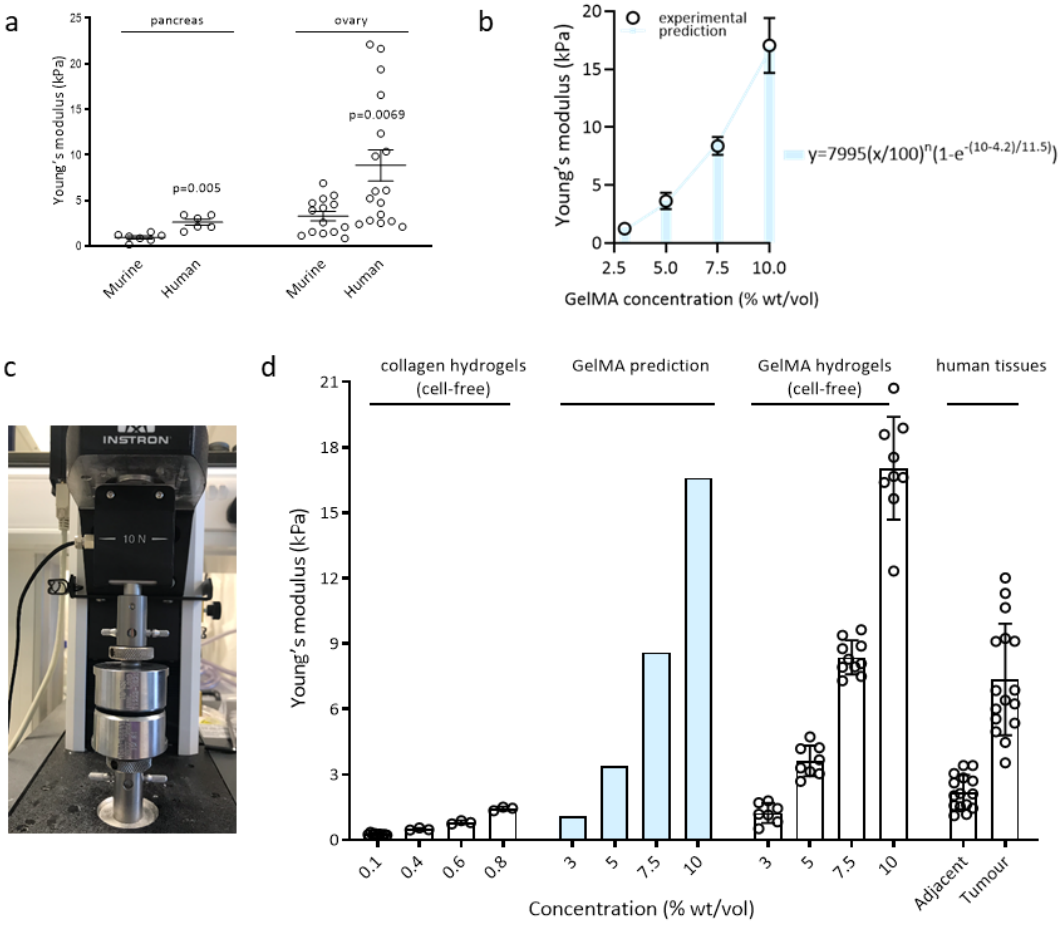

[31,147,204,367]

Figure 3.7. Biomechanical characterisation of murine and human tissues, collagen and GelMA hydrogels reveals tuneability of this semi-synthetic platform. (a) Characterisation of the mechanical properties of murine healthy pancreas and ovaries by indentation shows that in mice, these organs are much softer than their human equivalents. Pancreas: murine 0.96±0.44 kPa (n=7), human 2.62±0.78 kPa (n=4), Mann-Whitney U-test p=0.005; ovary: murine 3.30±1.9 kPa (n=14), human 8.84±7.1 kPa (n=5), Mann-Whitney U-test p=0.0069; **(b)** Measured Young's modulus of 3-10% wt/vol GelMA hydrogels (black) matches predicted stiffness (blue) as obtained with through our optimised equation. Experimental values: 3% GelMA 1.24±0.46 kPa, 5% GelMA 3.62±0.70 kPa, 7.5% GelMA 8.37±0.78 kPa, 10% GelMA 17.04±2.36 kPa. Predicted values: 3% GelMA= 1.1 kPa, 5% GelMA= 3.4 kPa, 7.5% GelMA= 8.6 kPa, 10% GelMA= 16.6 kPa; **(c)** Experimental setup for compression testing of GelMA hydrogels included an Instron E1000 machine equipped with a 10N load cell. **(d)** Young's modulus of acellular collagen (0.1-0.8% wt/vol) and GelMA (3-10% wt/vol) hydrogels as measured by rheometry and unconfined compression respectively (n=9). The blue bars represent the predicted stiffness for 3-10% wt/vol GelMA hydrogels after 10 min of crosslinking with a 365 nm wavelength. The Young's modulus of fresh adjacent non-diseased pancreas and PDAC tissues as measured by flat-end indentation (n=4, 6).

Next I wanted to ascertain whether the mechanical properties of the hydrogels were maintained upon incorporation of cells. For this I set up 3-10% (wt/vol) GelMA hydrogels with four commonly used PDAC cell lines: BxPC-3, Capan-2, MIAPaCa-2 and PANC-1. Cell-containing hydrogels were kept for 14 days in culture prior to mechanical testing. Hydrogel characterisation, functional analyses and viability of incorporated cells will be extensively described in Chapter 4. As shown in Figure 3.8 a, the stiffness of cell-containing GelMA hydrogels matched the prediction (n=5), where dotted lines represent prediction values for each stiffness. Hydrogel's Young's modulus was also maintained upon incorporation of the HGSOC cell line OvCar-4, as reported in our publication [235].

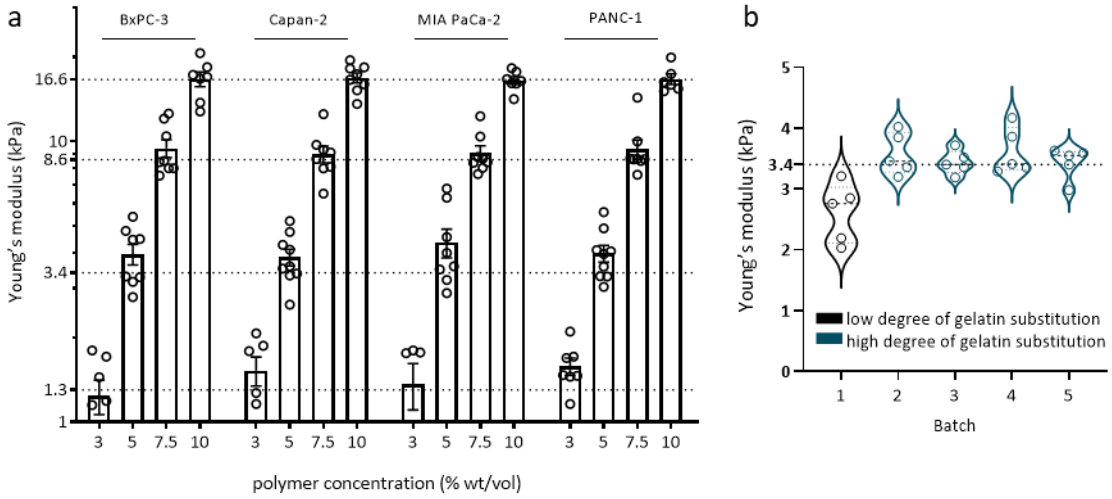

Figure 3.8 GelMA hydrogels are a tunable and reproducible platform for 3D stiffness modulation, even upon cell incorporation. (a) Young's modulus of cell-containing GelMA hydrogels at varying polymer concentrations (3-10% wt/vol) matched the prediction (dotted lines) upon incorporation of four PDAC cell lines at day 14 of culture. **(b)** Stiffness of 5% GelMA hydrogels using 5 different GelMA batches. Upon characterisation, Batch 1 showed low degree of methacryloyl substitution onto the gelatin backbone and was not used for 3D cell culture. Batches 2-5 produced hydrogels with consistent and reproducible stiffness.

Five different GelMA batches were synthesised by my group (Batch 1-5), of which Batches 3-5 were utilised in this thesis for 3D cell cultures. Figure 3.8 b shows no significant variation was found in the mechanical properties of hydrogels across the different batches used. The degree of methacryloyl substitution onto the gelatin backbone (GelMA's "degree of functionalisation" or DoF) was found to affect the mechanical properties of the resulting hydrogels. In particular, lower degree of substitution resulted in lower hydrogel crosslinking ability and therefore softer hydrogels (as it was the case with Batch 1). Hydrogels from batches with a low degree of substitution (<65%) do not follow the stiffness prediction described above and were therefore not used for this project. Low-degree-substitution batches are, however, widely used throughout the literature and have been reported to be softer compared to high-degree-substitution batches [242]. Quantification of the degree of

functionalisation for each batch will be detailed in Chapter 4, where the overall hydrogel and cell viability characterisation is analysed in more depth.

Overall, GelMA represented a suitable system for *in vitro* stiffness modulation. The resulting hydrogels had a stiffness ranging from 1 to 17 kPa making it a highly modular system when benchmarked against commonly used collagen gels. GelMA hydrogel's mechanical properties were predicted through a simple mathematical equation and reproducible across multiple batches, independent of cell incorporation.

3.3.4 GelMA and collagen hydrogels mimic key architectural features of PDAC tissues

3.3.4.1 The nanostructure of GelMA and collagen hydrogels

To further characterise these 3D cell culture systems, I investigated whether cells embedded in both matrices exhibited growth patterns and protein expression to resemble the architecture of native tissues. As shown in Figure 3.4, PDAC is characterised by a tightly packed interstitial ECM with very little vascularity. Like most epithelial tissues its stromal composition consists primarily of fibrous collagens assembled into bundles and fibrils. In addition to stiffness, recreating these architectural features is a prerequisite for a realistic model of the cellular TME for further functional and transcriptomics analyses. In order to validate collagen and GelMA hydrogels in this regard, their ultrastructure was determined via Scanning Electron Microscopy (SEM), and cellular structure via immunostaining.

For a more faithful recreation of tumour tissues, PANC-1 or BxPC-3 PDAC cells were embedded together with the monocytic cell line THP-1 and patient-derived CAFs (1:2:2 ratio) in both 0.1% collagen (1mg/ml) and 5% (wt/vol) GelMA hydrogels and grown for 14 days prior to SEM and IHC analyses. Both PDAC and THP-1 cells proliferated to form multicellular spheroids when cultured in the 3D models. Patient-derived CAFs had a much lower proliferation rate, even on tissue culture plastic, and in 3D they exhibited the typical elongated, fibroblastic morphology, remaining viable throughout the 14 days of culture.

The spatial distribution of cells and hydrogel topography differed between the two matrices. Qualitative analysis of GelMA hydrogels via SEM showed a highly compact and dense matrix in which cell clusters are interspersed (Figure 3.9 a-b). GelMA hydrogels presented as a much more compact matrix compared to collagen as their initial gelatin concentration (50 mg/ml) is 500-fold higher compared to that used for collagen gels synthesis (1 mg/ml). The pattern of cell growth in GelMA resembled tight cell clusters and multicellular spheroids surrounded by a dense cell- and hydrogel-derived matrix. Cells were therefore subjected to higher stiffness and interstitial pressure from their dense surroundings and exposed to higher matrix contents, similarly to what they would experience physiologically in tissues. Cross-sectional micrographs of the hydrogels showed an even distribution of spheroids (Figure 3.9 b). Some cells or entire clusters exhibited a 'budding' phenotype as they broke down the matrix and migrated out of the hydrogel. This phenotype was less prominent upon treatment with an broad-band MMP inhibitor, described later in Chapter 6.

Micrographs of collagen gels revealed the characteristic collagen fibres that these hydrogels are known to form during crosslinking (Figure 3.9 a-b). Despite the low concentration (0.1%), a high number of dense, disorganised fibres was observed. Quantification of collagen gel microfibres revealed a thickness of 23.5 ± 9.72 nm (n=4 gels), which was not quantifiable, with this resolution, in IHC micrographs (Figure 3.9 c). This is consistent with the reported average collagen microfibre (1-20 nm) and fibril (20-40 nm) diameter, which can generally range to up to 10 μm (fibres) and further increase to up to 1 cm once assembled in tissues [92]. Cells encapsulated within this hydrogel grew either as single cells or as cell clusters, in a disorganised fashion.

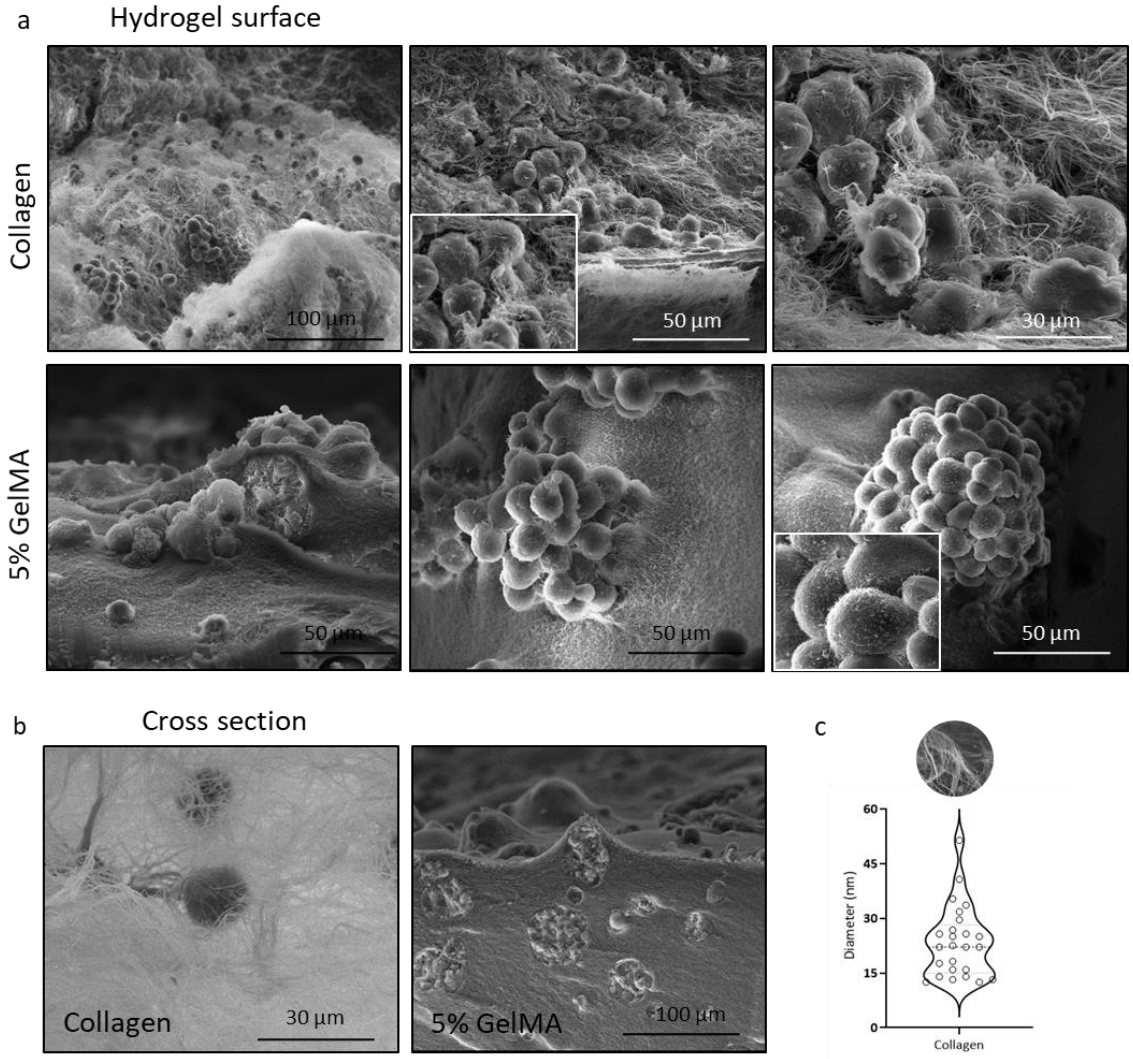

Figure 3.9 Characterisation of the nanostructure of collagen and GelMA hydrogels via Scanning Electron Microscopy (SEM). (a) Representative SEM micrographs of PANC-1 cells in collagen (upper row) and GelMA (bottom row) hydrogels at day 14 of culture. **(b)** Representative cross-section SEM micrographs of collagen and GelMA-encapsulated cells. Scale bars as indicated on each micrograph. **(c)** Analysis of collagen microfibre diameter as measured via ImageJ, average thickness= 23.5 ± 9.72 nm, n=4.

3.3.4.2 Extracellular components of the pancreatic TME

Given their biophysical properties, GelMA and collagen hydrogels provided adequate architectural support for the 3D culture of cells. Next, I sought to assess whether encapsulated cells displayed a matrix protein expression pattern similar to that observed in patient tissues. The pancreatic niche is composed of collagens, glycoproteins, proteoglycans, ECM regulators, ECM-affiliated proteins and secreted factors [268,269], whose different functions and contributions to pathogenesis were detailed in Section 1.2.2. Recent work by Tian and colleagues [86,87], characterised the first human PDAC matrisome revealing protein changes associated with human pancreatitis, PanIN and progression to PDAC. Stromal- and tumour-derived ECMs not only contribute to tissue architecture and stiffness (Figure 3.5, Figure 3.6) but also promote cancer cell behaviours and is consequently associated with clinical outcome [95,259]. I therefore assessed the expression of tumour-associated ECM proteins FN1, VCAN, COL1 and total collagens (MT) in cell-containing GelMA and collagen hydrogels and compared them to normal pancreas and PDAC tissues. For this, PDAC cells were co-cultured with THP-1 monocytes or in triple cultures with CAFs (1:2:2 ratio) for 14 days, as detailed in each figure legend.

Collagens make up the largest component of the PDAC-specific ECM [268]. Collagen type-I in particular is known to interact with a number of pro-survival signalling molecules including activation of focal adhesion kinase (FAK)[103] and Smad-interacting protein 1, which leading to a loss of E-cadherin, a crucial step during EMT [270]. High collagen type-I expression was found in both primary PDAC and metastatic lesions and was linked to an 8.2 months reduction in overall patient survival (6.4 months for high vs 14.6 months for low expression levels) [95]. Its abundance as a matrix protein, combined with its tumour-promoting and clinical role, make collagen a highly relevant and popular matrix for the 3D culture of PDAC cells. I therefore used collagen gels as a control matrix throughout this study. Because of their prominent role in PDAC progression, both COL1 and overall collagen expression was assessed via immunostaining in human tissues and 3D cell cultures (Figure 3.10, COL1 and MT). COL1 was highly upregulated in PDAC compared to adjacent tissues, and its expression was maintained in both 3D matrices. Both collagen and GelMA hydrogels provide a dense collagen-based scaffold (stained blue in MT) tightly surrounding cellular components, similarly to what is observed in PDAC tissues.

Fibronectin (FN1) is an ECM glycoprotein mainly secreted by pancreatic stellate cells and fibroblasts. Its main role is to bind to integrin receptors and collagens inducing cell-ECM

adhesion, cell migration and differentiation [271]. FN1 expression was highly upregulated in PDAC and maintained in the 3D cell cultures (Figure 3.10). Because of its interactions with collagens and the presence of gelatin-binding domains [109], FN1 immunostaining was positive in both GelMA and collagen, in the hydrogel itself. Its affinity to collagen and overexpression in tumours make FN1 a clinically relevant protein. In fact, FN1 has been reported to impede PDAC cell apoptosis and necrosis, leading to an increased tumour size in patients [124].

Although its role has not been well characterised in PDAC, versican (VCAN) is an ECM proteoglycan whose expression is driven by both epithelial and stromal cells [52]. Its accumulation is common during PDAC progression and correlates with CD8+ T cell exclusion [52]. Together with COL1 and FN1, VCAN is part of the "matrix index", a matrix signature common to many solid tumours and associated with poor prognosis [259]. VCAN protein expression increased from adjacent to PDAC tissues and was recapitulated in both collagen and GelMA 3D cell cultures (Figure 3.10). In GelMA triple cultures, all three cell types (PDAC and THP-1 cells, patient-derived CAFs) showed a high VCAN expression. The use of such 3D culture systems allows us to begin to investigate the cellular origin of ECM proteins in a direct and inexpensive fashion.

One of the most noticeable differences between hydrogel cultures and the human tissues was the level of cellularity, which is a common limitation of most *in vitro* culture systems. The average tumour is reported to contain around $1x10^5$ cells/μL [272] (or $1x10^8$ cells/ml) which is almost 300 times higher than the initial seeding density of GelMA monocultures ($3.5x10^5$ cells/ml) and almost 60 times higher than triple culture seeding densities ($1.75x10^6$ cells/ml). Patient-derived tissue and cell supply are the main limitations to increase cell numbers for 3D culture in these matrices. Very high seeding densities also resulted in high numbers of cells migrating out of the hydrogels during the 14 days of 3D culture.

Given that the expression of core matrix proteins was replicated in GelMA, I sought to investigate the expression of other PDAC-related markers in these hydrogels. Another key extracellular component of the pancreatic TME is hyaluronic acid (HA), a non-sulphated glycosaminoglycan known to be secreted by both tumour cells and CAFs. Similarly to COL1, HA expression was found in both primary and metastatic lesions, with high HA protein levels resulting in an average 15 months reduction in overall patient survival compared to low levels [95]. Among all ECM components, HA has been extensively studied in PDAC in relation to its high abundance and accumulation in the tumour [44], and its prominence in

clinical trials via pegylated recombinant human PH20 hyaluronidase (PEGPH20) depletion[46]. HA expression was assessed in human tissues and hydrogels via HA-binding protein (HABP) staining. HA was expressed in PDAC cell spheroids but not by the smaller THP-1 cell clusters (indicated by arrows, Figure 3.11).

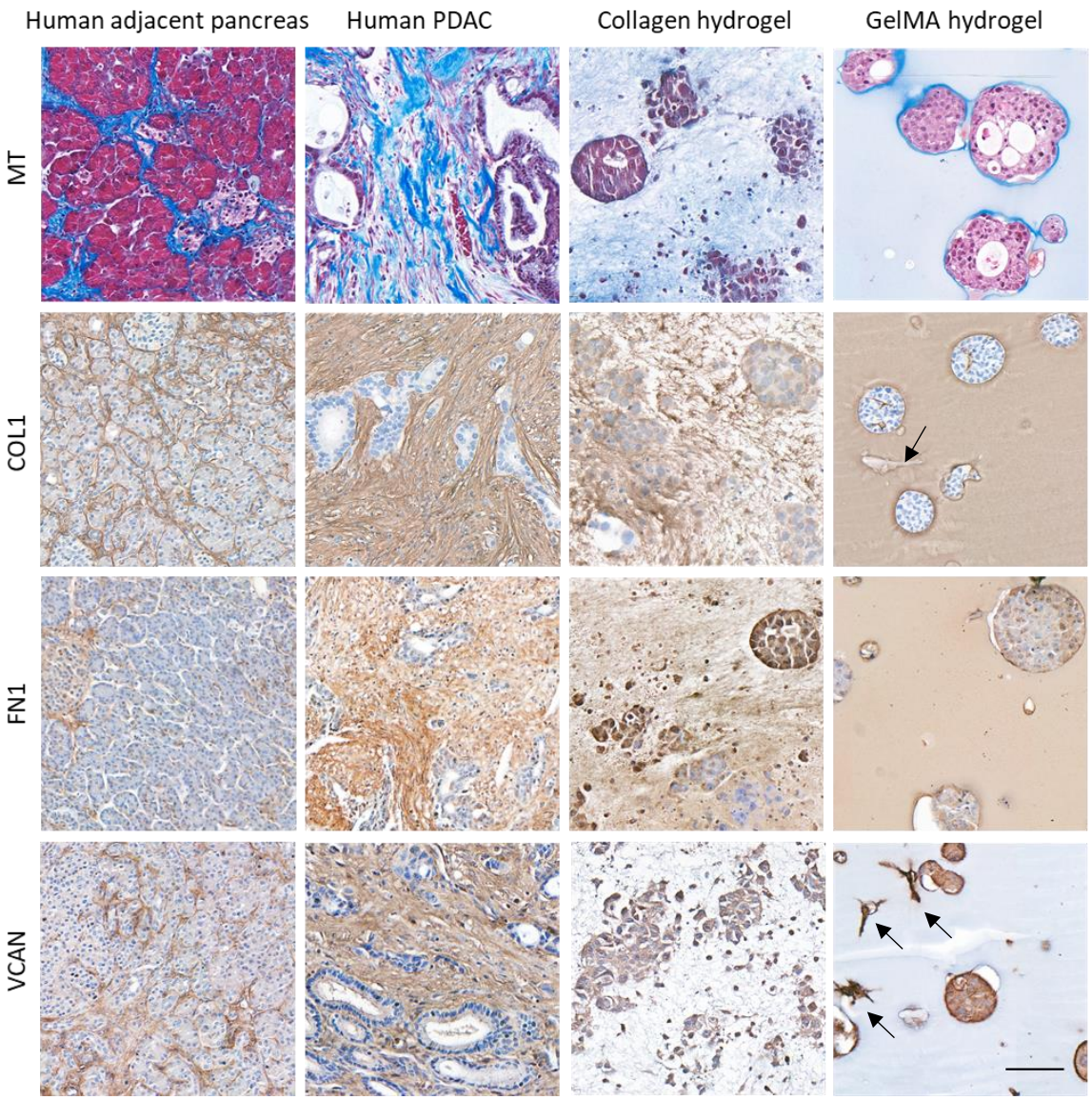

Figure 3.10 Immunostaining of FN1, VCAN, COL1 and total collagen (MT) staining in matched human tumour-adjacent pancreatic and PDAC tissues and in 3D triple cultures of PDAC and THP-1 cells and CAFs. FN, VCAN and COL1 positive cells are visualised with DAB staining (brown chromogen) while MT shows collagens stained blue. In the hydrogels, both THP-1 and PDAC cells grow as spherical multicellular aggregates while patient-derived CAFs (indicated by arrows) maintain their elongated fibroblastic morphology. Scale bar applies to all, 100 μm.

3.3.4.3 Cellular components of the pancreatic TME

Lastly, I investigated the expression of cellular components of the TME by imaging 3D cultures with cell type-specific markers (Figure 3.11). PDAC cells and THP-1 were co-cultured in 5% GelMA hydrogels for 4 days prior to immunostaining. Unfortunately, no

CAFs were incorporated for the purpose of this staining. Cytokeratin-19 (KRT19) is a cytoskeletal protein whose overexpression has been associated with PDAC tumorigenesis, progression and poor outcome[273]. KRT19 was used as a cancer marker and its expression in 3D cultures characterised further in Chapter 4. Additionally, KRT19 expression is linked to increased invasion and mechano-sensing via interactions with β-catenin and RAC1 [274]. More about the mechano-transduction pathways upregulated in GelMA-cultured cells will be discussed in Chapter 5. KRT19 was strongly expressed by PDAC cell spheroids in GelMA cultures, while absent in THP-1 clusters.

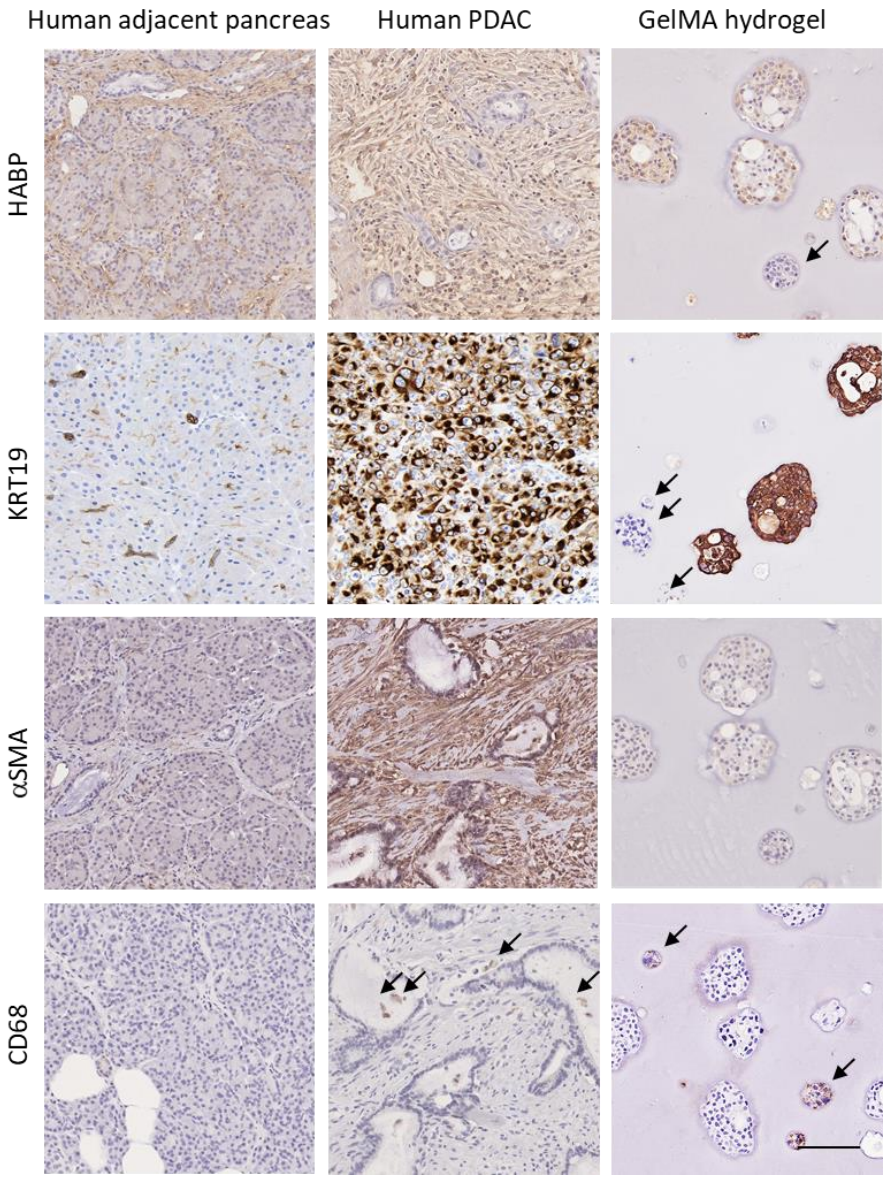

Figure 3.11 Immunostaining of KRT19, αSMA, CD68 and HABP in matched human tumour-adjacent pancreatic and PDAC tissues and 3D co-cultures of PDAC and THP-1 cells. Positive cells are visualised with DAB staining (brown chromogen). Arrows pointing at THP-1 spheroids, which become CD68 positive when co-cultured with cancer cells in GelMA. Scale bar applies to all, 100 μm.

Alpha-smooth muscle actin (αSMA) was used as a marker for CAFs. Immunostaining indicated both a higher αSMA expression and fibroblast disorganisation in PDAC tissues compared to tumour-adjacent normal tissues (Figure 3.11). PDAC and THP-1 co-cultures in GelMA showed no staining for this marker. In the future, it would be beneficial to repeat this stain on CAF-containing GelMA hydrogels to confirm the specificity of the stain. Finally, cluster of differentiation-68 (CD68) was used as a macrophage marker. Limited CD68+ cells were detected in our tissues (Figure 3.11). Interestingly in GelMA cultures, co-culture of PDAC cells with THP-1 monocytes led to differentiation of the latter into CD68+ macrophages.

In summary, the use of 3D culture approaches allowed us to begin to recapitulate some of the key architectural, cellular and extracellular features of the pancreatic TME. Upregulation of tumour-associated matrix proteins, such as FN1, VCAN, COL1 and HA, was observed in human PDAC compared to adjacent normal tissues and was induced in GelMA and collagen cultures. Patterns of cell growth and hydrogel nanostructure were visualised by SEM and IHC. Cellular components of the TME retained their cell-type-specific marker expression in the 3D matrices.

3.4 Conclusions

This chapter covered the characterisation of the biomechanics of human pancreatic and ovarian tissues and two 3D hydrogel-based cell culture models, using three techniques that can be applied for any biomaterial characterisation. Indentation testing revealed that for pancreatic tissues, tumours were significantly stiffer than matched, histologically normal tissues. Despite previous research having characterised the elastic modulus of human normal pancreas [275,276] and that of PDAC progression in mouse models [128], only one recent study has performed this analysis on fresh, human resected tissues [130]. As shown in Figure 3.7, murine tissues were softer than their human counterparts as well as more laborious compared to *in vitro* models.

My results show adjacent normal tissues had a stiffness of 2.2 ± 0.2 kPa which increased to 7.4 ± 0.6 kPa in matched tumours. This is consistent with previous work [130] where normal tissues where found to be 1.06 ± 0.25 kPa, increasing to 2.15 ± 0.41 kPa in pancreatitis and 5.46 ± 3.18 kPa in tumours. Though tumours are significantly stiffer in both cases, the adjacent tissues characterised in this study present a stiffness range that overlaps with that of chronic pancreatitis or PanIN of previous reports, being stiffer than normal tissues [130]. This is unsurprising as tumour-adjacent tissues probably present with a degree of inflammation accompanying the tumour, which might have still induced stromal activation, reduced permeability and increased tissue desmoplasia leading to higher tissue stiffness [277]. This was not the case for ovarian tissues, where no significant difference was found between diseased and healthy tissues (Figure 3.2). However, normal ovaries were surgically removed only when accompanying a gynaecological disorder, which might have contributed to an overall tissue inflammation and stiffening. Additionally, the tissues classed as ovarian tumours came from patients which had previously undergone chemotherapy. This affected the tissue architecture, cellularity (as detected by H&E staining, not shown) and, in turn, stiffness. Because of these limitations, ovarian tissues were not taken further for matrix protein analysis, which was instead conducted on pancreatic tissues.

Importantly, this analysis enabled me to directly compare these values to the stiffness of our 3D cultures, allowing for mechanics to be used as a readout. Over the last decades, basic research has begun to uncover the importance of substrate mechanics in the regulation of PDAC cell proliferation[128], invasion [129,278], EMT [128,203] and response to treatment [265,279]. However *in vivo*, stiffness is neither static or two-dimensional, and cell-ECM signalling has

been shown to play a role in governing tissue biomechanics [17,265]. My project focused on cell functions and molecular processes involved in proliferation and response to treatment, while being able to directly link these behaviours to changes substrate mechanics (Chapter 6).

I next conducted immunostaining for key ECM proteins on tissues post-mechanical testing. Unsurprisingly, the expression of all tested tumour-related matrix proteins, namely COL1, FN and VCAN, was significantly higher in tumour tissues compared to tumour-adjacent normal tissues. All three proteins, as well as overall collagen content, have been described as being highly expressed in PDAC and linked to shorter survival [52,95,124,268]. I also characterised collagen fibre thickness (Figure 3.5), which was significantly higher in tumour compared to tumour-adjacent tissues, similarly to previous reports [128]. Thanks to the use of tissue dye, I was next able to correlate percentage area marker stained with exact stiffness in each testing location, which is, to my knowledge, a novel characterisation technique. Ideally, I would like to extend this analysis to a larger sample pool (n>15), to increase the robustness and significance of the results.

Expression of all three proteins positively correlated with tissue stiffness, suggesting a combination of histological and mechanical assessment of the tumour may be predictive of disease. In physiologically normal conditions, soft and compliant matrices are rich in proteoglycans (such as VCAN) and hyaluronan, while rigid and stiff matrices are enriched in collagens and fibrous proteins (such as fibronectin) [118]. However, in disease, deregulated matrix production leads to a disturbance in tissue architecture and function. Proteins like VCAN, transit to a more fibrous, highly cross-linked ECM, which is conductive of tissue stiffening, promoting tumour cell proliferation [119]. Such ECM disturbance may impact the course of pathogenesis and also offer alternative therapeutic and/or stroma-targeting strategies (as it is the case for PEGPH20) [46,47,117].

Next, I characterised the mechanical properties of commonly-used collagen type-I gels and GelMA-based hydrogels. The stiffness of 3-10% (wt/vol) GelMA ranged between 1 to 17 kPa, which is in concordance with the literature [230,242]. Stiffness was highly reproducible across different batches and influenced by the degree of methacryloyl (MA) substitution onto the gelatin backbone [242]. Additionally, a simple mathematical relationship was established to predict GelMA hydrogel stiffness based on the initial concentration and crosslinking parameters. As this is only valid for GelMA with a high degree of substitution (DoF ≥ 65%), future work should consider into including the degree of substitution as a further parameter

in the equation. This tuneability, reproducibility and stiffness range is one of the key advantages of GelMA hydrogels over the commonly-used collagen type-I gels.
In order to be able to investigate stiffness changes upon treatment (Chapter 6), mechanical properties of both hydrogel platforms had to be maintained upon cell incorporation (Figure 3.8). Cell contractility, matrix protein production and deposition, matrix digestion and crosslinking, are processes which will be investigated in more detail in the following chapters, in relation to their association with matrix stiffness. For consistency, mechanical properties were assessed at day 14 of 3D cell culture throughout this study with limited variation in the final concentration of cells embedded in order to achieve comparable results between experimental conditions. Since cancer cells themselves are softer (~400-900 Pa) than the matrices they are embedded in, reasonable variations in cell numbers alone is not likely to be responsible for matrix stiffening [280].

Lastly, I wanted to ensure that the production of key pancreatic TME proteins by cancer and stromal cells would be maintained in the 3D culture systems. SEM analysis of the nanostructure of GelMA and collagen hydrogels revealed the pattern of cell growth differed between both models. Up to 80-90% of pancreatic tumours, depending on reports, can be made up by ECM and stroma, with very little vascularity and only a fraction of the tumour bulk comprising cancer cells [59,192,281]. With this in mind, GelMA hydrogels provided a dense, compact matrix, in which cancer cells grew as multicellular spheroids (Figure 3.9). In addition to structural support, GelMA-embedded cells retained the expression of key extracellular and cell-specific markers, namely FN1, VCAN, COL1, HA and KRT19, CD68. PDAC spheroids expressed all the tumour-associated ECM markers analysed, with darker stain rims along the spheroid edges, suggesting cells were able to produce they own matrix within the hydrogels. Further proteomics analyses could be conducted on these matrices to characterise overall changes in matrix molecules with successive incorporation of additional cellular components or, later on, with treatment.

Starting with the patient material available, my initial aim was to understand tissue biomechanics and related ECM protein expression in order to recapitulate them with the use of 3D cell culture platforms. The presented 3D culture approaches were able to mimic some of the key biomechanical, architectural, cellular and extracellular features of the PDAC microenvironment. The next chapters will focus on characterising behaviours, functions and transcriptomics of GelMA-encapsulated cells in order to decipher and target processes related to the mechano-biology of PDAC.

Chapter 4 - GelMA Hydrogels as a 3D Platform to Study Cell Behaviours

4.1 Background

The use of 3D cell culture platforms is an innovative and fairly recent approach to bridging the gap between traditional 2D cell culture, animal models, and clinical results. The advantages of such models include control over the inclusion of cellular and extracellular components of the TME, in order to unveil their individual and joint contributions to disease and treatment [249]. Increased need for biologically and architecturally accurate model systems has led to the development of a plethora of 3D platforms, with hydrogels (whether naturally-derived, semi-synthetic or synthetic) being of particular interest due to their rheology, and relatively easy and inexpensive synthesis.

Our group's 3D cell culture platform of choice is based on the use of a semi-synthetic biomaterial, named gelatin methacryloyl (GelMA), and its ability to crosslink to via photo-polymerisation to form biocompatible hydrogels. GelMA combines the advantages of both natural and synthetic hydrogels by retaining integrin cell-binding and protease-cleavage domains (from the gelatin backbone), as well as the chemically reactive substitution groups (methacryloyl groups) that allow tunable and reproducible mechanical and chemical properties [229]. This allows for cell adhesion, proliferation, migration and proteolytic degradation to take place within the hydrogel, while allowing the operator to finely tune hydrogel crosslinking and stiffness parameters (such as time, energy, source, photo-initiator, concentration, degree of substitution, etc.).

In the previous chapter, I have shown how GelMA's properties can be altered to obtain a desired hydrogel stiffness to match physiological conditions, and how expression of key matrix proteins was maintained by GelMA-embedded cells. In this chapter, I explore the establishment of GelMA as a novel PDAC cell culture system and how this was used to conduct a range of quantitative *in vitro* and *in vivo* analyses. I also describe validation steps for the characterisation of GelMA itself (degree of substitution) as well as the development of protocols for hydrogel digestion, cell recovery [235] and downstream gene and protein analyses.

Although GelMA has been studied for decades [236], its implementation as a cell culture system dates back to less than ten years ago [229], and almost exclusively limited to applications in the field of tissue engineering and regenerative medicine [231,232,238,250,251]. A handful of groups have now used GelMA as a cancer cell culture platform, mainly focusing on ovarian [235,252], glioblastoma [253,254], breast [255,256], prostate [257,258] and more recently colon cancer (Loessner,

Ryan unpublished). Thus far, there have been no reported uses of GelMA for the study of pancreatic cancer and the inclusion of patient-derived cells.

Following the approximation of the fibrotic PDAC matrix stiffness and tissue architecture (Chapter 3), the model was subjected to a systematic characterisation of GelMA-embedded cell behaviours and how these were altered in response to physicochemical changes. Finally, I looked at the incorporation of additional cell types for the formation of a multicellular pancreatic TME model. I assessed the effects of the inclusion of stromal and myeloid cells on cancer cell proliferation, matrix stiffness as well as *in vivo* tumorigenicity. The use of such 3D cell culture model allowed me to begin to evaluate the individual contributions of different elements of the pancreatic TME in cancer-related processes.

4.2 Aim and objectives

The aim of this chapter is to characterise GelMA hydrogels and assess their potential as a 3D PDAC cell culture system, by investigating various cancer cell functions in hydrogels with different biomechanical properties. I also aimed to increase the complexity of the model, by studying cancer cell interactions with additional cellular components of the TME and their effect on matrix stiffness.

I will:

- Characterise GelMA's degree of substitution (batch-to-batch consistency)
- Analyse biological characteristics and functions of GelMA-embedded cells
- Optimise techniques required for the analysis of GelMA-embedded cells
- Assess the degree of UV-induced DNA-damage in GelMA
- Understand the effects of additional TME components and multicellularity in GelMA hydrogels and how these affect cell growth, *in vivo* tumorigenicity, cytokine secretion and pro-survival signalling pathways

4.3 Results

4.3.1 Degree of functionalisation analyses show high GelMA batch consistency

In recent years, gelatin-methacryloyl (GelMA) has become one of the most commonly used photocrosslinkable materials in bio-applications [262]. The 'degree of substitution' or 'degree of functionalisation' (DoF) refers to the amount (%) of methacrylic anhydride (MA) that attaches onto the gelatin primary amine groups during GelMA synthesis (Figure 4.1 a). DoF can be broadly classified into high (≥65%), medium (30%≥ x ≥65%) or low (<30%). The DoF directly regulates the amount of crosslinking that the hydrogel can undergo during UV polymerisation, and therefore directly affects hydrogel's physicochemical properties, its highest achievable density, stiffness and porosity, all factors which ultimately affect cell behaviour. When other parameters (such as concentration and crosslinking time) are unchanged, a higher DoF leads to stiffer hydrogels, higher cross-linking density, improved shape maintenance[230], decreased pore size[246] and, importantly, higher consistency between hydrogels. Since cell behaviour can be influenced by these factors, and since hydrogel stiffness was used as a readout, I used DoF as a batch quality control to ensure result reproducibility. For my purposes, a high DoF was desirable as it resulted in higher consistency of crosslinked hydrogels.

After synthesis of each batch, I employed various analytical techniques in order to determine the DoF and conducted mechanical analysis of the resulting hydrogels (Figure 3.8 b). Most DoF characterisation methods work through quantifying the amount of free primary amine groups that are present on the gelatin backbone [229]. Since MA binds to amine groups during GelMA synthesis, a higher degree of substitution will lead to a lower amount of free amine groups. Colorimetric assays allow to compare the fluorescence/absorbance of GelMA against the gelatin used for its synthesis, and to infer DoF from the spectroscopy shift [229]. Three such methods were employed for DoF analysis of our in-house batch 1 (low DoF control) and batches 3-5 (used throughout this study): namely ninhydrin, fluoraldehyde and 2,4,6-trinitrobenzenesulfonic acid (TNBS) assays (Figure 4.1 b). All three methods returned consistent results with no significant difference between different methods used or between different batches (3-5). Our low DoF control batch 1 showed higher variation in the results as well as higher variation in the stiffness of the resulting hydrogels (Figure 3.8 b) underlining the importance, for the purpose of this study, of using higher DoF batches. These assays

work with the assumption that the reduction in free amine groups is solely due to MA substitution with 100% substitution efficiency. As this is not always the case, these methods tend to overestimate GelMA's DoF.

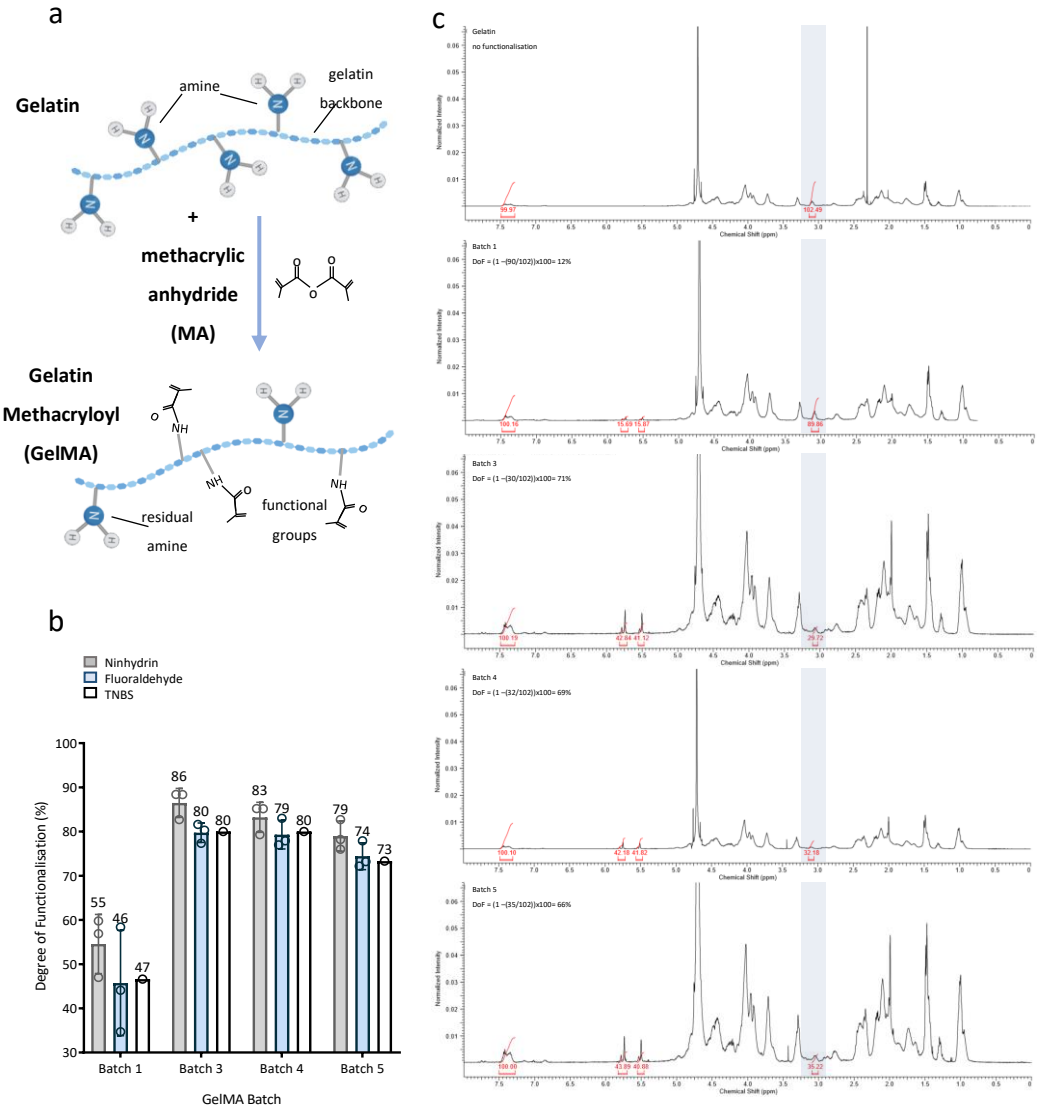

Figure 4.1 Analysis of GelMA degree of functionalisation (DoF) via spectrophotometric and ^{1}H NMR. **(a)** Schematic representation of the synthesis of gelatin methacryloyl (GelMA) through functionalisation of gelatin's primary amine groups by methacrylic anhydride (MA) addition. The DoF is defined as the percentage of MA substitution (functional groups) onto primary amines. The less residual amine groups are left onto the GelMA gelatin backbone, the higher the DoF is. GelMA's DoF can be adjusted by changing synthesis parameters such as MA feed ratio, gelatin concentration, reaction temperature to obtain GelMA with defined high, medium or low DoF. **(b)** GelMA DoF for batches 1 (low DoF), 3-5 (high DoF) as measured through three independent assays: ninhydrin (n=3), fluoraldehyde (n=3) and 2,4,6-trinitrobenzenesulfonic acid (TNBS) (n=1). All three assays are indirect measures of DoF through quantification of free amine groups in GelMA's gelatin backbone and comparison against unfunctionalised gelatin. Only batches 3-5 were used for this project. **(c)** Proton nuclear magnetic resonance (^{1}H NMR) spectra of gelatin and GelMA batches 1, 3-5 for DoF verification. The blue band highlights the lysine methylene proton peak for each spectra, where λ is the measured area under the peak. Higher λ indicates higher number of methylene protons (2H) of unreacted lysine groups.

To validate these results, proton nuclear magnetic resonance (^{1}H NMR) was performed on unfunctionalised gelatin and the different GelMA batches (Figure 4.1 c). This method looks at the lysine methylene proton present on the carbon atom that joins to the amino group (where the MA functionalisation takes place). This proton is known to give a peak (highlighted in blue in Figure 4.1 c) at 3 parts per million (ppm). The peak was highest in the gelatin NMR spectra and decreased as the amino group was connected to a methacryloyl group in GelMA. The annotated values indicate the integration number of each peak (λ), reflecting the area under the peak. DoF was calculated from the gelatin and GelMA NMR spectra, as follows:

$$DoF = \left[1 - \left(\frac{\lambda\ of\ lysine\ methylene\ proton\ of\ GelMA}{\lambda\ of\ lysisne\ methylene\ proton\ of\ gelatin}\right)\right] \times 100\%$$

The resulting DoF calculated were 12% for batch 1, 71% for batch 3, 69% for batch 4 and 66% for batch 5. The accuracy on this method rests on the assumption that MA functionalisation will not be affecting proton distribution on any of the remaining free amino groups. Since this is not always the case, this method could be slightly underestimating the overall DoF.

To summarise, all batches used during this study had a high degree of substitution when measured with both indirect amine quantification methods (73-86%) or ^{1}H NMR (66-71%). No single method gave an absolute quantification of MA functionalisation onto gelatin, however batch-to-batch consistency was evident regardless of the method used. Additional controls such as hydrogel stiffness and nanostructure were discussed in the previous chapter. A consistent, high DoF was important for reproducibility and consistency in GelMA hydrogel stiffness, stiffness predictability, biochemical properties and, in turn, biological effects.

4.3.2 GelMA hydrogels as a 3D platform to study cell behaviour

4.3.2.1 GelMA supports cell viability, proliferation and long-term 3D cell culture

Following mechanical and chemical characterisation of GelMA hydrogels, I aimed to assess the suitability of GelMA-based hydrogels for biological applications in PDAC research. Cell viability is a crucial parameter that any platform designed for cell culture must adequately support. For this, I incorporated BxPc-3, Capan-2, MIAPaCa-2, PANC-1 PDAC cells and the HGSOC cell line OvCar4 in 5% (wt/vol) GelMA hydrogels and observed the pattern of cell growth over time. A live/dead assay was used, looking at esterase activity (494/517 nm: calcein-AM Ca-AM) and loss of membrane integrity (528/617 nm: ethidium homodimer-1 Et-H1) as proxies for cell viability and cell death, respectively. Brightfield micrographs as well as live/dead confocal analysis of the cultures was conducted on day 1, 7, 14 and 28 post cell-encapsulation.

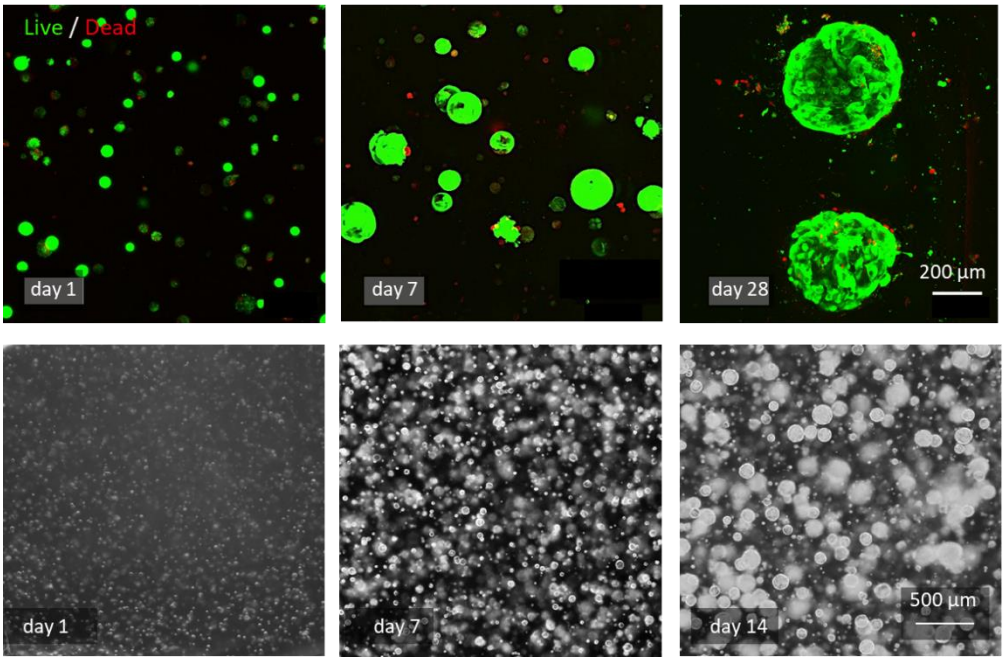

Figure 4.2 Cell proliferation and viability of OvCar4 cells in GelMA hydrogels. (top) Confocal z-stack micrographs show a high cell viability on day 1 to 14; live OvCar-4 cells were stained with green-fluorescent calcein-AM (Ca-AM, 494/517 nm); dead cells were stained with red-fluorescent ethidium homodimer-1 (Et-H1, 528/617 nm). Scale bar, 200 µm, applies to all. **(bottom)** Representative brightfield images indicate that GelMA hydrogels supported OvCar4 cell growth after encapsulation in 5% GelMA and allowed multicellular spheroids formation over 14 days of culture. Scale bar 500 µm, applies to all.

OvCar4 cells formed multicellular spheroids (Figure 4.2) already visible at day 7 of culture and ranging up to 500 µm in diameter by day 28 (Figure 4.3 a). Cells maintained a high viability throughout culture in GelMA, as indicated by the low amounts of red Et-H1 dye compared to green, viable cells. Spheroid diameter analysis revealed an increase from an

average 81.5 ± 64 μm on day 14 to almost double to 154.7 ± 101 μm on day 28 of culture (Figure 4.3 a). Heterogeneity of spheroid size is reflected in a large SD for these measurements.

The same analysis was conducted on four PDAC cell lines. Similarly to OvCar4, PDAC cell lines proliferated in 5% (wt/vol) GelMA to form spheroids by day 14 of culture, after which the hydrogels appeared overcrowded and cells began to migrate out of the hydrogel towards the bottom of the wells. Cultures were therefore kept for 14 days to prevent cell loss. Diameter quantification at day 14 of culture suggested that different cell lines proliferated at different rates within 5% GelMA hydrogels, reflected in different spheroid sizes, with MIA PaCA-2 cell forming the largest spheroids (188.7 μm), followed by PANC-1 (170.2 μm), Capan-2 (79.5 μm) and BxPC-2 (78.0 μm).

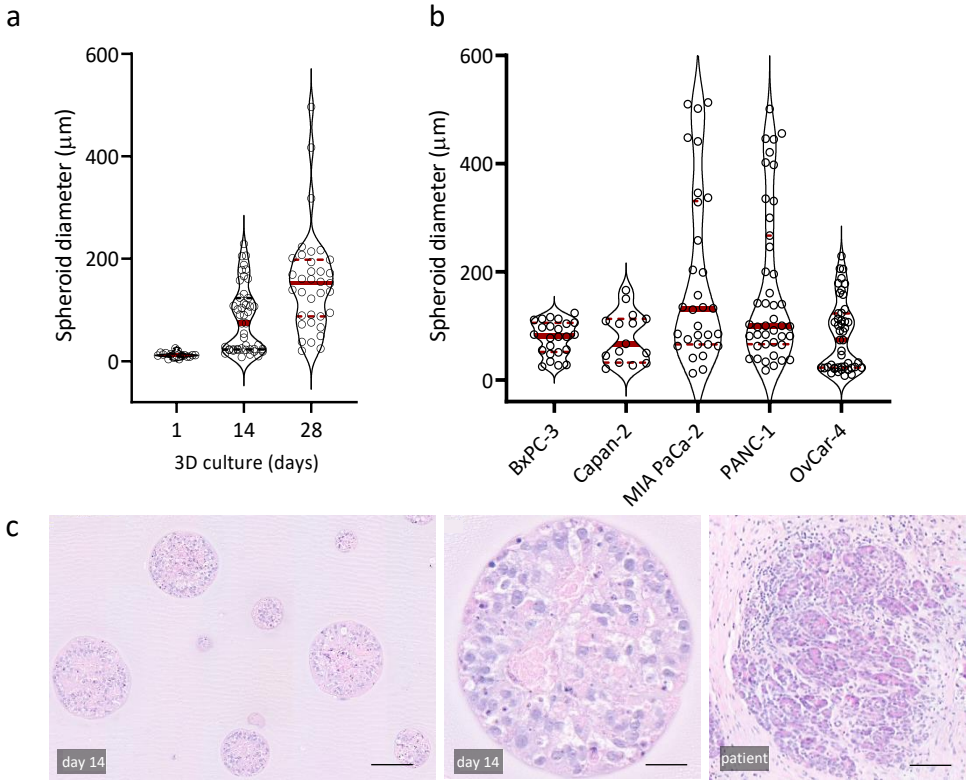

Figure 4.3 Spheroid-forming ability of HGSOC and PDAC cell lines in 5% GelMA. (a) Quantification of OvCar-4 spheroid diameter (μm) from day 1 to 28 of culture as measured via ImageJ. Median and interquartile ranges shown. **(b)** Quantification of spheroid diameter (μm) of 5 PDAC and HGSOC cell lines and on day 14 of culture as measured via ImageJ. Median and interquartile ranges shown. **(c)** PANC-1 cells formed multicellular spheroids in 5% GelMA. Haematoxylin and eosin (H&E) staining of 5% GelMA hydrogel section at day 14 of culture (left), single spheroid (middle) and PDAC patient tissue (right). Scale bars,100 μm, 50 μm, 50 μm.

The spheroids were reminiscent of tumour cell aggregates seen in PDAC patients (Figure 4.3 b) as well as spheroids that are found disseminating in tumour fluid (ascites) of cancer-

bearing patients, distinctively at late-stage disease [252]. PDAC cell viability was also ensured via live/dead imaging of 5% wt/vol GelMA cell cultures at day 1, 14 and 28 (Figure 4.4). Cell-containing GelMA hydrogels were kept for over four weeks in culture without compromising cell viability. The expression of the PDAC cancer-associated marker cytokeratin-19 (KRT19) [273] was also maintained over 14 days of culture assessed via whole-gel immunofluorescence (Figure 4.4 b). This confirmed the results obtained via immunohistochemistry in Chapter 3 (Figure 3.11) and underlines the amenability of GelMA hydrogels to various cell and molecular analyses.

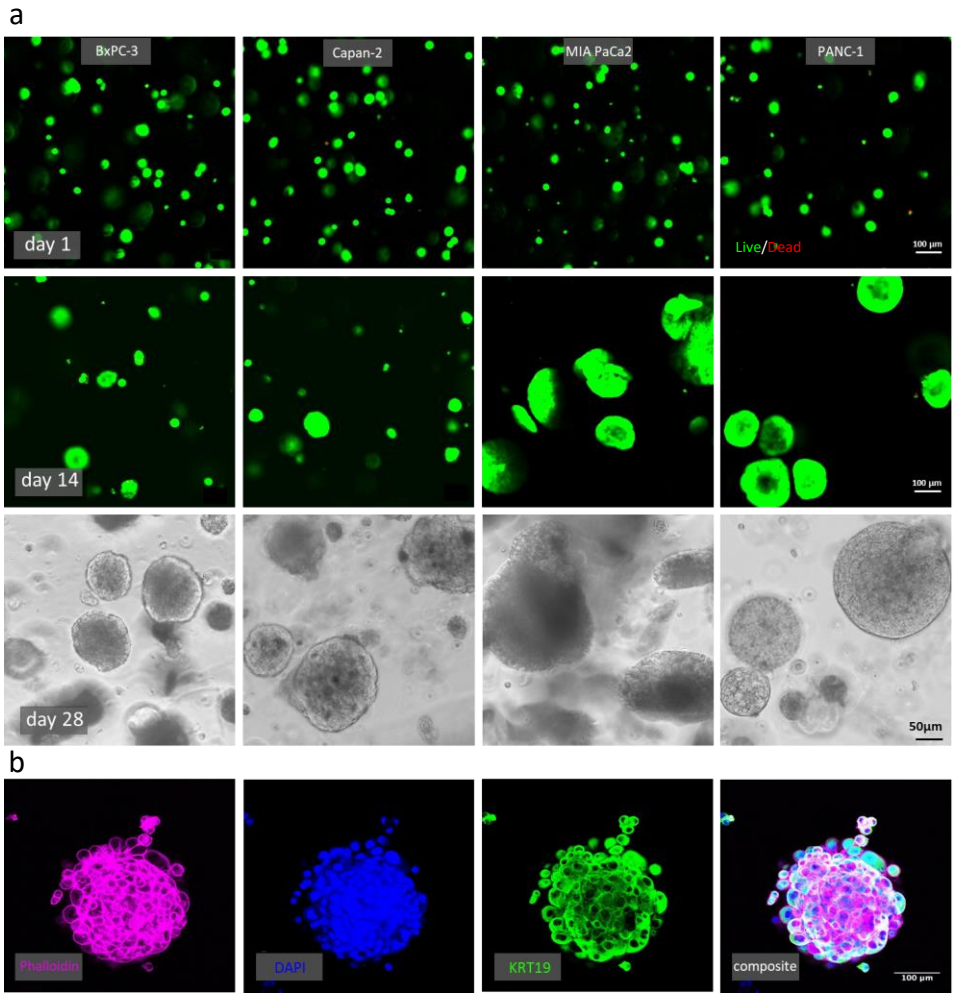

Figure 4.4 Cell proliferation and viability of BxPC-3, Capan-2, MIA PaCa-2 and PANC-1 cells in GelMA hydrogels. (a)(top) Confocal z-stack micrographs show a high cell viability on day 1 and 14; live cells were stained with green-fluorescent calcein-AM (Ca-AM, 494/517 nm); dead cells were stained with red-fluorescent ethidium homodimer-1 (Et-H1, 528/617 nm). Scale bar, 100 µm, applies to all. (bottom) Representative brightfield images at day 28 of culture after encapsulation in 5% GelMA. Scale bar 50 µm, applies to all. **(b)** Immunofluorescence images reveal high cytokeratin 19 (KRT19, 488 nm) expression in PANC-1 cells, cytoskeleton stained with phalloidin (647 nm), nuclei stained with DAPI (358 nm). Scale bar, 100 µm, applies to all.

4.3.2.2 Hydrogel stiffness influences PDAC cell proliferation

Next, I sought to quantify cell viability and proliferation by incorporating my four PDAC cell lines in GelMA hydrogels with increasing stiffness (3-10% GelMA). The proliferation of OvCar4 cells was also measured, and is presented in our publication [235]. The cells showed different proliferative and spheroid-formation abilities within different matrices (Figure 4.5).

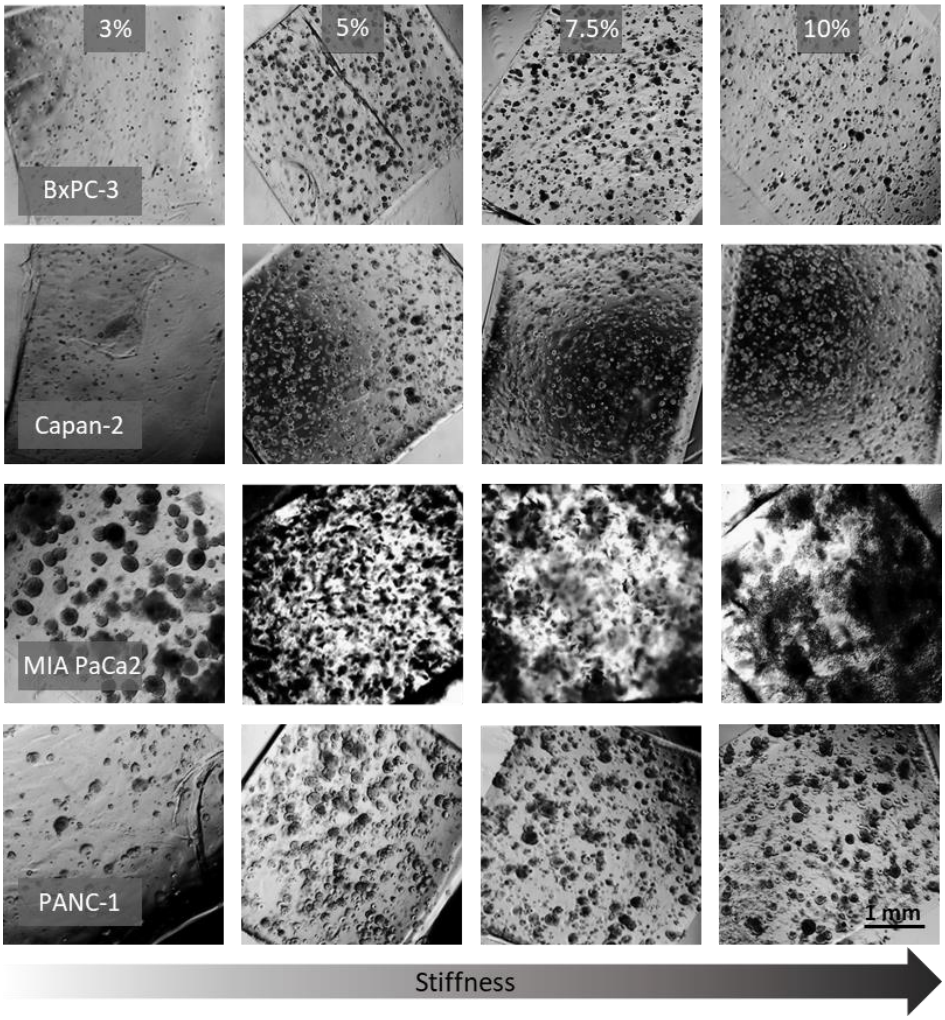

Figure 4.5 Representative brightfield micrographs of BxPC-3, Capan-2, MIA PaCa-2, PANC-1 cells embedded in GelMA hydrogels of increasing stiffness (3-10% wt/vol) at day 14 of culture. Scale bar, 1 mm, applies to all.

10% GelMA hydrogels, corresponding to 16 kPa, were not conducive of high cell proliferation in any of the cell lines, probably owning to its high stiffness. Capan-2 and BxPC-3 cells, which present with a more epithelial cell phenotype [203,282], did not grow very well in soft matrices but proliferated preferentially in matrices with medium-low (5% = 3.4 kPa) and medium-high stiffness (7.5% = 8.6 kPa). These values were also the ones closest to the stiffness of adjacent normal and diseased human tissues (Figure 3.2). On the other hand, micrographs of cell lines of a semi-mesenchymal (PANC-1) and mesenchymal (MIA PaCa-

2) phenotype [203,282], showed cells proliferated regardless of matrix stiffness. In addition, MIA PaCa-2 cells grew to form tight round spheroids in low-stiffness matrices whereas its growth pattern became disorganised and highly migratory (with high numbers of cells moved towards the edge and outside the hydrogels) in stiffer matrices, due to the mesenchymal nature of this cell line.

Cell metabolic activity and DNA quantification analyses were performed on hydrogels on day 1 and day 14 of cell culture in order to quantify cell proliferation (Figure 4.6). MIA PaCa-2 cells showed the highest inconsistencies in fluorescence measurements, due to their tendency to move outside of the hydrogel once confluency is reached. Quantification data strengthened the notion that cell's EMT status may play a role in stiffness-related proliferation as Capan-2 and BxPC-3 show behaviours opposite to PANC-1 and MIA PaCa-2 cells. In addition to their physiological relevance, 5% and 7.5% (wt/vol) GelMA (3.4 – 8.6 kPa) were the matrices in which cells showed the highest proliferation rates, across all four cell lines (Figure 4.6 a), and were therefore taken further for transcriptomics studies in Chapter 5 and treatment studies in Chapter 6.

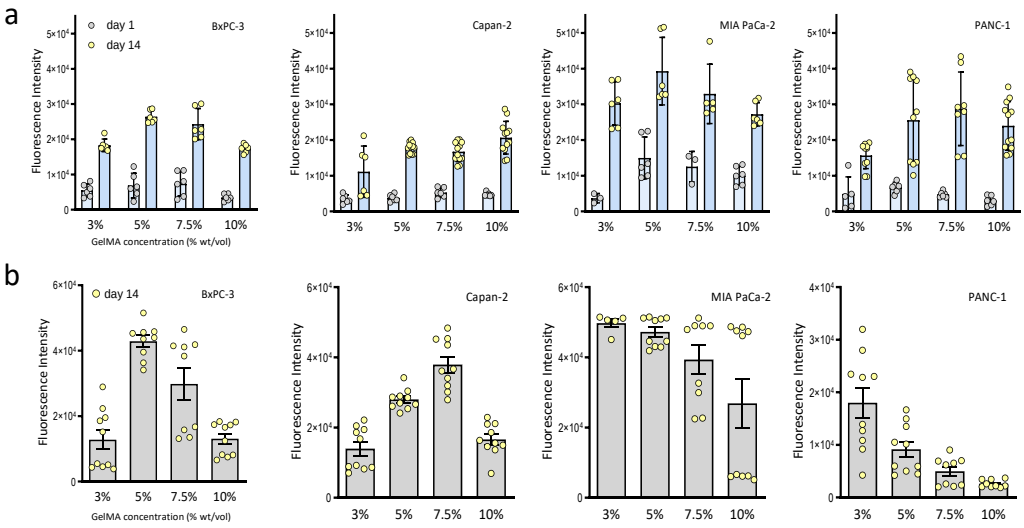

Figure 4.6 BxPC-3, Capan-2, MIA PaCa-2, PANC-1 cell viability and proliferation in GelMA hydrogels of increasing stiffness (3-10%) as measured via quantification of (a) endogenous cellular reducing ability and (b) DNA content. (a) Alamar Blue quantification of cells' metabolic activity was performed on day 1 and day 14 of culture, n=3. **(b)** CyQUANT quantification of DNA content was performed at day 14 of culture, n=3.

To summarise, GelMA-based hydrogels provided the adequate support for 3D culture of HGSOC and PDAC cells by allowing spheroid formation and quantification of cell viability, cell proliferation and cell-specific marker expression. Culture of PDAC cells in this matrix had not been previously characterised.

4.3.3 Optimisation of hydrogel digestion and cell retrieval for downstream analyses

For the successful implementation of GelMA as a 3D cell culture platform, it was next necessary to optimise various techniques for the isolation of GelMA-cultured cells whereby maintaining high viability, as well as quick hydrogel digestion for downstream molecular analyses [235]. I analysed the efficiency of five different enzymatic approaches for the degradation of cell-containing GelMA hydrogels by assessing their hydrogel digestion efficiency and performing flow cytometry analysis of the retrieved cells. OvCar4 and MIA PaCa-2 cells grown in 5% (wt/vol) GelMA were used for this analysis. As collagen is the main component of gelatin [283], the efficiency of different collagenases was assessed. Additionally, other enzymes and reagents such as dispase II and a combination of trypsin and EDTA were also used (Table 4.1). All the tested enzymatic approaches resulted in complete hydrogel degradation, although at different completion rates, suggesting different digestion approaches can be used depending on the intended downstream application.

Table 4.1. Digestion protocol specifications including enzyme names, origin, final concentration and representative pictures. EDTA= Ethylenediaminetetraacetic acid; PBS= Phosphate Buffered Saline; DMEM= Dulbecco's Modified Eagle Medium; FBS= Foetal Bovine Serum; P/S= penicillin/streptomycin

Label	Name, origin, diluent (working concentration)	Pictures Time (min)
1	Trypsin/EDTA in PBS (0.5%/0.2%)	
2	Collagenase I from Clostridium histolyticum in serum-free DMEM (1 mg/ml)	
3	Collagenase V from Clostridium histolyticum in Hank's Salt Balanced Solution (1 mg/ml)	
4	Dispase II from Bacillus polymyxa in PBS (2.5 U/ml)	
5	Collagenase XI from Clostridium histolyticum and Dispase II from Bacillus polymyxa in DMEM (10% FBS, 1% P/S) (0.125 mg/ml 0.625 U/ml)	

Next, the viability of the retrieved cells was assessed via flow cytometry. Figure 4.7 shows the general gating strategy for the sequential exclusion of cell debris (SSC-A/FSC-A), doublets (SSC-W/SSC-A and FSC-H/FSC-A) and detection of live cells. Following this analysis, all digestion protocols returned cells with high viability (>50%) with collagenase I achieving digestion with the highest number of viable cells (95%) and dispase II being the only condition with significantly lower cell viability (67%). Dispase is a protease which cleaves fibronectin (a component of GelMA, as shown in Figure 3.10), collagen IV, and to a lesser extent, collagen I [284] (the main component of GelMA). Increased specificity to collagen I and reduced digestion time might explain the higher efficiency of collagenase I digestion compared to other proteases. Trypsin also possesses collagenolytic activity [285] , but its digestion rate of GelMA was reduced compared to other enzymatic treatments making it a less attractive option for downstream applications. Prolonged cell exposure to trypsin is known to interfere with a number of cell surface molecules including integrins [286], hence why this digestion approach is not favourable for downstream molecular analyses.

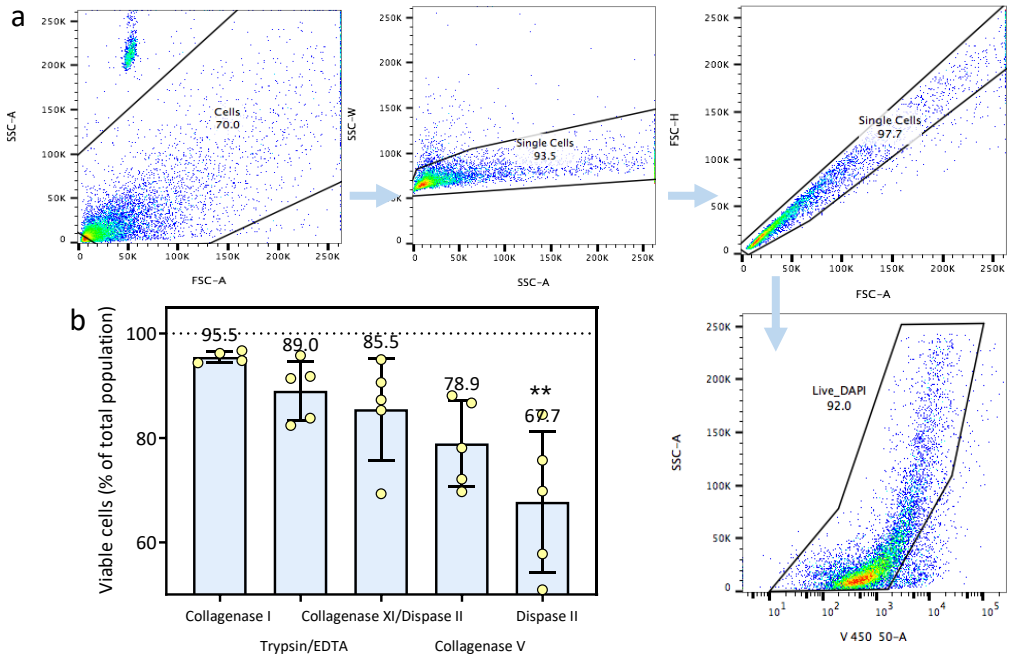

Figure 4.7 Flow cytometry and detection of MIA PaCa-2 cell viability after GelMA hydrogel digestion. **(a)** Representative flow cytometry gating strategy for exclusion of cell debris and doublets and detection of viable cells using DAPI (450/50, X-axis). (**b)** High cell viability was achieved across the five enzymatic approaches tested, with collagenase I: 95.5 ± 0.5%, trypsin/EDTA: 89.0 ± 2.6%, collagenase XI/dispase II: 85.5 ± 4.4%, collagenase V: 78.9 ± 3.7% and dispase II: 67.7 ± 6.0% cell viability (n = five biological replicates with five gels each). ANOVA (Tuckey multiple comparisons), p= 0.0015.

In order to further validate these results, an optimisation of live/dead viability/cytotoxicity dyes (Ca-AM and Et-H1) for flow cytometry was conducted. The two dyes (Ca-AM: 494/517 nm; Et-H1: 528/617 nm), together with DAPI (358/461 nm) staining were used to determine MIA PaCA-2 cell viability after retrieval (Table 4.2). For consistency, collagenase I was chosen for hydrogel digestion during this optimisation.

Table 4.2. Conditions for flow cytometry and details of calcein-AM (CaAM)/ethidium homodimer-1 (EtH1)/ 4',6-diamidino-2-phenylindole (DAPI) staining of GelMA-retrieved MIA PaCa-2 cells following collagenase I digestion.

Test conditions	Sample description	Staining	Ca-AM+ population (%)	Et-H1+ population (%)	DAPI- population (%)	Live/dead detection
1	Manufacturer's instructions; without DAPI	0.1 µM Ca-AM, 8µM Et-H1	84.5	7.0	0.3	Live
2	Manufacturer's instructions; with DAPI	0.1 µM Ca-AM, 8µM Et-H1, 1 µg/ml DAPI	90.5	7.3	91.2	Live
3	Double concentration	0.2 µM Ca-AM, 16 µM Et-H1, 1 µg/mL DAPI	No distinct separation	No distinct separation	91.7	Live
4	Ca-AM dye only	0.2 µM Ca-AM	89.9	-	-	Live
5	Et-H1 dye only	16 µM Et-H1	-	18.5	0.5	Live
6	Manufacturer's instructions; UV-treated	0.1 µM Ca-AM, 8 µM Et-H1, 1 µg/ml DAPI	3.4	81.7	5.8	Dead
7	Manufacturer's instructions; ethanol-treated: live cells (50:50)	0.1 µM Ca-AM, 8 µM Et-H1, 1 µg/ml DAPI	49.6	58.0	47.6	50:50
8	Manufacturer's instructions; phenol-red-free DMEM	0.2 µM Ca-AM, 8 µM Et-H1, 1 µg/ml DAPI	81.3	7.8	93.5	Live
9	Unstained control	Unstained	-	-	-	-

Ca-AM and Et-H1 dyes were used either individually or in conjunction with DAPI staining during optimisation, at both recommended concentrations and double concentration. UV-treated cells (40 min UV, 365 nm) and ethanol-treated cells, were used as dead cell controls, either on their own, or in a 50:50 mix with live cells to determine the accuracy of the live/dead staining (Table 4.2). Results from the three stainings were mostly in agreement and consistent. The removal of phenol-red from the digestion media did not have a significant effect on the staining as the cells underwent several wash rounds prior to flow cytometry, preventing any possible autofluorescence. Representative flow cytometry gating strategy for conditions 2 and 7 are shown in Figure 4.8 4a and 4b. These optimised procedures were published in our book chapter [235].

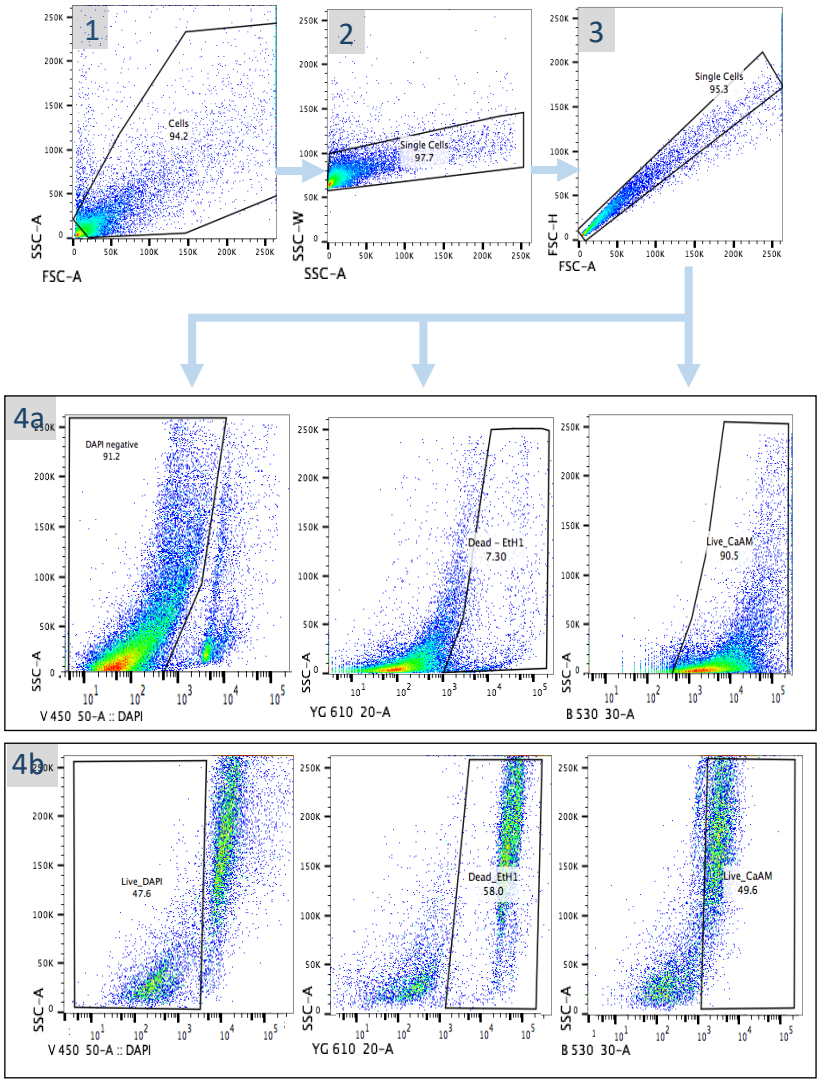

Figure 4.8 General flow cytometry gating strategy for Ca-AM/Et-H1/DAPI staining optimisation. CaAM/EtH1/DAPI staining of GelMa-retrieved cells is shown, following **(1)** exclusion of cell debris and **(2-3)** exclusion of doublets. Representative plots are from triple staining detection of **(4a)** samples 2 (Table 4.2; DAPI 450/50, EtH1 610/20, CaAM 530/30, X-axis) and **(4b)** sample 7 (Table 4.2; DAPI 450/50, EtH1 610/20, CaAM 530/30, X-axis), n=3.

In order to avoid affecting the expression profile of cells by exposing them to proteolytic enzymes, I also optimised a method for mechanical disruption of hydrogels, desirable when performing high-sensitivity assays (such as RNA analyses). This technique yielded a much lower number of cells compared to hydrogel digestion and did not ensure cell integrity/viability (as required for analyses such as flow cytometry). However, it allowed for a faster and enzyme-free hydrogel dissociation. Lastly, western blot analysis from GelMA-recovered cells was carried out successfully with the use of either collagenase I (1 mg/ml) or liberase (0.3 mg/ml) hydrogel digestion (Chapter 4, Chapter 6). The latter has unknown enzymatic composition but was efficient at dissolving GelMA at a much lower concentration.

To summarise, due to the increased popularity of 3D models, there is a need for the development of standardised and reproducible techniques for the recovery of cells cultured in 3D. Effective digestion of GelMA hydrogels for cell retrieval was achieved with a number of different enzymatic approaches, of which collagenase I/DMEM (1 mg/ml) was the most efficient at extracting cells with high (>95%) viability. Different cell retrieval approaches had to be optimised depending on intended downstream application as not many groups [229,235,287] have developed or published analytical techniques for GelMA hydrogels.

4.3.4 UV-induced DNA damage assessment in GelMA cell cultures

GelMA hydrogels crosslink through a photopolymerisation reaction between the methacryloyl functional groups, a photo-initiator and ultraviolet (UV) light (Figure 2.1). UV light exposure is limited to 10 minutes and a low energy 365 nm wavelength to limit UV-induced damage to the incorporated cells. However, I was interested in determining whether such exposure would cause any DNA damage in the used cell lines, as no other group had characterised this. Histone H2A variant (H2AX) levels were measured in the cell lines and in response to UV exposure firstly in 2D (monolayers) and then in 3D (GelMA hydrogels). H2AX becomes activated and phosphorylated on Ser139 (γH2AX) in response to chromatin relaxation, and can therefore be used as a marker for DNA double strand breaks (DSBs) [288]. H2AX phosphorylation was examined by immunofluorescence on monolayer untreated cells, and in cells after 10 minutes of UV exposure (this is the time normally employed during GelMA photo-crosslinking) or 30 minutes of UV exposure (positive control). γH2AX can already be detected a few minutes after irradiation and peaks ~30 min later [288], therefore 1 and 48 hours were chosen as analysis time points.

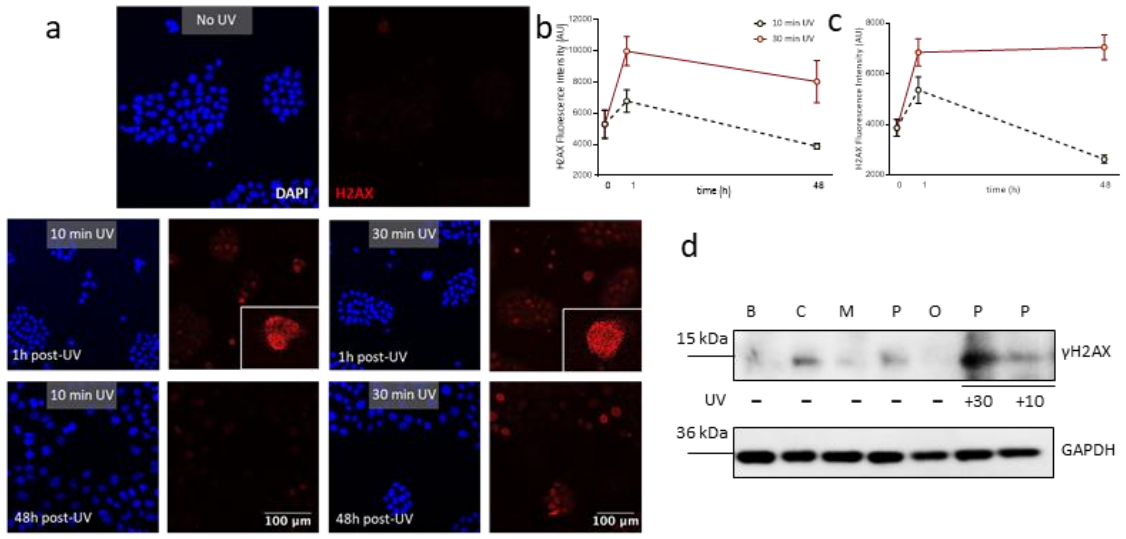

Figure 4.9 γH2AX staining and quantification reveals limited DNA damage following 10 minutes of UV light exposure. (a) BxPC-3 cells show no γH2AX staining (red) under normal conditions. After irradiation with either 10 or 30 minutes of 365nm UV light, γH2AX fluorescent staining peaks (1 hour post-UV irradiation). Levels of γH2AX staining revert to normal 48 hours later, while they remain higher when the UV exposure is increased (30 min). γH2AX, red; DAPI, blue. Scale bar, 100 µm, applies to all. **(b)** Quantification of BxPC-3 immunofluorescence pictures, n= 4 pictures per condition, 100 cells per picture. **(c)** Quantification of immunofluorescence pictures for PANC-1 cells (pictures not shown), n= 4 pictures per condition, 100 cells per picture. **(d)** Human γH2A.X was detected in BxPC-3 (B), Capan-2 (C), MIA PaCa-2 (M), PANC-1 (P) and OvCar4 (O) cell lysates either without treatment or, in the case of PANC-1 cells, after 10 or 30 minutes of UV light exposure. γH2A.X expression (15 kDa) increases marginally after 10 and significantly after 30 minutes of UV exposure. GAPDH (36 kDa) was used as loading control, n=1.

As shown in Figure 4.9 a-c, BxPC-3 and PANC-1 irradiation with 10 minutes UV-light did not cause sustained DNA damage, as the number of γH2AX-positive cells decreases reverting to control conditions at 48 hours. However, cells irradiated with 30 minutes of UV light show very high γH2AX expression after 1 hour, and the expression is maintained even 48 hours post-exposure. This was also confirmed via western blot on irradiated PANC-1 cells (Figure 4.9 d).

Immunofluorescent detection of γH2AX was then performed on cell-containing GelMA sections (day 14 of culture) to investigate its expression in established 3D cultures. Limited γH2AX expression was observed in PANC-1 spheroids at day 14 of culture, with its expression being mainly confined to the edges of the spheroid mass (Figure 4.10 bottom inserts).

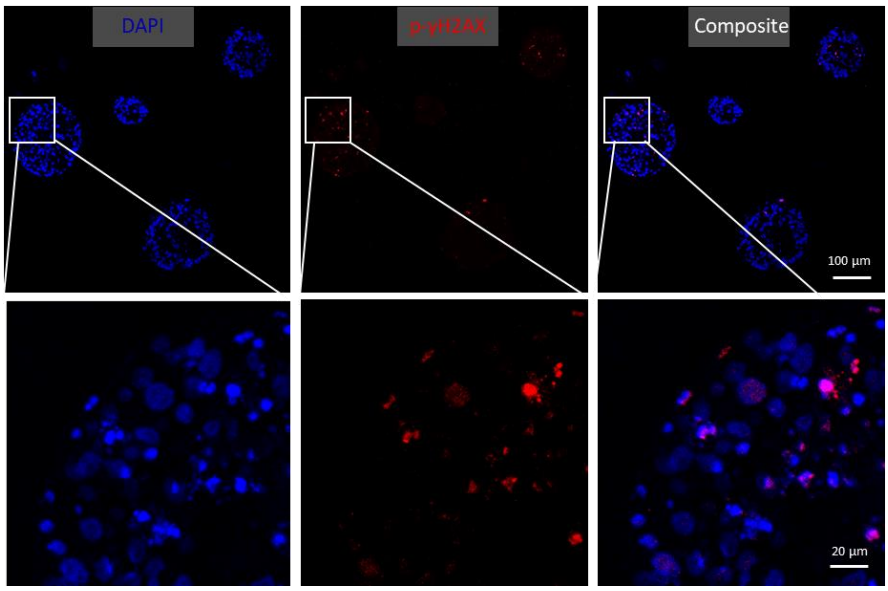

Figure 4.10 Immunofluorescent detection of γH2AX (red) as a marker of DNA double-strand breaks in GelMA-embedded cells. (a) PANC-1 cells were cultured in 5% GelMA for 14 days prior to fixing, sectioning (7 µm) and subjection to immunofluorescent staining. Phospho-H2AX, red; DAPI, blue. Scale bars 100 µm (top) and 20 µm (bottom), applies to all, n=4.

DSBs associated with replication stress or UV damage are detected by the ataxia-telangiectasia mutated and Rad3-Related (ATR) kinase, which in turn activates H2AX via phosphorylation [289]. In turn, ATR can be activated by a number of other proteins, such as ATRIP, which also recognises single-strand breaks, an extremely common phenomenon during cell replication [290]. As such, ATR-mediated H2AX phosphorylation is not necessarily indicative of DSBs, particularly for cells in the S-phase, which may explain the high number of γH2AX positive cells along the edges of GelMA spheroids. Looking at additional markers

such as phosphorylation of the ataxia-telangiectasia mutated (ATM) kinase (Ser1981), phosphorylation of the ATM/ATR substrate [291], or of the tumour suppressor p53 (Ser15) [292], in conjunction with γH2AX could provide additional information on the degree of DNA-damage incurred by the cells.

Despite this, a number of groups have now began investigating the use of visible light for GelMA crosslinking, replacing the need of a UV source [233,293]. For this, the effects of a different photo-initiator, lithium acylphosphinate salt (LAP) on cells and a higher wavelength (405 nm), would have to be fully characterised. Physicochemical properties, hydrogel rheology, pore size and operating procedures (such as light during hydrogel preparation) would also have to be adjusted accordingly.

To summarise, 10 minutes of exposure to high wavelength UV-light (365 nm) did not cause sustained DNA damage as quantified via γH2AX staining in monolayer or GelMA-cultured cells. Additional markers could be used to investigate the extent of UV-induced DNA-damage in GelMA further. Finally, the use of visible light as a crosslinking mechanism does not come without its own limitations, but is an interesting alternative for GelMA hydrogel crosslinking.

4.3.5 Investigating the effects of cellular components on the pancreatic TME

4.3.5.1 Cancer-associated fibroblasts promote cell proliferation and GelMA hydrogel stiffening

The expression of key matrix proteins as well as markers for cellular components of the pancreatic TME had already been investigated via tissue IHC in Figures 3.10 and 3.11. COL1, FN1, VCAN, HABP, KRT19 and CD68 protein expression was also maintained in 3D cell cultures. The cellular fractions of ascites fluid were further characterised via flow cytometry in order to gauge a better understanding of its composition (Figure 4.11 a). Ascites fluid from HGSOC patients was used for this, as our ethics did not cover collection of PDAC ascites. Flow cytometry data revealed a high proportion, nearly 95%, of ascites, was constituted by immune cells of leukocyte lineage ($CD45^+$). The remaining 5% represented cells of epithelial lineage ($CD45^-$). $CD45^+$ cells were further characterised based on their CD11b monocyte marker expression, of which around 80% were positive. Epithelial cells were further gated for epithelial cell adhesion molecule (EpCAM) expression, showing around 30% $EpCAM^+$ cells.

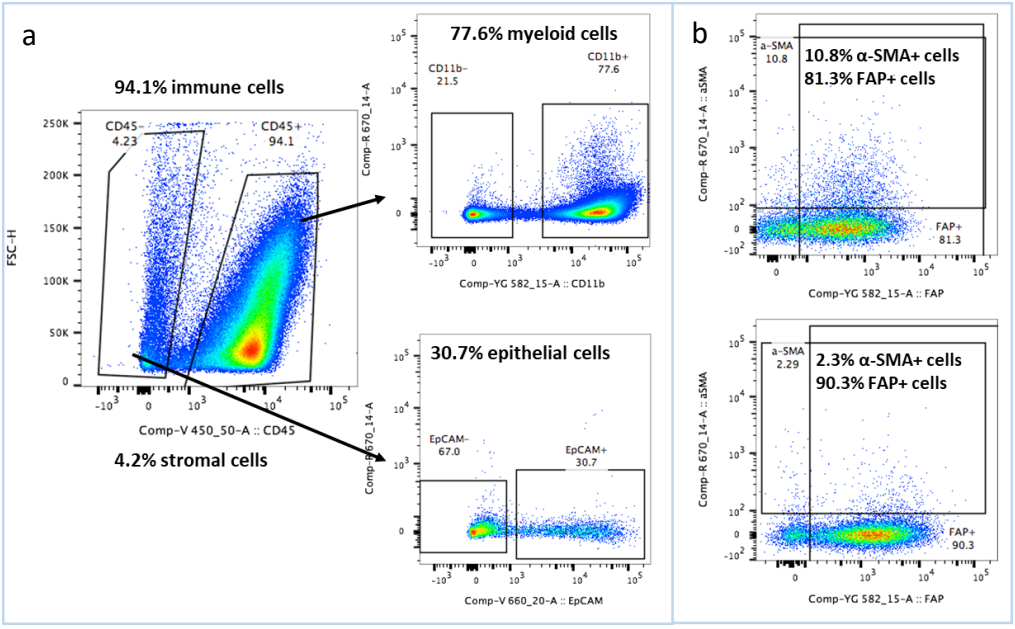

Figure 4.11 Characterisation of cellular fractions of a) HGSOC ascites fluid and (b) HGSOC and PDAC primary isolated CAFs, by flow cytometry. (a) Example of gating strategy to determine CD45 expression on cells (shown here in channel V450). Leukocyte marker CD45+ cells are further divided into macrophage marker CD11b+ or negative (YG582 channel). CD45- cells were further gated for EpCAM (V660). **(b)** Flow cytometry on HGSOC and PDAC patient-derived fibroblast population, characterised via α-SMA (R670) and FAP (YG582) markers expression. Plots correspond to patients 2, 17, 1 (Table 2.1), n=3.

According to this classification, less than 1.5% of the total ascites population corresponded to malignant cells. This is unsurprising as some reports have found tumour cells in ascites to be as little as 0.1% [294,295]. Even in primary PDAC tissues, malignant cells represent <20% of the tumour bulk [59,192,281]. Monocytes and fibroblasts were chosen as additional cell types for incorporation in GelMA alongside cancer cells, representing respectively an immune and epithelial cell component.

When not used for mechanical testing, both HGSOC and PDAC tissues, as well as HGSOC ascites, were used for isolation of primary cancer-associated fibroblasts (CAFs). Representative flow cytometry analysis for two patients is shown in Figure 4.11 b, where alpha-smooth muscle actin (α-SMA) and fibroblast activation protein (FAP) were used as fibroblast lineage markers. For each subsequent isolation, fibroblasts were characterised using immunofluorescence to confirm their CAF phenotype. Figure 4.12 shows an example from PDAC tissue-derived CAFs (top panels) and HGSOC omentum metastasis-derived CAFs (bottom panels), both showing typical fibroblast elongated or fried-egg morphologies and high α-SMA and vimentin (Vim) expression.

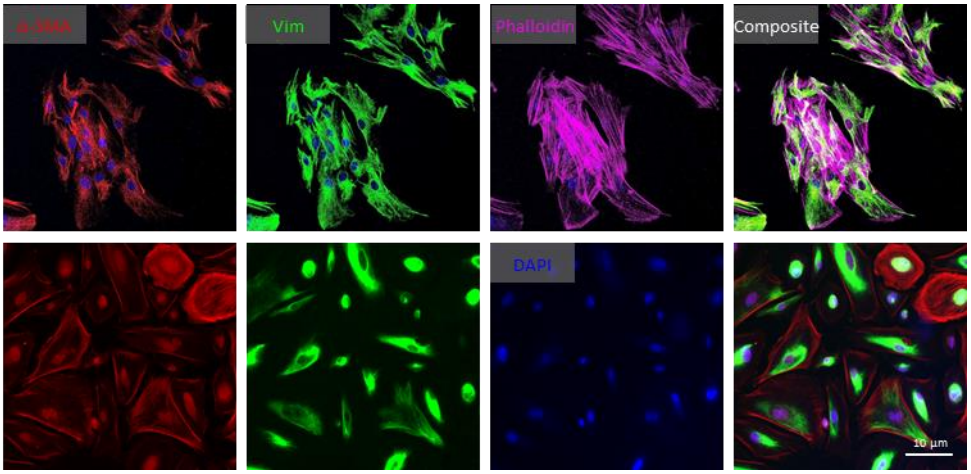

Figure 4.12 Immunofluorescence analysis of patient-derived cells confirmed CAF phenotype by co-expression of alpha-smooth muscle actin (αSMA, AF568) and fibroblast activation protein (FAP, AF488); phalloidin (AF647), DAPI (EX358). Cells were derived from patients 16 and 13 (Table 2.1). Scale bars 10 µm, applies to all. Representative pictures, n=9 patients assessed in total.

Because of the relatively low percentage of tumour cells in found the cancer bulk and ascites fluid, co-culture studies were always performed with a higher proportion (either 4:1 or 1:2, as stated each time) of stromal cells compared to tumour cells. Following isolation and characterisation, CAFs were seeded in a 4:1 ratio with PDAC cell lines, alongside appropriate monoculture controls, in 5% (wt/vol) GelMA hydrogels. Representative micrographs of cell

cultures at day 14 are shown in Figure 4.13 a. The presence of CAFs increased cell proliferation in co-culture hydrogels compared to monocultures for 3 out of 4 PDAC cell lines tested, with the exception of BxPC-3, as indicated by the Alamar Blue results (Figure 4.13 b). In monoculture, CAFs remained viable in GelMA hydrogels however, they did not proliferate, as reflected in the constant Alamar Blue values on day 1 throughout to 14 (live/dead staining not shown, see Figure 4.17). This is unsurprising as the doubling time of primary CAFs was extremely low even on tissue culture plastic. From this analysis, it is however unclear which cell population, if not both, had an increased proliferation rate as a result of being in co-culture. A dual staining of a proliferation (e.g. Ki67) and fibroblast or cancer marker could be conducted in order to answer this question.

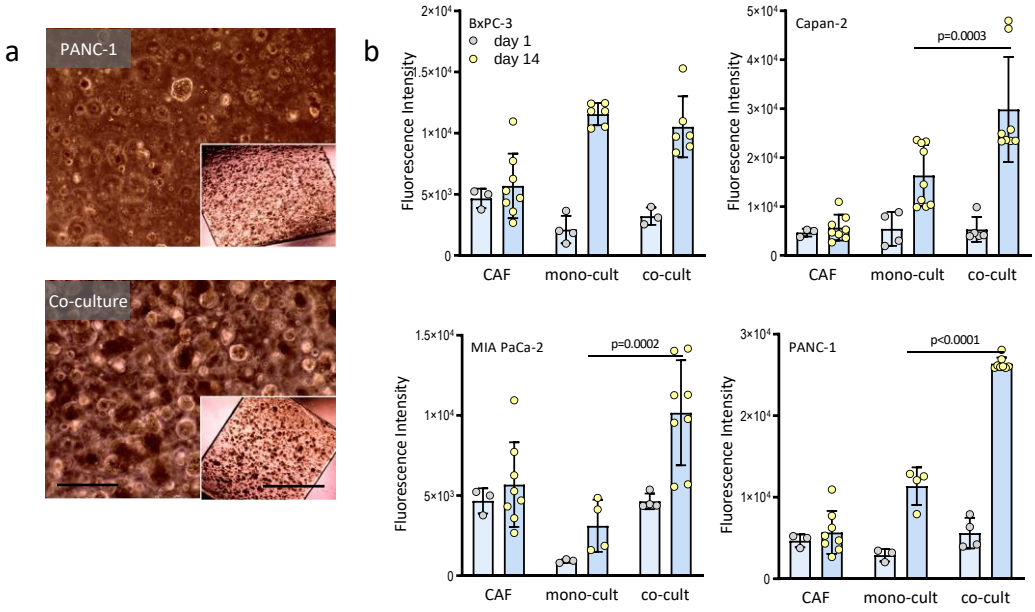

Figure 4.13 CAFs promote cell proliferation in 5% GelMA co-cultures with PDAC cells. (a) Representative brightfield micrographs of (top) PANC-1 monoculture and (bottom) PANC-1 and CAF co-culture (1:4 ratio), at day 14 of culture in 5% GelMA. Scale bars 500 µm and 2 mm (inserts), apply to all. **(b)** Alamar Blue quantification of cell viability of 3D cell cultures at day 1 (light blue) and day 14 (blue) in 5% GelMA monocultures and PDAC/CAF co-cultures (1:4 ratio). ANOVA (Tuckeys multiple comparisons), p-values as annotated, n=2.

Next, I assessed whether CAFs would impact GelMA hydrogel stiffness. For this analysis, BxPC-3 cells were chosen as their proliferation was not significantly affected by CAFs (Figure 4.13 b), ensuring that observed stiffness differences would not be due to different cell numbers within the hydrogels. BxPC-3 cells were incorporated in 3% (wt/vol) and 5% (wt/vol) GelMA hydrogels in a 1:2 ratio with either CAFs or normal fibroblasts (NFs). CAFs and NFs were isolated from matched PDAC and tumour-adjacent tissue samples respectively (Patient 17, see Table 2.1).

The presence of CAFs in the co-cultures significantly increased the hydrogel's Young's modulus in both 3% (wt/vol) and 5% (wt/vol) GelMA (Figure 4.14). Interestingly, NFs had no effect on hydrogel Young's modulus. As cells in GelMA are in close proximity but not necessarily in direct contact, it is likely that both proliferative and stiffening effects would be influenced by secreted factors. More about this will be discussed later in this Chapter.

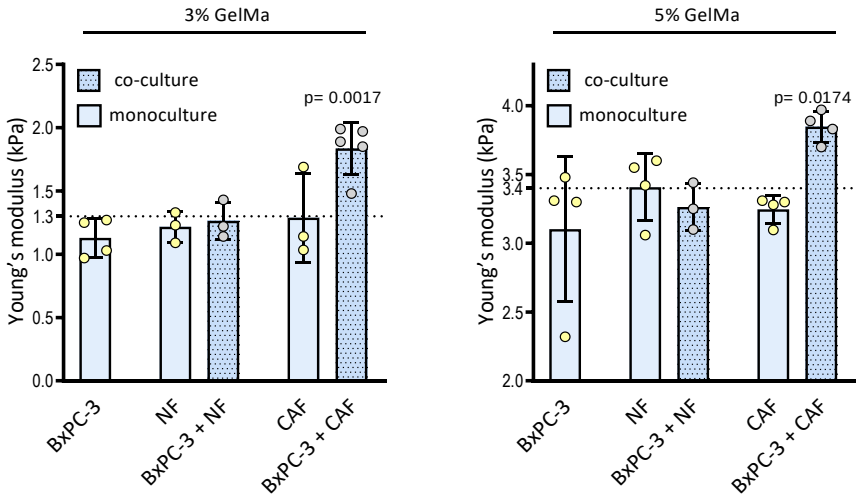

Figure 4.14 Young's modulus measurement of 3% and 5% GelMA BxPC-3 co-cultures with cancer-associated fibroblasts (CAFs) or non-malignant fibroblasts (NFs), and respective monoculture controls (day 14). Dotted lines represent GelMA stiffness prediction for 3% (1.3 kPa) and 5% (3.4 kPa) GelMA. ANOVA (Tuckeys multiple comparisons), p-values as annotated, n=4.

4.3.5.2 Co-culture of myeloid and cancer cells contribute to tumour development and metastasis *in vivo*

Macrophages are the dominant leukocyte population both in human PDAC stroma and autochthonous disease models [51]. Human THP-1 leukaemia-derived monocytes were used to model immune cells in our 3D platform. Due to tissue bank ethics restrictions we were not able to collect any fresh blood from human donors, which would have been a preferred source of cells of monocytic lineage. As discussed in Figure 3.11, once co-cultured with cancer cells in GelMA, monocytes not only proliferated to form cell clusters, but they also showed a positive CD68 expression indicating they had differentiated into macrophages (Figure 3.11).

In order to assess the effects of THP-1 on cancer cell survival and proliferation, monocytes were incorporated in a 2:1 ratio alongside either BxPC-3 or PANC-1 cells in 5% (wt/vol) GelMA hydrogels. Appropriate BxPC-3 or PDAC monoculture controls were also set up. After 14 days of culture, both mono- and co-culture GelMA hydrogels were implanted

orthotopically on top of the pancreas of 6 female NOD/SCID mice (Figure 4.15 a). In an effort to reduce the number of animals used, no GelMA vehicle-only group was kept, as this had already been shown to generate no inflammation or tumour formation in previous reports [252]. Animal appearance and weight was recorded weekly and once tumours reached a palpable size, usually around 10-14 weeks post-surgery, animals were sacrificed. Presence of ascites was noted, GelMA hydrogels, tumours, spleen and liver tissues were surgically removed, and the latter were subjected to histological and immunohistochemical analyses. Human-specific KRT19 and Ki67 detection on the resected tumours confirmed that PDAC cells were capable of migrating outside of GelMA hydrogel implants and colonising the murine pancreas forming tumours (Figure 4.15 b).

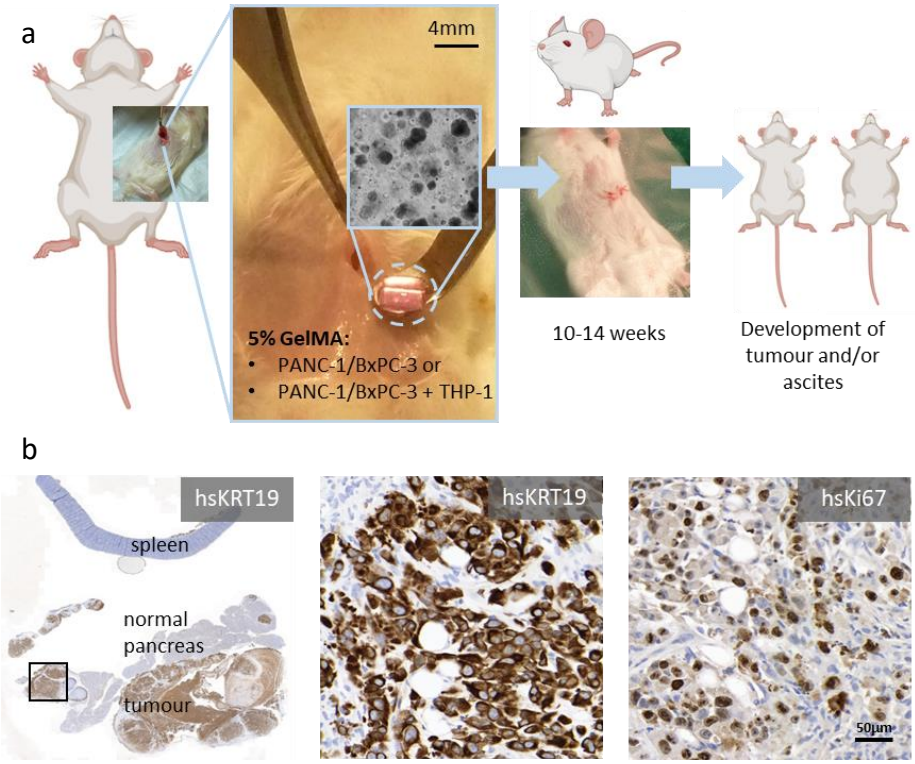

Figure 4.15 GelMA hydrogel orthotopic xenograft. (a) Schematic representation of xenograft implant procedure. BxPC-3 or PANC-1 cells were grown either in monocultures or in co-culture with THP-1 cells for 14 days in 5% GelMA prior to subcutaneous implant. Animals were sacrificed at the first sign of symptoms, around 10-14 weeks after implant. **(b)** Immunohistochemical analysis of human-specific cytokeratin-19 (KRT19) and Ki67 in resected xenograft tumours. Spleen serves as negative control tissue, while positive cells stain for DAB (brown chromogen). Scale bar, 50 µm for higher magnification.

Ascites fluid and xenograft tissues were subjected to flow cytometry or bulk mechanical testing. Detection of tumour marker EpCAM by flow cytometry using a human-specific antibody, revealed the presence of a subpopulation of human tumour cells with positive chemokine receptor type-4 (CXCR4) expression (Figure 4.16 a). CXCR4 expression in PDAC is correlated with worse prognosis as its expression on tumour cells promotes tumour

cell growth, migration, and invasiveness [296,297]. Here, CXCR4 was used as a cancer stem cell marker in conjunction with EpCAM to determine the malignant human cell population of the murine tumours.

No significant difference was found between the stiffness of xenograft tissues derived from monoculture (BxPC-3 or PANC-1) and co-culture (BxPC-3/PANC-1 + THP-1) implants, despite a clear trend towards an increase in stiffness of co-culture xenograft tissues (Figure 4.16 b, p=0.08). Increased sample size (n>3) would be necessary for significance to be detected via whole-tissue stiffness analysis, as only three tumours were available per condition. Some cell-containing GelMA hydrogels were also retrieved after post-mortem inspection and subsequently tested for stiffness. No significant difference was found between hydrogel stiffness in monoculture and co-culture groups, indicating that unlike CAFs, THP-1 cells might not be contributing to hydrogel stiffening (Figure 4.16 c). To note, that the long permanence of hydrogels in mice and the subsequent surgical procedures and handling might have compromised the integrity and original stiffness of these hydrogels.

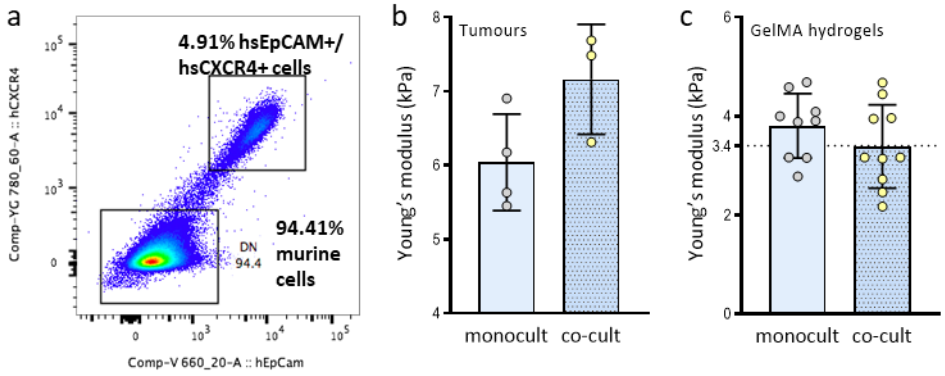

Figure 4.16 Analysis of resected orthotopic xenograft tumorigenic cell population and tumour stiffness. (a) Flow cytometry analysis of resected murine tumours. Human-specific EpCAM and CXCR4 positive cells allow the detection of human-specific cell components of the murine tumours. **(b)** Young's modulus of tumours from mice in monoculture groups (BxPC-3 and PANC-1) and co-culture groups (BxPC-3/PANC-1 and THP-1). Monocultures: 6.0 ± 0.65 kPa, co-cultures: 7.2 ± 0.74 kPa, t-test p= 0.086, n=3. **(c)** Young's modulus of mice-resected GelMA hydrogels for monoculture groups (BxPC-3 and PANC-1) and co-culture groups (BxPC-3/PANC-1 and THP-1). Dotted line represents stiffness prediction for 5% GelMA, 3.4 kPa. Monocultures: 3.8 ± 0.65 kPa, co-cultures: 3.4 ± 0.84 kPa, t-test p=0.24, n=9.

In addition to hydrogel and tumour resection, the presence of ascites and additional metastases was noted (Table 4.3). Implantation of THP-1 and cancer cell co-cultures resulted in both an increase in tumour occurrence as well as increased metastases incidence in both BxPC-3 and PANC-1 groups.

Table 4.3. Number of tumours, metastases and tumour stiffness of orthotopic xenografts of GelMA hydrogels.

Experimental group	Tumours (number of animals)	Metastases (number of animals, locations)	Tumour stiffness (Young's modulus, kPa)
BxPC-3	2/6	0/6	5.54 ± 0.13
BxPC-3 + THP-1	5/6	2/6 (diaphragm, omentum)	7.0 ± 0.97
PANC-1	2/6	1/6 (ascites)	6.54 ± 0.51
PANC-1+ THP-1	5/6	3/6 (ascites, omentum)	7.4

To summarise, patient-derived CAF inclusion in GelMA cultures resulted in an increased PDAC cell proliferation (in three of four cell lines analysed) and increased GelMA hydrogel stiffness, which was not observed with NFs. GelMA hydrogels were successfully employed as vehicles for cell delivery in orthotopic xenograft experiments. THP-1 monocytic cells contributed to both tumour development and formation of metastasis *in vivo*.

4.3.6 Mimicking the pancreatic TME in GelMA hydrogels using triple cell cultures

4.3.6.1 Stromal cells lead to increased cell proliferation in GelMA and collagen hydrogels

GelMA hydrogels allowed the simultaneous 3D culture of multiple cell types. In order to recapitulate a complex pancreatic TME, I next assessed the viability of triple cultures of PDAC cells, THP-1 cells and CAFs in GelMA hydrogels. Due to the high stromal content of pancreatic tumours [59,60], PDAC cells were embedded in a 1:2:2 ratio with stromal cells, in both 5% (wt/vol) and 7.5% (wt/vol) GelMA hydrogels, whose stiffness closely mimic that of human tumour tissues. Collagen hydrogels were used both as soft matrix control as well as for their prominence as 3D cell culture system in the literature [144,192,203,267]. Appropriate PDAC monoculture and stromal (CAF and THP-1) control hydrogels were also set up.

Brightfield and confocal imaging (Figure 4.17 a,b) revealed GelMA supported high viability of CAFs and THP-1 cells even without PDAC cell presence throughout the 14 days of culture. Confocal micrographs of triple cultures will be shown later on in Chapter 6. THP-1 cells formed round spheroids while CAFs retained their typical elongated fibroblast morphology. Proliferation of these cultures was assessed via metabolic activity (Figure 4.17 c) and DNA content quantification (Figure 4.17 d) from three independent experiments with CAFs isolated from patients 2, 3 and 14 (Table 2.1). DNA content analysis revealed a significantly higher proliferation in PANC-1 cells when cultured with CAFs and THP-1s compared to monoculture controls irrespective of stiffness. Despite remaining viable, stromal cells preferred soft matrices for proliferation (collagen and to a lesser extent 5% GelMA) as the number of viable cells was lower in the 7.5% GelMA stromal control.

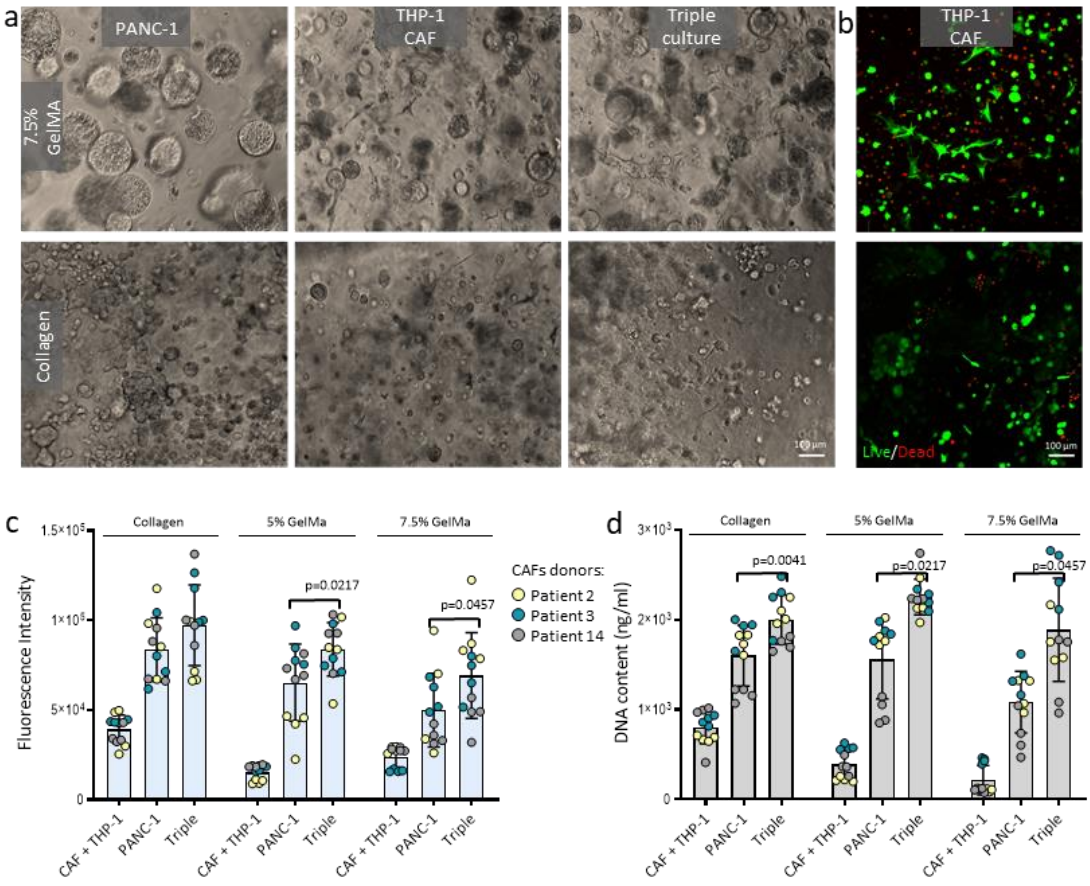

Figure 4.17 PDAC, THP-1 and CAF triple cultures in GelMA and collagen hydrogels. (a) Brightfield micrographs at day 14 of culture in 7.5% GelMA (top panels) and collagen (bottom panels) hydrogels. Triple cultures and relevant monoculture (PANC-1) and stroma (CAF and THP-1) controls shown. Scale bar, 100 µm, applies to all. **(b)** Confocal imaging of THP-1 and CAF stromal co-cultures (day 14) in 7.5% GelMA (top) and collagen (bottom); live cells were stained with green-fluorescent calcein-AM (Ca-AM, 494/517 nm); dead cells were stained with red-fluorescent ethidium homodimer-1 (Et-H1, 528/617 nm). Scale bar, 100 µm, applies to all. **(c)** Alamar blue cell viability quantification of PANC-1 monoculture, stromal cultures (THP-1+CAF) and triple cultures (PANC-1 + THP-1 + CAF) in collagen, 5% GelMA, 7.5% GelMA hydrogels on day 14. n=3, CAFs from patients 2 (yellow dots), 3 (blue dots), 14 (grey dots). ANOVA (Tuckey multiple comparisons), p-value wrt PANC-1 as annotated. **(d)** CyQUANT DNA content quantification of PANC-1 monoculture, stromal cultures (THP-1+CAF) and triple cultures (PANC-1 + THP-1 + CAF) in collagen, 5% GelMA, 7.5% GelMA hydrogels on day 14. n=3, CAFs from patients 2 (yellow dots), 3 (blue dots), 14 (grey dots). ANOVA (Tuckey multiple comparisons), p-value wrt PANC-1 as annotated.

4.3.6.2 Stromal cells in GelMA result in increased hydrogel stiffness

The stiffness of GelMA cultures was also assessed (Figure 4.18). The presence of stromal cells led to an increased hydrogel stiffness in 7.5% (wt/vol) GelMA triple cultures compared to PANC-1 monocultures. As THP-1 cells alone did not have a significant effect on matrix stiffness (Figure 4.16 c), hydrogel stiffening could likely be attributed to CAF interactions with the surrounding matrix and other cells of the triple culture (PANC-1 and THP-1). A similar trend was observed in 5% (wt/vol) GelMA hydrogels despite not being significant. A higher stiffness might also indicate that CAFs had an increased proliferation rate triple cultures, contributing to both a higher DNA content (Figure 4.17 d) and increased Young's

modulus (Figure 4.18). This could be tested via proliferative marker staining (Ki67) on mono- and triple-cultures.

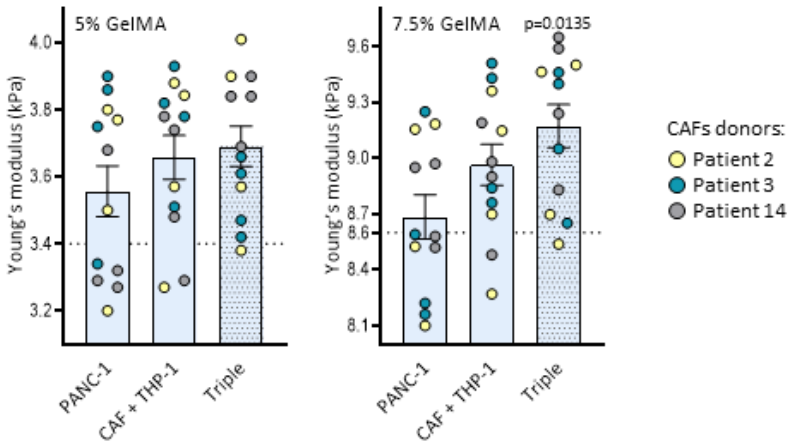

Figure 4.18 Young's modulus measurement of 5% and 7.5% GelMA PANC-1 co-cultures with CAFs and THP-1s, and respective stroma (CAF + THP-1) and PDAC-only controls (day 14). Dotted lines represent GelMA stiffness prediction for 5% (3.4 kPa) and 7.5% (8.6 kPa) GelMA. n=3, CAFs from patients 2 (yellow dots), 3 (blue dots), 14 (grey dots). ANOVA (Tuckey multiple comparisons), p-value as annotated.

4.3.6.3 Stromal cells lead to increased pro-inflammatory cytokines secretion in GelMA and collagen hydrogels

The expression of some key pro-inflammatory cytokines was assessed at day 14 of culture in the conditioned supernatant of either PANC-1 cells, stromal cells (CAF and THP-1) or triple cultures in collagen and GelMA hydrogels. Overall, the levels of secreted cytokines decreased in cultures from soft to stiff matrices. Secreted IL-6 levels were higher in triple cultures compared to controls in both collagen and 5% GelMA (Figure 4.19 a). In 7.5% GelMA, IL-6 levels decreased compared to stroma but were highly upregulated compared to PANC-1 levels. Secreted IL-8 levels were higher in triple cultures compared to controls in all three matrices (Figure 4.19 b). IL-6 and IL-8 are known to promote proliferation, migration and invasion in PDAC [298-300], hence higher levels of these cytokines are concordant with the observed increase in cell proliferation of these cultures. Importantly, as IL-6-dependant activation of STAT3 is a hallmark of PDAC progression [300], stroma-induced activation of pro-survival signalling pathways in collagen and GelMA hydrogels was assessed next.

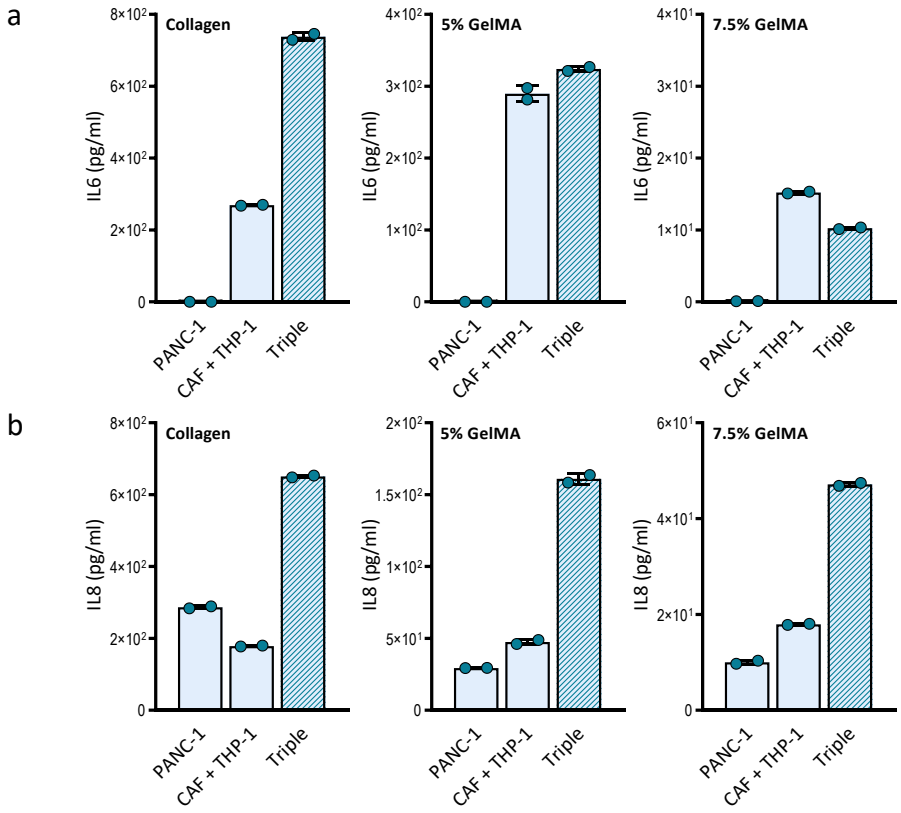

Figure 4.19 Secreted (a) interleukin (IL)-6 and (b) IL-8 levels in cell culture supernatants at day 14 of culture in either collagen, 5% or 7.5% GelMA hydrogels. CAFs isolated from patient 3 were used for this, n=1.

To conclude, GelMA hydrogels were employed for the 3D culture of multiple cell types including key cellular components of the pancreatic TME, namely CAFs and myeloid cells. Both primary cells and established cell lines maintained a high viability throughout long-term culture over 4 weeks, which was paramount for their implementation in treatment studies (Chapter 6). The presence of stromal cells increased both matrix stiffness and cell proliferation of PDAC cells. These effects were more evident in stiffer 7.5% (wt/vol) GelMA matrices, which are representative of physiological PDAC stiffness. Co-culture of stromal and PDAC cells led to increased IL-6 and IL-8 secretion in collagen and GelMA.

4.3.7 A novel hydrogel-based indirect co-culture system unveils stroma-induced upregulation of pro-survival signals in PDAC cells

In order to understand further the stromal (CAF and THP-1) cell's influence on PDAC cell signalling pathways, an indirect 3D co-culture experiment was devised (Figure 4.20 a). For this, patient-derived CAFs and THP-1 monocytes were co-embedded in collagen, 5% or 7.5% GelMA hydrogels. Monocultures of PANC-1 cells were also set up in collagen, 5% or 7.5% GelMA hydrogels. PDAC- and stroma-containing hydrogels were then cultured in the same medium-containing well (indirect co-culture) or in separate wells (controls) for 72 hours, after which hydrogels were separated visually under and inverted microscope and subjected to proliferation, stiffness and immunoblotting analyses (Figure 4.20 a).

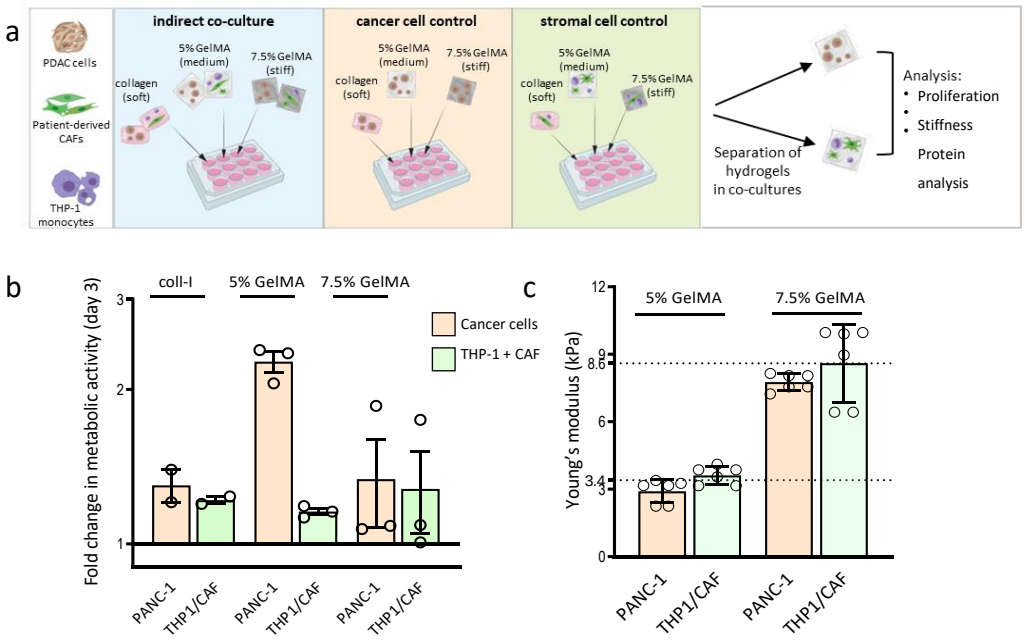

Figure 4.20 Indirect co-culture experimental setup and analysis of viability and mechanical properties. **(a)** Schematic representation of experimental setup. Collagen, 5% and 7.5% GelMA hydrogels were set up containing either cancer cells (PANC-1) or stromal cells (THP-1 and CAFs). Cancer and stroma hydrogels were either cultured in the same well of a 12-well plate (indirect co-culture) or placed in individual wells as controls. Hydrogels were kept for 72 hours in culture with no medium replacement, after which cancer cell-containing hydrogels in the co-culture were separated from the stroma-containing hydrogels (visually, with an inverted microscope). Hydrogels were then subjected to protein extraction for further analysis**. (b)** Fold change in metabolic activity of control hydrogels (PANC-1, THP-1/CAF) at day 3 of culture as measured via Alamar Blue assay, n=3. (c) Stiffness of cell-containing 5% and 7.5% GelMA hydrogels at day 3 of culture. Dotted line corresponds to predicted hydrogel stiffness, n=2.

Cell viability and hydrogel stiffness were analysed after 72 hour as control measures for this early time point (Figure 4.20 b, c). Compared to day 1, all conditions showed a fold change in metabolic activity of a value higher than 1, indicative of cell viability and a little initial cell proliferation, particularly of PANC-1 cells (Figure 4.20 b). GelMA hydrogel stiffness closely

matched the prediction (dotted line 3.4 kPa for 5% GelMA and 8.6 kPa for 7.5% GelMA) (Figure 4.20 c). Despite the early timepoint, there was a tendency for stromal hydrogels (CAF and THP-1) to be a little stiffer than their PDAC counterparts. The difference is not statistically significant on day 3 but could be indicative of matrix remodelling already starting at early stages of 3D cell culture. Once again, it would seem that CAFs are the main drivers of matrix stiffening in GelMA (as seen earlier in this Chapter).

Next, immunoblotting was performed on hydrogel-retrieved cells and further quantified via densitometry (Figure 4.21 a,b). Western blot analysis of protein lysates revealed an increase in phosphorylated signal transducer and activator of transcription 3 (pSTAT) in cancer cells following co-culture (blue bars) compared to monoculture (orange bars), indicating activation of pro-survival pathways [18]. This pattern was observed in all three hydrogels. Importantly, STAT3 activation is constitutive of PDAC pathogenesis and progression [301], hence its upregulation in co-culture settings could be responsible of the increased proliferation observed in co-cultures and triple cultures throughout the project (Figures 4.13, 4.15 and 4.17).

In stromal cells, STAT3 phosphorylation increased when co-cultured (blue bars) with PANC-1 in collagen hydrogels compared to control (green bar), but was unchanged in 5% and 7.5% GelMA. Similarly, stromal cells (CAF and THP-1) had a decreased proliferation in GelMA compared to collagen hydrogels as shown in Figure 4.17 d. STAT3 phosphorylation in CAFs is known to increase the expression of insulin-like growth factor 1 (IGF-1) to promote PDAC cell proliferation [302], concordant with the increase proliferation observed in PDAC co-cultured with CAFs and triple cultures. STAT3 phosphorylation also induces the emergence of pro-invasive and pro-survival characteristics of fibroblasts, ultimately leading to *in vitro* and *in vivo* ECM remodelling and stiffening [303]. In fact, crosstalk between the JAK1/STAT3 pathway and the mechanosensing RhoA/ROCK/MLC2 signalling pathway, links CAF survival to stiffness regulation, although more work needs to be done in order to fully clarify their interactions [304]. This mechanism could be underlying the observed increase of stiffness of triple-cultures in GelMA (Figure 4.18).

Since CAF and THP-1 cells have been incorporated in the same hydrogel for this assay, it is not possible to understand their individual contributions to the phosphorylation of STAT3 in PANC-1 cells and vice versa. A similar, indirect co-culture experiment with CAF and THP-1 cells in separated hydrogels could help clarify this. In fact, STAT3 activation in

macrophages has anti-tumour properties and leads to suppressed inflammation via IL-10-mediated suppression of TNF-α [305,306]. Hence, it could be possible that during indirect co-culture THP-1 cells downregulated their pSTAT3 expression while CAFs upregulated it, resulting in little difference in the overall levels of pSTAT3 in these hydrogels.

Unlike pSTAT3, phosphorylated extracellular-signal-regulated kinase (pERK) did not significantly increase in co-cultures (blue bars) versus controls in neither PANC-1 or stromal cells (orange, green bars) (Figure 4.21 b). In 7.5% GelMA, pERK/ERK levels in co-cultures are 30-40% lower than control conditions. Therefore both PANC-1 and stromal cells increased phosphorylation of STAT3 while reducing that of ERK in stiff matrices. A direct inverse correlation in expression levels of pERK and pSTAT3 has already been reported both *in vitro* and *in vivo,* where they were responsible for mediating resistance to treatment (specifically MAPK/ERK – RAS - pathway inhibitors) [307]. Stiffness-induced increase of pSTAT3 and reduction of pERK could therefore be responsible for increased drug resistance in stiffer tumours.

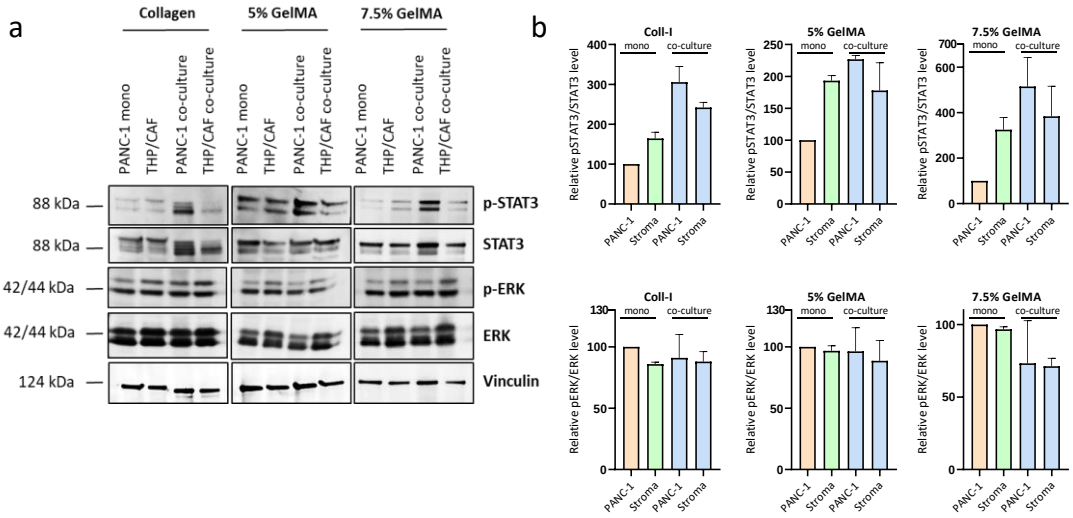

Figure 4.21 Indirect co-culture of PANC-1 cells with THP-1 cells and CAFs promotes activation of pro-survival pathways via STAT3 phosphorylation. (a) Immunoblots of phosphorylated MAPK (p-ERK) and STAT3 (p-STAT3) proteins with paired total proteins following 72 h of culture. Vinculin was used as protein loading control. **(b)** Relative STAT3 and MAPK densitometric analysis of phosphorylated/total protein bands in Figure 7a, data normalised to Vinculin control, change relative to PANC-1 monoculture controls (100%), n=2.

To conclude, indirect co-culture of PDAC and stromal (CAF and THP-1 cells) led to the upregulation of pSTAT3 levels in the cancer cells, together with a stiffness-dependant reduction in pERK levels. In the stromal cells, co-culture led to an increase in pSTAT3 in collagen and a decrease in pERK in 7.5% GelMA however, the individual protein levels in THP-1 and CAFs were not assessed.

4.4 Conclusions

In this chapter I covered a characterisation of the main biochemical properties of GelMA hydrogels which, together with biomechanics described in Chapter 3, provide an extensive characterisation of GelMA's versatility as a 3D cell culture platform. Since it was first described [236], it was clear that GelMA hydrogels' physical properties could be tuned by adjusting its degree of functionalisation (DoF), concentration, photo-initiator concentration and UV-exposure time during hydrogel polymerisation. We used ^{1}H NMR, alongside three spectroscopy-based techniques to characterise the DoF of our in-house GelMA batches (Figure 4.1). The DoF plays a role in GelMA's crosslinking efficiency, affecting in turn GelMA stiffness and stiffness predictability, hydrogel consistency and reproducibility, all leading to batch-to-batch and experimental variation. All tested batches had a very similar and high DoF (66-71%), minimising any inter-batch effects on biological assays. For GelMA batches with similar DoF, previous reports [230,242] have found hydrogel stiffness to be very similar (DoF 64%, 3.2± 0.18 kPa) [246] to what I previously reported in Figure 3.7 (DoF: 71%, 3.4 kPa). Pore size in GelMA hydrogels can also be tuned by its DoF and characterised via SEM. For DoFs between 60-75% the average GelMA hydrogel pore size has been found at 25-30 μm, a size which is conducive of cell proliferation and migration [246,247].

Next, the proliferation and spheroid formation abilities of cells in GelMA hydrogels was assessed (Figures 4.2-4.6). The work presented here showed that these hydrogels support long-term culture of both established cell lines and primary cells, which remained highly viable and proliferative. By day 14 of 3D culture, spherical aggregates were visible by brightfield imaging and resembled spheroids disseminating in the tumour fluid (ascites) of cancer-bearing patients, distinctively at late-stage disease [252,308]. The expression of biomarkers such as KRT19 was also maintained by GelMA-embedded cells throughout culture (Figure 4.4). Cell growth parameters such as spheroid diameter (Figure 4.3), shape (Figure 4.5), total hydrogel cell viability (Figure 4.6 a) and DNA content (Figure 4.6 b), were both stiffness-dependent and cell line specific.

All cell lines formed round spheroids with the exception of MIA PaCa-2 cells which proliferated in a disorderly fashion in stiffer matrices (7.5-10% (wt/vol) GelMA). A number of reports have described MIA PaCa-2 cells to form loose cell aggregates in 3D matrices compared to tighter clusters formed by the other three PDAC cell lines [201,203,309]. This phenotypic variability in spheroid formation can be attributed to the EMT status [203,282] and

aggressiveness of the cell lines, whereby Capan-2 and BxPC-3 formed tighter and compact spheroids whilst the more aggressive PANC-1 and MIA PaCa-2 formed irregular colonies. In a separate study, subcutaneous injection of these cell lines in mice resulted in well and moderately differentiated tumours for Capan-2 and BxPC-3 cells respectively, while PANC-1 and MiaPaCa-2 cell lines developed undifferentiated primary tumour masses, which proliferated in an unorganized way [201]. In PDAC, tissue stiffness is known to promote EMT, at least *in vitro* [128], which is evident through the loss of adhesion, circularity, and higher migration of cells towards the edges of stiff GelMA hydrogels (7.5-10% (wt/vol) GelMA). Cell lines with a highly epithelial phenotype (Capan-2 and BxPC-3) increased their proliferation in response to increased matrix stiffness (from 3% (wt/vol) to 5-7.5% (wt/vol) GelMA) whereas more mesenchymal cell lines did not increase their proliferation in response to stiffness.

In order to make molecular analyses feasible for my next chapters, I optimised techniques for the retrieval of cells from GelMA hydrogels without compromising their viability or expression profile. Gelatin retains a number of protease-sensitive and cell binding sites (such as RGD-binding and MMP-sensitive sites) [238] implicated in a number of physiological functions, including cell proliferation, migration, invasion, disease development and progression, and are therefore key components of any bioactive niche analogue. As such, it also retains collagen and fibronectin domains normally present in gelatin [109], which make it cleavable through digestion with collagenases and other proteolytic cocktails (Table 4.2, Figure 4.7). Other groups have developed different fast and non-invasive approaches for the digestion of synthetic hydrogels [310]. An example is the functionalisation of the polymer backbone with microbial protease-sensitive peptides. The resulting hydrogels would then allow controlled, immediate, on-demand degradation with the simple addition of a microbial protease [310].

Another aspect of working with GelMA is the use of UV light to which cells are subjected during hydrogel crosslinking. I used γH2AX as a marker to assess DSBs in the DNA as a result of UV-induced damage. Analysis was performed on cells after 10 minutes of UV exposure, the same amount of time normally employed for GelMA crosslinking. The number of γH2AX positive cells increased marginally 1-hour post-exposure but was back to control levels after 48 hours, suggesting affected cells either were unaffected, fully recovered, or underwent apoptosis (Figure 4.9a-c). An additional consideration is the higher UV dose to which monolayer cells were subjected, due to the lack of glass slide and hydrogel that would

normally be surrounding them during GelMA synthesis. For this reason, I also looked at γH2AX expression on GelMA sections at day 14 of culture (Figure 4.10). Some phosphorylated H2AX was detected in GelMA sections, particularly towards the rim of the spheroids, where the majority of proliferating cells are located. High γH2AX staining can be seen in S-phase cells even in the absence of DSBs [288], therefore the combined use of γH2AX together with other DSB-dependant markers, such as p53 binding protein (53BP1), RAD-51, or BRCA1 [311], would validate these results. The use of highly soluble, low concentration photo-initiators (e.g. LAP) and crosslinking via visible light, are rapidly changing the way GelMA is synthesised in order to reduce and remove risks associated with UV light exposure. Importantly, potential UV-induced DNA alterations might be responsible for changes in cell's sensitivity to chemotherapeutic agents, as tested later in Chapter 6. Future GelMA work should aim to characterise this in cultures pre and post-chemotherapy, with and without thee use of UV-photocrosslinking, to fully characterise the effects of crosslinking on treatment response.

Lastly, the effects of stromal and immune cell components on PDAC cells were assessed in GelMA hydrogels. Figure 4.11 showed ascites composition was largely attributable to stromal and immune cells, with less than 1.5% comprising malignant cells, which is largely concordant with other reports on both ascitic fluids [294,295] and primary tumour composition [59,192,281]. To reflect this, cell ratios in GelMA cultures always comprised more stromal (CAF and/or THP-1) cells than PDAC cells. Patient-derived CAF isolation and characterisation was conducted via flow cytometry and immunofluorescence on both ascites- and tissue-derived CAFs (Figure 4.11 b, Figure 4.12).

CAFs incorporation alongside PDAC cells increased both cell proliferation (Figure 4.13) and GelMA hydrogel stiffness (Figure 4.14). Interestingly, these effects were not observed when fibroblasts (NFs) isolated from normal tissue were used instead. Other groups identified Special AT-rich sequence-Binding protein-1 (SATB-1) and Stromal cell Derived Factor 1 (SDF-1) amongst the differentially upregulated genes in PDAC cells when exposed to CAFs versus NFs conditioned medium [64]. CAF-mediated SATB-1 upregulation of SDF-1 (also known as CXCL12) can signal through the SDF-1/CXCR4/SATB-1 axis increasing cell proliferation and chemotherapy resistance [64]. This could be of particular interest in our triple cultures as PDAC tumour-associated macrophages (TAMs) are also known to significantly upregulate CXCR4 [312]. This could be confirmed in the future via flow cytometry. Moreover,

CXCR4 overexpression represents a risk factor and is associated with increased incidence of distal metastases [313,314] and delayed PDAC diagnosis [315].

The ability of both malignant and stromal cells to remodel biomaterials, as they would do with the ECM, and affect their stiffness, has been known for decades [316]. CAFs specifically are capable of remodelling the surrounding matrix via both the platelet-derived growth factor receptor (PDGFR) and lysophosphatidic acid (LPA) receptors through phosphatidylinositol 3 kinase (PI3K) signalling [317]. Alternatively, LPA-stimulated remodelling can act through the Rho-kinase (ROCK) pathway [317]. In turn, both ROCK and PI3K lead to cofilin-mediated actin remodelling and matrix contraction [318]. It was therefore unsurprising that the culture of PDAC and CAFs would lead to matrix and hydrogel stiffening.

While CAFs presence supported spheroid formation and cell survival in GelMA hydrogels, macrophages alone did not have a significant effect on PDAC cell proliferation or hydrogel stiffness *in vitro* (Figure 4.16), concordant with other 3D studies [309,319]. The presence of THP-1 cells did, however, lead to an increased incidence of both tumours and metastases in orthotopic xenografts of PDAC cells with GelMA hydrogels as a delivery vector. Evidence of the crosstalk between PDAC cells and THP-1 is their differentiation into $CD68^{+}$ macrophages (Figure 3.11), which in turn, is known to increase PDAC cell migration and proliferation through increased IL-8 secretion and STAT3 expression [320,321]. This was indeed the case as both pSTAT3 and secreted IL-8 levels were higher in co-cultures compared to monocultures as shown in Figure 4.19 and Figure 4.21. Although not significant, resected tumour stiffness was also higher in PDAC+THP-1 groups compared to PDAC alone, suggesting increased tumour aggressiveness [322]. This also provided proof of application of GelMA hydrogels as a pancreatic and immune cell carrier. Implantation of the hydrogels was able to replicate tumour growth pattern, and, to a lesser extent, route of metastatic spread as observed in KPC mice (metastases: diaphragm 33%, peritoneal 5.5%) [323,324].

The addition of stromal cells (CAFs and THP-1s) to PDAC cells in GelMA triple-cultures led to increased cell proliferation and hydrogel stiffness compared to controls (Figure 4.17, 4.18). Tumour-fibroblast interactions and their importance in driving epithelial gene expression programs [325], as well as the tumour-macrophage crosstalk mentioned above, have been extensively characterised. However, more recently, new evidence suggests that macrophage suppression can directly affect CAF marker expression (αSMA downregulation) together with decrease in tenascin C, collagen and tissue stiffness [51]. This suggests a complex

multi-lateral crosstalk between all three cell types, as opposed to the traditional unilateral tumour-stroma interactions, could be in place for cell proliferation and hydrogel stiffness regulation in PDAC, and recapitulated in GelMA.

Lastly, the effects of co-culture on the activation of pro-survival signalling pathways was assessed in collagen and GelMA hydrogels, aiming to provide a better understanding of the tumour-stroma interactions leading to increased proliferation and matrix stiffness (Figure 4.17 and Figure 4.18). STAT3 activation was confirmed via immunoblotting following indirect co-culture of PDAC cells and stromal hydrogels, consistent with the increased proliferation observed in co-culture settings (Figure 4.21). Other groups also showed that exposure to CAF-conditioned media resulted in the induction of STAT3 phosphorylation in PDAC cells after 72 hours [18]. Furthermore, STAT3 inhibitors have successfully been employed in 3D models of PDAC cells and CAFs leading to a reduction in pSTAT3 levels and reduced cell proliferation and viability [326].

Previous reports in KPC mice identified a negative correlation between increased levels of pSTAT3 and decreased numbers of CAFs via TGFβ/SMAD signalling pathway [327], indicating a possible mechanism of treatment resistance due to stroma-depleting therapies. Importantly, STAT3 activity is also increased in a stiffness-dependant fashion (Figure 4.21). In several Kras-driven mouse models, both the loss of TGF-β signalling and elevated mechano-signalling via β1-integrin resulted in a positive feedback loop for the upregulation of STAT3 and a subsequent further increase in fibrosis, tissue tension and tumour progression [17]. This was also true in PDAC patients where elevated STAT3 expression corresponded to stiffer, matricellular-rich, fibrotic tumour linked with shorter survival [17]. This data suggests that a greater understanding of time-dependant resistance to both tumour- and stromal-targeting therapies is paramount for treatment durability. Stiffness-dependant and time-dependant changes in pSTAT3 and associated changes in CAF density and TGFβ signalling could be investigated further with the use of this indirect co-culture technique.

Contrariwise, no changes in phosphorylated ERK levels were detected upon co-culture with stromal cells, with a further decrease in expression within stiffer hydrogels (7.5% GelMA) (Figure 4.21). Concomitant activation of STAT3 and downregulation of ERK in PDAC cells has been associated with resistance [307]. ERK, but not STAT3, downregulation occurs also as a result of hypoxia [328], hence its reduction in 7.5% GelMA hydrogels might be indicative of lower oxygen diffusion within stiffer hydrogels. This mechanism is independent of hypoxia-

inducible factor 1 alpha (HIF-1α) [328], a master regulator of peri-tumoral stromal remodelling whose levels are significantly upregulated in stiffer matrices [134].

The aim of this Chapter was to characterise the biomechanical and bio-responsive features of GelMA hydrogels for their application in 3D cell culture. In addition to recapitulating key biomechanical, architectural, cellular and extracellular features depicted in Chapter 3, I showed how GelMA hydrogels allowed the culture of multiple cell types, both established and patient-derived cells, over an extended period of time, whereby maintain high cell viability. I started to investigate the effects of cellular TME components, namely fibroblasts and myeloid cells, on stiffness and cell proliferation both *in vitro* and *in vivo*. The next chapters will complement these data by looking at the transcriptomics of cells embedded in 3D matrices in order to identify and target mechanobiology-related processes.

Chapter 5 - Transcriptomics of PDAC cells in GelMA and Collagen hydrogels

5.1 Background

The *in vitro* modelling of PDAC using complex 3D models is crucial to predict treatment responses and bridge the gap between laboratory results and clinical data. Matrigel and collagen-based organotypic approaches are limited by undefined and varying composition, as well as in recapitulating tumour stiffness, which is known to affect treatment response. Both 2D and 3D cultures, as well as *in vivo* studies, have shown stiffness can affect cell morphology [329], proliferation [128], invasion [129], EMT [128] and cell-cell interactions [17,330], in experiments that span a wide variety of cell types and matrix-based cell culture approaches. In addition, transcriptome-wide changes are associated with the simple transition from 2D to 3D cell culture [331]. Mechanistic studies have shed light on a number of signal transduction modes that convert matrix-sensing to changes in intracellular signalling pathways and gene expression [17,128,332].

Here, I hypothesised that the use of GelMA hydrogels of different stiffness (5% and 7.5% GelMA) can provide a microenvironment capable of directing not only PDAC cell growth but also stiffness- and matrisome-related gene programs. BxPC-3 and PANC-1 cells were chosen for this analysis as representative epithelial and mesenchymal-like cell lines respectively [203,282]. Signatures of GelMA-embedded cells were compared against those of cells cultured in the commonly-used collagen hydrogels (Col). As an additional comparison, primary cells derived from three PDAC patients (12556, 12560, 12975) were cultured as organoids in Matrigel (Mat). These samples were set up, collected, and analysed as part of an ongoing project with another member of our group (Dr David Osuna de la Peña).

RNA sequencing (RNA-seq) was performed at the Oxford Genomics Centre to establish similarities and differences between the different 3D cell cultures in GelMA hydrogels and the control matrices collagen or Matrigel. In addition to differential gene expression between GelMA and controls, the transcriptional changes in epithelial-to-mesenchymal (EMT) status, PDAC matrisome [86,87], and other matrix [120] signatures were assessed.

5.2 Aim and objectives

Following biomechanical (Chapter 3) and functional (Chapter 4) characterisation of cell-laden GelMA matrices, the transcriptional profile of BxPC-3 and PANC-1 cells in collagen, 5% and 7.5% GelMA hydrogels will be explored in this Chapter.

I will:

- Compare and validate the transcriptional differences between 5% GelMA, 7.5% GelMA, collagen gels with Matrigel-cultured primary tumour organoids
- Explore the relevance of differentially expressed genes in biological pathways and processes
- Investigate associations between GelMA transcriptomes and reported PDAC matrisome [87] and matrix index [120] (MI) signatures
- Identify changes in secretome-related genes

5.3 Results

5.3.1 Exploratory analysis of differentially expressed genes in GelMA

To better understand the behaviour of PDAC cells in 3D matrices, transcriptomic profiling (Chapter 5) and further functional analyses (Chapter 6) were performed. BxPC-3 or PANC-1 cells were grown for 7 days is either collagen (1 mg/ml), 5% or 7.5% GelMA hydrogels prior to RNA extraction (as described in Section 4.3.3) and poly-A capture (Oxford Genomics). Samples were run in duplicates. BxPC-3 and PANC-1 cells showed distinct morphologies and behaviours in 3D cell cultures (Figures 4.5, 4.6), EMT statuses, and maintained *in vivo* tumorigenicity abilities (Table 4.3), hence why they were chosen for analysis. As an additional comparison, primary PDAC patient cells (patients 12556, 12560, 12975) were grown for 7 days as organoids in Matrigel and underwent simultaneous transcriptomic profiling as the collagen and GelMA samples. For ease of labelling collagen hydrogels are named COL, MAT refers to Matrigel cultures and _5 and _7.5 refer to 5% and 7.5% GelMA respectively.

Unsupervised cluster analysis showed good correlation between repeats (duplicates) and clustering of each cell line and matrix stiffness with each other (Figure 5.1 a-b), with clear separation between BxPC-3 and PANC-1 transcripts. Matrigel organoids clustered separately and showed higher similarity to BxPC-3 transcripts. To better understand the differences between cells cultured in stiff versus soft matrices, differential gene expression was analysed (false discovery rate, FDR < 0.05). A total of 4209 genes were found differentially expressed between collagen and 7.5% GelMA cultures for BxPC-3 cells and 7378 for PANC-1, of which ones with an absolute fold change greater than 2 (logFC ≥ 1 or logFC ≤ -1) are indicated in Figure 5.1 c. Venn diagrams were used to show overlapping of differentially expressed genes (DEGs) that were upregulated (Figure 5.1 d) or downregulated (Figure 5.1 e) of a factor of ≥ 2 amongst all the significant DEGs.

Next, genes were ranked by the $\log_{10}$ p-value against their fold change ($\log_2$FC) to identify genes that were significantly up- or down-regulated in a volcano plot (Figure 5.2). Plots for both 5% and 7.5% GelMA compared to collagen are shown. The top 20 up- and down-regulated genes of the comparison between collagen, 5% and 7.5% GelMA with associated logFC and p-values are listed in 9.4 Appendix 5.3.

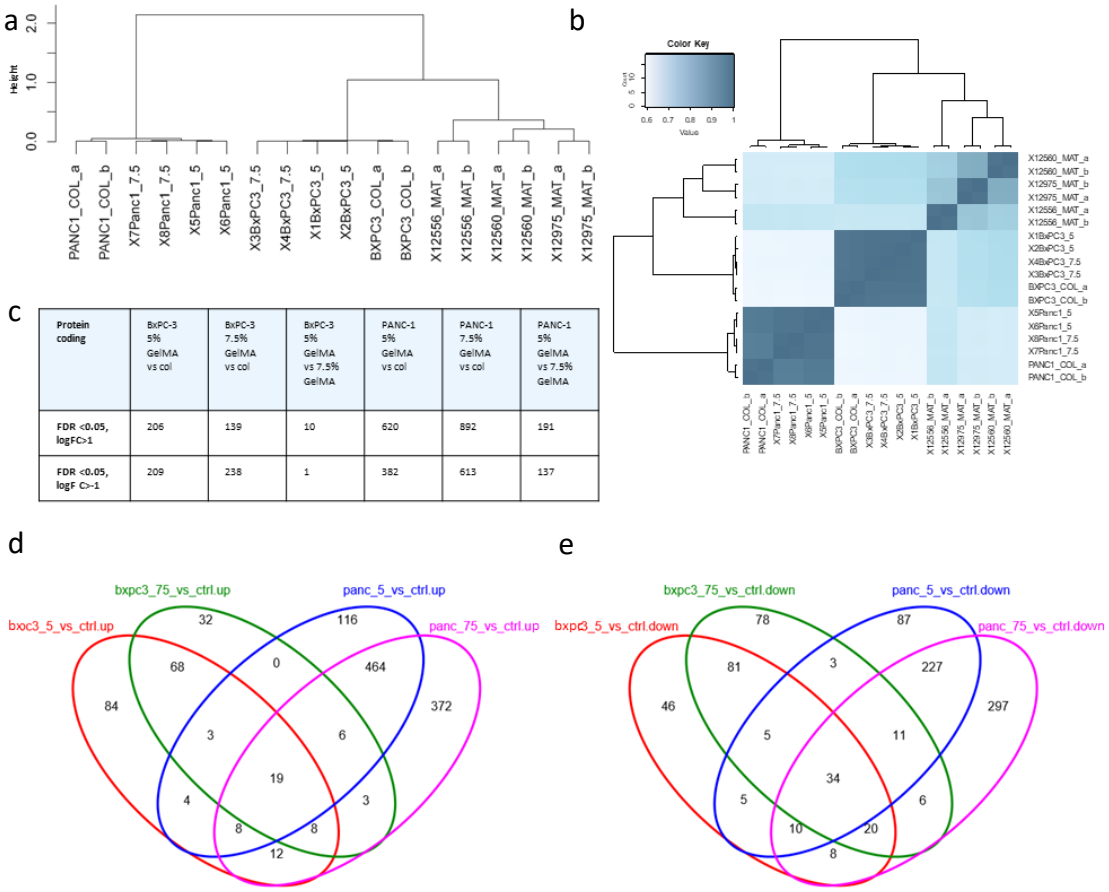

Protein coding	BxPC-3 5% GelMA vs col	BxPC-3 7.5% GelMA vs col	BxPC-3 5% GelMA vs 7.5% GelMA	PANC-1 5% GelMA vs col	PANC-1 7.5% GelMA vs col	PANC-1 5% GelMA vs 7.5% GelMA
FDR <0.05, logFC>1	206	139	10	620	892	191
FDR <0.05, logF C>-1	209	238	1	382	613	137

Figure 5.1 Exploratory clustering and number of differentially expressed genes (DEGs) of PDAC cells grown in Matrigel, collagen, 5% GelMA and 7.5% GelMA matrices. BxPC-3 or PANC-1 cells were grown for 7 days is either collagen, 5% or 7.5% GelMA prior to RNA extraction and poly-A capture (Oxford Genomics). Primary PDAC patient cells (12556, 12560, 12975) were grown for 7 days in Matrigel prior to analysis as additional comparison. **(a-b)** Cluster dendogram and unsupervised clustering of all genes. **(c)** Table of DEGs using the generalised linear model on EdgeR R package, FDR<0.05 FC≥1 or FC≤-1 (at least 2 fold change). **(d)** Venn diagram indicating individual and overlapping upregulated DEGs in collagen, 5% and 7.5% GelMA, FDR<0.05 FC≥1. **(e)** Venn diagram indicating individual and overlapping downregulated DEGs in collagen, 5% and 7.5% GelMA, FDR<0.05 FC≤-1.

In BxPC-3 cells, highly upregulated genes in 5% GelMA compared to collagen were associated with cell invasion, motility and EMT, and included for example bone morphogenic protein 7 (*BMP7*), chemokine ligand 14 (*CXCL14*), myosin light chain 9 (*MYL9*), CCN family member 1 (*CCN1*). In PDAC, BMP7 is known to induce EMT through transforming growth factor-β (TGF-β)/SMAD1 signalling [333] as well as cell invasiveness through matrix metalloproteinase (MMP2) expression [334]. Similarly, CXCL14 is upregulated during PDAC progression and implicated in invasion and metastasis through NF-kB signalling, while also acting as a chemoattractant for monocytes [335,336]. MYL9 is involved in actomyosin-mediated cell contractility and the Rho-associated protein kinase pathway (RhoA/ROCK) [337], while CCN1 is a tumour promoter, and plays a crucial role in gemcitabine resistance through deoxycytidine kinase production [338]. Downregulated genes

included structural molecules such as keratins, lysyl oxidase like 2 (*LOXL2*), mucin 2 (*MUC2*) and *ADAMTSL4*, as well as vascularisation-related proteins such as placental growth factor (*PGF*) and egl-9 family hypoxia inducible factor 3 (EGLN3), both involved in vascular endothelial growth factor (*VEGF*) transcription [339]. LOX family members are known to mediate collagen cross-linking and ECM stiffening [134], hence LOXL2 downregulation could be a result of stiffness-sensing in GelMA compared to collagen matrices.

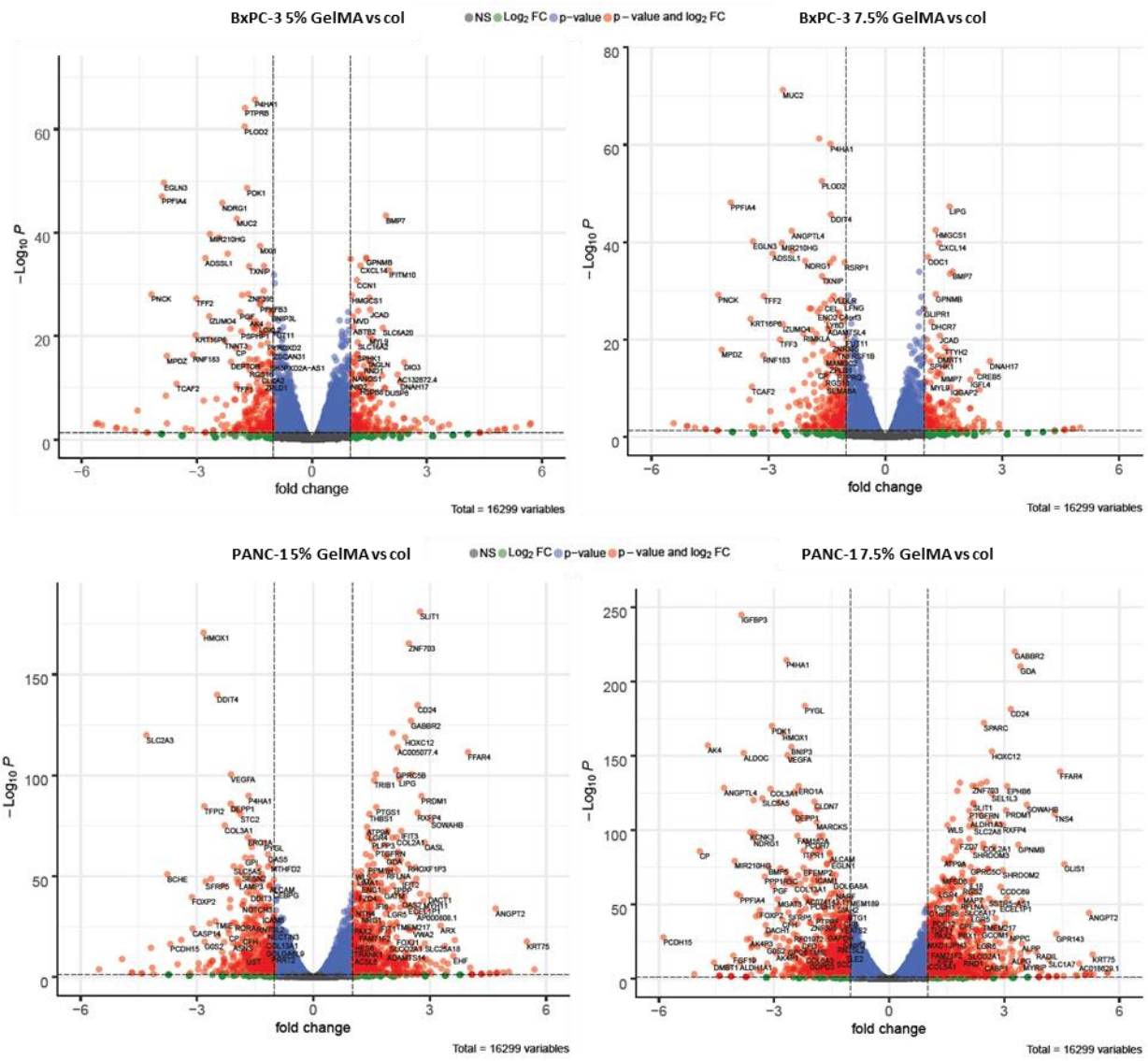

Figure 5.2 Volcano plots of p-value and log_2FC for each stiffness (5% and 7.5% GelMA) compared to collagen control. Labelled red dots represent genes with $p<0.05$ and $log_2FC \geq 1$ or ≤ -1 (at least two-fold change). Top panels, BxPC-3 cells, bottom panels PANC-1 cells. Left panes 5% GelMA vs collagen, right panels 7.5% vs collagen. [see Appendix 9.3 for a larger version of the above graphs]

When comparing BxPC-3 cells in 7.5% GelMA hydrogels and collagen, we found that upregulation of *BMP7, CXCL14* and *MYL9*, as well as downregulation of *MUC2* and *EGLN3*, was maintained. Interestingly, *MMP7*, involved in initiation and maintenance of metaplasia in PDAC [143], was also amongst the highest upregulated genes in 7.5% GelMA hydrogels. When comparing BxPC-3 cells in 7.5% GelMA to 5% GelMA, we noticed the

further upregulation of genes involved in cell adhesion and tissue structure, namely laminin gamma 3 (*LAMC3*), and the cell survival cystatin-M (*CST6*), both of which are associated with PDAC progression [340,341]. The upregulation of genes involved in matrix remodelling such as *BMP7, MYL9, LAMC3* and *MMP7* was encouraging, as this will be the focus of the targeting strategies discussed in Chapter 6.

PANC-1 cells in 5% GelMA showed an upregulation of cancer stem cell-associated genes compared to collagen hydrogels. These included *CD24*, commonly associated with worse prognosis [115], and leucine-rich repeat-containing G-protein coupled receptor 4 (*LGR4*) and *LGR5*, which are commonly used markers for the assessment of organoid development [223,342]. Other upregulated genes included structural factors like *COL2A1, ADAMTS14, KRT75* and the oncogenic transcription factor *PAX2*. A number of collagens (*COL3A1, COL13A1*) and structural adhesion genes (*ICAM5, ALCAM*) were also found amongst the top downregulated genes, suggesting proliferation in GelMA might require different set of matrix remodelling and cytoskeletal genes compared to cells in collagen hydrogels. Tumour angiogenic vascular endothelial growth factor A (*VEGFA*) was also significantly downregulated in GelMA, however, other interactome members of the VEGF signalling pathways such as angiopoietin 2 (*ANGPT2*) and interleukin 18 (*IL-18*) [343,344] were upregulated, indicating more complex and dichotomous processes might be in play.

Significantly upregulated and downregulated genes in 7.5% GelMA versus collagen PANC-1 genes were largely concordant with those observed in 5% GelMA with the addition of *LGR6, COL5A1* genes. Comparing 7.5% GelMA to 5% GelMA PANC-1 cells showed an upregulation in *ANGPTL2*, a factor associated with increased metastatic potential in PDAC [345,346], and the serine protease inhibitor *SERPINA3*, whose upregulation is linked with increased cancer cell migration and invasion [347]. The upregulation of structural and protease-related genes suggested that cells may be capable of undergoing protease-mediated matrix remodelling and migration in GelMA hydrogels.

Significantly DEGs in both BxPC-3 and PANC-1 cells were compared, in order to identify common overlapping genes. In 5% GelMA, 34 genes were upregulated in both BxPC-3 and PANC-1 cells compared to collagen hydrogels, while 54 genes were downregulated in both cell lines compared to collagen. In 7.5% GelMA, upregulation of 36 genes was overlapping between the two cell lines when compared to collagen controls, while 71 were downregulated. Overlapping genes were visualised as heatmaps in Figure 5.3 (5% GelMA,

left; 7.5% GelMA, right). Several of the matrix- and protease-related genes described above were found overlapping in both cell lines, including LOX, MMP7/9, ANGPTL4, SERPINA3, COL4A4, MUC5, ADAMTS14, suggesting regulation of mechanosensing pathways might be conserved in GelMA hydrogels.

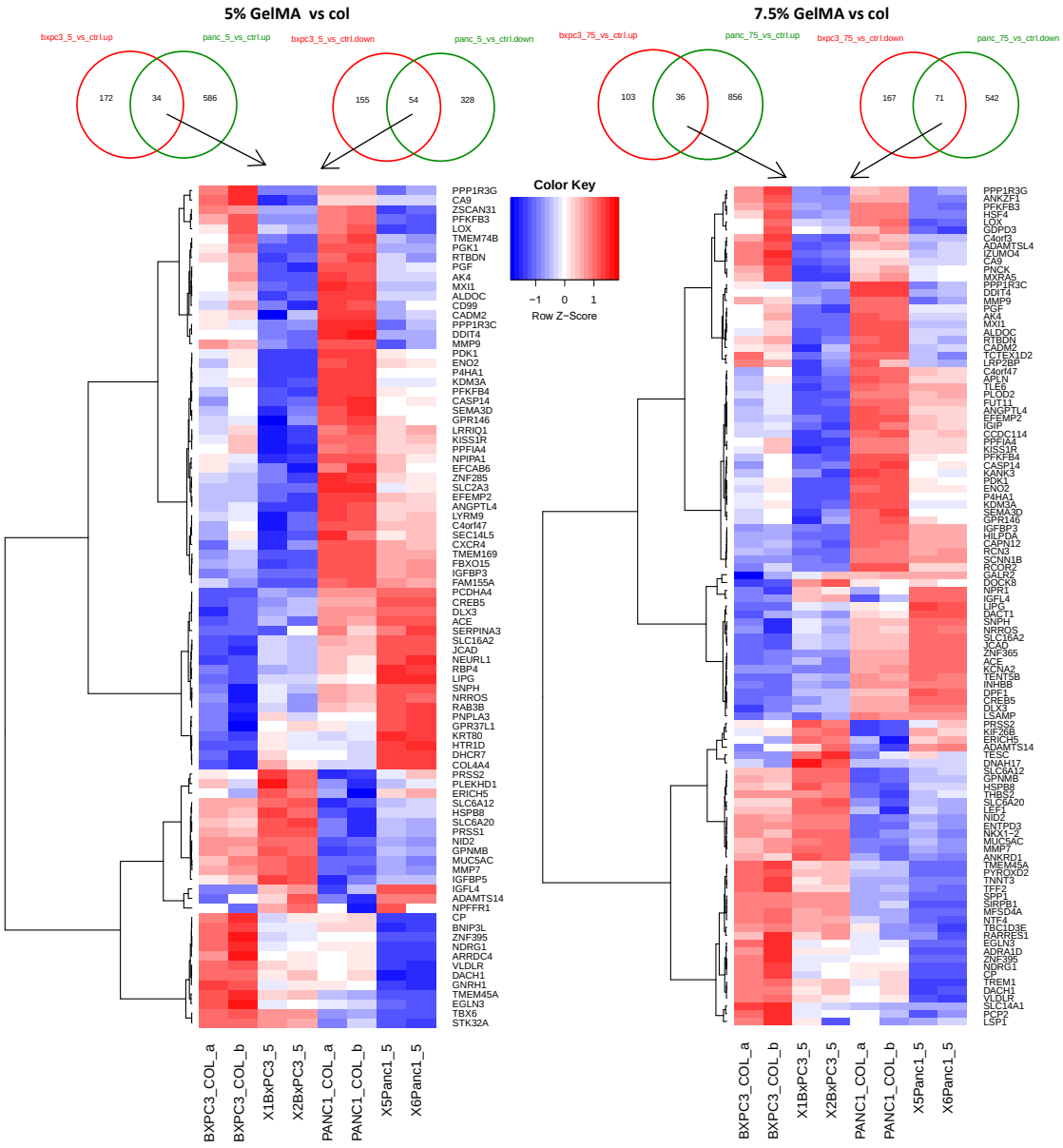

Figure 5.3 Overlap of significantly different protein-coding genes (FDR< 0.05) and at least two-fold change (logFC≥1 or logFC≤-1) in the 5% (left) and 7.5% (right) GelMA compared to collagen. Heatmap shows the common upregulated (red) and downregulated (blue) genes in the two cell lines.

Primary PDAC organoids grown in Matrigel offered an additional comparison thanks to the use of patient-derived PDAC cells, as well as Matrigel substrate, which is the gold standard for 3D organoid cultures [201,223,227,348]. In Figure 5.4 transcripts from collagen, 5% GelMA and 7.5% GelMA were compared to Matrigel organoids. This analysis identified a total of 1592 DEGs between Matrigel and collagen, 1644 between Matrigel and 5% GelMA and 1676 between Matrigel and 7.5% GelMA cultures. As cells and hydrogel composition were the

same in 5% and 7.5% GelMA cultures, it could be speculated that a minimum of 32 genes were differentially expressed as a result GelMA stiffness. Correlation analysis was also performed on these datasets and is illustrated in Figure 5.4 b. Pearson correlation coefficient (r) showed Matrigel organoids highly correlated with both collagen and GelMA cultures ($r > 0.6$), indicating high similarity between all the assessed 3D cell culture methods. With the exception of patient 12556, organoid transcripts had a higher correlation with BxPC-3 cells than PANC-1, which was surprising considered that PANC-1 showed upregulation of many stem cell and organoid markers in GelMA. This could be due to Matrigel being a very soft matrix, hence cell transcriptional profiles showed a higher correlation with cells in softer (collagen) matrices and epithelial phenotype (BxPC-3) as opposed to mesenchymal (PANC-1). Patient 12556 presented with the latest stage of disease (IIB) and the most mutations (KRAS, TP53) compared to the other patients (Figure 5.4 c). Concordantly, transcripts from 12556-derived organoids showed a slightly higher correlation for the more mesenchymal PANC-1 transcripts than BxPC-3 cells.

a

Protein coding	Col vs mat	5% GelMA vs mat	7.5% GelMA vs mat
FDR <0.05, logFC>1	909	978	990
FDR <0.05, logFC>-1	683	666	686

c

Patient ID	Gender	Stage	Histology	Mutations
12556	Male	IIB	PDAC	*KRAS, TP53*
12560	Male	IIB	PDAC	*KRAS*
12975	Female	IIA	IPMN/PDAC	*KRAS*

b

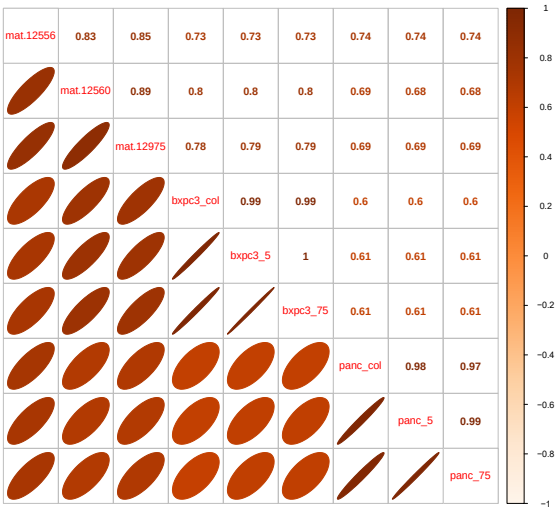

Figure 5.4 Number of differentially expressed (DEGs) and strength of correlation between genes of PDAC cells grown in Matrigel (mat) versus collagen, 5% GelMA and 7.5% GelMA matrices. (a) Table of DEGs using the generalised linear model on EdgeR R package, FDR<0.05 FC≥1 or FC≤-1 (at least 2 fold change). **(b)** Comparison of PDAC Matrigel organoids with the other models. Values correspond to r (Pearson correlation coefficients) based on average reads per kilobase of transcripts per million reads (RPKM) of 16,299 genes in pairwise alignments. Diameter of ellipses is proportional to r, thinner ellipses represent higher correlation coefficients. **(c)** Patient information for PDAC-derived organoids. IPMN = Intraductal papillary mucinous neoplasm.

5.3.2 Transcriptome-wide associations with biological pathways

To assess the importance of these DEGs in biological pathways, KEGG, Reactome and Naba [269] pathways and gene set enrichment analyses (GSEA) were performed (Figure 5.5). The DEGs between collagen and GelMA were grouped into 35 canonical pathways and displayed in Figure 5.5 a. Lower p-values equal higher the $\log_{10}$ p-values, resulting in bigger dots, while normalised enrichment score (NES) indicates sample activity relative to control (blue for weaker, red for stronger enrichment). Pathway analysis indicated that across both BxPC-3 and PANC-1 cells, upregulated DEGs were involved in multiple tumorigenic pathways including Wnt, Rho GTPases and G-protein coupled receptor (GPCR) signalling, all of which have been associated with increased tumorigenicity and are linked to mechano-transduction in PDAC [16,134,135,349,350] (Figure 5.11). Interestingly, O-linked glycosylation and associated disease pathways were also upregulated, and will be discussed in Section 5.3.3. Across both cell lines, downregulated pathways included metabolism (glucose, glycolysis, gluconeogenesis, mannose), IL-6 receptor-ligand interactions and cellular responses to hypoxia.

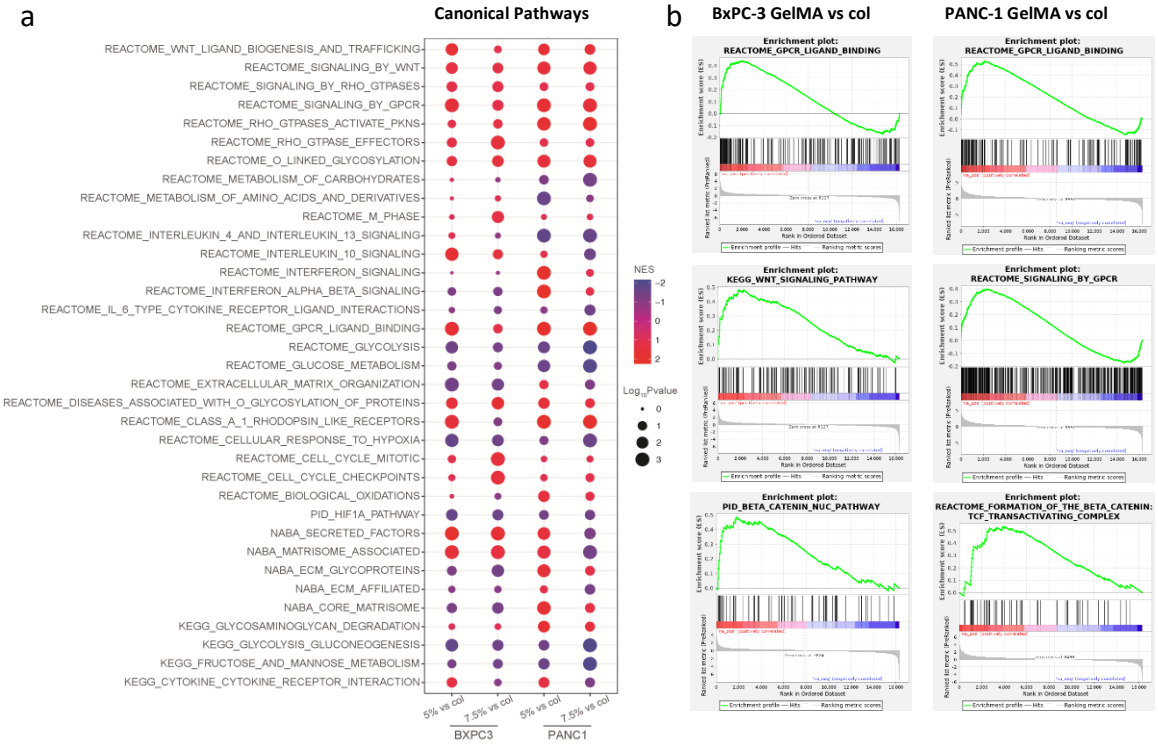

Figure 5.5 Analysis of differentially regulated pathways and Gene Set Enrichment Analysis (GSEA) for BxPC-3 and PANC-1 cells in collagen versus 5% and 7.5% GelMA. (a) Enrichment in KEGG, Reactome and Naba pathways. Colour represents the normalised enrichment score (NES) while the size of the dot indicates significance (log10p-value). **(b)** GSEA-enrichment plots (Broad Institute) using all genes for canonical pathways, ranked by the logFC for BxPC-3 (left) and PANC-1 (right) in 7.5% GelMA versus collagen.

Figure 5.5 b shows GSEA plots for some of the above-mentioned pathways comparing cells in GelMA and collagen hydrogels. Selected plots showed the enrichment of mechano-sensing and mechano-transduction pathways in GelMA, namely through GPCR, Wnt and β-Catenin/TCF signalling [128] (Figure 5.11).

To further assess the importance of genes in biological processes, gene sets were selected, related to processes relevant for cell adaptation within matrices of different stiffness, including proteases (Figure 5.6 a), EMT (Figure 5.6 b) and mechano-sensing (Figure 5.6 c). As seen from the heatmaps, expression of most genes highly differed between BxPC-3 and PANC-1 cells. Unsurprisingly, PANC-1 cells exhibited higher expression of EMT markers including vimentin, N-cadherin, Snail and Zeb1, compared to BxPC-3 cells which showed higher expression of E-cadherin [128,203,282].

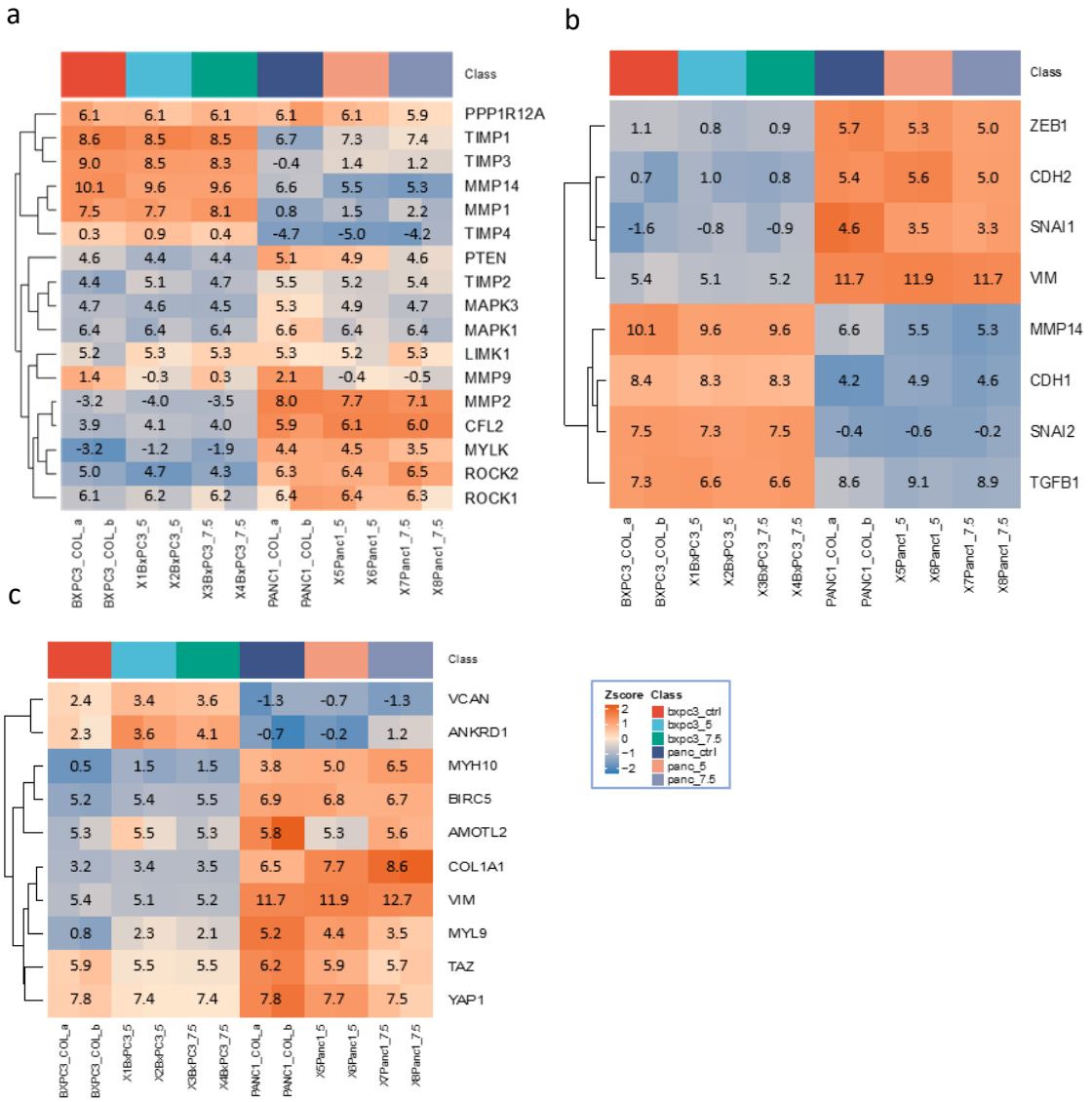

Figure 5.6 Expression heatmaps of genes related to (a) proteases, (b) EMT and (c) mechanosensing pathways in BxPC-3 and PANC-1 PDAC cells grown in collagen, 5% GelMA and 7.5% GelMA. Number of read counts after count normalisation are indicated on the heatmaps for comparison of absolute abundances.

Amongst mechano-sensing related genes, ankyrin (*ANKRD1*), myosin (*MYH10*) and collagen I (*COL1A1*) expression increased in both BxPC-3 and PANC-1 cells in response to stiffness. Versican (*VCAN*) and *MYL9* expression increased in BxPC-3 but not PANC-1 cells in stiffer matrices, while PANC-1 had an increased expression in vimentin (*VIM*). Neither cell line had an increased expression of the mechano-transductor genes Yes-associated protein and transcriptional coactivator with PDZ-binding motif (YAP/TAZ) in GelMA compared to collagen. However, YAP/TAZ signal primarily through translocation to the nucleus, therefore immunofluorescence rather than gene analytical techniques, should be used to assess its activation [17].

In summary, cells retained the expression of genes important for mechano-transduction in GelMA, namely through Wnt, GPCR, Rho GTPase and β-catenin pathways. They also showed high variability between cell lines, concordant to their EMT status.

5.3.3 Post-translational modifications and matrisome-related gene profiles in GelMA and collagen hydrogels

Attempting to replicate the tumour biomechanics and matrix structure, signatures of genes involved in matrisome composition as well as unusual protein glycosylation patterns were assessed. The matrisome is defined as the proteome subset that constitutes the ECM. It comprises over 1000 secreted proteins, of which around a quarter are categorised as "core matrisome" due to their fundamental ECM organisation role, while the remaining ones fall under "matrisome-associated" nomenclature [91]. Naba et al. [269], classified ECM proteins into categories that are now widely used in proteomics and during matrisome classification. The various categories and their involvement in PDAC pathogenesis have been described in detail in Section 1.2.2.

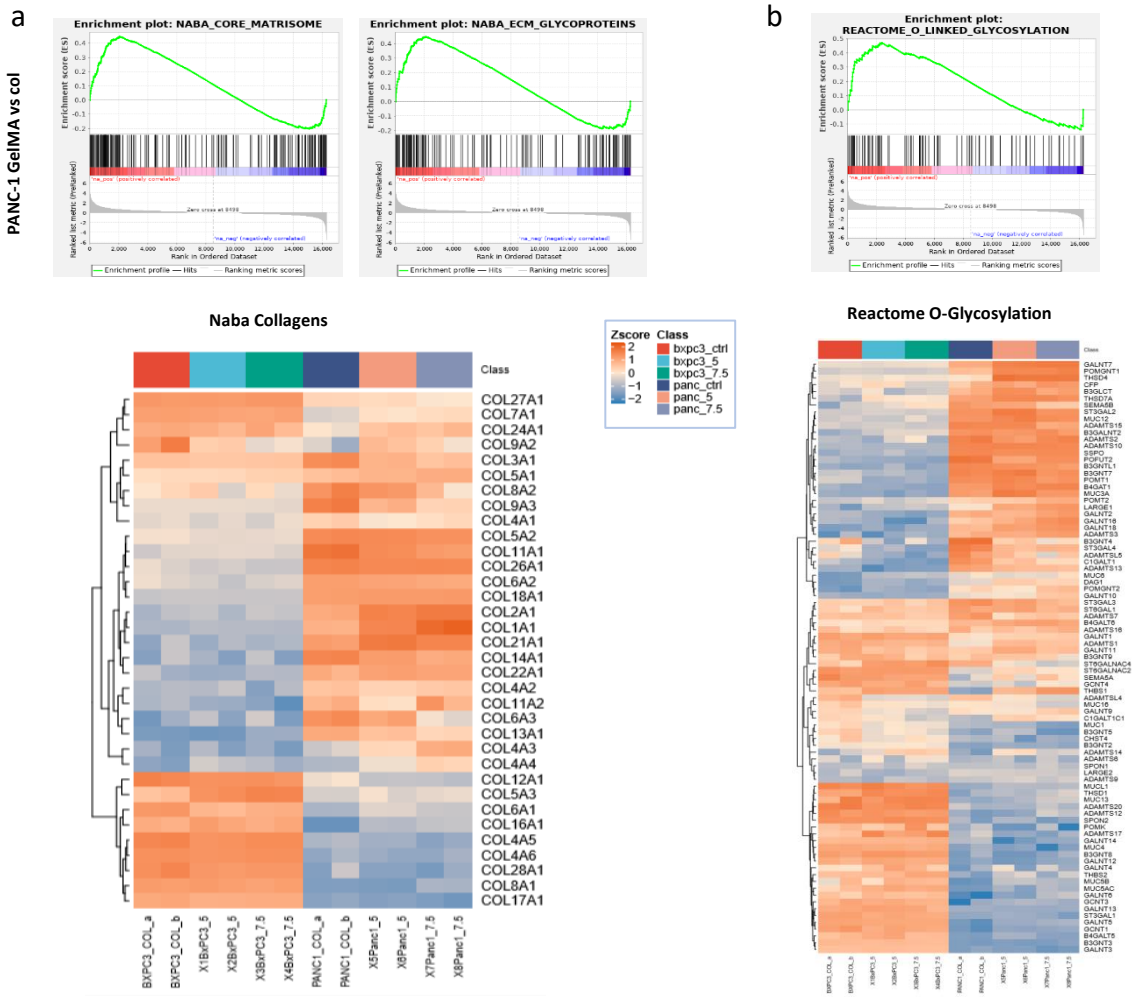

Figure 5.7 Gene set enrichment analysis (GSEA) and expression heatmaps of (a) Naba's core matrisome and (b) O-linked glycosylation in BxPC-3 and PANC-1 cells in collagen, 5% and 7.5% GelMA hydrogels.

Despite proteomics usually being the favourable technique for this analysis, GSEA was performed instead on Naba matrisome-associated gene categories (Figure 5.7 a). Naba "core matrisome" proteins were enriched in GelMA, as well as the ECM glycoprotein subset component. Despite Naba's collagens category not being found amongst DEGs, the heatmap in Figure 5.7a shows differential expression of several collagens (*COL1A1, COL11A1, COL9A2, COL3A1*) while expression of others was conserved (*COL5A2, COL17A1, COL4A6, COL18A1*).

Interestingly, the O-linked protein glycosylation pathway was also highly enriched in GelMA hydrogels in both BxPC-3 and PANC-1 cells (Figure 5.5a, Figure 5.7 b). O-linked β-N-acetylglucosamine (O-GlcNAc) is a post-translational modification mechanism by which a sugar is attached to the serine residues of a protein, thereby modifying protein activity [351]. The expression heatmap of all the genes constituting the O-glycosylation gene set (Reactome) is shown in Figure 5.7 b. In PDAC, hyper-*O*-GlcNAcylation is anti-apoptotic and contributes to NF-κB oncogenic activation [351].

In 2019, Tian et al. [86,87] reported the first study on the PDAC matrisome. The authors were able to discriminate between tumour cell and stroma-derived ECM proteins and indicated that the tumour-produced proteins correlated with poor patient survival. In contrast, despite the majority of the tumour bulk comprising stromal-derived ECM, the role of these in disease and survival was much more heterogeneous [87]. The authors identified a PDAC-specific signature, against which our RNA-seq data was compared (Figure 5.8 a).

The majority of matrisome-associated genes were upregulated in PANC-1 cells compared to BxPC-3. A subset of these genes was further upregulated in PANC-1 cells cultured in 7.5% GelMA compared to 5% GelMA and collagen hydrogels, including collagens (*COL1A1, COL2A1, COL5A1*), elastin microfibril interfacer (*EMILIN1*), fibrillin (*FBN1*), and heparan sulphate proteoglycan (*HSPG2*), which are associated with poorer prognosis [120,352]. This supports the notion that tumour cells alone can contribute to adverse ECM protein production in concordance with their EMT status and increased substrate stiffness.

In order to further assess the contribution of PDAC cells to matrix production and prognosis, the matrix index (MI) was calculated and shown in Figure 5.8 b, alongside that of KPC mouse model (LSL-$Kras^{G12D/+}$; LSL-$Trp53^{R172H/+}$; Pdx-1-Cre) and TCGA data. The MI is an ECM-associated signature (comprising 22 molecules), that predicted both extent of

disease and tissue stiffness at gene transcription level, where it was first discovered, and validated at protein level [120]. It was originally characterised in HGSOC but also correlated with 12 other solid cancers including PDAC [120]. MI analysis of our tumour cell cultures provided a measure of their contribution to ECM-associated gene expression directly linked to their prognostic value.

Unsurprisingly, PANC-1 cultures showed a higher MI compared to BxPC-3 cells (Figure 5.8 b). Although not significant, 5% GelMA cultures had a higher MI compared to cells cultured in collagen hydrogels. Both KPC mice and TCGA data had MIs that closely resembled that of PANC-1 cells. MI did not however correlate with stiffness, at least in GelMA, as both cell lines showed a lower MI in 7.5% GelMA when compared to 5% GelMA. As MI was characterised in omental tissues, the mechanics and therefore correlation with stiffness are likely to be different from PDAC (as shown in Chapter 3) and even more so in hydrogels. Taken together, these data suggested that despite the MI having been originally characterised at a whole-tissue level (tumour and stroma), it also correlated to tumour cell phenotypes alone and was closely linked to matrisome-associated gene expression, at least for BxPC-3 and PANC-1 PDAC cells.

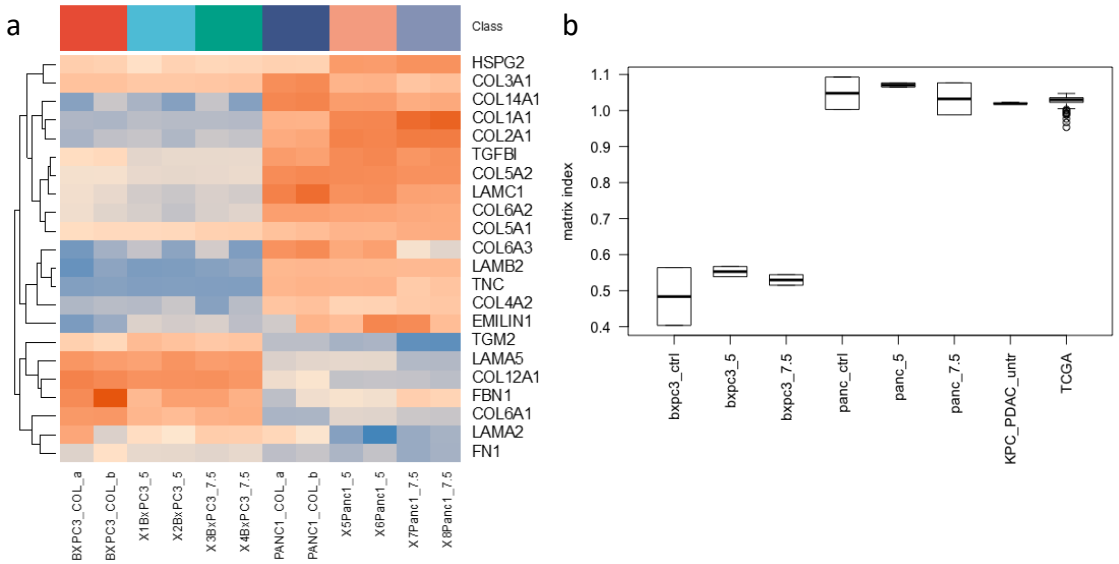

Figure 5.8 Expression of PDAC matrisome signature (Tian et al.) and Matrix Index (MI) (Pearce et al.) in BxPC-3 and PANC-1 cells in collagen, 5% and 7.5% GelMA hydrogels. (a) Expression heatmap of PDAC matrisome-associated genes, Tian et al. 2019. **(b)** Calculated MI for BxPC-3 an PANC-1 cells in 3D models, alongside KPC PDAC mouse model and TCGA data, accessed at https://www.cancer.gov/tcga. AGT, CTSG, COL15A1, COL6A6 not detected for MI calculation.

5.3.4 Validation of RNA-seq data in GelMA and collagen hydrogels

A total of 8 genes were selected for validation of RNA-seq gene expression by quantitative RT-PCR using independent RNA samples. Genes selected belonged either to the MI (*COL1A1, COL11A1, CTSB, FN1, VCAN*), or mechanobiology and proteases categories (*MMP9, TGFBI, YAP1*). Expression of collagen-I, fibronectin and versican had also been confirmed at protein level in 5% GelMA hydrogels (Figures 3.10-3.11), while proteases will be the focus of the next Chapter. Of these, all except *VCAN* were highly expressed (Ct < 28 cycles). RNA-seq (Figure 5.9 a) and qRT-PCR data (Figure 5.9 b) were largely in agreement and showed a comparable trend in expression.

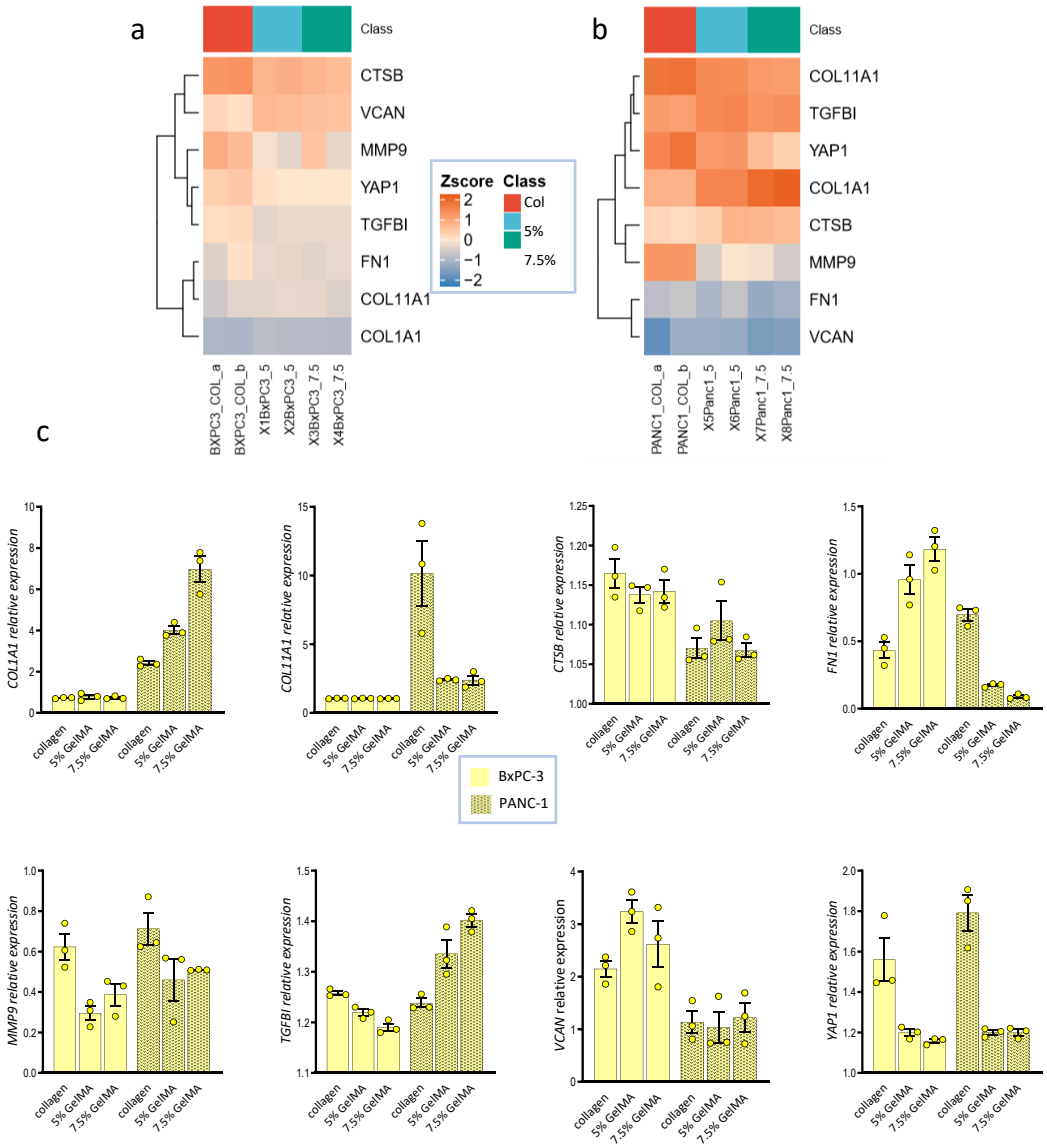

Figure 5.9 qRT-PCR validation of RNA-seq data. (a) Gene expression heatmap of selected genes in BxPC-3 cells cultured in collagen, 5% and 7.5% GelMA. **(b)** Gene expression heatmap of selected genes in PANC-1 cells. **(c)** qRT-PCR validation of genes shown in (a-b), expression relative to *HPRT-1*, n=1 hence no statistics.

5.3.5 Secretome-related gene profiles and validation in GelMA and collagen hydrogels

Lastly, the expression of secretome-related genes was assessed in our dataset. The secretome is a subset of the proteome which comprises between 13-20% of all human proteins including cytokines, growth factors, and receptors [324]. These often constitutes the largest proportion of Naba's "matrisome-associated" genes and include secreted factors that may interact with core ECM proteins [91] such as BMPs and Wnts, some of which were found amongst the DEGs in collagen and GelMA, as well as TGFβ and cytokines. Naba's secreted factors are shown in Figure 5.10 alongside including the GSEA (Figure 5.10 b) in GelMA. Secreted factors were largely upregulated in BxPC-3 cells compared to PANC-1. Figure 5.10 c showed the differential expression of cytokines in the two cell lines. Amongst these, *CXCL8* and *CCL22* were upregulated in BxPC-3 cells in GelMA compared to collagen, while *IL-16* was upregulated in PANC-1. Upregulation of IL-16 was also significantly associated with disease score in the tissues used for MI characterisation in HGSOC [120], and is a key regulator of fibrosis [353], suggesting this cytokine could be a mediator of tissue stiffness.

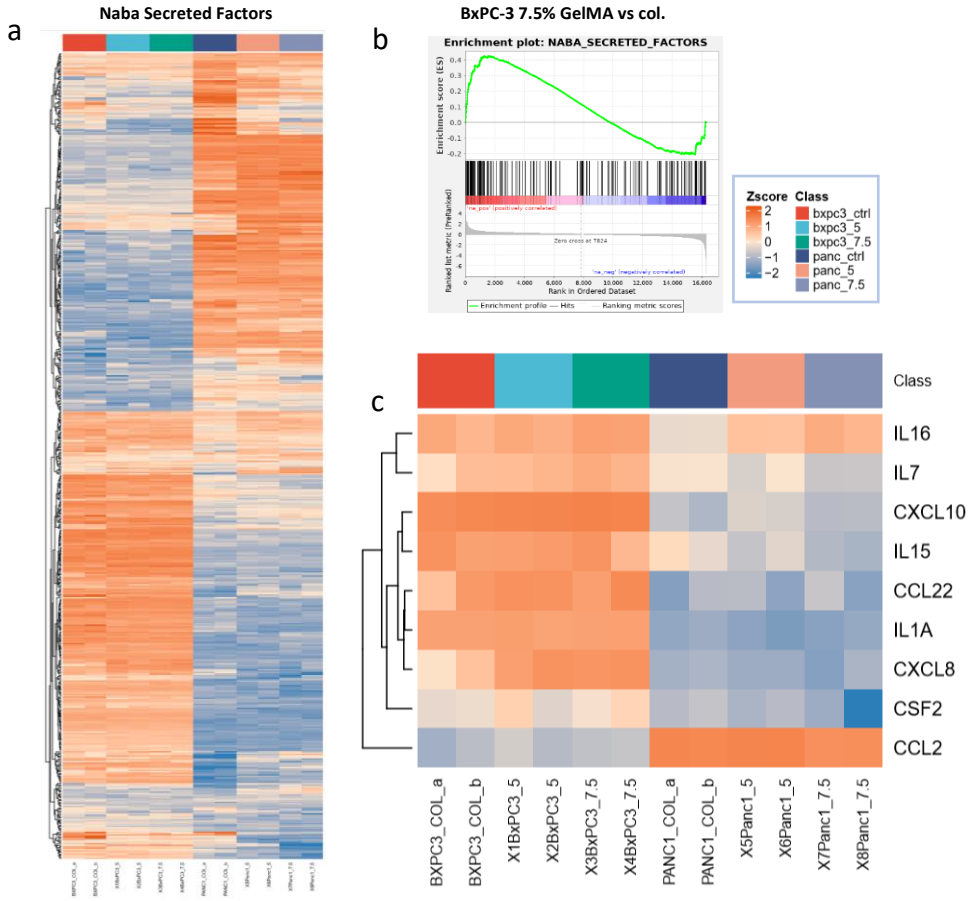

Figure 5.10 Expression heatmaps and Gene Set Enrichment Analysis (GSEA) of (a-b) Naba's matrisome-associated secreted factors and (c) selected cytokines (from MSD panel).

5.4 Conclusions

This chapter provided the first transcriptomics analysis of GelMA-embedded cells of its kind, by directly comparing three different 3D cell culture matrices with varying stiffness and cell types. Together with the biomechanical and functional characterisations in Chapters 3 and 4, the signatures and pathways uncovered at the gene level suggested the activation of mechanosensing and ECM-associated programmes in GelMA. Transcriptomics analyses performed on GelMA cultures showed how cells maintained their expression and cellular identities compared to collagen cultures, underlying the suitability of GelMA as a matrix for 3D PDAC cell culture. Correlation analysis between patient-derived organoids and collagen/GelMA cultures further highlighted the similarity between collagen and GelMA transcripts, reflected in similar correlation scores (Figure 5.4). This suggested that GelMA cultures retained gene signatures comparable to those of cells cultured in commonly-used collagen gels and Matrigel.

Amongst the DEGs in BxPC-3 and PANC-1 cells in GelMA compared to collagen, several structural and matrix organisation genes as well as effectors of GPCR, Wnt and Rho GTPase pathways were identified. Specifically, GPCR ligand-binding, signalling through GPCR, Wnt signalling, β-catenin pathway and TCF transactivation were some of the highly enriched pathways in both BxPC-3 and PANC-1 GelMA cultures (Figure 5.5), all of which are involved in mechano-sensing (Figure 5.11). Some of these pathways are also key in regulating EMT. In fact, EMT is a multifaceted process which involves many morphological changes affecting the expression of proteins including high vimentin and N-cadherin expression, attenuated E-cadherin, high β-catenin [354], YAP and TAZ [138]. This was also highlighted by the differential expression of these markers in the mesenchymal PANC-1 cells compared to epithelial BxPC-3 cells, in our 3D matrices (Figure 5.6 b-c). Stiffness is associated with EMT in a number of cancers [128,355] where it is induced through mechano-transduction. Vimentin for instance can be altered by the *in vitro* mechanical environment [356], while mechanical activation of β-catenin has also been observed *in vivo* (in murine colon) [357]. YAP/TAZ has also recently emerged as player in the response to ECM stiffness [128,137]. Taken together, these data suggest cells in GelMA activate a number of mechano-transduction pathways (Figure 5.11), as well as retaining characteristics concordant with their EMT status.

Aside from mechano-transduction pathways, O-linked glycosylation was also highly enriched in GelMA hydrogels compared to collagen (Figure 5.5 a, Figure 5.7 a). O-linked glycosylation

is a post-translational modification that occurs on many cytosolic and nuclear proteins by *O*-GlcNAc [351]. In PDAC, increased O-GlcNAcylation of kinases upstream of NF-κB signalling impede cell apoptosis and support anchorage-independent growth [351]. Significant alterations in O-linked glycosylation are also present on cell surface molecules during PDAC progression [107]. In collagen, increased cell glycosylation has been reported to contribute to hydrogel stiffening through fibril crosslinking, resulting in a pro-inflammatory, profibrotic cascade. This ultimately affects MMPs and tissue inhibitors of MMPs (TIMPs) promoting an abnormal matrix accumulation [358]. Finally, O-GlcNAcylation of YAP disrupts its interactions with upstream kinase LATS1, thereby promoting transcriptional activity [359]. YAP glycosylation is therefore capable of integrating and coordinating both mechanical and intracellular signals to promote tumorigenesis [359].

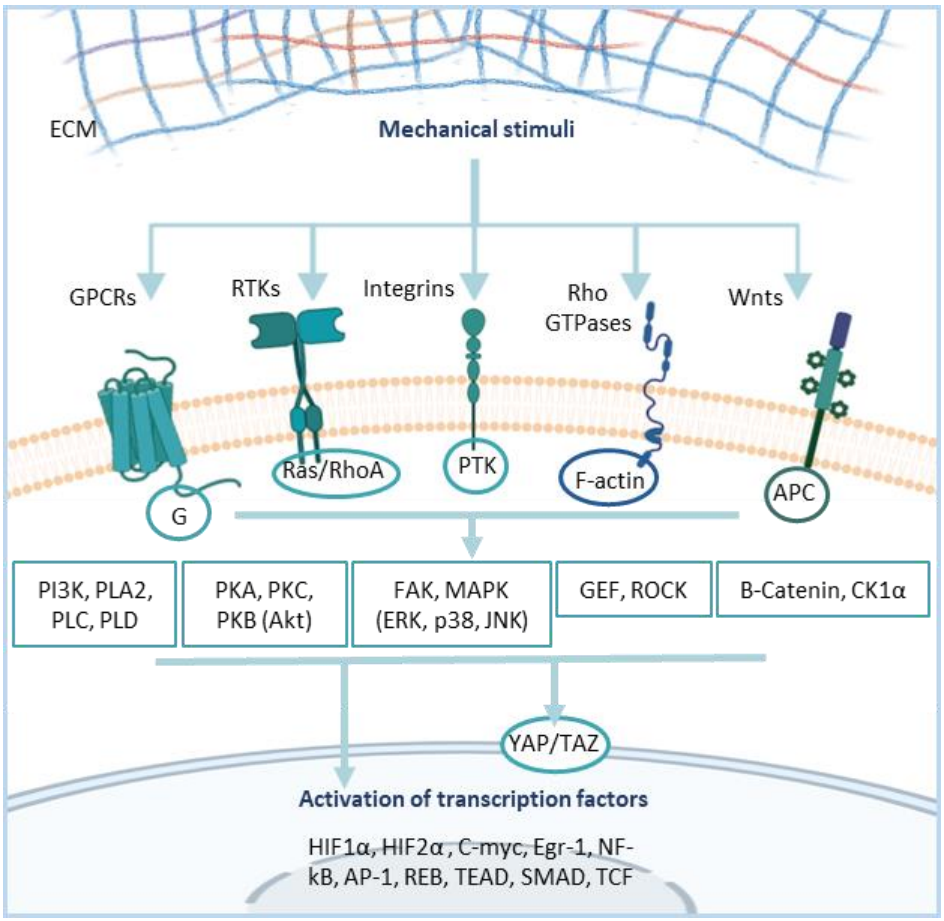

Figure 5.11 Schematic representation of cell mechanotransduction mechanisms. Mechanical forces induce receptor activation on the cell surface, converting physical stimuli into biochemical signals. These include G-protein coupled receptors (GPCRs), Receptor Tyrosine Kinase (RTKs) and Ras homologous GTPases through Ras, RhoA and F-actin signalling, Integrins through tyrosine protein kinase (PTK), and Wingless-related integration site (Wnts) through Axin or APC. As a result, these can co-activate a number of different signalling pathways which lead to changes in gene expression and modulate cell functions including cell shape, structure, proliferation, migration and invasion. For instance, YAP/TAZ can be induced by RTKs through either FGFR-MAPK/PI3K signalling (Azad et al., 2020), or through the RTK-Ras-Rac1 cascade (Panciera et al., 2020). Alternatively, it can be activated through the Wnt/β-catenin axis (Liu et al., 2019). Adapted from Liedert at al., 2006; Moroishi et al., 2015.

Together, these data suggest GelMA cultures possess gene signatures comparable to those of cells grown in popular 3D matrices, and therefore have the potential for applications in the field of bioengineering and clinical translation. With the advent of 'omics' technologies, this kind of systematic evaluation of mechanical (Chapter 3), phenotypic (Chapter 4) and transcriptional (Chapter 5) responses to biomaterials has gained significant interest in recent years [223,348,360] and is poised to become the gold standard of the field. Finally, the following and concluding result chapter will investigate the pre-clinical and translational applications of these hydrogels by looking at the effects of matrix remodelling and mechano-modulating treatments on cell-containing GelMA hydrogels.

Chapter 6 - Targeting the Tumour Microenvironment using *in vitro* Models of PDAC

6.1 Background

Compared to other malignancies in which we are witnessing the progressive implementation of immunotherapies or other advanced targeted therapies [361,362], resection and systemic chemotherapy remain the standard treatments for PDAC patients (Figure 1.1). Despite our advances in understanding the molecular, genetic and biophysical mechanisms driving this cancer, a breakthrough in its treatment is still lacking [26]. This is highlighted by the fact that as little as 3.4% of oncology drugs entering the clinical trial pipeline end being approved for clinical use [363]. Reasons for the discrepancy in the number of drugs investigated and approved include the lack of models capable of fully recapitulating the distribution and off-target toxicities of systemic drug administration as well as the complex tumour-stroma interactions inherent to human tissues. Despite 2D cell culture and animals being the most widely used testing approaches, they are inadequate to accurately reflect all aspects and complexity of the human tumour microenvironment (TME) [171,172,187].

Thus far, this body of work was aimed at characterising gelatin methacryloyl (GelMA) hydrogels as a PDAC 3D cell culture platform, demonstrating how embedded cells recreate complex 3-dimentional structures reminiscent of tissue architecture, as well as being conducive to the culture of multiple cellular TME components. GelMA-embedded cells also had transcriptional profiles similar to those of cells grown in commonly used collagen gels but showed an enrichment in mechano-sensing pathways. Stiffness modulation in these matrices represented a major advantage to traditional collagen or Matrigel-based gels. Importantly, GelMA allowed the culture of primary cells, circumventing the need for long, costly animal experiments, which are currently incompatible with PDAC personalised medicine due to its dismal median survival. The use of alternative biomaterials with defined composition and controllable biophysical properties could therefore represent an advantage in the modelling of pre-clinical drug responses.

In order to test this, drug responses were assessed in GelMA hydrogels of varying stiffness and compared to those of other *in vitro* platforms including monolayer cell cultures and collagen gels. The current standard of care for PDAC patients, namely combination of the chemotherapeutic agents gemcitabine and nab-paclitaxel (known by its commercial name abraxane), will be tested in the models. Additionally, the effect of matrix-remodelling and stromal targeting therapies will also be assessed. In particular, the matrix remodelling, proliferative and invasive abilities of cells will be tested following the addition of a broadband

matrix metalloproteinase (MMP) inhibitor ilomastat (GM6001). The roles of MMPs in cancer span a number of pro-tumorigenic pathways and cell behaviours including ECM-remodelling, proliferation, migration, invasion and metastasis [142]. Since GelMA is primarily composed of hydrolysed collagens, and because of the clinical relevance of collagen in PDAC [95], the use of a potent inhibitor of collagenases is of particular interest.

Additionally, cells are capable of remodelling the surrounding extracellular matrix (ECM) through the regulation of Rho-associated protein kinase (ROCK)-mediated cytoskeletal re-arrangement, via which they exert cell contractility and contribute to tissue tension and stiffness [149,151]. As suggested by Vennin et al. [155,364], transient tumour targeting with a ROCK inhibitor prior to the administration of standard chemotherapeutic agents may release local tissue tension and increase cell susceptibility to treatment, enhancing chemotherapy efficiency. Importantly, transient tissue targeting or 'priming' circumvents the risks associated with chronic ablation of restraining stromal components, which could have negative clinical effects, similarly to those observed with hyaluronidase treatment (PEGPH20 trial) [47] (Figure 1.5). Hence, I will assess the efficacy of ROCK inhibition with fasudil in combination with chemotherapeutic agents, and its effects on matrix stiffness, in our models. In the previously presented RNA-seq analysis, ROCK1, ROCK2, MMP9, MMP12, MMP14, MMP19, amongst other genes, were differentially expressed in collagen compared to GelMA matrices. The role of collagens, MMPs, ROCK and ROCK targeting in PDAC have been discussed in more detail in Sections 1.2.2.3 and 1.2.2.4.

6.2 Aim and objectives

Following mechanical, functional and transcriptional characterisations of Chapters 3-5, in this Chapter I will assess the responses of PDAC cells (BxPC-3, Capan-2, MIA PaCa-2 and PANC-1), one HGSOC cell line (OvCar-4) and stromal cells (CAFs and THP-1s) to matrix remodelling and stroma-modulating treatments both in 2D and 3D cell cultures. GelMA hydrogels of increasing stiffness (5 – 7.5 %) will be used alongside collagen control gels.
I will:

- Assess the effects of GM6001, fasudil, gemcitabine plus abraxane treatment on cell functions (viability, proliferation, spheroid formation, invasion) in both 2D and 3D, as well as treatment effects on matrix stiffness in GelMA and collagen hydrogels.
- Understand changes in matrix stiffness at the nanoscale following GM6001 treatment, using atomic force microscopy (AFM).

- Assess the effect of a matrix priming regime with fasudil on the efficacy of gemcitabine plus abraxane treatment, in triple cultures of PDAC (PDAC cells, CAFs and THPs), via assessment of cell functions, matrix stiffness, gene expression and secreted factors analysis.

6.3 Results

6.3.1 Epithelial-mesenchymal transition status and extracellular collagen dictate cell proliferation and treatment response in 2D

The effects of MMP and ROCK inhibition on PDAC cell proliferation were tested via the addition of inhibitors, namely GM6001 and fasudil respectively. Additionally, a combination of gemcitabine and nab-paclitaxel (abraxane), the standard chemotherapeutic agents used for the treatment of PDAC patients, was also used. The therapeutic effects of these agents were first assessed in 2D and, subsequently, in collagen and GelMA hydrogel models. A treatment dose of 20 μM GM6001, 10 μM fasudil, 100 nM gem/abx (each) and 20 μM control peptide were chosen, as these concentrations have been shown to elicit biological effects in the literature, even in 3D matrices [155,252].

The epithelial-to-mesenchymal (EMT) status of the cell lines was confirmed via immunoblotting for the EMT markers E-cadherin, vimentin and the epithelial PDAC-associated marker cytokeratin 19 (KRT19) (Figure 6.1 a). Capan-2 and BxPC-3 showed high expression of the epithelial marker KRT19 and E-cadherin together with low vimentin expression, overall indicative of their epithelial-like phenotype. Conversely, PANC-1 and MIA PaCa-2 show an upregulation of vimentin accompanied by loss of E-cadherin and lower KRT19 expression, typical of a more mesenchymal phenotype. The mutational status and phenotype of the four cell lines is indicated in Table 6.1. OvCar4 HGSOC cells were used as control as they have a mesenchymal phenotype and show no expression of the PDAC-specific marker KRT19.

In order to test the effects of treatment on the proliferative ability of the cells, PDAC cell lines were seeded on plates coated with either 10 μg/ml of poly-L-lysine (control) or 10 μg/ml of collagen type-I. As collagen type-I is known to induce EMT and affect treatment response [104,128,203,355], I hypothesised that different cell lines would respond to treatment in an opposite fashion to one another, based on their EMT status and plate coating (collagen versus control). After 24 hours from seeding, cells were treated with either 20 μM GM6001, 10 μM fasudil or 100 nM gem/abx (each), and their proliferation recorded (Figure 6.1 b-c). On poly-L-lysine control plates, mesenchymal cell lines (namely PANC-1 and MIA PaCa-2) showed higher proliferation compared to Capan-2 and BxPC-3. Conversely, collagen type-I coating stimulated the proliferation of Capan-2, BxPC-3 and PANC-1 cells while inhibiting

the growth of MIA PaCa-2 cells. The stimulatory effect of collagen on cell proliferation via induction of EMT is well characterised in PDAC [355].

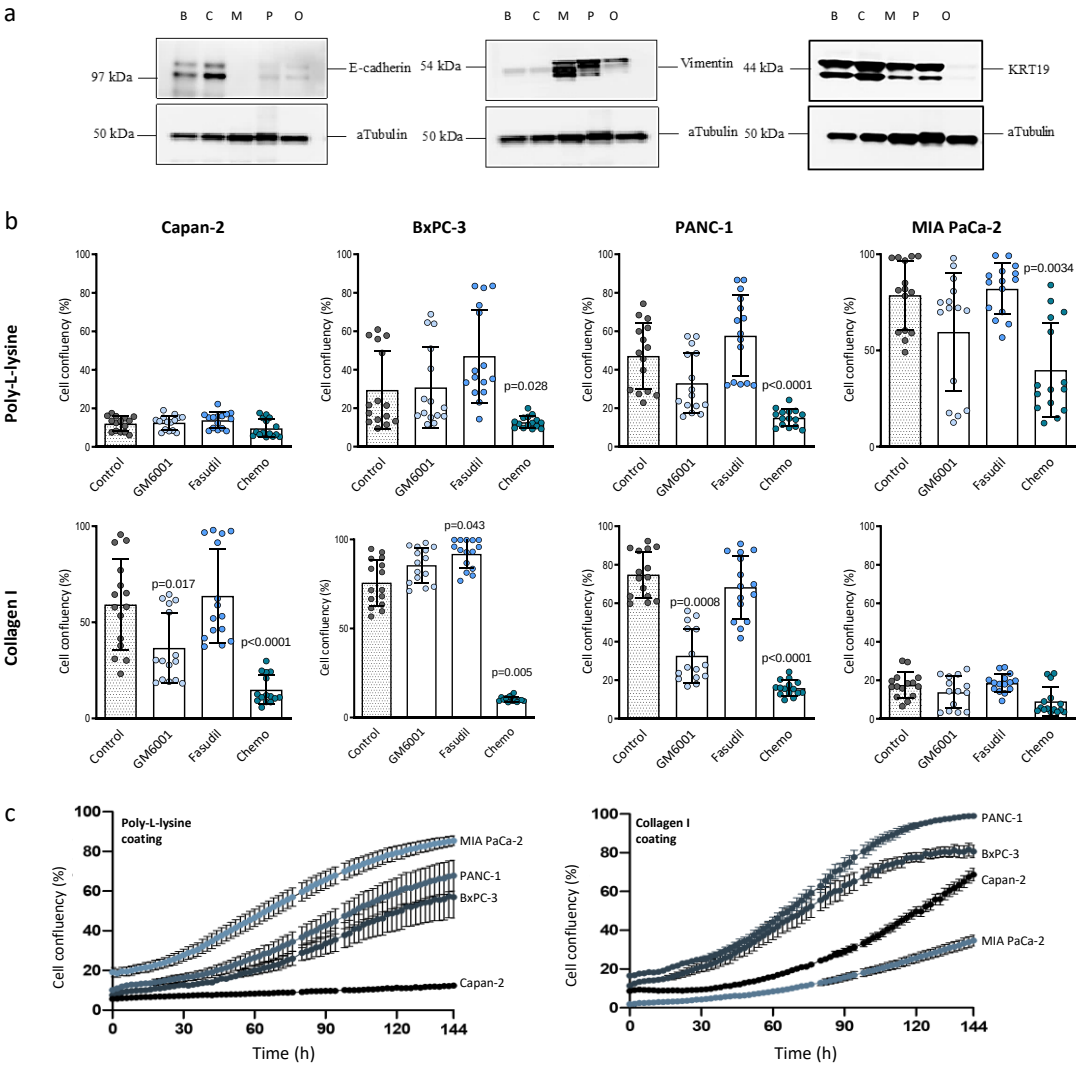

Figure 6.1 Effects of epithelial-to-mesenchymal transition (EMT) status and GM6001, fasudil and gemcitabine/abraxane treatment on the proliferation of PDAC cells in 2D. (a) Immunoblots of EMT markers E-cadherin (97 kDa), vimentin (54 kDa) and cytokeratin 19 (44 kDa) and protein loading control alpha-tubulin (50 kDa) from BxPC-3, Capan-2, MiaPaCA-2, PANC-1 and OvCar4 cells grown in monolayers. **(b)** BxPC-3, Capan-2, MiaPaCA-2 and PANC-1 cells were seeded on either 10 µg/ml collagen-I or 10 µg/ml poly-L-lysine (control) and treated at t=0 with either GM6001 (20 µM), fasudil (10 µM), Gem/Abx (100 nM each) or control peptide (20 µM). Proliferation was analysed every 24 hours for six days (t=96 hours shown) (n=3). Cell lines are ordered based or their EMT status from more epithelial-like to mesenchymal. Data shown as mean ± SEM, significance tested with Kruskal-Wallis one-way ANOVA, p-values as annotated, n=3. (c) Proliferation of the four PDAC cell lines on poly-L-lysine (control) and collagen-I matrices. Collagen I stimulates the proliferation of PDAC cell lines with the exception of MiaPaCa-2 cells which, having a mesenchymal phenotype, have a decreased proliferation rate when plated on collagen, n=3.

Representative proliferation plots at 96 hours of treatment are shown in Figure 6.1 b. Unsurprisingly, gem/abx treatment significantly reduced the growth of highly proliferative cells (hence, it had no effect on Capan-2 cells on poly-L-lysine or MIA PaCa-2 cells on collagen-coated plates, as these conditions showed very little overall proliferation). Overall,

fasudil had no effect on cell proliferation in 2D, on neither poly-L-lysine or collagen-coated plates. Conversely, although not always significant, GM6001-treated cells showed a trend towards decreased proliferation in three out of four cell lines. Despite having similar mutations, the different proliferation rates of MIA PaCa-2 and PANC-1 on collagen can be partially explained by the different affinity of these cell lines to collagen type-I (Table 6.1 [365]). Overall, collagen type-I stimulation increased sensitivity of Capan-2, BxPC-3 and PANC-1 to gem/abx, and of Capan-2 and PANC-1 to GM6001.

Table 6.1 Genotype and phenotype of PDAC cell lines. Mutational status for four of the most common mutations in PDAC [365]. WT= wildtype, HD=homozygous deletion.

Cell line	KRAS	TP53	CDKN2A/p16	SMAD4/DPC4	Coll I adhesion
BxPC-3	WT	220 Cys	WT; HD	HD	High
Capan-2	12 Val	WT	WT; insertion	WT	Medium
MIA PaCa-2	12 Cys	248 Trp	HD	WT	Low
PANC-1	12 Asp	273 His	HD	WT	High

6.3.2 Inhibition of MMPs, but not ROCK, leads to reduced cell proliferation in 3D

6.3.2.1 Effects of GM6001 treatment on PDAC cell proliferation and invasion

Next, the effects of MMP inhibition was assessed in collagen, 5% and 7.5% GelMA hydrogels via GM6001 treatment. GM6001 is a potent broad-spectrum human MMP inhibitor with low reported Ki values of 0.1 nM for MMP8, 0.2 nM for MMP9, 0.4 nM for MMP1, 0.5 nM for MMP2 and 27 nM for MMP3. As MMP expression is upregulated by PDAC cells in response to matrix stiffness [131], I hypothesised GM6001 efficacy would vary across matrices of different stiffness. For this, collagen and GelMA hydrogels were set up with four PDAC cell lines and one HGSOC cell line as monocultures. Treatment molarities were kept consistent - 20 μM GM6001 and 20 μM of control peptide in cell culture medium – added on day 1 of culture and subsequently replaced every 72 hours until endpoint analysis on day 14 (Figure 6.2 a). Treatment with GM6001 generally reduced the proliferation of hydrogel-embedded cells over 14 days of culture and led to the formation of smaller spheroids (Figure 6.2 b).

Proliferation was analysed using DNA content analysis on day 1 and 14 as a proxy for cell content quantification within the hydrogels. Interestingly, the more mesenchymal cell lines PANC-1 and MIA PaCa-2 had a reduced sensitivity to the treatment, only showing significantly reduced proliferation when treated with the inhibitor in stiffer conditions (7.5% GelMA). These were followed by BxPC-3 and OvCar4, with a significant reduction of proliferation in both 5% and 7.5% GelMA upon treatment, and lastly Capan-2 showing susceptibility to GM6001 in all three 3D cell culture matrices. This pattern largely reflects the results observed in 2D whereby the intrinsic proliferative, metastatic and EMT status of the cell lines determined their response to GM6001 treatment on collagen-coated plates. The effectiveness of GM6001 treatment in GelMA hydrogels was encouraging as a further confirmation of the retention of cleavage-sensitive motifs (MMP-binding domains) within the hydrogel backbone.

Across all cell lines, GM6001 efficacy was increased with increased matrix stiffness (Figure 6.2 b). One possible reason could be the stiffness-induced increase in the production and activity of MMPs which, in turn, would lead to more significant reduction in proliferation upon treatment. This is the case for PANC-1 cells, in which a 3-to-10 fold increase in secreted MMP activity has been shown in stiff compared to soft collagen hydrogels [131]. In the same

study, secreted MMPs activity was higher in BxPC-3 cells compared to PANC-1, and did not significantly vary across hydrogels of different stiffness [131]. Taken together, these data might explain the higher sensitivity of BxPC-3 cells to the MMP inhibitor in both 5% and 7.5% GelMA as well as the significant reduction in PANC-1 proliferation only in stiffer matrices. GelMA stiffness was not only inducive of increased MMP activity but also of proliferation of untreated controls in the case of BxPC-3, MIA PaCa-2 and PANC-1, highlighting further the inhibitory effects of GM6001 treatment.

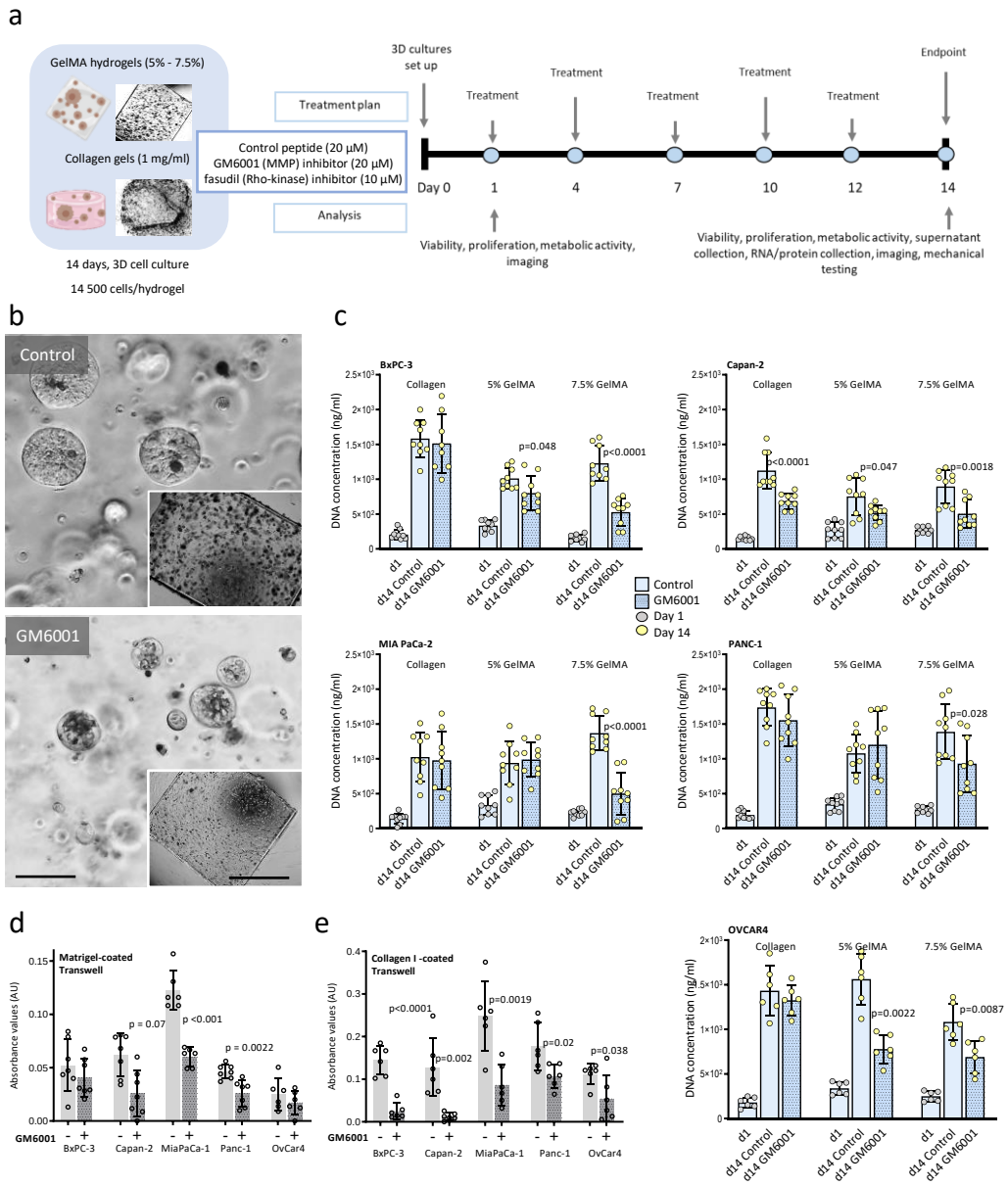

Figure 6.2 Effects of GM6001 treatment on PDAC cell proliferation in collagen, 5% and 7.5% GelMA and Transwell cell invasion in collagen and Matrigel. (a) Schematic representation of treatment strategy for 3D GM6001 and fasudil experiments. **(b)** Representative brightfield micrographs of PANC-1 treated with 20 µM control peptide (top) or 20 µM GM6001 (bottom), at day 14 of culture in 7.5% GelMA. Scale bars 500 µm and 2 mm (inserts), apply to all. **(c)** CyQUANT quantification of cell proliferation of 3D cell cultures at day 1 (grey dots) and day 14 (yellow dots) in matrices of increasing stiffness (collagen, 5% and 7.5% GelMA). Cells were treated with either 20 µM control peptide or GM6001 in medium, replaced every 72 hours. ANOVA (Tuckeys multiple comparisons), p-values as annotated, n=3. **(d)** Matrigel-coated Transwell invasion assays (48 hours) on cells treated with 20 µM control peptide (light grey) or GM6001 (dark grey). **(e)** Collagen I-coated Transwell invasion assays (48 hours). Mann-U-Whitney, p-values as annotated, n=3.

MMPs are not only involved in matrix degradation during proliferative and metastatic cancer cell dissemination, they also play a pivotal role in invasion and during the degradation of the basal membrane [142]. Because of this, I next assessed the effects of GM6001 treatment on invasive cell behaviours though Matrigel and collagen-coated Transwells after 48 hours of treatment (Figure 6.2 d, e). Three out of five cell lines showed reduced Transwell invasion upon treatment in Matrigel while all of the analysed cell lines had a significantly lower invasive ability upon treatment in collagen. Overall, all of the cell lines showed much higher invasion in collagen compared to Matrigel as indicated by their respective mean absorbance values. Because of their increased invasiveness, it is likely that GM6001 effects would be augmented in collagen compared to Matrigel. MIA PaCa-2 cells showed a higher invasive ability amongst the analysed cell lines followed by Capan-2, PANC-1 and BxPC-3 which is concordant with the literature [365-367]. Finally, although not measured in this project, the stiffness of Matrigel is considerably lower than that of collagen (100 Pa vs 1.2 kPa) [266], suggesting increased stiffness might be stimulating invasive behaviours in the latter.

In order to validate these results further, gene and protein assays were conducted on cells following GM6001 treatment (Figure 6.3). At gene level, vimentin expression increased in GelMA compared to collagen in all three cell lines analysed (Figure 6.3 a). Vimentin is a cytoplasmic intermediate filament widely associated with PDAC cell stiffness [129], mechanosensing *in vivo* [356], EMT [354], as well as treatment response [128]. Increased vimentin expression is therefore expected upon culture in stiffer substrates. Concordant with the protein data (Figure 6.1 a), in 2D its expression was higher in PANC-1 cells compared to BxPC-3 and Capan-2. In collagen, *MMP9* expression was low in the three PDAC cells assessed, and its expression was reduced further upon GM6001 treatment (Figure 6.3 b). In GelMA, *MMP2* levels were also reduced upon GM6001 treatment, with the exception of Capan-2 cells, whose MMP2 levels were five-fold increased upon treatment. GM6001 inhibits MMPs by binding to the active-site zinc atom that is critical for the activity of these proteases [368]. Therefore a decrease of *MMP2* and *MMP9* at gene level is not necessarily to be expected, even at this late time point (14 days). Combined gene expression techniques and activity-based assays (such as zymography) at earlier time points would be able to better characterise the extent of MMP inhibition during treatment.

In collagen, vimentin levels did not significantly change upon GM6001 treatment, with the exception of Capan-2 cells which showed a decreased expression. Importantly, Vimentin expression was also decreased in all of the cell lines in 7.5% GelMA hydrogels, which might

explain the observed reduction in the proliferation of these cells. Taken together, this data would suggest that mechanosensing via regulation of vimentin and EMT at gene level, rather than MMPs, are determinant of differential cell proliferation rates and GM6001 treatment responses in 3D. This is exemplified in the case of Capan-2 cells, where cells responded to treatment in GelMA despite having increased *MMP2* expression, or BxPC-3 and PANC-1 in collagen which, despite a decrease in *MMP9* levels, showed no significant changes in proliferation concordant with an unchanged expression of vimentin.

Overall protein content of GM6001-treated GelMA hydrogels was also lower compared to their untreated counterparts as shown via Coomassie protein staining (Figure 6.3 c). Importantly, acellular GelMA hydrogels (lane 6) only resulted in one strong band following separation by electrophoresis, instead of a large smear as in the case of unfuctionalised gelatin (lane 7). This was an important result, indicating for the first time, that GelMA-recovered cells could be used for successive protein analysis via Western blot without interference from gelatin-derived protein bands.

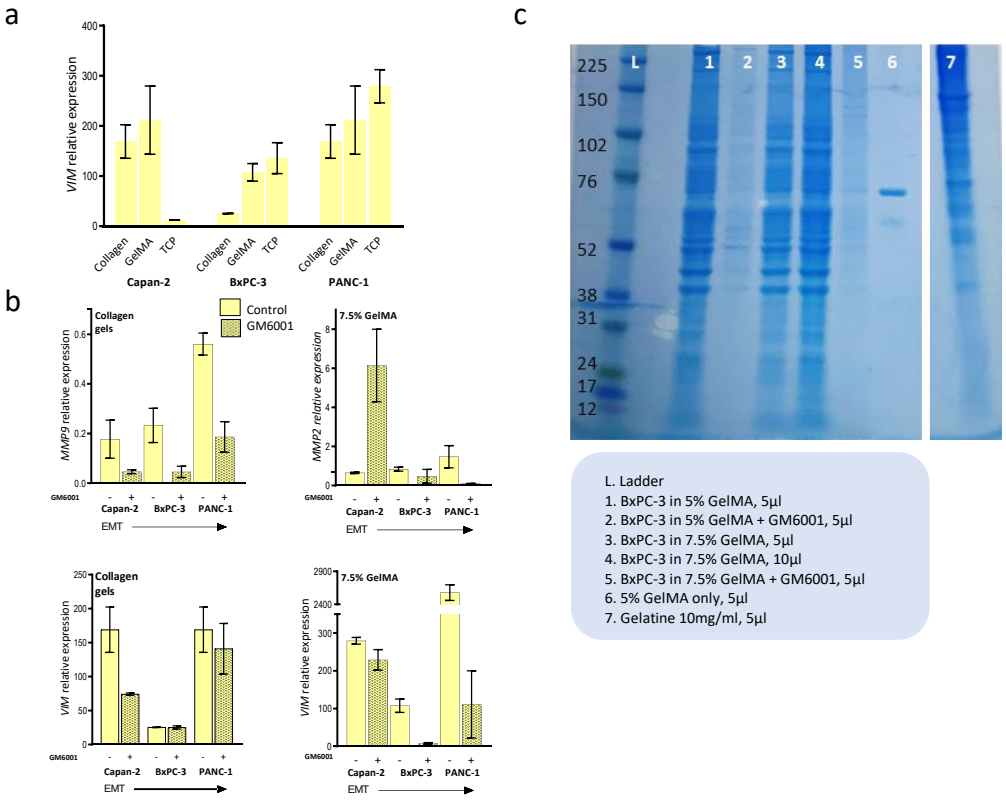

Figure 6.3 Effects of GM6001 treatment on gene and protein expression in collagen and 7.5% GelMA hydrogels. (a) RTqPCR analysis of BxPC-3, Capan-2 and PANC-1 cells in collagen, 7.5% GelMA day 14 of culture and tissue culture plastic (TCP). Expression relative to *RPS13*, mean and standard deviation shown, n=2. **(b)** RTqPCR analysis of BxPC-3, Capan-2 and PANC-1 cells in collagen, 7.5% GelMA at day 14 of culture, following treatment with 20 µM control peptide (yellow) or GM6001 (pattern) - replaced every 72 hours in culture medium. Expression relative to *RPS13*, mean and standard deviation shown, n=2. **(c)** Coomassie protein staining of proteins following separation via electrophoresis, loading conditions as indicated.

6.3.2.2 Effects of fasudil treatment on PDAC cell proliferation

The effects of ROCK inhibition on cell behaviours in 3D matrices was assessed via treatment with 10 μM fasudil hydrochloride. fasudil is a potent Rho-kinase pan-inhibitor, targeting the ATP-dependant kinase domain of both ROCK1 and ROCK2 and is currently the only ROCK inhibitor clinically employed [369]. The treatment was added into cell culture medium at day 1 and replaced every 72 hours (Figure 6.2 a). Unlike treatment with GM6001, there were no apparent effects on cell proliferation following 14 days of treatment with this ROCK inhibitor (Figure 6.4 a, b). Assessment of cell proliferation via quantification of hydrogel DNA content revealed no decrease in cell proliferation in either collagen or GelMA hydrogels, with the exception of MIA PaCa-2 cells in GelMA. In collagen, Capan-2 and MIA PaCa-2 even showed a significant increase in cell proliferation with treatment. Visually, cells formed clusters which were similar in numbers to control condition but showed more disorganised morphologies (Figure 6.4 b). Despite no apparent reduction of cell proliferation as a single treatment, the effects of fasudil as well as GM6001 treatment on overall hydrogel stiffness will be described in the next Section.

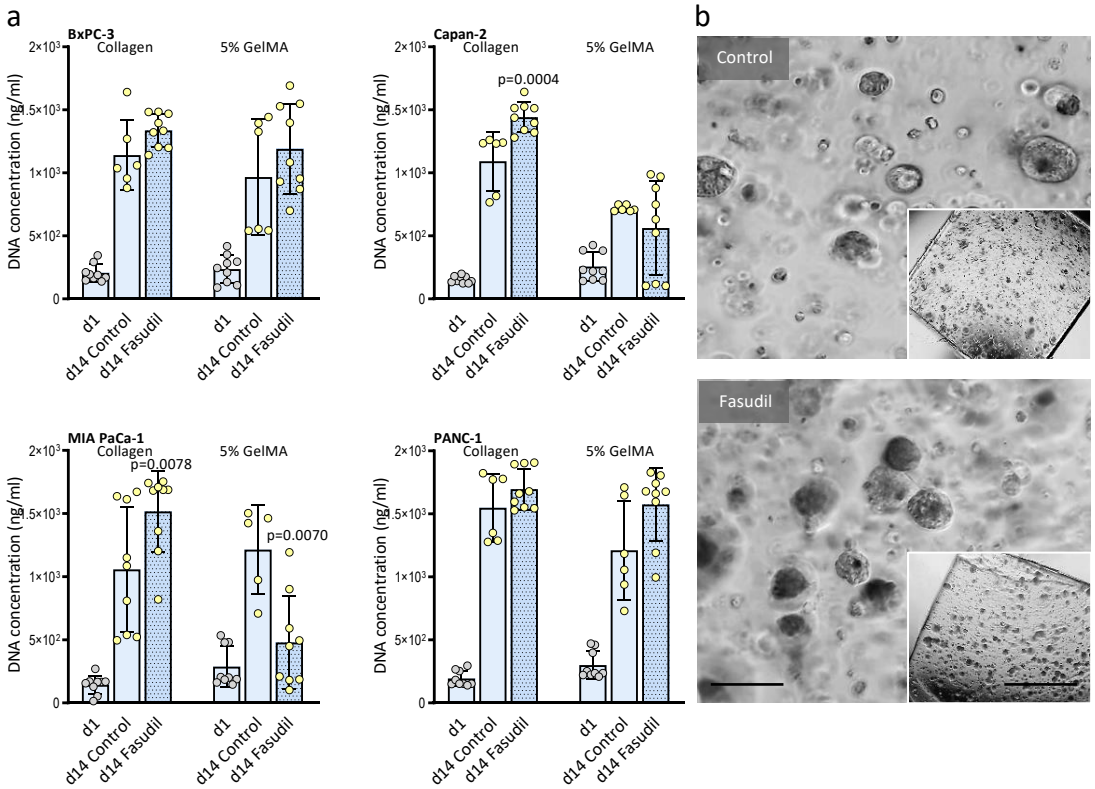

Figure 6.4 Effects of fasudil treatment on PDAC cell proliferation in collagen and 5% GelMA. (a) CyQUANT quantification of cell proliferation of 3D cell cultures at day 1 (grey dots) and day 14 (yellow dots) in matrices of increasing stiffness (collagen and 5% GelMA). Cells were treated with either 10 μM control peptide or fasudil in medium, replaced every 72 hours. ANOVA (Tuckeys multiple comparisons), p-values as annotated, n=3. **(b)** Representative brightfield micrographs of Capan-2 cells treated with 10 μM fasudil (bottom) or control (top), at day 14 of culture in 7.5% GelMA. Scale bars 500 μm and 2 mm (inserts), apply to all.

6.3.3 Inhibition of ROCK, but not of MMPs, lead to cell-mediated stiffness changes in GelMA hydrogels

The stiffness of cell-containing hydrogels was assessed via rheometry (collagen hydrogels) and confined compression (GelMA hydrogels) (Figure 6.5 a). Despite having no significant effect on cell proliferation, fasudil treatment significantly reduced the stiffness of cell-containing 5% and 7.5% GelMA hydrogels compared to control conditions. Due to collagen gels being very soft, compression testing could not be performed, and rheology was used instead. No significant difference in matrix stiffness was detected using this method despite a tendency towards decreased stiffness was observed in GM6001 treated gels. In the future, a consistent, unified method should be used for stiffness assessment in both collagen hydrogels. For instance, a specialised rheometer with combined frequency sweep, amplitude sweep, and compression modalities could be used for the assessment of both hydrogel types.

A yet different and highly sensitive methodology was used for the assessment of local stiffness at the nano-scale in 5% and 7.5% GelMA hydrogels. Atomic force microscopy (AFM) is a type of scanning probe microscopy which uses the deflection of a laser generated by the movement of a cantilever to scan topography or stiffness at a very high resolution. This technique was employed in order to precisely detect the stiffness of GelMA-embedded spheroids at day 14 of culture after calibration of the tip on an acellular hydrogel (Figure 6.5 b). BxPC-3 and PANC-1 cells grown in 5% and 7.5% GelMA hydrogels at day 14 of treatment with GM6001 were used for this. Surprisingly, mean stiffness values of PDAC cell spheroids within GelMA were very close to the predicted stiffness of the hydrogel itself (3.4 kPa for 5% GelMA hydrogels and 8.6 kPa for 7.5% GelMA hydrogels). This indicated that cells embedded in stiffer matrices had the tendency to form tighter spheroids, with a stiffness similar to that of their surroundings. It also indicated that despite AFM being a very different technique than compression, the results are relatively comparable.

Spheroids treated with GM6001 had a lower stiffness in 5% GelMA compared to their untreated counterparts. Upon GM6001 treatment, BxPC-3 and PANC-1 cells formed smaller spheroids due to their impaired MMP-mediated matrix remodelling ability. This could explain why GM6001-treated spheroid were softer compared to their untreated counterparts. This effect seems lost in 7.5% GelMA where the surrounding matrix is very stiff. Taken together, this could indicate that the tumour mass stiffens and relaxes in response to treatment, but generally matches the stiffness of its surrounding. This could have

interesting implications *in vivo*, whereby matrix stiffness alone could determine, and possibly re-establish, the stiffness of the tumour cell mass. As fasudil-treated hydrogels showed a significant reduction in stiffness, I was interested in taking this treatment further with the hypothesis that it could be used in combination with gem/abx in order to relax hydrogel stiffness increasing the efficiency of chemotherapeutics delivery.

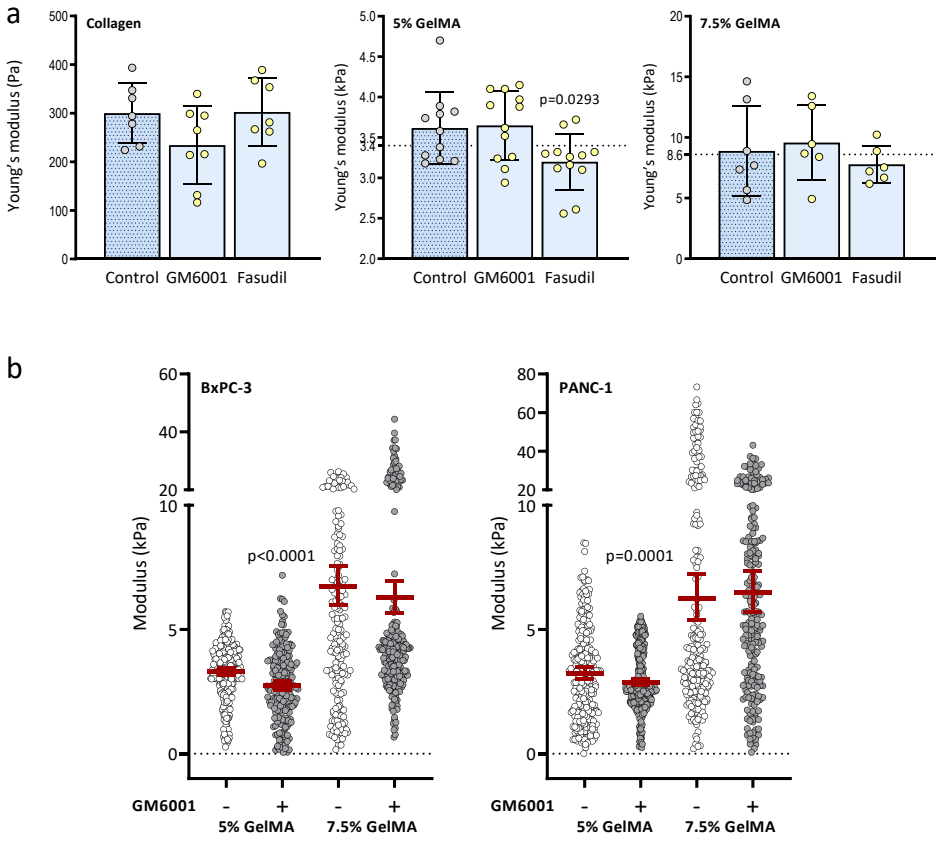

Figure 6.5 Effects of GM6001 treatment on matrix stiffness as measured by (a) rheometry, confined compression and (b) atomic force microscopy (AFM). (a) Cells were cultured for 14 days in either collagen, 5% or 7.5% GelMA and treated with either 20 μM GM6001, 10 μM fasudil, or control peptide in medium (replaced every 72 hours). Collagen hydrogel stiffness was measured via rheometry testing in amplitude sweep mode while GelMA hydrogels were tested via compression. Dotted lines correspond to GelMA stiffness prediction. ANOVA, p-values as annotated, n=3. **(b)** AFM testing of BxPC-3 and PANC-1 cell-laden 5% and 7.5% GelMA hydrogels. Hydrogels were cultured for 14 days and treated with GM6001 as previously described. Each sample was indented on three separate 1x1mm areas, in which 100 indents were performed. Acellular hydrogels were used as calibration, allowing the precise detection of 'spheroids' and cell cluster' areas within cell-laden hydrogels. Kolmogorov-Smirnov (multiple comparisons), p-value as annotated, n≥3.

6.3.4 Effects of matrix priming with ROCK inhibitors on chemotherapy efficiency in 3D cell cultures

6.3.4.1 Combined treatment of fasudil and chemotherapy lead to reduced cell viability

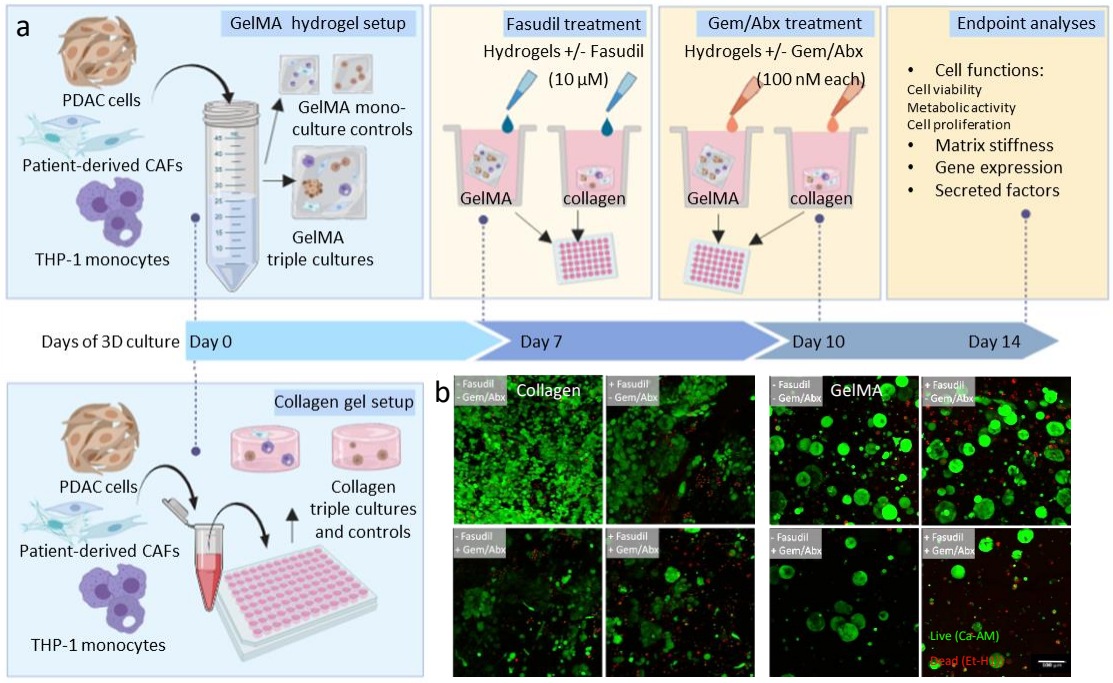

Figure 6.6 Experimental setup of triple culture experiments. (a) Schematic representation of triple culture experimental setup. Collagen, 5% and 7.5% GelMA hydrogels were used for this. Triple cultures consisted of PDAC cells, THP-1 monocytes and patient-derived CAFs in a 1:2:2 ratio. Monoculture control hydrogels (PDAC only and THP-1/CAFs stroma only) were also set up. CAFs were isolated from patients number 2, 3 and 15. Cultures were kept for 14 days prior to readout. **(b)** Confocal z-stack micrographs of PANC-1 cells in collagen (left) and 5% GelMA (right) hydrogels at day 14 of culture following treatment as indicates. Live cells were stained with green fluorescent calcein-AM (Ca-AM, 494/517 nm) and dead cells with ethidium homodimer 1 (Et-H1, 528/517 nm). Scale bar 100 µm applies to all.

In order to test the effects of combined fasudil and chemotherapy treatment, collagen, 5% and 7.5% GelMA hydrogels were set up as triple cultures (PDAC, CAF, THP-1 cells in a 1:2:2 ratio) and respective controls (PDAC cells monocultures and stroma). Cells were grown within the hydrogels for 7 days prior to treatment with 10 µM fasudil or control medium. Following 72 hours from the addition of fasudil, the treatment groups were further divided for treatment with gem/abx (100 nm of each) or saline diluent control in cell culture medium. Hydrogels were then collected at day 14 for endpoint analyses including imaging, proliferation, hydrogel stiffness, gene and secreted factors expression (Figure 6.6 a). The experiment was repeated with patient-derived CAFs from three distinct patients and a minimum of three technical replicates for each condition. Micrographs of live (green, Ca-AM) and dead (red, Et-H1) cells at day 14 of culture revealed an increase in the number of

dead cells in fasudil-treated conditions compared to untreated, despite no change in the overall number of viable cells (Figure 6.6 b). As expected, treatment with gem/abx reduced the number of viable cells in both collagen and GelMA hydrogels.

Cell viability and cell counts were quantified on day 14 via measurement of endogenous reducing enzyme activity (Alamar Blue, unfilled dots) and DNA content (CyQUANT, filled dots)(Figure 6.7 a,b). Similarly to what had been observed in the previous sections, treatment with fasudil alone did not overall decrease the viability and proliferation of PANC-1 cells (p=0.95 and p=0.96, ns), and had a limited effect on triple cultures (slight reduction of proliferation in 5/9 cases, p=0.92 and p=0.89, ns). Individual patient data is indicated as a line plot in Appendix 9.5. Without the presence of cancer cells, CAF and THP-1 cells proliferated less than their malignant counterparts within the hydrogels, especially in stiffer ones (7.5% GelMA). However, in 8/9 cases, fasudil decreased the proliferation of stromal cells.

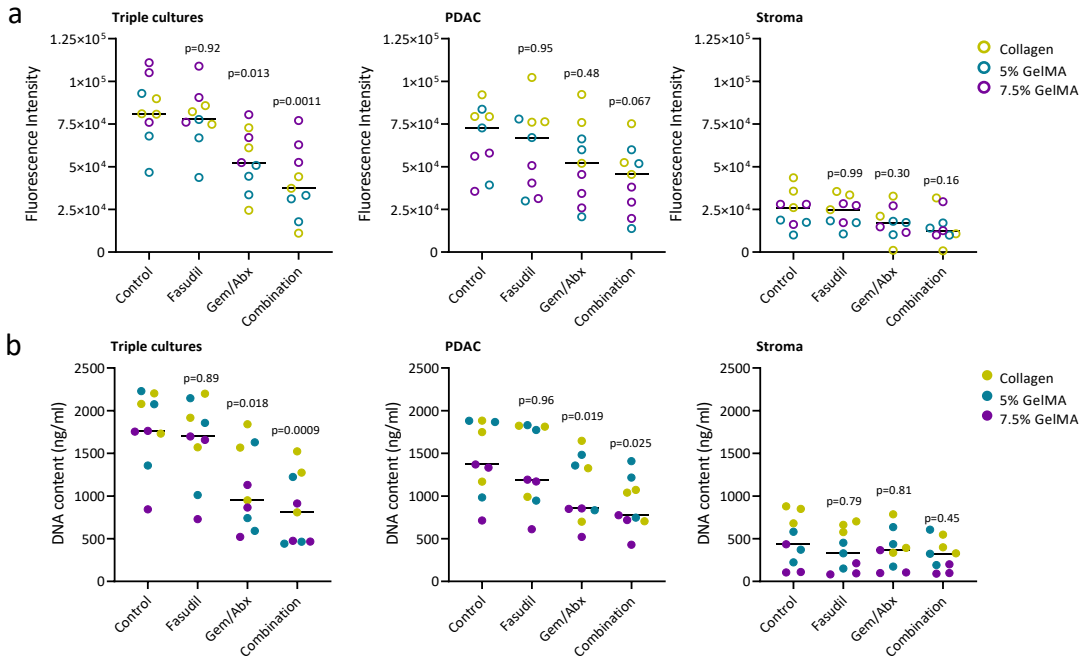

Figure 6.7 Effects of fasudil priming on the efficacy of gemcitabine and abraxane (Gem/Abx) in collagen (yellow), 5% (blue) and 7.5% (purple) GelMA hydrogels as measured via quantification of (a) endogenous cellular reducing ability and (b) DNA content. (a) Alamar Blue quantification of cells' metabolic activity at day 14 of culture. Cultures were treated with 10 µM fasudil on day 7 and 100 nm of each Gem/Abx on day 10. Appropriate untreated and single treatment controls were also set up. Triple cultures consisted of PDAC cells, THP-1 monocytes and patient-derived CAFs in a 1:2:2 ratio. Monoculture control hydrogels (PDAC only and THP-1/CAFs stroma only) were also set up. CAFs were isolated from patients number 2, 3 and 15, n=3, p-values as indicated. **(b)** CyQUANT quantification of DNA content was performed at day 14 of culture. n=3, p-values as indicated.

Treatment with gem/abx decreased the viability and proliferation of triple cultures and PANC-1 cells and but was less efficient in targeting stromal cells (response in 3/9 cases, p-value >0.05, ns). When combined with fasudil, there was a further decrease in the proliferation of triple cultures (8/9 cases showed further reduction in DNA content, p=0.0009), as well as PANC-1 (7/9, p=0.025) and, to a lesser extent, stromal cells (3/9, p=0.45). Interestingly, similar effects were observed across collagen and GelMA hydrogels as well as different stiffness, suggesting its mechanism of action may be overcoming stiffness-related resistance mechanisms.

Overall, these data indicate that fasudil had a greater effect on stromal cells compared to malignant cells, while the opposite was true for gem/abx treatment. When pre-treated with fasudil, gem/abx treatment led to a further decrease in overall cell numbers in all the conditions, suggesting this combination may be advantageous in reducing cell proliferation. Importantly, even in combination, there was no overall ablation of stromal cells following treatment in GelMA, suggesting a number of residual stromal cells were preserved in these hydrogels. This was not the case in collagen hydrogels, in which stromal cells responded to all three treatment conditions. As stroma-ablating treatments have so far proved controversial or failed in PDAC [45,47,49], the ability of stiffer tissues to retain some restraining or re-educating stromal cells may be an advantage.

6.3.4.2 Treatment with fasudil, but not chemotherapy, led to reduced matrix stiffness in GelMA

In order to understand the mechanisms involved in fasudil-enhanced chemotherapy efficiency, the stiffness of cell-containing hydrogels was recoded at day 14 of culture in GelMA hydrogels (Figure 6.8 a, b). When all conditions were combined, fasudil, but not gem/abx treatment, led to a significant reduction in GelMA hydrogels stiffness (Figure 6.8 a). Despite fasudil having no direct effects on proliferation as a monotherapy, this data suggests treatment could be decreasing overall matrix stiffness to either facilitate subsequent gem/abx delivery, or reprogramming of stromal cells. In fact, fasudil is known to decrease fibroblast contractility in 3D models, as well as disrupting collagen matrix integrity via ROCK/pMLC (myosin light chain)-mediated downregulation of acto-myosin contractility [155]. GelMA hydrogels show a reduction of overall stiffness even when treated in combination with chemotherapy. As stiffness alone is able to induce chemoresistance to abraxane [128], relaxation of overall matrix tension after treatment would be advantageous in order to limit relapse.

Figure 6.8 b shows the distribution of stiffness data based on different culture groups: triple cultures (blue dots) generally result stiffer compared to PDAC and stroma-containing hydrogels (brown and pink dots). In order to understand further the molecular changes involved in stiffness regulation, gene analyses on the treated samples were conducted.

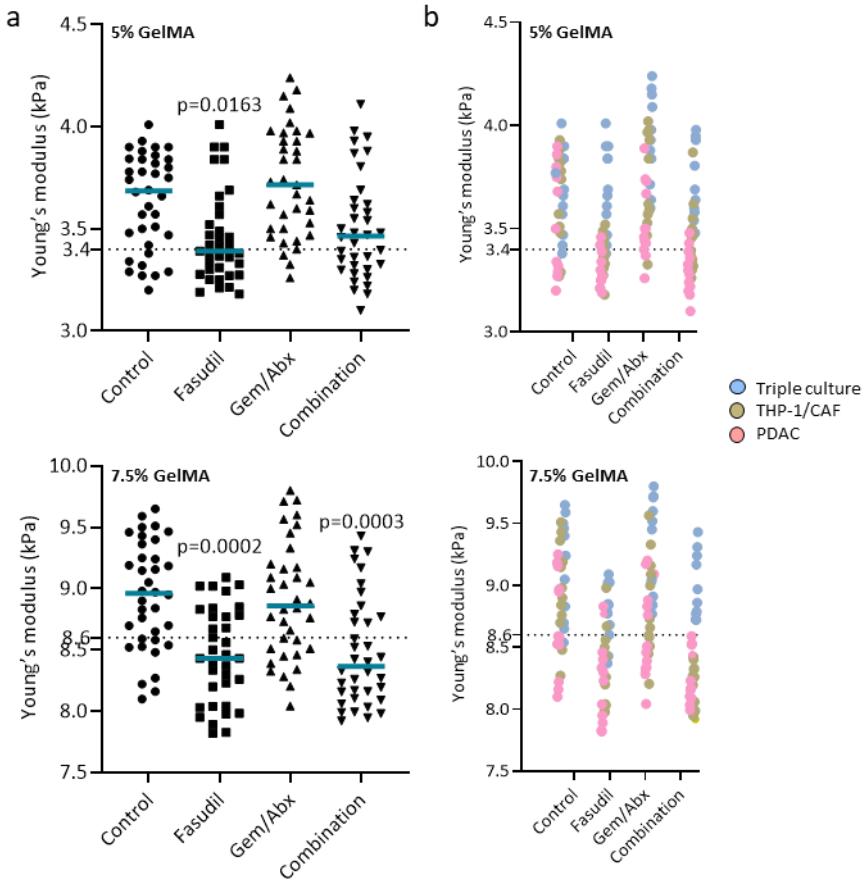

Figure 6.8 Effects of fasudil, Gemcitabine and abraxane (Gem/Abx) treatment on the stiffness of collagen, 5% and 7.5% GelMA hydrogels. (a) Stiffness of cell-laden 5% (top) and 7.5% (bottom) GelMA hydrogels, as measured via unconfined-compression at day 14 of culture. Cultures were treated with 10 μM fasudil on day 7 and 100 nm of each Gem/Abx on day 10. Appropriate untreated and single treatment controls were also set up. Triple cultures consisted of PDAC cells, THP-1 monocytes and patient-derived CAFs in a 1:2:2 ratio. Monoculture control hydrogels (PDAC only and THP-1/CAFs stroma only) were also set up. CAFs were isolated from patients number 2, 3 and 15. Kruskal-Wallis, p-value as annotated, n=3. **(b)** Stiffness of cell-laden 5% (top) and 7.5% (bottom) GelMA hydrogels. Here, the different hydrogels groups are indicated as follows: triple cultures (blue), stroma (brown), PDAC cells (pink), n=3.

6.3.4.3 Effects of ROCK inhibition and chemotherapy on matrisome-related genes and secreted factors

The effects of fasudil, gem/abx and combination treatment on matrix-related gene expression was assessed. For this, a panel of nine genes was used as either belonging either to matrix and matrix remodelling (*FN1, VCAN, CTSB, COL1A1, COL11A1, MMP9*), EMT (*VIM, MMP9*) or mechano-sensing (*YAP1, VIM, TGFBI*) groups. PDAC or stromal (CAFs

and THP-1) cells were cultured for 14 days in either collagen, 5% or 7.5% GelMA hydrogels prior to RNA extraction. Gene expression heatmaps showed a downregulation of all assessed genes upon combinational treatment in cancer cells, with the exception of *TGFBI* in 5% GelMA and *YAP1* in 7.5% GelMA hydrogels (Figure 6.9 top). This suggested that upon treatment, cancer cells had a reduced matrix and EMT gene expression leading to reduced matrix production and malignant cell behaviours. In soft (collagen) and medium stiffness (5% GelMA) hydrogels, chemotherapy was responsible for an upregulation of most of the assessed genes. As a monotherapy, fasudil also led to the upregulation of all the tested genes with the exception of matrix proteins *FN1, VCAN, MMP9* and *TGFBI, CTSB, COL1A1, VCAN,* that were unaffected in collagen and 5% GelMA hydrogels respectively.

Gene expression analysis of stromal (CAF and THP-1) cells showed a more heterogeneous picture (Figure 6.9 bottom). In collagen and 5% GelMA hydrogels, the majority of assessed genes were downregulated upon combinational treatment, while all genes showed an upregulation in 7.5% GelMA hydrogels. Chemotherapy alone was responsible for the upregulation of the assessed genes in collagen and was maintained for 4 out of 9 genes in 7.5% GelMA hydrogels. fasudil treatment resulted in an upregulation of the assessed genes in stromal cells cultured in 5% GelMA hydrogels. Overall, the decreased expression of matrix and mechanosensing genes following combinational treatment in all assessed PDAC conditions as well as largely in stromal cells was encouraging. The large upregulation in pro-tumorigenic gene expression by stromal cells in stiffer matrices (7.5% GelMA) suggests these cells might be exerting a tumour-protecting role upon treatment and contribute to resistance. Future work will investigate the changes in gene expression of triple cultures in response to treatment. Following gene expression analyses, the effects of treatment on other gene signatures [120] and secreted proteins was assessed.

The matrix index (MI) is an ECM-associated signature (comprising 22 molecules), that predicts both extent of disease and tissue stiffness at gene and protein levels [120]. The MI inversely correlated with prognosis [120] as well as EMT status of the analysed PDAC cells (Chapter 5). *FN1, VCAN, CTSB, COL1A1, COL11A1* are part of the MI signature. Here, the MI of normal untreated pancreas was compared to that of PDAC untreated or gem-treated samples (Figure 6.10 a) in publicly available gene datasets. Unsurprisingly, normal untreated pancreatic samples had a lower MI compared to PDAC samples. The MI increased further in gemcitabine-treated samples, indicating that despite its cytotoxic effects, chemotherapy may alter the tumour niche causing an increase in pro-tumorigenic matrix

deposition, contributing to resistance. This effect was also seen in 3D cultures in both PDAC and stromal cells (Figure 6.9). In the absence of other treatments, aberrant matrix deposition (Figure 6.9, Figure 6.10 a), together with an unaltered tissue stiffness (Figure 6.8 a), may work synergistically to promote chemoresistance and reoccurrence post-chemotherapy.

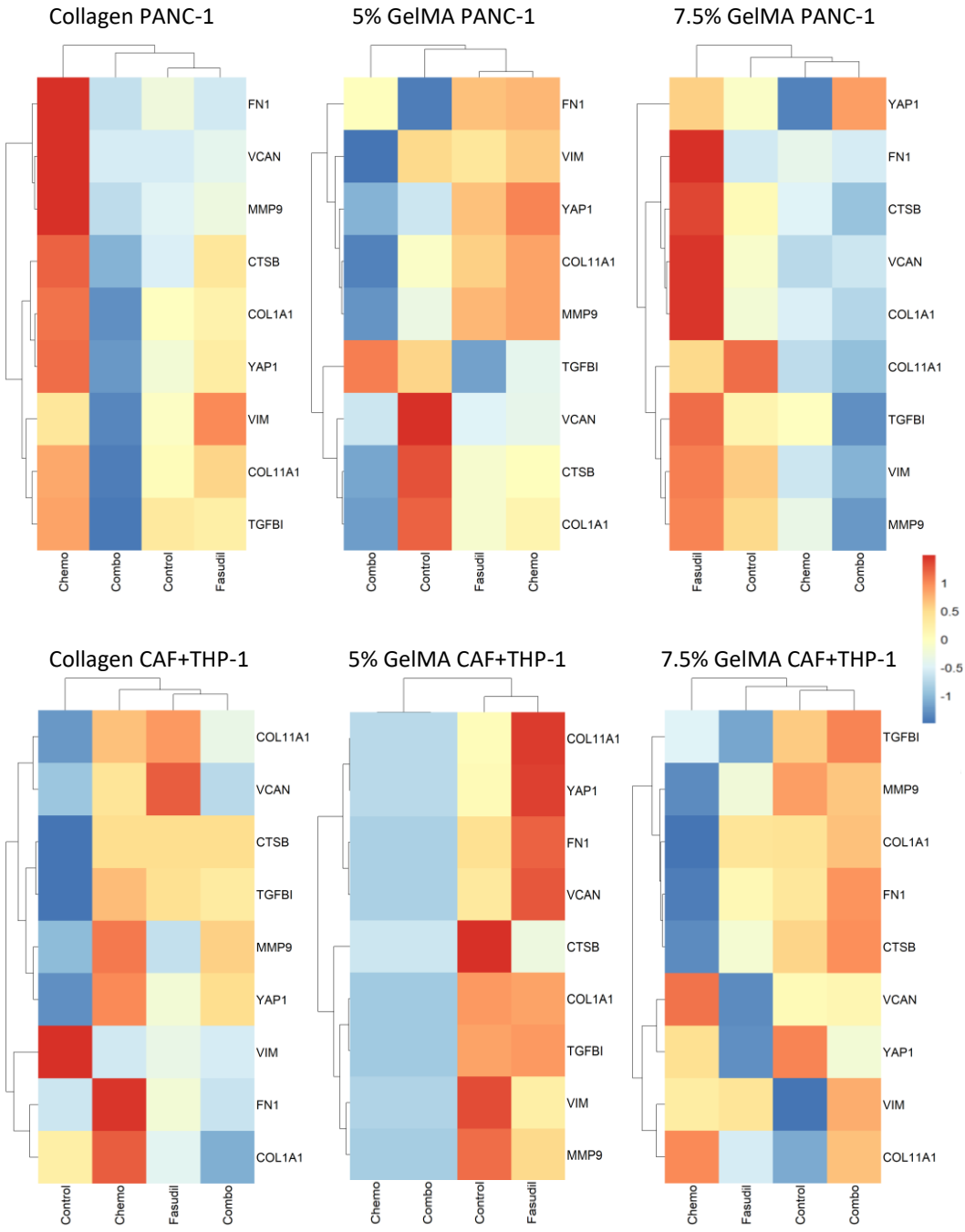

Figure 6.9 Expression heatmaps of selected genes following treatment with fasudil, chemotherapy (Gemcitabine/abraxane), combination treatment or control for PANC-1 (top graphs) or stromal cells (THP-1 and CAF, bottom graphs) at day 14 of culture in collagen, 5% or 7.5% GelMA hydrogels. Gene expression was quantified via RT-qPCR and expression analysed relative to *HPRT1*. Ward.D2 was used on R for data clustering based on the indicated Z-score. n=1.

It could be hypothesised that due to the decrease in ECM gene expression and consequently matrix deposition, the MI of fasudil-treated cultures would also be lower compared to untreated conditions. Unfortunately, not enough data are publicly available to determine whether this is the case. Gene sequencing or proteomics analyses of fasudil and gem/abx-treated hydrogels should be conducted in order to characterise changes in the MI following treatment.

Next, a cytokine array was used to determine changes in the levels of secreted factors following fasudil, gem/abx and combination treatments. The measured levels of some key cytokines in the ascitic fluid of patient 3 are shown in Figure 6.10 b. Elevated interleukin (IL) -6 and -8 levels are associated with poor prognosis in a number of cancers [370]. In PDAC, their expression is significantly upregulated compared to healthy tissues [371], so much so that they are considered as PDAC biomarkers [372,373]. A high concentration of both IL-6 and -8 was recorded in the ascitic fluid of patient 3.

IL-6 and -8 levels were measured in the conditioned supernatant of triple culture hydrogels (PANC-1:CAF:THP-1 in a 1:2:2 ratio) at day 14 of culture and following fasudil, gem/abx or combination treatment, as previously described. CAFs isolated from patient 3 were used for this (Figure 6.10 c). Following treatment, IL-6 levels were elevated compared to control in collagen gels, while IL-8 levels remained unchanged. This was not the case in 5% and 7.5% GelMA hydrogels. Interestingly, despite both IL-6 and IL-8 levels increasing with fasudil and gem/abx as a single treatment, the expression of both cytokines resulted lower in the combinational setting. This effect was evident in both 5% and 7.5% GelMA (Figure 6.10 c). Taken together, this suggested that matrix priming with fasudil followed by gem/abx might be not only relaxing matrix stiffness but also leading to decreased secretion of proinflammatory cytokines, such as Il-6 and IL-8. As IL-6 and IL-8 are known to promote proliferation, migration and invasion in PDAC [298-300], lower levels following combinational treatment is concordant with the observed reduction in cell proliferation of these cultures. Importantly, as IL-6-dependant activation of STAT3 is required for PDAC progression [300], its inactivation could slow tumorigenesis or, in this case, reoccurrence after treatment (Figure 6.10 b, Figure 4.21 b). In control conditions, both IL-6 and IL-8 levels decreased in GelMA cultures compared to collagen cultures, and even further from 5% to 7.5% GelMA (Figure 6.10 d).

To conclude, successive treatment of triple cultures with fasudil and gem/abx led to reduced cell viability and cell counts compared to chemotherapy alone, in all three matrices at day 14

of culture. Treatment with fasudil led to a significant reduction of GelMA hydrogel stiffness. This was accompanied by a downregulation of matrix-, EMT- and mechanosensing-related genes in the cancer cells. Finally, while secreted IL-6 and IL-8 levels increased upon monotherapy, their levels were decreased to control levels during combinational treatment.

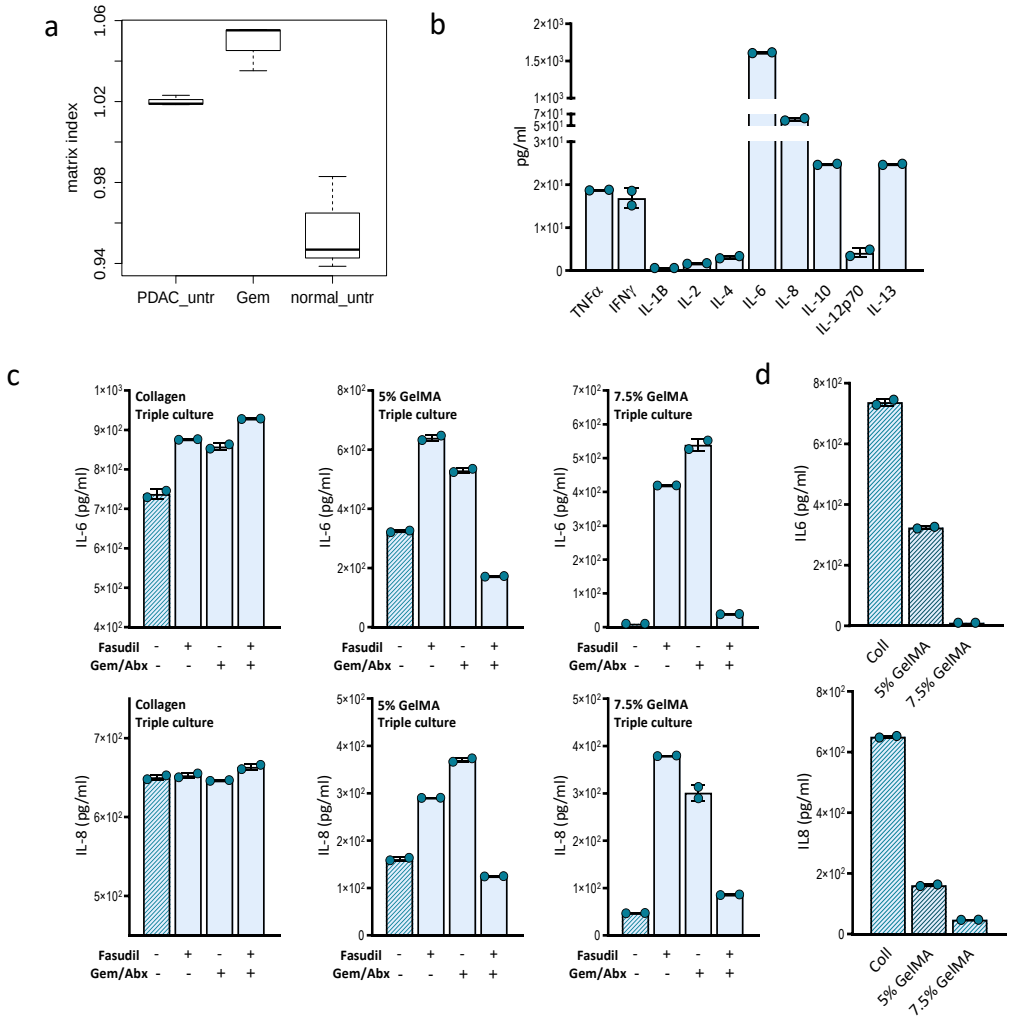

Figure 6.10 Effects of treatment with fasudil and chemotherapy (gemcitabine/abraxane) on matrix proteins and secreted factors. (a) Matrix index of PDAC untreated samples, gemcitabine-treated, and normal untreated samples from publicly available gene data from The Cancer Genome Atlas. **(b)** Secretory profile of some of the main cytokines in patient 3 (ascitic liquid), n=1. **(c)** Interleukin (IL-) -6 and -8 levels in cell culture supernatants of triple cultures (PANC-1:CAF:THP-1 1:2:2 ratio) at day 14 of culture in collagen, 5% and 7.5% GelMA. Hydrogels were treated with 10 μM fasudil on day 7 of culture and 100 nm Gem/Abx (each) on day 10 of culture. TNFα= tumour necrosis factor alpha, IFNγ = interferon gamma.

6.4 Conclusions

In this Chapter, I explored the changes in cell behaviours and hydrogel properties following treatment with inhibitors of matrix-remodelling and matrix-sensing pathways. For this, I used a potent broad-spectrum MMP inhibitor (GM6001), a ROCK inhibitor (fasudil) and three hydrogel-based matrices for the 3D cell culture of PDAC and stromal cells.

Degradation of the local microenvironment through MMPs is a key process during spheroid formation, cell growth and migration [142,145,164]. Altered MMP expression and activity in the TME lead to loss of homeostasis of the ECM, thereby driving PDAC progression [163]. Hence decreased MMP levels are considered important markers of the anti-tumorigenic potential of several compounds and genes under study. The gelatinases MMP2 and MMP9 are among the most studied in PDAC due to their significant upregulation in patients [163,374] and contribution to prognosis (Figure 1.4). In this study, MMP inhibition via the broad-band inhibitor GM6001 led to a reduction in the expression of *MM2* and *MMP9* in collagen and GelMA hydrogels which was accompanied by a downregulation of *vimentin* in three PDAC cell lines cultured in collagen and GelMA hydrogels (Figure 6.3). Recent work showed that anti-MMP9 antibody targeting in PDAC led to the formation of smaller tumours in xenograft models accompanied by a downregulation of stromal markers (collagen-I, α-SMA) and EMT markers including vimentin [375]. A number of other groups have implemented MMP inhibitors in pre-clinical animal models with promising results [163,252,376,377].

GM6001 successfully reduced the proliferation of four PDAC cell lines in 2D, where its effects were more marked on epithelial-like cell lines rather than mesenchymal ones (Figure 6.1). Stimulation of EMT by collagen coating or increasing matrix stiffness (GelMA) resulted in increased susceptibility of cells and higher response rates to GM6001 (Figure 6.1, Figure 6.2). Upon treatment, all the cell lines showed significantly lower invasive potential (Figure 6.2). Limited cell-mediated matrix remodelling and proliferation, as well as loss of vimentin, led to the formation of markedly smaller spheroids in GM6001-treated hydrogels compared to controls (Figure 6.2). The dual reduction in cell proliferation and spheroid size further highlighted the regulatory role of MMPs in spheroid formation and growth as well as emphasising the importance of using MMP-sensitive and biodegradable 3D cell culture systems for the study of biological processes. Lastly, although there was no difference in the overall stiffness GelMA hydrogels upon treatment, AFM revealed local changes in the stiffness of spheroids and cell-clusters embedded within the hydrogels (Figure 6.5). GM6001-

treated spheroids were not only smaller than their untreated counterparts but also softer and, possibly due to their limited matrix remodelling abilities, they did not affect overall hydrogel stiffness.

Despite promising results at pre-clinical stages in both *in vitro* and *in vivo* models, there has yet been no breakthrough for the clinical implementation of MMP inhibitors. In fact, only two phase III trials were published with the use of broad-band MMP inhibitors in PDAC (marimastat and tanomastat), both of which with no clear response or survival benefit for the patients [161,162]. A number of speculations can be made in regard to the discrepancies between experimental and clinical results for these inhibitors. First is the lack of adequate TME in pre-clinical models, which prevent the accurate understanding of the complex MMP dynamics within the tumour niche. CAFs for instance can secrete high amounts of MMPs and their tissue inhibitors TIMPs and are active contributors to matrix remodelling in PDAC [59]. Matrix remodelling is essential for the maintenance of CAFs and as such, is a self-sustained function. In addition, stromal cytokine levels (such as interferon gamma – IFNγ – or C-C motif chemokine ligand 2 - CCL2) can direct monocyte-mediated regulation of MMPs in PDAC [378]. In order to accurately model the effects of MMP inhibitors at a pre-clinical level, a model would have to take into consideration not only effects of MMP inhibition on cancer cells themselves (or on tumour burdens) but also on the self-sustaining and co-regulated secretion of MMPs by other components of the pancreatic TME. In this regard, the inclusion of multiple TME elements in collagen and GelMA hydrogels for these experiments would give us a better understanding of the mechanistic processes regulating MMP inhibition in the context of the TME.

Disappointing clinical trials results of MMP inhibitors do not imply that MMPs do not contribute to PDAC progression. The lack of clinical benefits may also be due to inclusion of the inhibitors at advanced stage of disease, when both the tumour cells and other TME components have an already established co-stimulatory networks for the secretion of several matrix remodelling enzymes. In fact, the MMP pathway is highly multifaceted and only constitutes a minority of expressed human proteases. Serine, cysteine, threonine and aspartic proteases are also deregulated in cancer, and can contribute to tumorigenesis both dependently and independently of MMPs [379,380]. Finally, certain MMPs can play both a pro- and anti-tumour role, therefore their inhibition is not always beneficial. This is in fact the case for MMP9 deficiency which, on a *Kras(G12D)* background enhances tumour progression and invasion [164] rather than inhibiting it. Nonetheless, a continued understanding

of the processes regulating matrix degradation in cancer and their roles in stiffness modulation is pivotal to our understanding of PDAC biology.

Next, the effects of ROCK inhibition on PDAC cells cultured in collagen and GelMA were presented (Figure 6.4, Figure 6.5). Unlike GM6001, treatment with fasudil did not lead to a significant reduction in cell proliferation and the overall number of spheroids remained unchanged between treated and untreated conditions (Figure 6.4). This is concordant with previous reports where treatment with fasudil did not significantly affect cell proliferation in 2D or 3D (collagen gels) [155]. However, fasudil significantly decreased the stiffness of cell-containing GelMA hydrogels (Figure 6.5 a). When analysed by microscopy, fasudil treated cultures showed a higher number of dead (Et-H1 stained) PANC-1 cells compared to control conditions, despite the overall number of spheroids being unchanged (Figure 6.6 b). Because of this, the effects of fasudil were investigated in conjunction with the standard chemotherapeutic agents gem/abx on 3D cell cultures of PDAC, CAFs and THP-1 cells. A staggered administration regime was devised, whereby cultures received an initial dose of fasudil followed by chemotherapy. Monotherapy as well as monoculture controls were also analysed. Matrix priming with fasudil in combination with chemotherapy led to a further reduction in cell viability and proliferation compared to chemotherapy alone (Figure 6.6, Figure 6.7).

As previously observed in monocultures, fasudil alone had no effect on cell proliferation of the triple culture hydrogels however, it had a mild effect on stromal cells. Importantly, fasudil treatment led to a reduction in the overall stiffness of triple culture GelMA hydrogels, even in the presence of gem/abx (Figure 6.7). In addition to impeding drug delivery, matrix stiffness alone can induce resistance to abraxane and relapse [128], hence a reduction in tension was an encouraging outcome of this combinational treatment (Figure 6.8). In PDAC cells, combinational treatment led to the downregulation of matrix and matrix remodelling genes (*FN1, VCAN, CTSB, COL1A1, COL11A1, MMP9*), EMT genes (*VIM, MMP9*) and mechano-sensing genes (*YAP1, VIM, TGFBI*), in all three matrices. This suggested treatment led to an impaired expression of pro-survival, pro-tumorigenic genes and matrisome-related genes. *FN1, VCAN, CTSB, COL1A1, COL11A1* specifically, have been associated with poor prognosis in a number of cancers including HGSOC and PDAC [120]. Hence, their downregulation was an encouraging feature of the treatment. Contrariwise, chemotherapy alone caused an upregulation of EMT genes, a phenomenon which has been described in a number of cancers [381,382]. In turn, EMT can promote chemotherapy resistance further [128,382].

Lastly, a common matrix signature (the matrix index – MI [120]) and secreted cytokines were analysed upon treatment in order to establish further treatment effects at the gene and protein level (Figure 6.9, Figure 6.10). At gene level, the MI was significantly increased in the progression from healthy pancreas to PDAC, and was further upregulated in gem-treated samples (Figure 6.10 a). An increased expression was also recorded in IL-6 and IL-8 cytokines upon gem/abx treatment (Figure 6.10 c), both of which are associated with poorer prognosis in PDAC [371-373]. High, sustained levels of IL-6 and IL-8 were also observed upon fasudil treatment as a monotherapy. Combined treatment with fasudil and chemotherapy resulted in lower IL-6 and IL-8 levels in GelMA but not collagen hydrogels. Because of their involvement in promoting PDAC cells proliferation, migration and invasion [298-300], a decrease in these cytokines would be a beneficial feature of this combinational treatment, especially as a conserved feature in stiffer GelMA hydrogels.

Host tissue properties and its alterations play a vital role in tumorigenesis by providing initial pro-survival signals as well as subsequent maintenance of cancer cell proliferation, invasion and metastasis [17,278]. Combined, these results suggest that short-term inhibition of matrix and cellular tension at a whole hydrogel level prior to chemotherapy may improve response to treatment. The data revealed similar effect in all hydrogels analysed, as well as monoculture controls suggesting this phenomenon may be common to multiple microenvironments and across multiple physiologically-relevant tissue rigidities. This suggests that temporal disruption of signalling between tumour cells and their surrounding microenvironment renders cancer cells momentarily more sensitive to cytotoxic drugs. Additional mechanisms of action of ROCK inhibitors include impaired integrin signalling and induced accumulation of mitotic defects upon treatment [149,383]. This is supported by other recent findings such as the inhibition of collagen crosslinking via temporal lysyl oxidase (LOX) antibody targeting in combination with chemotherapy, which effectively impaired PDAC progression [133]. These effects have also been characterised and shown to be maintained in secondary sites [155].

Additional work should be carried out in order to establish which patients are more likely to benefit from ROCK inhibitors and which biomarkers would be used for accurate stratification and characterisation of response. Patient stratification could facilitate a more targeted and efficient intervention strategy, as single "all inclusive" chronic targeting approaches have so far had limited success in PDAC [45,47-49,364]. As for the presented data, combinational ROCK and cytotoxic drugs targeting was efficient in triple cultures regardless of the stiffness of the hydrogel (Figure 6.7). However, in the absence of cancer cells, stromal

cells were more susceptible to the treatment in collagen hydrogels compared to 5% and 7.5% GelMA hydrogels. This suggests that despite no apparent advantage in overall co-culture proliferation, stiffer matrices serve a protective role over stromal cells. This may prove advantageous as previous studies have shown that complete fibrosis ablation in PDAC via either α-smooth muscle actin fibroblasts targeting [48], or pro-fibrotic Sonic Hedgehog signalling pathway silencing [49], enhance invasion, metastasis and reduced survival. Hence, transient administration of stromal-targeting therapies, rather than chronic ablation of fibrosis may represent an advantageous strategy. A similar intervention strategy could be applied to other ECM-targeting therapies such as the abovementioned LOX [133] or hyaluronic acid [44,45].

Because of its reduced toxicity as a monotherapy, fasudil could be administered systemically at higher doses, where it would target not only the primary but also act as a priming agent on potentially unknown metastatic sites, followed by standard chemotherapy. Additionally, fasudil has been approved for use in Japan in the treatment of cerebral vasospasm since 1995 and has now been approved by the US Food and Drugs Administration (FDA) in clinical trials of Raynaud's disease, atherosclerosis, and amyotrophic lateral sclerosis (ALS). Among its benefits is the vasodilatory properties of the drug, which might also be beneficial for increased vessel perfusion and drug delivery in cancer [384]. Alternative ROCK inhibitors such as CCT129254, AT13148, K-115 (ripasudil), GSK269962A have shown promising effects in melanoma [385,386] and glaucoma [387,388], as well as different specificity to ROCK1 and ROCK2. As such, the field of mechano-transduction in PDAC is still its infancy and the role of ROCK still widely unexplored in this cancer. Continued work will not only help uncover significant mechanobiological processes but also pave the way for improved targeting of this lethal malignancy.

Taken together, these results suggest that GelMA hydrogels are a viable and informative platform for *in vitro* drug testing, with many potential applications in the field of bioengineering as well as drug development and pre-clinical drug screening.

Chapter 7 - Discussion and Concluding Remarks

7.1 Summary of key findings

This thesis presents the first instance of the use of GelMA hydrogels of different stiffness for the modelling of the pancreatic TME. The suitability of GelMA hydrogels was evaluated by conducting several cell behaviour and molecular profiling assays on the encapsulated cells and benchmarked against collagen gels. For this, PDAC cells were used alongside THP-1 cells and patient-derived CAFs. The formation of a multicellular 3D model, as well as the use of primary cells, represent a novel aspect compared to other reported GelMA-based models [252,255-257,389].

Characterisation of GelMA hydrogel stiffness, nanostructure and the expression of selected matrix proteins were largely concordant with that of native PDAC ECM. To the best of my knowledge, this thesis presented the second-largest characterisation of fresh, human resected PDAC and adjacent normal tissues. In line with previous work [130], adjacent normal tissues had a stiffness of 2.2 ± 0.2 kPa which significantly increased to 7.4 ± 0.6 kPa in matched tumour tissues. Patient-derived pancreatic tissues were often stiffer than their murine counterparts, which prompted the investigation of 3D model's rigidities via the stiffness testing of commonly-used hydrogel platforms. The stiffness range of GelMA hydrogels was much larger and easily tuneable compared to that of collagen gels, as well as Matrigel, which is an order of magnitude softer compared to human PDAC tissues [266]. GelMA hydrogels stiffness was highly reproducible, even upon cell incorporation, and predictable through a simple mathematical relationship. To this end, 5% and 7.5% GelMA hydrogels were deemed the closest to the observed human tissue stiffness (3.4 and 8.6 kPa respectively) and were employed for transcriptomic and *in vitro* drug testing analyses. Importantly, following optimisation, biomechanics were used as a readout for direct comparison of cell-mediated matrix remodelling or stiffness modulation.

Recent work has begun to uncover the importance of substrate mechanics in the regulation of PDAC intracellular signalling [17], proliferation [128], invasion [129,278], EMT [128,203] and response to treatment [265,279], of which cell-ECM signalling is a vital mediator [139,155]. Because of this, the association between stiffness and the expression of some key matrix proteins was investigated. Collagen-I, fibronectin, versican, as well as total collagen expression was significantly higher in diseased tissues compared to matched healthy pancreas. Collagen fibre thickness was also increased [128]. Importantly, increased local expression of any of these three matrix proteins positively correlated with increased tissue stiffness. In PDAC, the role of collagen and fibronectin is well characterised and associated with shorter survival [95,124,268],

whereas versican and its roles in carcinogenesis are much less studied [52]. Finally, the expression of these three extracellular proteins as well as hyaluronic acid and the cellular markers cytokeratin-19 (PDAC cells) and CD68 (macrophages) was validated in cell-laden GelMA hydrogels.

Next, the suitability of GelMA hydrogels for 3D PDAC cell culture and the inclusion of patient-derived cells was assessed and extensively characterised. ^{1}H NMR and spectroscopy-based analyses revealed high consistency in the degree of methacryloyl substitution onto the gelatin backbone across different GelMA batches. Cancer cell culture and viability in GelMA hydrogels was supported for over 28 days in hydrogels of ranging stiffness 3%, 5%, 7.5% and 10% GelMA. PDAC cells formed round, spherical colonies with distinct cell-specific morphologies, proliferation patterns and rates. Several *in vitro* and *in vivo* studies have now shown a appositive association between matrix stiffness and upregulation of EMT markers and pro-survival signalling pathways [17,128,139]. In GelMA, epithelial-like cell lines, such as Capan-2 and BxPC-3, showed an increased proliferation in matrices of increasing stiffness (from 3% to 7.5% GelMA) while mesenchymal cell lines, such as PANC-1 and MIA PaCa-2, did not. The presence of myeloid cells and patient-derived CAFs (but not normal fibroblasts) increased PDAC cell proliferation, as well as GelMA hydrogel stiffness via the upregulation of IL-6, IL-8 and pSTAT3, concordant with other reports [188,320]. Unsurprisingly, the presence of myeloid cells in GelMA hydrogels increased the number of both tumours and metastases formed in orthotopic xenografts compared to control hydrogels with PDAC cells only. Furthermore, this supported the use of GelMA hydrogels as an alternative to collagen and Matrigel for use as carrier during *in vivo* studies. Although not tested here, the effects of hydrogel stiffness as well as patient-derived cells on tumorigenicity may be investigated *in vivo* using this approach. Indirect co-culture experiments revealed that STAT3, but not ERK, was upregulated during culture of PDAC cells with myeloid cells and fibroblasts. In stiffer matrices, concomitant upregulation of STAT3 and downregulation of ERK was observed, a phenomenon that has been associated with treatment resistance [307].

Transcriptomics analysis of PDAC cells grown in GelMA hydrogels revealed matrix signatures that correlated with those of cells grown in collagen hydrogels, as well as primary tumour organoids cultured in Matrigel. Amongst the differentially expressed pathways of cells grown in soft collagen and stiffer GelMA hydrogels were a number of structural and matrix organisation genes. These included effectors of the GPCR, Wnt, β-catenin and Rho GTPase pathways, all of which are involved in mechano-sensing. Selected core matrisome and mechano-transduction genes were validated by RT-qPCR. Importantly, GelMA-cultured PANC-1 and BxPC-3 cells retained a gene expression profiles concordant with their EMT

status and distinct between the two cell lines. This suggested that cells were capable of maintaining cell-specific characteristics upon culture in GelMA which would be an advantage for the potential application of these hydrogels as personalised medicine or diagnostic tools.

In order to understand the translational value of GelMA for PDAC research, treatment response to matrix-modulating and cytotoxic agents was assessed, alongside collagen gels. The effects of the broad-band MMP inhibitor GM6001, the ROCK inhibitor fasudil as well as a combination of gemcitabine and abraxane were tested on PDAC cell behaviours in 2D and 3D. Unfortunately, too little is known about patient's responses to these agents to be able to infer any correlation between cell responses in GelMA and clinical efficacy. However, GelMA represented a suitable model for the investigation of all tested therapeutic agents, as well as the effects of stiffness, which could not be assessed to this extent in collagen gels. In 2D, cell's susceptibility to GM6001 and cytotoxic agents increased on collagen-coated wells compared to control, while fasudil had little effect on cell proliferation. Transwell invasion assays revealed that cell invasion through collagen and Matrigel-coated wells was significantly reduced upon MMP inhibition. In 3D, GM6001 treatment led to impaired spheroid formation and cell proliferation in both GelMA- and collagen-embedded cells [252]. This was mediated by a reduction in PDAC cell *MMP2* expression in collagen gels and *MMP9* and *VIM* expression in GelMA. Treatment with GM6001 did not affect bulk hydrogel stiffness as measured by compression. However, atomic force microscopy revealed a decrease in local spheroid stiffness upon treatment with the MMP inhibitor, possibly indicative of a reduced matrix remodelling capacity.

Unlike GM6001, treatment with fasudil did not significantly affect PDAC cell proliferation in 2D or 3D models as previously reported [155]. Treatment with fasudil did however lead to decreased bulk hydrogel stiffness and increased cell death, prompting the investigation of this treatment in combination with the cytotoxic agents gemcitabine and abraxane. For this, triple cultures of PDAC, CAF and THP-1 cells were treated with the mechano-modulating agent fasudil on day 7 of 3D culture prior to chemotherapy on day 10 of culture. Endpoint analysis revealed that the addition of matrix priming with fasudil further reduced the proliferation of triple cultures compared to chemotherapy alone. Additionally, combinational treatment samples (fasudil plus gemcitabine/abraxane) showed lower levels of secreted IL-6 and IL-8 compared to monotherapy treatments. Gene expression analyses revealed a downregulation of matrix proteins (*COL1A1, COL11A1, CTSB, FN1, VCAN*) and EMT markers (*MMP9, TGFBI, VIM, YAP1*) in the combination treatment samples compared to controls. These genes were largely upregulated in chemotherapy-treated and fasudil-treated

samples but not in combination. Overall, these effects were more prominent in PDAC cells compared to stromal (CAF and THP-1) cultures. On the other hand, stromal cells cultured in stiffer matrices (7.5% GelMA) did not respond to treatment as their proliferation was unchanged and matrix protein and EMT gene expression increased. Hence, the use of GelMA hydrogels allowed to discern between the behaviours of specific cells, in 3D monoculture or co-culture settings, unveiling differential responses to treatment and matrix stiffness. Taken together, these data supported the use of GelMA-based hydrogels for pre-clinical drug testing, accurate assessment of *in vitro* stiffness modulation and multi-modal assessment of cell functions and behaviours.

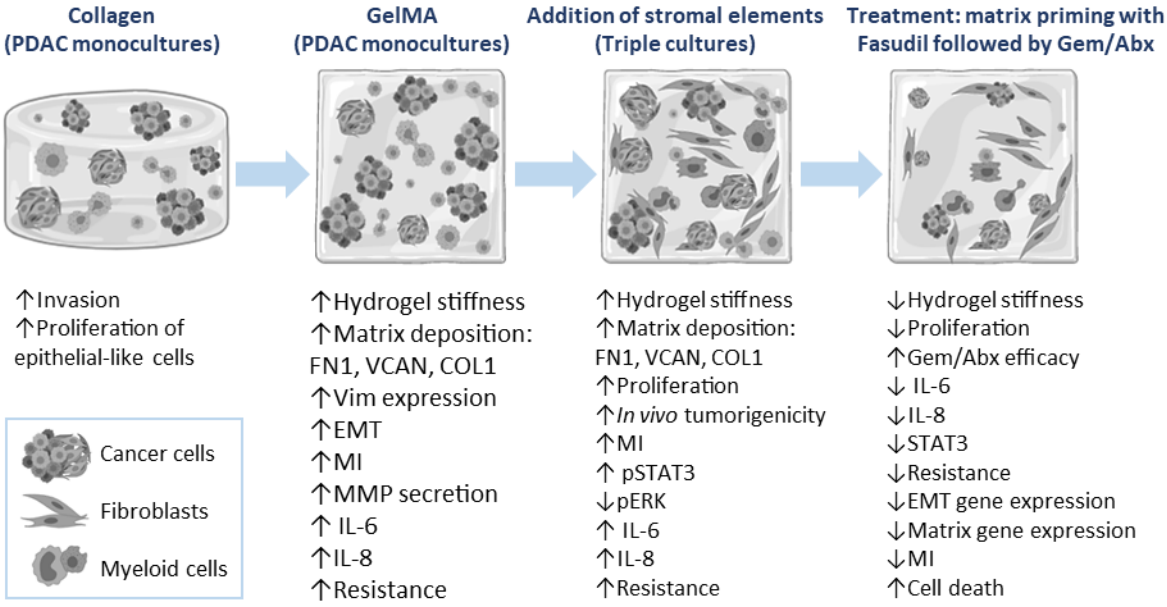

Figure 7.1 Schematic representation of some of the investigated key processes involved during the progression from 2D cultures to 3D collagen gels, GelMA-based hydrogel cultures, the addition of relevant tumour microenvironment components, and treatment.

7.2 Future experiments

In the light of findings presented, I suggest the following experiments for the continuation of this work:

Related to Chapter 3:

- Increase the number of tissues for stiffness and matrix protein analysis to strengthen and validate the described correlations with tissue stiffness. Associations between specific matrix molecules and stiffness have not been previously characterised, at a local level, in PDAC. Additional matrix markers, such as hyaluronic acid, markers identified via transcriptomics analyses, such as ROCK, LOX, TGFBI, or cellular

markers such as CD68, αSMA, FAP, KRT19, should be validated at protein level and checked against local stiffness for potential correlations.

- The expression of these markers should be investigated further in GelMA hydrogels, which also allow to determine the cellular origins for each marker.

Related to Chapter 4:

- Increase the translation value of GelMA hydrogels by including primary PDAC and myeloid cells alongside patient-derived CAFs. These could be isolated from matched resected tissues and plasma/blood samples.
- Fully understand the effects of UV crosslinking on cells by conducting protein analyses on GelMA-extracted cells for the DNA damage markers γH2AX, p53 binding protein, RAD-51, or BRCA1 and consider visible light crosslinking alternatives.
- Optimise conditions for the 3D printing of cell-laden GelMA hydrogels [230,233,238]. This would be a high-throughput, fast, multimodal and standardised alternative for 3D modelling, conducive to the incorporation of multiple cell types.

Related to Chapter 5:

- Understand transcriptional changes upon incorporation of multiple cell types within GelMA hydrogels, and comparison with primary organoids (Matrigel). For this, RNA-seq could be performed on co- and triple-cultures in GelMA.
- Perform proteomics analysis of cells (this has never been done on GelMA-cultured cells before) and integrate the results with the transcriptional data. This could provide us with cues to stiffness-induced protein changes and complement the transcriptomic data. This could be further compared to human data (depending on tissue availability) or against published matrisome datasets [86,87]. Phospho-proteomics could be employed for the understanding of fasudil-induced changes in phosphorylation (such as those of downstream targets MLC, PTEN, LIMK, Cofilin).

Related to Chapter 6:

- Further elucidate the efficacy of combined ROCK and chemotherapy treatment (and relevant monotherapy controls) by assessing the expression of cell proliferative (Ki67) and cell death (Cc3) markers in GelMA triple cultures and monoculture controls.

- Understand the changes in ROCK expression (and downstream targets) during treatment in GelMA and subsequent addition of chemotherapy. Proteomics, western blotting or phospho-protein arrays could be used to this end.
- Confirm the ROCK-mediated mechanisms of stiffness relaxation in GelMA through validation with different ROCK inhibitors and performing a gene knockout.

7.3 Wider research implications and future perspectives

Despite several clinical trials and a considerable increase in our understanding of PDAC biology, there has been little improvement in the survival rates of pancreatic cancer patients over the past decades. Compared to other cancers, PDAC's dismal prognosis remains virtually unchanged and efficient treatment options rather stagnant [1]. This is accompanied by an overall high failure rate of oncology drugs entering the clinical trial pipeline, where only around 3.4% end up being approved for market use [363]. This can be partially explained by a number of discrepancies observed between pre-clinical and clinical results which is fostered by over-reliance on traditional 2D cell culture and the use of immortalised cell lines. The development of pre-clinical models that accurately capture multiple fundamental aspects of the TME, such as stiffness, architecture, matrix protein expression, tumour and stromal heterogeneity, is paramount to bridge the gap between pre-clinical and clinical efficacy. The development of advanced *in vitro* models and their analytical techniques would impact not only translational but also basic research.

A novel approach for 3D modelling of PDAC was presented in this thesis. Following a bottom-up approach, I aimed to dissect and then recapitulate certain key features of PDAC pathobiology in order to understand their individual contribution to pathogenesis. Characterisation of GelMA hydrogels themselves, as well as optimisation of analytical techniques for their analysis, were inherent to the successful implementation of this platform as a 3D cell culture model. These aspects are often overlooked as commonly-used matrices, such as collagen gels and Matrigel, have little tractability and tuneability, often leaving no room for optimisation. A crucial consideration for the purpose of this work was the range and tuneability of mechanical properties of these popular cell culture platforms. In fact, both collagen and Matrigel undergo chemical and temperature-dependant crosslinking resulting in weakly crosslinked matrices with a stiffness of less than 1 kPa, irrespective of polymer concentration. This is below both the physiological stiffness of pancreatic tissues as well as that of diseased ones. Both Matrigel and collagen gels have a batch-to-batch variability that is much higher than that of gelatin. These matrices undoubtedly provide microenvironmental

cues to support cell viability and proliferation but make it hard to discern between matrix-induced and cell-inherent behaviours. On the other hand, as gelatin is the most abundant protein in our body [237,287], it provides a more inert yet highly relevant matrix for 3D cell culture. A better-defined matrix composition represented an advantage during transcriptomic analysis of the embedded cells, allowing the dissection of pathways that were directly involved in stiffness regulation via direct comparison of 5% and 7.5% GelMA hydrogels. As the composition of GelMA is defined [234,242], cells could be subjected to proteomics analyses to further understand stiffness and treatment-induced matrisome changes. This would pave the way for more detailed and integrated multi-omics analyses of a single 3D system, which many groups have now adopted as standard characterisation approach [18,223,348,360].

An additional consideration is the number of cells that can be incorporated. In the case of Matrigel, high cell seeding densities preclude organoid formation because of high matrix degradation rates [226]. A similar phenomenon is observed in collagen, whereby low mechanical properties allow for increased matrix degradation and poor hydrogel stability upon incorporation of high cell numbers. For this reason, stiffness changes in collagen gels presented in this thesis were harder to detect and less consistent compared to compression-based and atomic force microscopy GelMA analyses. Although not investigated here, the observed movement of certain cell lines towards the edge of the hydrogels suggests a nutrient and oxygen gradient may be forming in GelMA. The formation of a nutrient gradient and hypoxic regions are hallmarks of pancreatic cancers, hence future work could investigate hypoxia-induced cell behaviours in GelMA hydrogels further. Three-dimensional studies have now shown that cells grown in highly compact multicellular spheroids - over 500 μm in diameter as observed in GelMA, as opposed to the traditional sphere culture – are capable of inducing tumour-like metabolic switches similarly to tumours, in response to hypoxic conditions [390]. Thanks to changes in tensional homeostasis, encapsulation of cells within hydrogels has been reported to induce the acquisition and sustainment of malignant and invasive cell phenotypes via upregulation of ROCK/Rho-generated contractility and downregulation of ERK [391]. The latter was also observed in cells cultured in GelMA hydrogels of increasing stiffness.

Another factor which is paramount for successful 3D cell culture is the biocompatibility of the matrix, which determines whether an environment is a conducive environment for cell proliferation. Malignant cells were highly viable in GelMA hydrogels for over 28 days of

culture. Stromal cells, including patient-derived cells, had a lower proliferation rate compared to malignant ones, but nonetheless maintained their viability throughout culture, highlighting the biocompatibility of these hydrogels. Taken together, these considerations suggest GelMA-based hydrogels constitute a valid alternative platform for the multicellular culture of PDAC and modelling of its extracellular TME, while being amenable, following optimisation, to most applications and analyses as showcased in this thesis.

GelMA hydrogels also hold potential as personalised medicine pre-clinical tools for PDAC, where lengthy animal experiments are not possible due to the dismal prognosis of this malignancy. While some features do not necessarily require 3D cell culture to be carried out (such as genomics, transcriptomics or proteomics), the presence of a 3D matrix is required for both the modelling and long-term maintenance of original tumour features. Additionally, most functional traits including response to treatment, stiffness, matrix deposition or cytokines, just to name some, require 3D culture for analysis. Here, the two employed treatment schedules - either from day 1 of 3D culture (replaced every 72 hours, chronic treatment) or staggered regime on day 7 and day 10 – allowed respectively for the investigation of treatment efficacy on early proliferative events, as well as "treatment" of previously-established tumour spheroids. Similar treatment regimens could be employed in GelMA hydrogels for drug testing as part of pre-clinical drug development or personalised medicine. To this end, a significant improvement would be the development of a fast and efficient protocol for the isolation of PDAC cells from resected tissues for incorporation and culture in GelMA. Current approaches including xenotransplantation or cell immortalisation require lengthy expansion procedures which severely limit the applications of these models as personalised diagnostic tools [18,392].

In its current state, the field of 3D models is still in its infancy, and many physiologically important aspects such as the presence of a fully functional immune system, or multifaceted TME components are yet to be entirely replicated. In fact, many aspects of cytotoxic drugs assessment, such as off-target effects, efficiency of second and third line of defence, pharmacokinetics and drug metabolism, cannot be fully characterised by any one *in vitro* system. Novel 3D models such as GelMA hydrogels should aim to integrate and complement *in vivo* data, by providing fast, cheap and easily tuneable systems capable of answering specific questions that would otherwise be limited to 2D models. Some additional challenges remain unaddressed, such as the inclusion of immune cells to modulate a fully functional immune system, the development of complex vascular networks and the recapitulation of exact tissue

architectures and matrix composition. For this, novel bioengineering approaches, such as the use of microfluidics devices, 3D printing and decellularised tissue scaffolds, hold great promise [195,223]. Microfluidic devices and 3D bioprinting require a crosslinkable material which is conductive to cell viability as well as extrusion, for which GelMA is a perfect candidate [238]. GelMA hydrogels also offer a scalability that would not be achievable with any *in vivo* model, leaving 3D models the system of choice for drug screening. Additionally, as showcased in Chapter 4, GelMA hydrogels can be employed as cell carriers for grafting, allowing the investigation of parameters such as matrix stiffness and composition on *in vivo* tumour growth and dissemination.

An evident advantage is the sequential incorporation of multiple cell types within the matrix, allowing to investigate both individual and collective contribution of cells of the TME. In the future, PDAC cells, patient-matched fibroblasts from resected tissues, and autologous serum should be collected from the same patient for isolation and subsequent 3D co-culture. The results presented in Chapter 4 indicated that stromal cells, although limited to CAFs and myeloid cells in this study, contributed to both increased cell proliferation and increased matrix stiffness via concomitant upregulation of STAT3, ERK downregulation and increased expression of pro-inflammatory cytokines in a stiffness-dependant fashion. Interestingly, stromal and malignant cells showed different responses to matrix modulating agents, which could not have been investigated to this extent in 2D cultures.

This work presented the first report of the use of GelMA hydrogels for the culture of PDAC cells and analysis of cell functions, transcriptomics and comparison against other popular hydrogel matrices, Matrigel and collagen gels. Transcripts from GelMA-cultured cells showed high correlation with both collagen and Matrigel-cultured patient-derived organoids, suggesting important pathways may be conserved across 3D cell culture platforms and recapitulated in GelMA. An encouraging outcome was the upregulation of mechano-sensing and mechano-related pathways within the stiffer GelMA hydrogels, suggesting this model could be a useful tool in the investigation of stiffness-related processes. These applications were highlighted further in Chapter 6, where the use of hydrogels of increased stiffness induced the expression of matrix remodelling proteases (MMPs) as well as the cytoskeletal EMT marker vimentin, ultimately affecting response to an MMP inhibitor. Using three distinct bioengineering approaches, the bulk and local stiffness of GelMA-embedded spheroids was assessed. Because of the high, sustained, viability of cells in GelMA, these hydrogels allowed for the investigation of a matrix-targeting treatment (fasudil) with a

staggered administration regime, in combination with cytotoxic agents. Preliminary results showed that this treatment regimen was favourable in that it decreased overall matrix tension, facilitating the diffusion of chemotherapy and reducing the expression of matrisome-related and EMT genes as well as the levels of secreted pro-inflammatory cytokines. These effects were more prominent in stiffer hydrogels, compared to collagen.

The biomechanics of the TME and regulation of tumorigenesis by mechanical forces and stiffness are relatively novel and under-studied fields [126,391,393,394]. However, mounting evidence has now linked matrix stiffness as well as cell-mediated solid stress increases to tumour progression and maintenance [139,322,357], and with it, efforts to target both the matrix- and cell-induced mechanical abnormalities have spiked [117,133,134,154,155,165,369,385]. These effects and targeting strategies are of particular interest in PDAC, because of its increased desmoplasia and tumour stiffness compared to other solid malignancies [95,128]. The present work highlighted the contribution of stromal cells and matrix molecules in determining matrix stiffness changes, highlighting the need to implement advanced, multicellular systems for the understanding of mechano-related processes. The use of mechanics as a high-sensitivity readout constituted one of the main advantages of GelMA over conventional 3D matrices. New experimental setups should consider introduction of further TME elements in an additive fashion, in combination and separately, to broaden our knowledge of the role of each component in the evolution and mechanobiology of pancreatic cancer.

Efforts in increasing our understanding of tumour biomechanics are driven by the clinical applications of this knowledge. In fact, many stromal targeting therapies are based on the premises that matrix molecules, as well as stromal cells, exert a pro-tumorigenic function by induction of local desmoplasia and pro-survival signalling [44,45,58,133,159,185]. However, stromal ablation in PDAC has had mixed results in both pre-clinical and clinical trials [44,46-48], hence why transient targeting and matrix priming regimes were devised [155,364]. With this in mind, the effects of matrix priming with a ROCK inhibitor followed by chemotherapy were tested. The overall decrease in matrix tension following ROCK inhibition was an encouraging result, as was the reduced viability of cells following combinational treatment. Reduced mechano-signalling, matrix stiffness and matrix gene expression could lead to both increased drug delivery, increased sensitivity and reduced cell motility. Future work should dwell into the mechanical and molecular mechanisms linking ROCK downregulation to increased chemotherapy efficiency, as well as the efficacy of this treatment at preventing further relapse.

7.4 Concluding remarks

Taken together, these findings suggest that GelMA-based hydrogels constitute a suitable and informative platform for the 3D culture of pancreatic cancer cells and associated TME components as well as *in vitro* drug testing. This work sets a precedent in the optimisation of analytical techniques for GelMA-embedded cells and the first extensive transcriptomics analysis in the context of other popular 3D cell culture matrices. The present experimental design also represents a minimal and reliable bottom-up approach required for the design and characterisation of any novel *in vitro* platform including assessment of its mechanics, reproducibility, matrix composition and architecture (Chapter 3), biocompatibility and cell functions (Chapter 4), transcriptomics (Chapter 5) and translational applications (Chapter 6). The use of collagen gels constituted an optimal control because of their prevalence in the literature while highlighting the tuneability of GelMA. Nonetheless, more work remains to be conducted in order to fully demonstrate the translational potential of GelMA hydrogels as well as required validation against clinical data. Given the virtually unchanged mortality of PDAC, and the predicted rise in its incidence, advances in the understanding and modelling of this cancer will be imperative for both research and clinical success.

Since the introduction of "biology's new dimension" in the early 2000s [395], 3D models have held great promises and excited a generation of scientists, including myself. In the words of Mina Bissell, "scientists started to realize just how much a cell's context matters". Over two decades later, a variety of 3D cell culture platforms, biomaterials and analysis techniques have been and continue being developed to this end, however, the majority of *in vitro* research is still carried out in 2D. The variety and complementarity of applications of 3D cell culture options – from spheroids to organoids, natural gels, (semi)synthetic hydrogels, self-assembling materials and polymers – may be both an advantage for their versatility, but equally slow the transition from 2D to a standardised 3D cell culture approach. So far, the optimal method, depends on the question and hypothesis to be tested. In the future, it may be possible to screen an individual's cells against chemo and radio-therapeutics using quick, standardised culture models for personalised treatment regimens. Additionally, with the advent of more complex culture systems came the realisation that we needed to understand more about the biology and biophysics regulating cancer, before we could accurately model them in 3D. For this reason, studies that aim to "deconstruct" aspects of the tumour microenvironment in order to "recapitulate" them in 3D models [120], are necessary and poised to become the norm of the field. For this, interdisciplinary collaborations between tumour biologists, material scientists and tissue engineers will be vital for the successful implementation of such tools.

Chapter 8 - Bibliography

1. Siegel RL, Miller KD, Jemal A. Cancer statistics, 2019. CA: A Cancer Journal for Clinicians. 2019;69(1):7-34.
2. Lekka K, Tzitzi E, Giakoustidis A, Papadopoulos V, Giakoustidis D. Contemporary management of borderline resectable pancreatic ductal adenocarcinoma. Annals of Hepato-Biliary-Pancreatic Surgery. 2019;23(2):97-108.
3. Stark AP, Sacks GD, Rochefort MM, et al. Long-term survival in patients with pancreatic ductal adenocarcinoma. Surgery. 2016;159(6):1520-1527.
4. Rahib L, Smith BD, Aizenberg R, Rosenzweig AB, Fleshman JM, Matrisian LM. Projecting cancer incidence and deaths to 2030: the unexpected burden of thyroid, liver, and pancreas cancers in the United States. Cancer Research. 2014;74(11):2913-2921.
5. Haeberle L, Esposito I. Pathology of pancreatic cancer. Translational Gastroenterology and Hepatology. 2019;4:50.
6. Turati F, Edefonti V, Bosetti C, et al. Family History of Cancer and the Risk of Cancer: A Network of Case-Control Studies. Annals of oncology. 2013;24(10):6.
7. Becker AE, Hernandez YG, Frucht H, Lucas AL. Pancreatic ductal adenocarcinoma: Risk factors, screening, and early detection. World Journal of Gastroenterology. 2014;20(32):11182-11198.
8. Basturk O, Hong SM, Wood LD, et al. A Revised Classification System and Recommendations From the Baltimore Consensus Meeting for Neoplastic Precursor Lesions in the Pancreas. Am J Surg Pathol. 2015;39(12):1730-1741.
9. Andea A, Sarkar F, Adsay VN. Clinicopathological correlates of pancreatic intraepithelial neoplasia: a comparative analysis of 82 cases with and 152 cases without pancreatic ductal adenocarcinoma. Modern Pathology. 2003;16(10):996-1006.
10. Bilimoria KY, Bentrem DJ, Ko CY, Stewart AK, Winchester DP, Talamonti MS. National Failure to Operate on Early Stage Pancreatic Cancer. Annals of Surgery. 2007 Aug; 246(2): 173–180.
11. Matsuda Y, Furukawa T, Yachida S, et al. The Prevalence and Clinicopathological Characteristics of High-Grade Pancreatic Intraepithelial Neoplasia: Autopsy Study Evaluating the Entire Pancreatic Parenchyma. Pancreas. 2017;46(5):658-664.
12. Kleeff J, Korc M, Apte M, et al. Pancreatic cancer. Nature Reviews. 2016;2:16022.
13. Hingorani SR, Petricoin EF, Maitra A, et al. Preinvasive and invasive ductal pancreatic cancer and its early detection in the mouse. Cancer Cell. 2003;4(6):437-450.
14. Feldmann G, Beaty R, Hruban RH, Maitra A. Molecular genetics of pancreatic intraepithelial neoplasia. Journal of Hepatobiliary Pancreatic Surgery. 2007;14(3):224-232.
15. Preis M, Korc M. Signaling pathways in pancreatic cancer. Critical reviews in Eukaryotic gene Expression. 2011;21(2):115-129.
16. Sano M, Driscoll DR, DeJesus-Monge WE, et al. Activation of WNT/beta-Catenin Signaling Enhances Pancreatic Cancer Development and the Malignant Potential Via Up-regulation of Cyr61. Neoplasia. 2016;18(12):785-794.
17. Laklai H, Miroshnikova YA, Pickup MW, et al. Genotype tunes pancreatic ductal adenocarcinoma tissue tension to induce matricellular-fibrosis and tumor progression. Nature Medicine. 2016;22(5):497-505.
18. Ligorio M, Sil S, Malagon-Lopez J, et al. Stromal Microenvironment Shapes the Intratumoral Architecture of Pancreatic Cancer. Cell. 2019;178(1):160-175.e127.
19. Gore AJ, Deitz SL, Palam LR, Craven KE, Korc M. Pancreatic cancer–associated retinoblastoma 1 dysfunction enables TGF-β to promote proliferation. Journal of Clinical Investigation. 2014;124(1):338-352.

20. Collisson EA, Sadanandam A, Olson P, et al. Subtypes of Pancreatic Ductal Adenocarcinoma and Their Differing Responses to Therapy. Nature Medicine. 2011;17(4):500-503.

21. Bailey P, Chang DK, Nones K, et al. Genomic analyses identify molecular subtypes of pancreatic cancer. Nature. 2016;531(7592):47-52.

22. Waddell N, Pajic M, Patch AM, et al. Whole genomes redefine the mutational landscape of pancreatic cancer. Nature. 2015;518(7540):495-501.

23. Moffitt RA, Marayati R, Flate EL, et al. Virtual microdissection identifies distinct tumor- and stroma-specific subtypes of pancreatic ductal adenocarcinoma. Nature Genetics. 2015;47(10):1168-1178.

24. Khalaf N, Yuan C, Hamada T, et al. Regular Use of Aspirin or Non-Aspirin Nonsteroidal Anti-Inflammatory Drugs Is Not Associated With Risk of Incident Pancreatic Cancer in Two Large Cohort Studies. Gastroenterology. 2018;154(5):1380-1390 e1385.

25. Garrido-Laguna I, Hidalgo M. Pancreatic cancer: from state-of-the-art treatments to promising novel therapies. Nature Reviews Clinical Oncology. 2015;12(6):319-334.

26. Neoptolemos JP, Kleeff J, Michl P, Costello E, Greenhalf W, Palmer DH. Therapeutic developments in pancreatic cancer: current and future perspectives. Nature Reviews in Gastroenterology and Hepatology. 2018;15(6):333-348.

27. Burris HA, Moore MJ, Andersen J, et al. Improvements in survival and clinical benefit with gemcitabine as first-line therapy for patients with advanced pancreas cancer: a randomized trial. Journal of Clinical Oncology. 1997;15(6):2403-2413.

28. Von Hoff DD, Ervin T, Arena FP, et al. Increased Survival in Pancreatic Cancer with nab-Paclitaxel plus gemcitabine. New England Journal of Medicine. 2013;369(18):1691-1703.

29. Conroy T, Desseigne F, Ychou M, et al. FOLFIRINOX versus gemcitabine for Metastatic Pancreatic Cancer. New England Journal of Medicine. 2011;364(19):1817-1825.

30. Kim S, Signorovitch JE, Yang H, et al. Comparative Effectiveness of nab-Paclitaxel Plus gemcitabine vs FOLFIRINOX in Metastatic Pancreatic Cancer: A Retrospective Nationwide Chart Review in the United States. Advances in Therapy. 2018;35(10):1564-1577.

31. Tahara J, Shimizu K, Otsuka N, Akao J, Takayama Y, Tokushige K. gemcitabine plus nab-paclitaxel vs. FOLFIRINOX for patients with advanced pancreatic cancer. Cancer Chemotherapy and Pharmacology. 2018;82(2):245-250.

32. Neoptolemos JP, Palmer DH, Ghaneh P, et al. Comparison of adjuvant gemcitabine and capecitabine with gemcitabine monotherapy in patients with resected pancreatic cancer (ESPAC-4): a multicentre, open-label, randomised, phase 3 trial. Lancet. 2017;389(10073):1011-1024.

33. Conroy T, Hammel P, Hebbar M, et al. FOLFIRINOX or gemcitabine as Adjuvant Therapy for Pancreatic Cancer. New England Journal of Medicine. 2018;379(25):2395-2406.

34. Kindler HL, Niedzwiecki D, Hollis D, et al. gemcitabine Plus Bevacizumab Compared With gemcitabine Plus Placebo in Patients With Advanced Pancreatic Cancer: Phase III Trial of the Cancer and Leukemia Group B (CALGB 80303). Journal of Clinical Oncology. Vol 282010.

35. Kindler HL, Ioka T, Richel DJ, et al. Axitinib plus gemcitabine versus placebo plus gemcitabine in patients with advanced pancreatic adenocarcinoma: a double-blind randomised phase 3 study. Lancet Oncology. 2011;12(3):256-262.

36. Rougier P, Riess H, Manges R, et al. Randomised, placebo-controlled, double-blind, parallel-group phase III study evaluating aflibercept in patients receiving first-line treatment with gemcitabine for metastatic pancreatic cancer. European Journal of Cancer. 2013;49(12):2633-2642.

37. Kindler HL, Wroblewski K, Wallace JA, et al. gemcitabine plus sorafenib in patients with advanced pancreatic cancer: a phase II trial of the University of Chicago Phase II Consortium. Investigational New Drugs. 2012;30(1):382-386.

38. O'Neil BH, Scott AJ, Ma WW, et al. A phase II/III randomized study to compare the efficacy and safety of rigosertib plus gemcitabine versus gemcitabine alone in patients with previously untreated metastatic pancreatic cancer. Annals of Oncology. 2015;26(9):1923-1929.

39. Deplanque G, Demarchi M, Hebbar M, et al. A randomized, placebo-controlled phase III trial of masitinib plus gemcitabine in the treatment of advanced pancreatic cancer. Annals of Oncology. 2015;26(6):1194-1200.

40. Fuchs CS, Azevedo S, Okusaka T, et al. A phase 3 randomized, double-blind, placebo-controlled trial of ganitumab or placebo in combination with gemcitabine as first-line therapy for metastatic adenocarcinoma of the pancreas: the GAMMA trial. Annals of Oncology. 2015;26(5):921-927.

41. Moore MJ, Goldstein D, Hamm J, et al. Erlotinib plus gemcitabine compared with gemcitabine alone in patients with advanced pancreatic cancer: a phase III trial of the National Cancer Institute of Canada Clinical Trials Group. Journal of Clinical Oncology. 2007;25(15):1960-1966.

42. Hurwitz HI, Uppal N, Wagner SA, et al. Randomized, Double-Blind, Phase II Study of Ruxolitinib or Placebo in Combination With Capecitabine in Patients With Metastatic Pancreatic Cancer for Whom Therapy With gemcitabine Has Failed. Journal of Clinical Oncology. 2015;33(34):4039-4047.

43. Hidalgo M, Plaza C, Musteanu M, et al. SPARC Expression Did Not Predict Efficacy of nab-Paclitaxel plus gemcitabine or gemcitabine Alone for Metastatic Pancreatic Cancer in an Exploratory Analysis of the Phase III MPACT Trial. Clinical Cancer Research. 2015;21(21):4811-4818.

44. Jacobetz MA, Chan DS, Neesse A, et al. Hyaluronan impairs vascular function and drug delivery in a mouse model of pancreatic cancer. Gut. 2013;62(1):112-120.

45. Provenzano PP, Cuevas C, Chang AE, Goel VK, Von Hoff DD, Hingorani SR. Enzymatic targeting of the stroma ablates physical barriers to treatment of pancreatic ductal adenocarcinoma. Cancer Cell. 2012;21(3):418-429.

46. Hingorani SR, Zheng L, Bullock AJ, et al. HALO 202: Randomized Phase II Study of PEGPH20 Plus Nab-Paclitaxel/gemcitabine Versus Nab-Paclitaxel/gemcitabine in Patients With Untreated, Metastatic Pancreatic Ductal Adenocarcinoma. Journal of Clinical Oncology. 2018;36(4):359-366.

47. Hakim N, Patel R, Devoe C, Saif MW. Why HALO 301 Failed and Implications for Treatment of Pancreatic Cancer. Pancreas. 2019;3(1):e1-4.

48. Özdemir BC, Pentcheva-Hoang T, Carstens JL, et al. Depletion of Carcinoma-Associated Fibroblasts and Fibrosis Induces Immunosuppression and Accelerates Pancreas Cancer with Diminished Survival. Cancer Cell. 2014;25(6):719-734.

49. Rhim AD, Oberstein PE, Thomas DH, et al. Stromal elements act to restrain, rather than support, pancreatic ductal adenocarcinoma. Cancer Cell. 2014;25(6):735-747.

50. Hanahan D, Weinberg RA. Hallmarks of cancer: the next generation. Cell. 2011;144(5):646-674.

51. Candido JB, Morton JP, Bailey P, et al. CSF1R(+) Macrophages Sustain Pancreatic Tumor Growth through T Cell Suppression and Maintenance of Key Gene Programs that Define the Squamous Subtype. Cell Reports. 2018;23(5):1448-1460.

52. Rainiero HR, Emmerich PB, Sievers CK, et al. Versican production is driven by both epithelial and stromal cells in pancreatic cancer [abstract 1904]. Proceedings of the American Association for Cancer Research Annual Meeting 2019. 2019;79(13 Supplement).

53. Farren MR, Mace TA, Geyer S, et al. Systemic immune activity predicts overall survival in treatment naïve patients with metastatic pancreatic cancer. Clinical Cancer Reseaarch. 2016;22(10):2565-2574.

54. Kamath SD, Kalyan A, Kircher S, et al. Ipilimumab and gemcitabine for Advanced Pancreatic Cancer: A Phase Ib Study. Oncologist. Vol 252020.

55. Hilmi M, Bartholin L, Neuzillet C. Immune therapies in pancreatic ductal adenocarcinoma: Where are we now? World Journal of Gastroenterology. 2018;24(20):2137-2151.

56. Palmer DH, Valle JW, Ting Ma Y, et al. TG01/GM-CSF and adjuvant gemcitabine in patients with resected RAS-mutant adenocarcinoma of the pancreas (CT TG01-01): a single-arm, phase 1/2 trial. British Journal of Cancer. 2020;122(7):971-977.

57. Hanahan D, Coussens LM. Accessories to the crime: functions of cells recruited to the tumor microenvironment. Cancer Cell. 2012;21(3):309-322.

58. Erkan M, Hausmann S, Michalski CW, et al. The role of stroma in pancreatic cancer: diagnostic and therapeutic implications. Nature Reviews in Gastroenterology and Hepatology. 2012;9(8):454-467.

59. Neesse A, Algul H, Tuveson DA, Gress TM. Stromal biology and therapy in pancreatic cancer: a changing paradigm. Gut. 2015;64(9):1476-1484.

60. Djurec M, Grana O, Lee A, et al. Saa3 is a key mediator of the protumorigenic properties of cancer-associated fibroblasts in pancreatic tumors. Proceedings of the National Academy of Sciences of the USA. 2018;115(6):E1147-e1156.

61. Kohler I, Bronsert P, Timme S, et al. Detailed analysis of epithelial-mesenchymal transition and tumor budding identifies predictors of long-term survival in pancreatic ductal adenocarcinoma. Journal of Gastroenterology and Hepatology. 2015;30 Suppl 1:78-84.

62. Galván JA, Zlobec I, Wartenberg M, et al. Expression of E-cadherin repressors SNAIL, ZEB1 and ZEB2 by tumour and stromal cells influences tumour-budding phenotype and suggests heterogeneity of stromal cells in pancreatic cancer. British Journal of Cancer. 2015;112(12):1944-1950.

63. Ram Makena M, Gatla H, Verlekar D, Sukhavasi S, M KP, K CP. Wnt/β-Catenin Signaling: The Culprit in Pancreatic Carcinogenesis and Therapeutic Resistance. International Journal of Molecular Sciences. 2019;20(17).

64. Wei L, Ye H, Li G, et al. Cancer-associated fibroblasts promote progression and gemcitabine resistance via the SDF-1/SATB-1 pathway in pancreatic cancer. Cell Death and Disease. 2018;9(11):1065.

65. Scarlett CJ, Colvin EK, Pinese M, et al. Recruitment and Activation of Pancreatic Stellate Cells from the Bone Marrow in Pancreatic Cancer: A Model of Tumor-Host Interaction. PLoS One. 2011;6(10).

66. von Ahrens D, Bhagat TD, Nagrath D, Maitra A, Verma A. The role of stromal cancer-associated fibroblasts in pancreatic cancer. Journal of Hematology and Oncology. 2017;10.

67. Karagiannis GS, Poutahidis T, Erdman SE, Kirsch R, Riddell RH, Diamandis EP. Cancer-Associated Fibroblasts Drive the Progression of Metastasis through both Paracrine and Mechanical Pressure on Cancer Tissue. Molecular Cancer Research. 2012;10(11):1403-1418.

68. Lonardo E, Frias-Aldeguer J, Hermann PC, Heeschen C. Pancreatic stellate cells form a niche for cancer stem cells and promote their self-renewal and invasiveness. Cell Cycle. 2012;11(7):1282-1290.

69. Neuzillet C, Tijeras-Raballand A, Ragulan C, et al. Inter- and intra-tumoural heterogeneity in cancer-associated fibroblasts of human pancreatic ductal adenocarcinoma. Journal of Pathology. 2019;248(1):51-65.

70. Puleo F, Nicolle R, Blum Y, et al. Stratification of Pancreatic Ductal Adenocarcinomas Based on Tumor and Microenvironment Features. Gastroenterology. 2018;155(6):1999-2013.e1993.

71. Clark CE, Hingorani SR, Mick R, Combs C, Tuveson DA, Vonderheide RH. Dynamics of the immune reaction to pancreatic cancer from inception to invasion. Cancer Research. 2007;67(19):9518-9527.

72. Knudsen ES, Vail P, Balaji U, et al. Stratification of Pancreatic Ductal Adenocarcinoma: Combinatorial Genetic, Stromal, and Immunological Markers. Clinical Cancer Reseaarch. 2017;23(15):4429-4440.

73. Noy R, Pollard JW. Tumor-associated macrophages: from mechanisms to therapy. Immunity. 2014;41(1):49-61.

74. Ino Y, Yamazaki-Itoh R, Shimada K, et al. Immune cell infiltration as an indicator of the immune microenvironment of pancreatic cancer. British Journal of Cancer. 2013;108(4):914-923.

75. Qian B, Pollard JW. Macrophage Diversity Enhances Tumor Progression and Metastasis. Cell. 2010;141(1):39-51.

76. Mantovani A, Marchesi F, Malesci A, Laghi L, Allavena P. Tumor-Associated Macrophages as Treatment Targets in Oncology. Nature Reviews Clinical Oncology. 2017;14(7):399-416.

77. Carstens JL, Correa de Sampaio P, Yang D, et al. Spatial computation of intratumoral T cells correlates with survival of patients with pancreatic cancer. Nature Communications. 2017; 8:15095.

78. Ryschich E, Nötzel T, Hinz U, et al. Control of T-cell-mediated immune response by HLA class I in human pancreatic carcinoma. Clinical Cancer Research. 2005;11(2 Pt 1):498-504.

79. Evans RA, Diamond MS, Rech AJ, et al. Lack of immunoediting in murine pancreatic cancer reversed with neoantigen. Journal for clinical Investigation. 2016;1(14).

80. Hiraoka N, Onozato K, Kosuge T, Hirohashi S. Prevalence of FOXP3+ regulatory T cells increases during the progression of pancreatic ductal adenocarcinoma and its premalignant lesions. Clinical Cancer Research. 2006;12(18):5423-5434.

81. Pickup MW, Mouw JK, Weaver VM. The extracellular matrix modulates the hallmarks of cancer. EMBO Reports. 2014;15(12):1243-1253.

82. Apte MV, Park S, Phillips PA, et al. Desmoplastic reaction in pancreatic cancer: role of pancreatic stellate cells. Pancreas. 2004;29(3):179-187.

83. Kleeff J, Beckhove P, Esposito I, et al. Pancreatic cancer microenvironment. International Journal of Cancer. 2007;121(4):699-705.

84. Afik R, Zigmond E, Vugman M, et al. Tumor macrophages are pivotal constructors of tumor collagenous matrix. Journal of Experimental Medicine. 2016;213(11):2315-2331.

85. Weniger M, Honselmann KC, Liss AS. The Extracellular Matrix and Pancreatic Cancer: A Complex Relationship. Cancers (Basel). 2018;10(9).

86. Tian C, Ohlund D, Rickelt S, et al. Cancer Cell-Derived Matrisome Proteins Promote Metastasis in Pancreatic Ductal Adenocarcinoma. Cancer Research. 2020;80(7):1461-1474.

87. Tian C, Clauser KR, Ohlund D, et al. Proteomic analyses of ECM during pancreatic ductal adenocarcinoma progression reveal different contributions by tumor and stromal cells. Proceedings of the National Academy of Sciences of the USA. 2019;116(39):19609-19618.

88. Naba A, Clauser KR, Whittaker CA, Carr SA, Tanabe KK, Hynes RO. Extracellular matrix signatures of human primary metastatic colon cancers and their metastases to liver. BMC Cancer. 2014;14(1):518.

89. Ojalill M, Rappu P, Siljamäki E, Taimen P, Boström P, Heino J. The composition of prostate core matrisome in vivo and in vitro unveiled by mass spectrometric analysis. Prostate. 2018;78(8):583-594.

90. Naba A, Pearce OMT, Del Rosario A, et al. Characterization of the Extracellular Matrix of Normal and Diseased Tissues Using Proteomics. Journal of Proteome Research. 2017;16(8):3083-3091.

91. Naba A, Clauser KR, Ding H, Whittaker CA, Carr SA, Hynes RO. The extracellular matrix: Tools and insights for the "omics" era. Matrix Biology. 2016;49:10-24.

92. Ricard-Blum S. The collagen family. Cold Spring Harbor Perspectives in Biology. 2011;3(1):4978.

93. Imamura T, Iguchi H, Manabe T, et al. Quantitative analysis of collagen and collagen subtypes I, III, and V in human pancreatic cancer, tumor-associated chronic pancreatitis, and alcoholic chronic pancreatitis. Pancreas. 1995;11(4):357-364.

94. Olivares O, Mayers JR, Gouirand V, et al. Collagen-derived proline promotes pancreatic ductal adenocarcinoma cell survival under nutrient limited conditions. Nature Communications. 2017;(8):1603.

95. Whatcott CJ, Diep CH, Jiang P, et al. Desmoplasia in Primary Tumors and Metastatic Lesions of Pancreatic Cancer. Clinical Cancer Reseaarch. 2015;21(15):3561-3568.

96. Clementz AG, Mutolo MJ, Leir SH, et al. Collagen XV Inhibits Epithelial to Mesenchymal Transition in Pancreatic Adenocarcinoma Cells. PLoS One. 2013;8(8):e72250.

97. van der Zee JA, van Eijck CH, Hop WC, et al. Tumour basement membrane laminin expression predicts outcome following curative resection of pancreatic head cancer. British Journal of Cancer. 2012;107(7):1153-1158.

98. Öhlund D, Franklin O, Lundberg E, Lundin C, Sund M. Type IV collagen stimulates pancreatic cancer cell proliferation, migration, and inhibits apoptosis through an autocrine loop. BMC Cancer. 2013;13:154.

99. Tulla M, Pentikäinen OT, Viitasalo T, et al. Selective binding of collagen subtypes by integrin alpha 1I, alpha 2I, and alpha 10I domains. Journal of Biological Chemistry. 2001;276(51):48206-48212.

100. Berchtold S, Grünwald B, Krüger A, et al. Collagen type V promotes the malignant phenotype of pancreatic ductal adenocarcinoma. Cancer Letters. 2015;356(2 Pt B):721-732.

101. Grzesiak JJ, Tran Cao HS, Burton DW, et al. Knockdown of the β1 integrin subunit reduces primary tumor growth and inhibits pancreatic cancer metastasis. International Journal of Cancer. 2011;129(12):2905-2915.

102. Lu J, Zhou S, Siech M, Habisch H, Seufferlein T, Bachem MG. Pancreatic stellate cells promote hapto-migration of cancer cells through collagen I-mediated signalling pathway. British Journal of Cancer. 2014;110(2):409-420.

103. Koenig A, Mueller C, Hasel C, Adler G, Menke A. Collagen type I induces disruption of E-cadherin-mediated cell-cell contacts and promotes proliferation of pancreatic carcinoma cells. Cancer Research. 2006;66(9):4662-4671.

104. Shintani Y, Fukumoto Y, Chaika N, Svoboda R, Wheelock MJ, Johnson KR. Collagen I–mediated up-regulation of N-cadherin requires cooperative signals from integrins and discoidin domain receptor 1. Journal of Cell Biology. 2008;180(6):1277-1289.

105. Yang J, Zhang Y, He S, et al. TM4SF1 Promotes Metastasis of Pancreatic Cancer via Regulating the Expression of DDR1. Scientific Reports. 2017;(7):45895.

106. Pan S, Brentnall TA, Chen R. Glycoproteins and glycoproteomics in pancreatic cancer. World Journal of Gastroenterology. 2016;22(42):9288-9299.

107. Remmers N, Anderson JM, Linde EM, et al. Aberrant expression of mucin core proteins and o-linked glycans associated with progression of pancreatic cancer. Clinical Cancer Reseaarch. 2013;19(8):1981-1993.

108. Pan S, Chen R, Tamura Y, et al. Quantitative Glycoproteomics Analysis Reveals Changes in N-Glycosylation Level Associated with Pancreatic Ductal Adenocarcinoma. Journal of Proteome Research. 2014;13(3):1293-1306.

109. Ingham KC, Brew SA, Isaacs BS. Interaction of fibronectin and its gelatin-binding domains with fluorescent-labeled chains of type I collagen. Journal of Biological Chemistry. 1988;263(April 5):4624-4462.

110. Miyamoto H, Murakami T, Tsuchida K, Sugino H, Miyake H, Tashiro S. Tumor-stroma interaction of human pancreatic cancer: acquired resistance to anticancer drugs and proliferation regulation is dependent on extracellular matrix proteins. Pancreas. 2004;28(1):38-44.

111. Dallas SL, Sivakumar P, Jones CJ, et al. Fibronectin regulates latent transforming growth factor-beta (TGF beta) by controlling matrix assembly of latent TGF beta-binding protein-1. Journal of Biological Chemistry. 2005;280(19):18871-18880.

112. Yao H, Zeng ZZ, Fay KS, et al. Role of α5β1 Integrin Up-regulation in Radiation-Induced Invasion by Human Pancreatic Cancer Cells1. Translational Oncology. 2011;4(5):282-292.

113. Lundahl J, Sköld CM, Halldén G, Hallgren M, Eklund A. Monocyte and neutrophil adhesion to matrix proteins is selectively enhanced in the presence of inflammatory mediators. Scandinavian Journal of Immunology. 1996;44(2):143-149.

114. Li X, Truty MA, Kang Y, et al. Extracellular lumican inhibits pancreatic cancer cell growth and is associated with prolonged survival after surgery. Clinical Cancer Reseaarch. 2014;20(24):6529-6540.

115. Durko L, Wlodarski W, Stasikowska-Kanicka O, et al. Expression and Clinical Significance of Cancer Stem Cell Markers CD24, CD44, and CD133 in Pancreatic Ductal Adenocarcinoma and Chronic Pancreatitis. Disease Markers. 2017;2017.

116. Aruffo A, Stamenkovic I, Melnick M, Underhill CB, Seed B. CD44 is the principal cell surface receptor for hyaluronate. Cell. 1990;61(7):1303-1313.

117. Hingorani SR, Harris WP, Hendifar AE, et al. High response rate and PFS with PEGPH20 added to nab-paclitaxel/gemcitabine in stage IV previously untreated pancreatic cancer patients with high-HA tumors: Interim results of a randomized phase II study. Journal of Clinical Oncology. 2015;33(15_suppl):4006-4006.

118. Wight TN. Provisional matrix: A role for versican and hyaluronan. Matrix Biology. 2017;60-61:38-56.

119. Wight TN, Kinsella MG, Evanko SP, Potter-Perigo S, Merrilees MJ. Versican and the regulation of cell phenotype in disease. Biochimica et Biophysica Acta. 2014;1840(8):2441-2451.

120. Pearce OMT, Delaine-Smith RM, Maniati E, et al. Deconstruction of a Metastatic Tumor Microenvironment Reveals a Common Matrix Response in Human Cancers. Cancer Discov. 2018;8(3):304-319.

121. Kaur S, Kumar S, Momi N, Sasson AR, Batra SK. Mucins in pancreatic cancer and its microenvironment. Nature Reviews in Gastroenterology and Hepatology. 2013;10(10):607-620.

122. Zhao X, Fan W, Xu Z, et al. Inhibiting tumor necrosis factor-alpha diminishes desmoplasia and inflammation to overcome chemoresistance in pancreatic ductal adenocarcinoma. Oncotarget. 2016;7(49):81110-81122.

123. Maniati E, Berlato C, Gopinathan G, et al. Mouse Ovarian Cancer Models Recapitulate the Human Tumor Microenvironment and Patient Response to Treatment. Cell Reports. 2020;30(2):525-540 e527.

124. Hu D, Ansari D, Zhou Q, Sasor A, Said Hilmersson K, Andersson R. Stromal fibronectin expression in patients with resected pancreatic ductal adenocarcinoma. World Journal of Surgical Oncology. 2019;17(1):29.

125. Tung JC, Barnes JM, Desai SR, et al. Tumor Mechanics and Metabolic Dysfunction. Free Radical Biology & Medicine. 2015;0:269-280.

126. Stylianopoulos T, Martin JD, Chauhan VP, et al. Causes, consequences, and remedies for growth-induced solid stress in murine and human tumors. Proceedings of the National Academy of Sciences of the USA. 2012;109(38):15101-15108.

127. Erkan M, Michalski CW, Rieder S, et al. The activated stroma index is a novel and independent prognostic marker in pancreatic ductal adenocarcinoma. Clin Gastroenterol Hepatol. 2008;6(10):1155-1161.

128. Rice AJ, Cortes E, Lachowski D, et al. Matrix stiffness induces epithelial–mesenchymal transition and promotes chemoresistance in pancreatic cancer cells. Oncogenesis. 2017;6(7):e352-.

129. Nguyen AV, Nyberg KD, Scott MB, et al. Stiffness of pancreatic cancer cells is associated with increased invasive potential. Integrative Biology. 2016;8(12):1232-1245.

130. Rubiano A, Delitto D, Han S, Hughes S, Simmons C. Viscoelastic properties of human pancreatic tumors and in vitro constructs to mimic mechanical properties | Elsevier Enhanced Reader. Acta Biomaterialia. 2018;67:331-340.

131. Haage A, Schneider IC. Cellular contractility and extracellular matrix stiffness regulate matrix metalloproteinase activity in pancreatic cancer cells. Faseb Journal. 2014;28(8):3589-3599.

132. Barker HE, Cox TR, Erler JT. The rationale for targeting the LOX family in cancer. Nature Reviews Cancer. 2012;12(8):540-552.

133. Miller BW, Morton JP, Pinese M, et al. Targeting the LOX/hypoxia axis reverses many of the features that make pancreatic cancer deadly: inhibition of LOX abrogates metastasis and enhances drug efficacy. EMBO Molecular Medicine. 2015;7(8):1063-1076.

134. Cortes E, Lachowski D, Robinson B, et al. Tamoxifen mechanically reprograms the tumor microenvironment via HIF-1A and reduces cancer cell survival. EMBO Reports. 2019;20(1).

135. Cortes E, Sarper M, Robinson B, et al. GPER is a mechanoregulator of pancreatic stellate cells and the tumor microenvironment. EMBO Reports. Vol 202019.

136. Lee J, Condello S, Yakubov B, et al. Tissue Transglutaminase Mediated Tumor-Stroma Interaction Promotes Pancreatic Cancer Progression. Clinical Cancer Reseaarch. 2015;21(19):4482-4493.

137. Piccolo S, Cordenonsi M, Dupont S. Molecular pathways: YAP and TAZ take center stage in organ growth and tumorigenesis. Clinical Cancer Reseaarch. 2013;19(18):4925-4930.

138. Moroishi T, Hansen CG, Guan KL. The emerging roles of YAP and TAZ in cancer. Nature Reviews Cancer. 2015;15(2):73-79.

139. Panciera T, Citron A, Di Biagio D, et al. Reprogramming normal cells into tumour precursors requires ECM stiffness and oncogene-mediated changes of cell mechanical properties. Nature Materials. 2020.

140. Dupont S, Morsut L, Aragona M, et al. Role of YAP/TAZ in mechanotransduction. Nature. 2011;474(7350):179-183.

141. Bonnans C, Chou J, Werb Z. Remodelling the extracellular matrix in development and disease. Nature Reviews in Molecular and Cell Biology. 2014;15(12):786-801.

142. Knapinska AM, Estrada CA, Fields GB. The Roles of Matrix Metalloproteinases in Pancreatic Cancer. Progress in Molecular Biology and Translational Sciences. 2017;148:339-354.

143. Crawford HC, Scoggins CR, Washington MK, Matrisian LM, Leach SD. Matrix metalloproteinase-7 is expressed by pancreatic cancer precursors and regulates acinar-to-ductal metaplasia in exocrine pancreas. Journal of Clinical Investigation. 109(11):1437-44.

144. Dangi-Garimella S, Krantz SB, Barron MR, et al. Three-dimensional collagen I promotes gemcitabine resistance in pancreatic cancer through MT1-MMP-mediated expression of HMGA2. Cancer Res. 2011;71(3):1019-1028.

145. Nguyen HL, Kadam P, Helkin A, et al. MT1-MMP Activation of TGF-β Signaling Enables Intercellular Activation of an Epithelial-mesenchymal Transition Program in Cancer. Current Cancer Drug Targets. 2016;16(7):618-630.

146. D'Costa Z, Jones K, Azad A, et al. gemcitabine-Induced TIMP1 Attenuates Therapy Response and Promotes Tumor Growth and Liver Metastasis in Pancreatic Cancer. Cancer Research. 2017;77(21):5952-5962.

147. Lachowski D, Cortes E, Rice A, Pinato D, Rombouts K, del Rio Hernandez A. Matrix stiffness modulates the activity of MMP-9 and TIMP-1 in hepatic stellate cells to perpetuate fibrosis. Science Reports. 2019;(9)7299.

148. Guan Y, Wu Y, Liu Y, Ni J, Nong S. Association of microRNA-21 expression with clinicopathological characteristics and the risk of progression in advanced prostate cancer patients receiving androgen deprivation therapy. Prostate. 2016;76(11):986-993.

149. Rath N, Olson MF. Rho-associated kinases in tumorigenesis: re-considering ROCK inhibition for cancer therapy. EMBO Reports. 2012;13(10):900-908.

150. Rath N, Morton JP, Julian L, et al. ROCK signaling promotes collagen remodeling to facilitate invasive pancreatic ductal adenocarcinoma tumor cell growth. EMBO Molecular Medicine. 2017;9(2):198-218.

151. Samuel MS, Lopez JI, McGhee EJ, et al. Actomyosin-mediated cellular tension drives increased tissue stiffness and β-catenin activation to induce interfollicular epidermal hyperplasia and tumor growth. Cancer Cell. 2011;19(6):776-791.

152. Awaji M, Singh RK. Cancer-Associated Fibroblasts' Functional Heterogeneity in Pancreatic Ductal Adenocarcinoma. Cancers (Basel). 2019;11(3).

153. Shimoda M, Principe S, Jackson HW, et al. Loss of the Timp gene family is sufficient for the acquisition of the CAF-like cell state. Nature Cell Biology. 2014;16(9):889-901.

154. Whatcott CJ, Ng S, Barrett MT, Hostetter G, Von Hoff DD, Han H. Inhibition of ROCK1 kinase modulates both tumor cells and stromal fibroblasts in pancreatic cancer. PLoS One. 2017;12(8):e0183871).

155. Vennin C, Chin VT, Warren S, et al. Transient tissue priming via ROCK inhibition uncouples pancreatic cancer progression, sensitivity to chemotherapy, and metastasis. Science Translational Medicine. 2017;9(384:e8504.

156. Calvo F, Ege N, Grande-Garcia A, et al. Mechano-transduction and YAP-dependent matrix remodelling is required for the generation and maintenance of cancer associated fibroblasts. Nature Cell Biology. 2013;15(6):2756.

157. Avery D, Govindaraju P, Jacob M, Todd L, Monslow J, Puré E. Extracellular Matrix Directs Phenotypic Heterogeneity of Activated Fibroblasts. Matrix Biology. 2018;67:90-106.

158. Sarper M, Cortes E, Lieberthal TJ, del Río Hernández A. ATRA modulates mechanical activation of TGF-β by pancreatic stellate cells. Scientific Reports. 2016;(6):27639.

159. Carapuça EF, gemenetzidis E, Feig C, et al. Anti-stromal treatment together with chemotherapy targets multiple signalling pathways in pancreatic adenocarcinoma. Journal of Pathology. 2016;239(3):286-296.

160. North B, Kocher HM, Sasieni P. A new pragmatic design for dose escalation in phase 1 clinical trials using an adaptive continual reassessment method. BMC Cancer. 2019;19:632.

161. Bramhall SR, Schulz J, Nemunaitis J, Brown PD, Baillet M, Buckels JAC. A double-blind placebo-controlled, randomised study comparing gemcitabine and marimastat

with gemcitabine and placebo as first line therapy in patients with advanced pancreatic cancer. British Journal of Cancer. 2002;87(2):161-167.

162. Moore MJ, Hamm J, Dancey J, et al. Comparison of gemcitabine versus the matrix metalloproteinase inhibitor BAY 12-9566 in patients with advanced or metastatic adenocarcinoma of the pancreas: a phase III trial of the National Cancer Institute of Canada Clinical Trials Group. Journal of Clinical Oncology. 2003;21(17):3296-3302.

163. Slapak EJ, Duitman J, Tekin C, Bijlsma MF, Spek CA. Matrix Metalloproteases in Pancreatic Ductal Adenocarcinoma: Key Drivers of Disease Progression? Biology (Basel). 2020;9(4).

164. Grünwald B, Vandooren J, Gerg M, et al. Systemic Ablation of MMP-9 Triggers Invasive Growth and Metastasis of Pancreatic Cancer via Deregulation of IL6 Expression in the Bone Marrow. Molecular Cancer Research. 2016;14(11):1147-1158.

165. Fukushima M, Nakamuta M, Kohjima M, et al. fasudil hydrochloride hydrate, a Rho-kinase (ROCK) inhibitor, suppresses collagen production and enhances collagenase activity in hepatic stellate cells. Liver International. 2005;25(4):829-838.

166. Rückert F, Pilarsky C, Grützmann R. Establishment of Primary Cell Lines in Pancreatic Cancer. Pancreatic Cancer-Molecular Mechanism and Targets. 2012:259-275.

167. Carrel A. On the permanent life of tissues outside of the organism. Journal of Experimental Medicine. 1912;15(5):516-528.

168. Caliari SR, Burdick JA. A Practical Guide to Hydrogels for Cell Culture. Nature Methods. 2016;13(5):405-414.

169. Krempley BD, Yu KH. Preclinical models of pancreatic ductal adenocarcinoma. Chinese Clinical Oncology. 2017;6(3):25.

170. Voskoglou-Nomikos T, Pater JL, Seymour L. Clinical predictive value of the in vitro cell line, human xenograft, and mouse allograft preclinical cancer models. Clinical Cancer Research. 2003;9(11):4227-4239.

171. Johnson JI, Decker S, Zaharevitz D, et al. Relationships between drug activity in NCI preclinical in vitro and in vivo models and early clinical trials. British Journal of Cancer. 2001;84(10):1424-1431.

172. Frese KK, Tuveson DA. Maximizing mouse cancer models. Nature Reviews Cancer. 2007;7(9):645-658.

173. Bruns CJ, Harbison MT, Davis DW, et al. Epidermal growth factor receptor blockade with C225 plus gemcitabine results in regression of human pancreatic carcinoma growing orthotopically in nude mice by antiangiogenic mechanisms. Clinical Cancer Research. 2000;6(5):1936-1948.

174. Philip PA, Benedetti J, Corless CL, et al. Phase III Study Comparing gemcitabine Plus Cetuximab Versus gemcitabine in Patients With Advanced Pancreatic Adenocarcinoma: Southwest Oncology Group–Directed Intergroup Trial S0205. Journal of Clinical Oncology. 2010;28(22):3605-3610.

175. Thomas JP, Arzoomanian RZ, Alberti D, et al. Phase I pharmacokinetic and pharmacodynamic study of recombinant human endostatin in patients with advanced solid tumors. Journal Clinical Oncology. 2003;21(2):223-231.

176. Kulke MH, Demetri GD, Sharpless NE, et al. A phase II study of troglitazone, an activator of the PPARgamma receptor, in patients with chemotherapy-resistant metastatic colorectal cancer. Cancer Journal. 2002;8(5):395-399.

177. Fu X, Guadagni F, Hoffman RM. A metastatic nude-mouse model of human pancreatic cancer constructed orthotopically with histologically intact patient specimens. Proceedings of the National Academy of Sciences of the USA. 1992;89(12):5645-5649.

178. Rubio-Viqueira B, Hidalgo M. Direct in vivo xenograft tumor model for predicting chemotherapeutic drug response in cancer patients. Clinical Pharmacology and Therapeutics. 2009;85(2):217-221.

179. Duconseil P, Gilabert M, Gayet O, et al. Transcriptomic analysis predicts survival and sensitivity to anticancer drugs of patients with a pancreatic adenocarcinoma. American Journal of Pathology. 2015;185(4):1022-1032.

180. Kim MP, Evans DB, Wang H, Abbrusseze JL, Fleming JB, Gallick GE. Orthotopic and heterotopic generation of murine pancreatic cancer xenografts. Nature Protocols. 2009;4(11):1670-1680.

181. He J, Ahuja N, Makary MA, et al. 2564 resected periampullary adenocarcinomas at a single institution: trends over three decades. HPB (Oxford). 2014;16(1):83-90.

182. Aguirre AJ, Bardeesy N, Sinha M, et al. Activated Kras and Ink4a/Arf deficiency cooperate to produce metastatic pancreatic ductal adenocarcinoma. Genes and Development. 2003;17(24):3112-3126.

183. Hingorani SR, Wang L, Multani AS, et al. Trp53R172H and KrasG12D cooperate to promote chromosomal instability and widely metastatic pancreatic ductal adenocarcinoma in mice. Cancer Cell. 2005;7(5):469-483.

184. Gilabert M, Calvo E, Airoldi A, et al. Pancreatic cancer-induced cachexia is Jak2-dependent in mice. Journal of Cell Physiology. 2014;229(10):1437-1443.

185. Olive KP, Jacobetz MA, Davidson CJ, et al. Inhibition of Hedgehog Signaling Enhances Delivery of Chemotherapy in a Mouse Model of Pancreatic Cancer. Science. 2009;324(5933):1457-1461.

186. Sharpless NE, DePinho RA. The mighty mouse: genetically engineered mouse models in cancer drug development. Nature Reviews Drug Discovery. 2006;5(9):741-754.

187. Barros AS, Costa EC, Nunes AS, de Melo-Diogo D, Correia IJ. Comparative study of the therapeutic effect of Doxorubicin and Resveratrol combination on 2D and 3D (spheroids) cell culture models. International Journal of Pharmacology. 2018;551(1-2):76-83.

188. Chen CS. 3D biomimetic cultures – the next platform for cell biology. Trends in Cell Biology. 2016;26(11):798-800.

189. Yamada KM, Cukierman E. Modeling tissue morphogenesis and cancer in 3D. Cell. 2007;130(4):601-610.

190. Golan T, Atias D, Barshack I, Avivi C, Goldstein RS, Berger R. Ascites-derived pancreatic ductal adenocarcinoma primary cell cultures as a platform for personalised medicine. British Journal of Cancer. 2014;110(9):2269-2276.

191. Mitchell MJ, Jain RK, Langer R. Engineering and physical sciences in oncology: challenges and opportunities. Nature Reviews Cancer. 2017;17(11):659-675.

192. Drifka CR, Eliceiri KW, Weber SM, Kao WJ. A bioengineered heterotypic stroma-cancer microenvironment model to study pancreatic ductal adenocarcinoma. Lab Chip. 2013;13(19):3965-3975.

193. Ware MJ, Keshishian V, Law JJ, et al. Generation of an in vitro 3D PDAC stroma rich spheroid model. Biomaterials. 2016;108:129-142.

194. Gioeli D, Snow CJ, Simmers MB, et al. Development of a multicellular pancreatic tumor microenvironment system using patient-derived tumor cells. Lab Chip. 2019;19(7):1193-1204.

195. Tomás-Bort E, Kieler M, Sharma S, Candido JB, Loessner D. 3D approaches to model the tumor microenvironment of pancreatic cancer. Theranostics. 2020;10(11):5074-5089.

196. Harrison RG. Observations on the living developing nerve fiber. Proceedings of the society for experimental biology and medicine. 1906;4(1):140-143.

197. Longati P, Jia X, Eimer J, et al. 3D pancreatic carcinoma spheroids induce a matrix-rich, chemoresistant phenotype offering a better model for drug testing. BMC Cancer. 2013;13:95.

198. Solanki A, King D, Thibault G, Wang L, Gibbs SL. Quantification of fluorophore distribution and therapeutic response in matched in vivo and ex vivo pancreatic cancer model systems. PLoS One. 2020;15(2):e0229407.

199. Misra S, Moro CF, Del Chiaro M, et al. Ex vivo organotypic culture system of precision-cut slices of human pancreatic ductal adenocarcinoma. Scientific Reports. 2019;9(1):2133.

200. Bi H, Ye K, Jin S. Proteomic analysis of decellularized pancreatic matrix identifies collagen V as a critical regulator for islet organogenesis from human pluripotent stem cells. Biomaterials. 2020;233:119673.

201. Zeeberg K, Cardone RA, Greco MR, et al. Assessment of different 3D culture systems to study tumor phenotype and chemosensitivity in pancreatic ductal adenocarcinoma. International Journal of Oncology. 2016;49(1):243-252.

202. Öhlund D, Handly-Santana A, Biffi G, et al. Distinct populations of inflammatory fibroblasts and myofibroblasts in pancreatic cancer. Journal of Experimental Medicine. 2017;214(3):579-596.

203. Puls TJ, Tan X, Whittington CF, Voytik-Harbin SL. 3D collagen fibrillar microstructure guides pancreatic cancer cell phenotype and serves as a critical design parameter for phenotypic models of EMT. PLoS One. 2017;12(11):e0188870.

204. Shields MA, Dangi-Garimella S, Krantz SB, Bentrem DJ, Munshi HG. Pancreatic Cancer Cells Respond to Type I Collagen by Inducing Snail Expression to Promote Membrane Type 1 Matrix Metalloproteinase-dependent Collagen Invasion. Journal of Biological Chemistry. 2011;286(12):10495-10504.

205. Chopra A, Murray ME, Byfield F, et al. Augmentation of integrin-mediated mechanotransduction by hyaluronic acid. Biomaterials. 2014;35(1):71-82.

206. Sherman MH, Yu RT, Tseng TW, et al. Stromal cues regulate the pancreatic cancer epigenome and metabolome. Proceedings of the National Academy of Sciences. 2017;114(5):1129.

207. Broguiere N, Isenmann L, Hirt C, et al. Growth of Epithelial Organoids in a Defined Hydrogel. Advanced Materials. 2018;30(43):1801621.

208. Guvendiren M, Burdick JA. Stiffening hydrogels to probe short- and long-term cellular responses to dynamic mechanics. Nature Communications. 2012;3(1):792.

209. Liu HY, Korc M, Lin CC. Biomimetic and enzyme-responsive dynamic hydrogels for studying cell-matrix interactions in pancreatic ductal adenocarcinoma. Biomaterials. 2018;160:24-36.

210. Ki CS, Shih H, Lin CC. Effect of 3D matrix compositions on the efficacy of EGFR inhibition in pancreatic ductal adenocarcinoma cells. Biomacromolecules. 2013;14(9):3017-3026.

211. Ki CS, Lin TY, Korc M, Lin CC. Thiol-ene hydrogels as desmoplasia-mimetic matrices for modeling pancreatic cancer cell growth, invasion, and drug resistance. Biomaterials. 2014;35(36):9668-9677.

212. Raza A, Ki CS, Lin CC. The influence of matrix properties on growth and morphogenesis of human pancreatic ductal epithelial cells in 3D. Biomaterials. 2013;34(21):5117-5127.

213. Scaife CL, Shea JE, Dai Q, Firpo MA, Prestwich GD, Mulvihill SJ. Synthetic Extracellular Matrix Enhances Tumor Growth and Metastasis in an Orthotopic Mouse Model of Pancreatic Adenocarcinoma. Journal of Gastrointestinal Surgery. 2008;12(6):1074-1080.

214. Allison Logan S, Brissenden AJ, Szewczuk MR, Neufeld RJ. Combinatorial and sequential delivery of gemcitabine and oseltamivir phosphate from implantable

poly(d,l-lactic-co-glycolic acid) cylinders disables human pancreatic cancer cell survival. Drug Design Development and Therapy. 2017;11:2239-2250.

215. Smink AM, Hertsig DT, Schwab L, et al. A Retrievable, Efficacious Polymeric Scaffold for Subcutaneous Transplantation of Rat Pancreatic Islets. Annals of Surgery. 2017;266(1):149-157.

216. Marchioli G, Luca AD, de Koning E, et al. Hybrid Polycaprolactone/Alginate Scaffolds Functionalized with VEGF to Promote de Novo Vessel Formation for the Transplantation of Islets of Langerhans. Adv Healthc Mater. 2016;5(13):1606-1616.

217. Yeon SE, No DY, Lee SH, et al. Application of Concave Microwells to Pancreatic Tumor Spheroids Enabling Anticancer Drug Evaluation in a Clinically Relevant Drug Resistance Model. PLoS One. 2013; 8(9):e73345.

218. Clausell-Tormos J, Azevedo MM, Miranda-Lorenzo I, et al. Nano-volume well array chip for large-scale propagation and high-resolution analysis of individual cancer stem cells. Journal of Nanomedicine and Nanotechnology. 2014; 114(12): 1305–1312.

219. Beer M, Kuppalu N, Stefanini M, et al. A novel microfluidic 3D platform for culturing pancreatic ductal adenocarcinoma cells: comparison with in vitro cultures and in vivo xenografts. Scientific Reports. 2017;7:1325.

220. Lee JH, Kim SK, Khawar IA, Jeong SY, Chung S, Kuh HJ. Microfluidic co-culture of pancreatic tumor spheroids with stellate cells as a novel 3D model for investigation of stroma-mediated cell motility and drug resistance. Journal of Experimental & Clinical Cancer Research. 2018;34:4.

221. Nguyen DHT, Lee E, Alimperti S, et al. A biomimetic pancreatic cancer on-chip reveals endothelial ablation via ALK7 signaling. Science Advances. 2019; 5(8): e6789.

222. Drifka CR, Loeffler AG, Esquibel CR, Weber SM, Eliceiri KW, Kao WJ. Human pancreatic stellate cells modulate 3D collagen alignment to promote the migration of pancreatic ductal adenocarcinoma cells. Biomedical Microdevices. 2016;18(6):105.

223. Giobbe GG, Crowley C, Luni C, et al. Extracellular matrix hydrogel derived from decellularized tissues enables endodermal organoid culture. Nature Communications. 2019;10(1):5658.

224. Sackett SD, Tremmel DM, Ma F, et al. Extracellular matrix scaffold and hydrogel derived from decellularized and delipidized human pancreas. Scientific Reports. 2018;8(1):10452.

225. Gaetani R, Aude S, DeMaddalena LL, et al. Evaluation of Different Decellularization Protocols on the Generation of Pancreas-Derived Hydrogels. Tissue Engineering Part C. 2018;24(12):697-708.

226. Gjorevski N, Sachs N, Manfrin A, et al. Designer matrices for intestinal stem cell and organoid culture. Nature. 2016;539(7630):560-564.

227. Boj SF, Hwang CI, Baker LA, et al. Organoid Models of Human and Mouse Ductal Pancreatic Cancer. Cell. 2015;160(0):324-338.

228. Lin CC, Korc M. Designer hydrogels: Shedding light on the physical chemistry of the pancreatic cancer microenvironment. Cancer Letters. 2018;436:22-27.

229. Loessner D, Meinert C, Kaemmerer E, et al. Functionalization, preparation and use of cell-laden gelatin methacryloyl-based hydrogels as modular tissue culture platforms. Nature Protocols. 2016;11(4):727-746.

230. Schuurman W, Levett PA, Pot MW, et al. Gelatin-methacrylamide hydrogels as potential biomaterials for fabrication of tissue-engineered cartilage constructs. Macromolecular Bioscience. 2013;13(5):551-561.

231. Kirsch M, Birnstein L, Pepelanova I, et al. Gelatin-Methacryloyl (GelMA) Formulated with Human Platelet Lysate Supports Mesenchymal Stem Cell Proliferation and Differentiation and Enhances the Hydrogel's Mechanical Properties. Bioengineering (Basel). Vol 62019.

232. Pepelanova I, Kruppa K, Scheper T, Lavrentieva A. Gelatin-Methacryloyl (GelMA) Hydrogels with Defined Degree of Functionalization as a Versatile Toolkit for 3D Cell Culture and Extrusion Bioprinting. Bioengineering (Basel). 2018;5(3).

233. Wang Z, Kumar H, Tian Z, et al. Visible Light Photoinitiation of Cell-Adhesive Gelatin Methacryloyl Hydrogels for Stereolithography 3D Bioprinting. ACS Applied Materials and Interfaces. 2018;10(32):26859-26869.

234. Yue K, Santiago G, Alvarez MM, Tamayol A, Annabi N, Khademhosseini A. Synthesis, properties, and biomedical applications of gelatin methacryloyl (GelMA) hydrogels. Biomaterials. 2015;73:254-271.

235. Peerani E, Candido JB, Loessner D. Cell Recovery of Hydrogel-Encapsulated Cells for Molecular Analysis. Methods in Molecular Biology: Springer; 2019.

236. Van Den Bulcke AI, Bogdanov B, De Rooze N, Schacht EH, Cornelissen M, Berghmans H. Structural and rheological properties of methacrylamide modified gelatin hydrogels. Biomacromolecules. 2000;1(1):31-38.

237. Di Lullo GA, Sweeney SM, Korkko J, Ala-Kokko L, San Antonio JD. Mapping the ligand-binding sites and disease-associated mutations on the most abundant protein in the human, type I collagen. Journal of Biological Chemistry. 2002;277(6):4223-4231.

238. Klotz BJ, Gawlitta D, Rosenberg A, Malda J, Melchels FPW. Gelatin-Methacryloyl Hydrogels: Towards Biofabrication-Based Tissue Repair. Trends Biotechnol. 2016;34(5):394-407.

239. Maji K, Dasgupta S, Pramanik K, Bissoyi A. Preparation and Evaluation of Gelatin-Chitosan-Nanobioglass 3D Porous Scaffold for Bone Tissue Engineering. International Journal of Biomaterials. 2016;2016.

240. Han F, Dong Y, Su Z, Yin R, Song A, Li S. Preparation, characteristics and assessment of a novel gelatin-chitosan sponge scaffold as skin tissue engineering material. International Journal of Pharmacology. 2014;476(1-2):124-133.

241. Liu Y, Chan-Park MB. A biomimetic hydrogel based on methacrylated dextran-graft-lysine and gelatin for 3D smooth muscle cell culture. Biomaterials. 2010;31(6):1158-1170.

242. Nichol JW, Koshy S, Bae H, Hwang CM, Yamanlar S, Khademhosseini A. Cell-laden microengineered gelatin methacrylate hydrogels. Biomaterials. 2010;31(21):5536-5544.

243. Benton JA, DeForest CA, Vivekanandan V, Anseth KS. Photocrosslinking of Gelatin Macromers to Synthesize Porous Hydrogels That Promote Valvular Interstitial Cell Function. Tissue Engineering Part A. 2009;15(11):3221-3230.

244. Xiao W, He J, Nichol JW, et al. Synthesis and characterization of photocrosslinkable gelatin and silk fibroin interpenetrating polymer network hydrogels. Acta Biomaterialia. 2011;7(6):2384-2393.

245. Xu F, Inci F, Mullick O, et al. Release of Magnetic Nanoparticles from Cell-Encapsulating Biodegradable Nanobiomaterials. ACS Nano. 2012;6(8).

246. Chen YC, Lin RZ, Qi H, et al. Functional Human Vascular Network Generated in Photocrosslinkable Gelatin Methacrylate Hydrogels. Advanced Functional Materials. 2012;22(10):2027-2039.

247. Lee Y, Lee JM, Bae PK, Chung IY, Chung BH, Chung BG. Photo-crosslinkable hydrogel-based 3D microfluidic culture device. Electrophoresis. 2015;36(7-8):994-1001.

248. Dubruel P, Unger R, Vlierberghe SV, et al. Porous gelatin hydrogels: 2. In vitro cell interaction study. Biomacromolecules. 2007;8(2):338-344.

249. Loessner D, Stok KS, Lutolf MP, Hutmacher DW, Clements JA, Rizzi SC. Bioengineered 3D platform to explore cell-ECM interactions and drug resistance of epithelial ovarian cancer cells. Biomaterials. 2010;31(32):8494-8506.

250. Sun M, Sun X, Wang Z, Guo S, Yu G, Yang H. Synthesis and Properties of Gelatin Methacryloyl (GelMA) Hydrogels and Their Recent Applications in Load-Bearing Tissue. Polymers (Basel). 2018; 10(11):1290.

251. Levett PA, Melchels FP, Schrobback K, Hutmacher DW, Malda J, Klein TJ. A biomimetic extracellular matrix for cartilage tissue engineering centered on photocurable gelatin, hyaluronic acid and chondroitin sulfate. Acta Biomaterialia. 2014;10(1):214-223.

252. Kaemmerer E, Melchels FP, Holzapfel BM, Meckel T, Hutmacher DW, Loessner D. Gelatine methacrylamide-based hydrogels: an alternative three-dimensional cancer cell culture system. Acta Biomater. 2014;10(6):2551-2562.

253. Chen JWE, Lumibao J, Blazek A, Gaskins HR, Harley B. Hypoxia activates enhanced invasive potential and endogenous hyaluronic acid production by glioblastoma cells. Biomaterials Science. 2018;6(4):854-862.

254. Erkoc P, Seker F, Bagci-Onder T, Kizilel S. Gelatin Methacryloyl Hydrogels in the Absence of a Crosslinker as 3D Glioblastoma Multiforme (GBM)-Mimetic Microenvironment. Macromolecular Bioscience. 2018;18(3):34501-34506.

255. Arya AD, Hallur PM, Karkisaval AG, et al. Gelatin Methacrylate Hydrogels as Biomimetic Three-Dimensional Matrixes for Modeling Breast Cancer Invasion and Chemoresponse in Vitro. ACS Applied Materials and Interfaces. 2016;8(34):22005-22017.

256. Li Y, Li X, Zheng L, Wang L, Zhang X, Xu F. Polyacrylamide/GelMA Hydrogel Templates for Breast Cancer Cell Spheroids Fabrication. Journal of Nanotechnology in Engineering and Medicine. 2016;6(3).

257. Meinert C, Theodoropoulos C, Klein TJ, Hutmacher DW, Loessner D. A method for prostate and breast cancer cell spheroid cultures using gelatin methacryloyl-based hydrogels. Prostate Cancer: Springer; 2018.

258. Berger AJ, Linsmeier K, Kreeger PK, Masters KS. Decoupling the effects of stiffness and fiber density on cellular behaviors via an interpenetrating network of gelatin-methacrylate and collagen. Biomaterials. 2017;141:125-135.

259. Pearce OMT, Delaine-Smith RM, Maniati E, et al. Deconstruction of a Metastatic Tumor Microenvironment Reveals a Common Matrix Response in Human Cancers. Cancer Discovery. 2018;8(3):304-319.

260. Macintyre G, Goranova TE, De Silva D, et al. Copy-number signatures and mutational processes in ovarian carcinoma. Nature Genetics. 2018;50(9):1262-1270.

261. Leinster DA, Kulbe H, Everitt G, et al. The peritoneal tumour microenvironment of high-grade serous ovarian cancer. Journal of Pathology. 2012;227(2):136-145.

262. Shirahama H, Lee BH, Tan LP, Cho NJ. Precise Tuning of Facile One-Pot Gelatin Methacryloyl (GelMA) Synthesis. Science Reports. Vol 62016.

263. Delaine-Smith RM, Burney S, Balkwill FR, Knight MM. Experimental validation of a flat punch indentation methodology calibrated against unconfined compression tests for determination of soft tissue biomechanics. Journal Mechanical Behaviour of Biomedical Materials. 2016;60:401-415.

264. Marshall J. Transwell® Invasion Assays. In: Springer. Cell Migration: Springer; 2011.

265. Vennin C, Chin VT, Warren SC, et al. Transient tissue priming via ROCK inhibition uncouples pancreatic cancer progression, sensitivity to chemotherapy, and metastasis. Science Translational Medicine. 2017;9(384):e8504.

266. Chaudhuri O, Koshy ST, Branco da Cunha C, et al. Extracellular matrix stiffness and composition jointly regulate the induction of malignant phenotypes in mammary epithelium. Nature Materials. 2014;13(10):970-978.

267. Hwang HJ, Oh MS, Lee DW, Kuh HJ. Multiplex quantitative analysis of stroma-mediated cancer cell invasion, matrix remodeling, and drug response in a 3D co-culture model of pancreatic tumor spheroids and stellate cells. Journal of Experimental & Clinical Cancer Research. 2019;38(1):258.

268. Tian C, Clauser KR, Ohlund D, et al. Proteomic analyses of ECM during pancreatic ductal adenocarcinoma progression reveal different contributions by tumor and stromal cells. Proceedings of the Natlonal Academy of Sciences of the USA. 2019;116(39):19609-19618.

269. Naba A, Clauser KR, Hoersch S, Liu H, Carr SA, Hynes RO. The matrisome: in silico definition and in vivo characterization by proteomics of normal and tumor extracellular matrices. Molecular Cell Proteomics. 2012;11(4):M111.014647.

270. Imamichi Y, Konig A, Gress T, Menke A. Collagen type I-induced Smad-interacting protein 1 expression downregulates E-cadherin in pancreatic cancer. Oncogene. 2007;26(16):2381-2385.

271. Veenstra VL, Garcia-Garijo A, van Laarhoven HW, Bijlsma MF. Extracellular Influences: Molecular Subclasses and the Microenvironment in Pancreatic Cancer. Cancers (Basel). Vol 102018.

272. Del Monte U. Does the cell number 10(9) still really fit one gram of tumor tissue? Cell Cycle. 2009;8(3):505-506.

273. Yao H, Yang Z, Liu Z, et al. Glypican-3 and KRT19 are markers associating with metastasis and poor prognosis of pancreatic ductal adenocarcinoma. Cancer Biomarkers. 2016;17(4):397-404.

274. Saha SK, Choi HY, Kim BW, et al. KRT19 directly interacts with β-catenin/RAC1 complex to regulate NUMB-dependent NOTCH signaling pathway and breast cancer properties. Oncogene. 2017;36(3):332-349.

275. Sugimoto M, Takahashi S, Kojima M, et al. What is the nature of pancreatic consistency? Assessment of the elastic modulus of the pancreas and comparison with tactile sensation, histology, and occurrence of postoperative pancreatic fistula after pancreaticoduodenectomy. Surgery. 2014;156(5):1204-1211.

276. Kuwahara T, Hirooka Y, Kawashima H, et al. Quantitative evaluation of pancreatic tumor fibrosis using shear wave elastography. Pancreatology. 2016;16(6):1063-1068.

277. Hammer AM, Sizemore GM, Shukla VC, et al. Stromal PDGFR-α Activation Enhances Matrix Stiffness, Impedes Mammary Ductal Development, and Accelerates Tumor Growth. Neoplasia. 2017;19(6):496-508.

278. Kai F, Laklai H, Weaver VM. Force Matters: Biomechanical Regulation of Cell Invasion and Migration in Disease. Trends in Cell Biology. 2016;26(7):486-497.

279. Dalin S, Sullivan MR, Lau AN, et al. Deoxycytidine Release from Pancreatic Stellate Cells Promotes gemcitabine Resistance. Cancer Research. 2019;79(22):5723-5733.

280. Lin HH, Lin HK, Lin IH, et al. Mechanical phenotype of cancer cells: cell softening and loss of stiffness sensing. Oncotarget. 2015;6(25):20946-20958.

281. Djurec M, Grana O, Lee A, et al. Saa3 is a key mediator of the protumorigenic properties of cancer-associated fibroblasts in pancreatic tumors. Proceedings of the Natlonal Academy of Sciences of the USA. 2018;115(6):E1147-e1156.

282. Kopantzev EP, Kopantseva MR, Grankina EV, Mikaelyan A, Egorov VI, Sverdlov ED. Activation of IGF/IGF-IR signaling pathway fails to induce epithelial-mesenchymal transition in pancreatic cancer cells. Pancreatology. 2019;19(2):390-396.

283. Young S, Wong M, Tabata Y, Mikos AG. Gelatin as a delivery vehicle for the controlled release of bioactive molecules. Journal of Controlled Release. 2005;109(1-3):256-274.

284. Stenn KS, Link R, Moellmann G, Madri J, Kuklinska E. Dispase, a neutral protease from Bacillus polymyxa, is a powerful fibronectinase and type IV collagenase. Journal of Investigative Dermatology. 1989;93(2):287-290.

285. Jung KH, Choi YC, Chun JY, Min SG, Hong GP. Effects of Concentration and Reaction Time of Trypsin, Pepsin, and Chymotrypsin on the Hydrolysis Efficiency of Porcine Placenta. Korean Journal for Food Science of Animal Resources. Vol 342014.

286. Brown MA, Wallace CS, Anamelechi CC, Clermont E, Reichert WM, Truskey GA. The use of mild trypsinization conditions in the detachment of endothelial cells to promote subsequent endothelialization on synthetic surfaces. Biomaterials. 2007;28(27):3928-3935.
287. Shirahama H, Lee BH, Tan LP, Cho NJ. Precise Tuning of Facile One-Pot Gelatin Methacryloyl (GelMA) Synthesis. Scientific Reports. Vol 62016.
288. Kinner A, Wu W, Staudt C, Iliakis G. γ-H2AX in recognition and signaling of DNA double-strand breaks in the context of chromatin. Nucleic Acids Research. Vol 362008.
289. Hanasoge S, Ljungman M. H2AX phosphorylation after UV irradiation is triggered by DNA repair intermediates and is mediated by the ATR kinase. Carcinogenesis. 2007;28(11):2298-2304.
290. Paulsen RD, Cimprich KA. The ATR pathway: fine-tuning the fork. DNA Repair. 2007;6(7):953-966.
291. Zhao H, Traganos F, Darzynkiewicz Z. Kinetics of the UV-induced DNA damage response in relation to cell cycle phase. Correlation with DNA replication. Cytometry Part A. 2010;77(3):285-293.
292. Nikitaki Z, Hellweg CE, Georgakilas AG, Ravanat JL. Stress-induced DNA damage biomarkers: applications and limitations. Frontiers in Chemistry. 2015;3.
293. Noshadi I, Hong S, Sullivan KE, et al. In Vitro and In Vivo Analysis of Visible Light Crosslinkable Gelatin Methacryloyl (GelMA) Hydrogels. Biomaterials Science. 2017;5(10):2093-2105.
294. Kipps E, Tan DS, Kaye SB. Meeting the challenge of ascites in ovarian cancer: new avenues for therapy and research. Nature Reviews Cancer. Vol 13. England2013.
295. Sheid B. Angiogenic effects of macrophages isolated from ascitic fluid aspirated from women with advanced ovarian cancer. Cancer Letters. 1992;62(2):153-158.
296. Sleightholm RL, Neilsen BK, Li J, et al. Emerging roles of the CXCL12/CXCR4 axis in pancreatic cancer progression and therapy. Pharmacology and Therapeutics. 2017;179:158-170.
297. Scotton CJ, Wilson JL, Scott K, et al. Multiple actions of the chemokine CXCL12 on epithelial tumor cells in human ovarian cancer. Cancer Research. 2002;62(20):5930-5938.
298. Kuwada Y, Sasaki T, Morinaka K, Kitadai Y, Mukaida N, Chayama K. Potential involvement of IL-8 and its receptors in the invasiveness of pancreatic cancer cells. International Journal of Oncology. 2003;22(4):765-771.
299. Ikeda O, Egami H, Ishiko T, et al. Signal of proteinase-activated receptor-2 contributes to highly malignant potential of human pancreatic cancer by up-regulation of interleukin-8 release. International Journal of Oncology. 2006;28(4):939-946.
300. Lesina M, Kurkowski MU, Ludes K, et al. Stat3/Socs3 activation by IL-6 transsignaling promotes progression of pancreatic intraepithelial neoplasia and development of pancreatic cancer. Cancer Cell. 2011;19(4):456-469.
301. Corcoran RB, Contino G, Deshpande V, et al. STAT3 plays a critical role in KRAS-induced pancreatic tumorigenesis. Cancer Research. 2011;71(14):5020-5029.
302. Xiao Q, Zhou D, Rucki AA, et al. Cancer associated fibroblasts in pancreatic cancer are reprogrammed by tumor-induced alterations in genomic DNA methylation. Cancer Research. 2016;76(18):5395-5404.
303. Sun Q, Zhang B, Hu Q, et al. The impact of cancer-associated fibroblasts on major hallmarks of pancreatic cancer. Theranostics. 2018;8(18):5072-5087.
304. Albrengues J, Bourget I, Pons C, et al. LIF mediates proinvasive activation of stromal fibroblasts in cancer. Cell Reports. 2014;7(5):1664-1678.
305. Prêle CM, Keith-Magee AL, Murcha M, Hart PH. Activated signal transducer and activator of transcription-3 (STAT3) is a poor regulator of tumour necrosis factor-α

production by human monocytes. Clinical and Experimental Immunology. 2007;147(3):564-572.

306. Nishiki S, Hato F, Kamata N, et al. Selective activation of STAT3 in human monocytes stimulated by G-CSF: implication in inhibition of LPS-induced TNF-alpha production. American Journal of Physiology and Cell Physiology. 2004;286(6):C1302-1311.

307. Nagathihalli NS, Castellanos JA, Lamichhane P, et al. Inverse Correlation of STAT3 and MEK Signaling Mediates Resistance to RAS Pathway Inhibition in Pancreatic Cancer. Cancer Research. 2018;78(21):6235-6246.

308. Shield K, Ackland ML, Ahmed N, Rice GE. Multicellular spheroids in ovarian cancer metastases: Biology and pathology. Gynecologic Oncology. 2009;113(1):143-148.

309. Kuen J, Darowski D, Kluge T, Majety M. Pancreatic cancer cell/fibroblast co-culture induces M2 like macrophages that influence therapeutic response in a 3D model. PLoS One. 2017;12(7):e0182039.

310. Valdez J, Cook CD, Ahrens CC, et al. On-demand dissolution of modular, synthetic extracellular matrix reveals local epithelial-stromal communication networks. Biomaterials. 2017;130:90-103.

311. Wang H, Adhikari S, Butler BE, Pandita TK, Mitra S, Hegde ML. A Perspective on Chromosomal Double Strand Break Markers in Mammalian Cells. Jacobs Journal of Radiation Oncology. 2014;1(1).

312. Zhu Y, Herndon JM, Sojka DK, et al. Tissue-Resident Macrophages in Pancreatic Ductal Adenocarcinoma Originate from Embryonic Hematopoiesis and Promote Tumor Progression. Immunity. 2017;47(2):323-338.e326.

313. Ding Y, Du Y. Clinicopathological significance and prognostic role of chemokine receptor CXCR4 expression in pancreatic ductal adenocarcinoma, a meta-analysis and literature review. International Journal of Surgery. 2019;65:32-38.

314. Krieg A, Riemer JC, Telan LA, Gabbert HE, Knoefel WT. CXCR4-A Prognostic and Clinicopathological Biomarker for Pancreatic Ductal Adenocarcinoma: A Meta-Analysis. PLoS One. 2015;10(6):e0130192.

315. Demir IE, Kujundzic K, Pfitzinger PL, et al. Early pancreatic cancer lesions suppress pain through CXCL12-mediated chemoattraction of Schwann cells. Proceedings of the National Academy of Sciences of the USA. 2017;114(1):E85-e94.

316. Lutolf MP, Hubbell JA. Synthetic biomaterials as instructive extracellular microenvironments for morphogenesis in tissue engineering. Nature Biotechnology. 2005;23(1):47-55.

317. Abe M, Ho CH, Kamm KE, Grinnell F. Different molecular motors mediate platelet-derived growth factor and lysophosphatidic acid-stimulated floating collagen matrix contraction. Journal of Biological Chemistry. 2003;278(48):47707-47712.

318. Rhee S, Grinnell F. P21-activated kinase 1: convergence point in PDGF- and LPA-stimulated collagen matrix contraction by human fibroblasts. Journal of Cell Biology. 2006;172(3):423-432.

319. Lee SWL, Seager RJ, Litvak F, et al. Integrated in silico and 3D in vitro model of macrophage migration in response to physical and chemical factors in the tumor microenvironment. Integrative Biology. 2020;12(4):90-108.

320. Karnevi E, Andersson R, Rosendahl AH. Tumour-educated macrophages display a mixed polarisation and enhance pancreatic cancer cell invasion. Immunology and Cell Biology. 2014;92(6):543-552.

321. Chen S, Lian G, Li J, et al. Tumor-driven like macrophages induced by conditioned media from pancreatic ductal adenocarcinoma promote tumor metastasis via secreting IL-8. Cancer Medicine. Vol 72018.

322. Acerbi I, Cassereau L, Dean I, et al. Human breast cancer invasion and aggression correlates with ECM stiffening and immune cell infiltration. Integrative Biology. 2015;7(10):1120-1134.

323. Aiello NM, Bajor DL, Norgard RJ, et al. Metastatic progression is associated with dynamic changes in the local microenvironment. Nature Communications. 2016;7:12819.

324. Feygenzon V, Loewenstein S, Lubezky N, et al. Unique cellular interactions between pancreatic cancer cells and the omentum. PLoS One. Vol 122017.

325. Tape CJ, Ling S, Dimitriadi M, et al. Oncogenic KRAS Regulates Tumor Cell Signaling via Stromal Reciprocation. Cell. 2016;165(4):910-920.

326. Arpin CC, Mac S, Jiang Y, et al. Applying Small Molecule Signal Transducer and Activator of Trancription-3 (STAT3) Protein Inhibitors as Pancreatic Cancer Therapeutics. Molecular Cancer Therapeutics. 2016;15(5):794-805.

327. Jiang H, Liu X, Knolhoff BL, et al. The development of resistance to FAK inhibition in pancreatic cancer is linked to stromal depletion. Gut. 2020;69(1):122-132.

328. Kučera J, Netušilová J, Sladeček S, et al. Hypoxia Downregulates MAPK/ERK but Not STAT3 Signaling in ROS-Dependent and HIF-1-Independent Manners in Mouse Embryonic Stem Cells. Oxidative Medicine and Cellular Longevity. 2017;2017:4386947.

329. Pelham RJ, Jr., Wang Y. Cell locomotion and focal adhesions are regulated by substrate flexibility. Proceedings of the National Academy of Sciences of the USA. 1997;94(25):13661-13665.

330. Das A, Fischer RS, Pan D, Waterman CM. YAP Nuclear Localization in the Absence of Cell-Cell Contact Is Mediated by a Filamentous Actin-dependent, Myosin II- and Phospho-YAP-independent Pathway during Extracellular Matrix Mechanosensing*. Journal of Biological Chemistry. Vol 2912016.

331. Tekin H, Simmons S, Cummings B, et al. Effects of 3D culturing conditions on the transcriptomic profile of stem-cell-derived neurons. Nature Biomedical Engineering. 2018;2(7):540-554.

332. Mammoto A, Mammoto T, Ingber DE. Mechanosensitive mechanisms in transcriptional regulation. Journal of Cell Science. 2012;125(Pt 13):3061-3073.

333. Jiramongkolchai P, Owens P, Hong CC. Emerging roles of the bone morphogenetic protein pathway in cancer: potential therapeutic target for kinase inhibition. Biochemical Society Transactions. 2016;44(4):1117-1134.

334. Gordon KJ, Kirkbride KC, How T, Blobe GC. Bone morphogenetic proteins induce pancreatic cancer cell invasiveness through a Smad1-dependent mechanism that involves matrix metalloproteinase-2. Carcinogenesis. 2009;30(2):238-248.

335. Geismann C, Schäfer H, Gundlach JP, et al. NF-κB Dependent Chemokine Signaling in Pancreatic Cancer. Cancers (Basel). Vol 112019.

336. Wente MN, Mayer C, Gaida MM, et al. CXCL14 expression and potential function in pancreatic cancer. Cancer Letters. 2008;259(2):209-217.

337. Licht AH, Nubel T, Feldner A, et al. Junb regulates arterial contraction capacity, cellular contractility, and motility via its target Myl9 in mice. Journal of Clinical Investigation. 2010;120(7):2307-2318.

338. Maity G, Ghosh A, Gupta V, et al. CYR61/CCN1 Regulates dCK and CTGF and Causes gemcitabine-resistant Phenotype in Pancreatic Ductal Adenocarcinoma. Molecular Cancer Therapeutics. 2019;18(4):788-800.

339. Xia YJ, Jiang XT, Jiang SB, et al. PHD3 affects gastric cancer progression by negatively regulating HIF1A. Molecular Medicine Reports. 2017;16(5):6882-6889.

340. Buchholz M, Braun M, Heidenblut A, et al. Transcriptome analysis of microdissected pancreatic intraepithelial neoplastic lesions. Oncogene. 2005;24(44):6626-6636.

341. Hosokawa M, Kashiwaya K, Eguchi H, et al. Over-expression of cysteine proteinase inhibitor cystatin 6 promotes pancreatic cancer growth. Cancer Science. 2008;99(8):1626-1632.

342. Van den broeck A, Vankelecom H, Van Delm W, et al. Human Pancreatic Cancer Contains a Side Population Expressing Cancer Stem Cell-Associated and Prognostic Genes. PLoS One. 2013;8(9): e73968

343. Craven KE, Gore J, Korc M. Overview of Pre-Clinical and Clinical Studies Targeting Angiogenesis in Pancreatic Ductal Adenocarcinoma. Cancer Letters. 2016;381(1):201-210.

344. Kim KE, Song H, Kim TS, et al. Interleukin-18 is a critical factor for vascular endothelial growth factor-enhanced migration in human gastric cancer cell lines. Oncogene. 2007;26(10):1468-1476.

345. Schulz P, Fischer C, Detjen KM, et al. Angiopoietin-2 drives lymphatic metastasis of pancreatic cancer. Faseb Journal. 2011;25(10):3325-3335.

346. Katsuta E, Qi Q, Peng X, Hochwald SN, Yan L, Takabe K. Pancreatic adenocarcinomas with mature blood vessels have better overall survival. Science Reports. 2019; 9:1310.

347. Zhou J, Cheng Y, Tang L, Martinka M, Kalia S. Up-regulation of SERPINA3 correlates with high mortality of melanoma patients and increased migration and invasion of cancer cells. Oncotarget. 2017;8(12):18712-18725.

348. Velez DO, Tsui B, Goshia T, et al. 3D collagen architecture induces a conserved migratory and transcriptional response linked to vasculogenic mimicry. Nature Communications. 2017;8(1):1651.

349. Timpson P, McGhee EJ, Morton JP, et al. Spatial regulation of RhoA activity during pancreatic cancer cell invasion driven by mutant p53. Cancer Research. 2011;71(3):747-757.

350. Moreno-Vicente R, Pavon DM, Martin-Padura I, et al. Caveolin-1 Modulates Mechanotransduction Responses to Substrate Stiffness through Actin-Dependent Control of YAP. Cell Reports. 2018;25(6):1622-1635.e1626.

351. Ma Z, Vocadlo DJ, Vosseller K. Hyper-O-GlcNAcylation Is Anti-apoptotic and Maintains Constitutive NF-κB Activity in Pancreatic Cancer Cells*. Journal of Biological Chemistry. Vol 2882013.

352. Wang Z, Liu Y, Lu L, et al. Fibrillin-1, induced by Aurora-A but inhibited by BRCA2, promotes ovarian cancer metastasis. Oncotarget. 2015;6(9):6670-6683.

353. Tamaki S, Mano T, Sakata Y, et al. Interleukin-16 promotes cardiac fibrosis and myocardial stiffening in heart failure with preserved ejection fraction. PLoS One. 2013;8(7):e68893.

354. Zeisberg M, Neilson EG. Biomarkers for epithelial-mesenchymal transitions. Journal of Clinical Investigation. 2009; 119(6):1429-37.

355. Wei SC, Fattet L, Tsai JH, et al. Matrix stiffness drives Epithelial-Mesenchymal Transition and tumour metastasis through a TWIST1-G3BP2 mechanotransduction pathway. Nature Cell Biology. 2015;17(5):678-688.

356. Murray ME, Mendez MG, Janmey PA. Substrate stiffness regulates solubility of cellular vimentin. Molecular Biology of the Cell. 2014; 25(1):87-94.

357. Fernandez-Sanchez ME, Barbier S, Whitehead J, et al. Mechanical induction of the tumorigenic beta-catenin pathway by tumour growth pressure. Nature. 2015;523(7558):92-95.

358. Van Buren P, LeWinter MM. Heart Failure as a Consequence of Diabetic Cardiomyopathy. In: Elsevier. Heart Failure: A Companion to Braunwald's Heart Disease. Second Edition ed: Elsevier; 2011.

359. Peng C, Zhu Y, Zhang W, et al. Regulation of the Hippo-YAP Pathway by Glucose Sensor O-GlcNAcylation. Molecular Cell. 2017;68(3):591-604.e595.

360. Baker BM, Trappmann B, Wang WY, et al. Cell-mediated fiber recruitment drives extracellular matrix mechanosensing in engineered fibrillar microenvironments. Nature Materials. 2015;14(12):1262-1268.

361. Schmid P, Chui SY, Emens LA. Atezolizumab and Nab-Paclitaxel in Advanced Triple-Negative Breast Cancer. Reply. New England Journal of Medicine. 2019;380(10):987-988.
362. Eggermont AMM, Blank CU, Mandala M, et al. Adjuvant Pembrolizumab versus Placebo in Resected Stage III Melanoma. New England Journal of Medicine. 2018;378(19):1789-1801.
363. Wong CH, Siah KW, Lo AW. Estimation of clinical trial success rates and related parameters. Biostatistics. 2019;20(2):273-286.
364. Vennin C, Cox TR, Pajic M, Timpson P. Transient targeting of the pancreatic cancer stroma as a 'fine-tuned' anti-tumor and anti-metastatic therapy. Oncotarget. 2017;8(49):84635-84636.
365. Deer EL, Gonzalez-Hernandez J, Coursen JD, et al. Phenotype and genotype of pancreatic cancer cell lines. Pancreas. 2010;39(4):425-435.
366. Ellenrieder V, Hendler SF, Ruhland C, Boeck W, Adler G, Gress TM. TGF-beta-induced invasiveness of pancreatic cancer cells is mediated by matrix metalloproteinase-2 and the urokinase plasminogen activator system. International Journal of Cancer. 2001;93(2):204-211.
367. Greco E, Basso D, Fogar P, et al. Pancreatic cancer cells invasiveness is mainly affected by interleukin-1beta not by transforming growth factor-beta1. International Journal of Biological Markers. 2005;20(4):235-241.
368. Kocer SS, Walker SG, Zerler B, Golub LM, Simon SR. Metalloproteinase Inhibitors, Nonantimicrobial Chemically Modified Tetracyclines, and Ilomastat Block Bacillus anthracis Lethal Factor Activity in Viable Cells. Infection and Immunity. 2005;73(11):7548-7557.
369. Olson MF. Applications for ROCK kinase inhibition. Current Opinions in Cell Biology. 2008;20(2):242-248.
370. Coward J, Kulbe H, Chakravarty P, et al. Interleukin-6 as a therapeutic target in human ovarian cancer. Clinical Cancer Reseaarch. 2011;17(18):6083-6096.
371. Babic A, Schnure N, Neupane NP, et al. Plasma inflammatory cytokines and survival of pancreatic cancer patients. Clinical Transnational Gastroenterology. 2018;9(4).
372. Kim HW, Lee J, Paik K, Kang J, Kim J, Hwang JH. Serum interleukin-6 is associated with pancreatic ductal adenocarcinoma progression pattern. Medicine (Baltimore). 2017;96(5):15926.
373. Yako YY, Kruger D, Smith M, Brand M. Cytokines as Biomarkers of Pancreatic Ductal Adenocarcinoma: A Systematic Review. PLoS One. 2016; 11(5):e0154016.
374. Ohlund D, Ardnor B, Oman M, Naredi P, Sund M. Expression pattern and circulating levels of endostatin in patients with pancreas cancer. International Journal of Cancer. 2008;122(12):2805-2810.
375. Awasthi N, Mikels-Vigdal AJ, Stefanutti E, et al. Therapeutic efficacy of anti-MMP9 antibody in combination with nab-paclitaxel-based chemotherapy in pre-clinical models of pancreatic cancer. Journal of Cell Molecular Medicine. 2019;23(6):3878-3887.
376. Haq M, Shafii A, Zervos EE, Rosemurgy AS. Addition of matrix metalloproteinase inhibition to conventional cytotoxic therapy reduces tumor implantation and prolongs survival in a murine model of human pancreatic cancer. Cancer Research. 2000;60(12):3207-3211.
377. Gao CC, Gong BG, Wu JB, et al. MMI-166, a selective matrix metalloproteinase inhibitor, promotes apoptosis in human pancreatic cancer. Medical Oncology. 2015;32(1):418.
378. Long KB, Gladney WL, Tooker GM, Graham K, Fraietta JA, Beatty GL. IFN-γ and CCL2 cooperate to redirect tumor-infiltrating monocytes to degrade fibrosis and enhance chemotherapy efficacy in pancreatic carcinoma. Cancer Discovery. 2016;6(4):400-413.

379. Rückert F, Hennig M, Petraki CD, et al. Co-expression of KLK6 and KLK10 as prognostic factors for survival in pancreatic ductal adenocarcinoma. British Journal of Cancer. 2008;99(9):1484-1492.

380. Felix K, Gaida MM. Neutrophil-Derived Proteases in the Microenvironment of Pancreatic Cancer -Active Players in Tumor Progression. International Journal of Biological Sciences. 2016;12(3):302-313.

381. Bulle A, Dekervel J, Libbrecht L, et al. gemcitabine induces Epithelial-to-Mesenchymal Transition in patient-derived pancreatic ductal adenocarcinoma xenografts. American Journal of Translational Research. 2019;11(2):765-779.

382. Loret N, Denys H, Tummers P, Berx G. The Role of Epithelial-to-Mesenchymal Plasticity in Ovarian Cancer Progression and Therapy Resistance. Cancers (Basel). 2019;11(6):838.

383. Hirata E, Girotti M, Viros A, et al. Intravital Imaging Reveals How BRAF Inhibition Generates Drug-Tolerant Microenvironments with High Integrin β1/FAK Signaling. Cancer Cell. 2015;27(4):574-588.

384. Gupta V, Gupta N, Shaik IH, et al. Liposomal fasudil, a Rho-Kinase Inhibitor, for Prolonged Pulmonary Preferential Vasodilation in Pulmonary Arterial Hypertension. Journal of Controlled Release. 2013;167(2):189-199.

385. Sadok A, McCarthy A, Caldwell J, et al. Rho kinase inhibitors block melanoma cell migration and inhibit metastasis. Cancer Research. 2015;75(11):2272-2284.

386. Orgaz JL, Crosas-Molist E, Sadok A, et al. Myosin II Reactivation and Cytoskeletal Remodeling as a Hallmark and a Vulnerability in Melanoma Therapy Resistance. Cancer Cell. 2020;37(1):85-103 e109.

387. Boland S, Bourin A, Alen J, et al. Design, synthesis, and biological evaluation of novel, highly active soft ROCK inhibitors. Journal of Medical Chemistry. 2015;58(10):4309-4324.

388. Garnock-Jones KP. Ripasudil: first global approval. Drugs. 2014;74(18):2211-2215.

389. Wu Y, Xiang Y, Fang J, et al. The influence of the stiffness of GelMA substrate on the outgrowth of PC12 cells. Bioscience Reports. 2019;39(1).

390. Riffle S, Hegde RS. Modeling tumor cell adaptations to hypoxia in multicellular tumor spheroids. Journal of Experimental & Clinical Cancer Research. 2017;36:102.

391. Paszek MJ, Zahir N, Johnson KR, et al. Tensional homeostasis and the malignant phenotype. Cancer Cell. 2005;8(3):241-254.

392. Ehrenberg KR, Gao J, Oppel F, et al. Systematic Generation of Patient-Derived Tumor Models in Pancreatic Cancer. Cells. 2019;8(2).

393. Paszek MJ, Weaver VM. The tension mounts: mechanics meets morphogenesis and malignancy. Journal of Mammary Gland Biology and Neoplasia. 2004;9(4):325-342.

394. Butcher DT, Alliston T, Weaver VM. A tense situation: forcing tumour progression. Nature Reviews Cancer. 2009;9(2):108-122.

395. Abbott A. Cell culture: biology's new dimension. Nature. Vol 424. England2003.

396. Monteran L, Erez N. The Dark Side of Fibroblasts: Cancer-Associated Fibroblasts as Mediators of Immunosuppression in the Tumor Microenvironment. Frontiers Immunology 2019;10:1835.

397. Kleeff J, Korc M, Apte M, et al. Pancreatic cancer. Nature Reviews. Disease Primers. 2016;2:16022.

398. Tang Y, Rowe RG, Botvinick EL, et al. MT1-MMP-dependent control of skeletal stem cell commitment via a β1-integrin/YAP/TAZ signaling axis. Developmental Cell. 2013;25(4):402-416.

Chapter 9 - Appendices

9.1 Appendix Chapter 2

MATLAB R2019 (MathWorks) code employed for the analysis of flat-end tissue indentation data (see Chapter 2 – section 2.4.1). Original code author: Stephen Thorpe, modified by Eleonora Peerani (December 2019, version 5.2)

```
dataRate = 100; %Spacing of data in results file (ms)
strainEndPt = 30; %Strain end point in absolute terms for first ramp
strainRate = 1; %Strain rate in %/s for first ramp
holdTime = 600; %Hold time in s after first ramp
IMStart = 2.5; %Initial modulus start strain in percent
IMEnd = 7.5; %Initial modulus end strain in percent
DMStart = 20; %Deep modulus start strain in percent
DMEnd = 30; %Deep modulus end strain in percent

headerlines1 = 3; %headerlines before gauge length value
headerlines2 = 5; %headerlines before data

% Indices for regions of interest in data lists
dataFreq = 1000/dataRate;
indEstPkF = (strainEndPt/strainRate)*dataFreq; %Estimate of peak force point
indEq = holdTime*dataFreq+indEstPkF; %Estimate of equilibrium force point
indRelax = indEq-2*dataFreq:indEq; %indices for relaxation (hold) step over last 2 sec

% Output file details
XLfilename = 'IndentationResults.csv'; %Filename for results output
resultsList = {'Filename','Pathname','GaugeLength [mm]','mIMFDfit [N/mm]',...
    'mDMFDfit [N/mm]','PkF [N]','PkFD [N/mm]','PkStrain','EqF [N]',...
    'EqFD [N/mm]','EqStrain'};
l = 2; %line number to start results input

% Algorithm repeats for each .csv file
runAgain = 'Y';
while runAgain == 'Y'
    close all
    % Get file for analysis and import data
    [File,PathName] = uigetfile('*.csv','Select the file for analysis');
    fileID = fopen(File);
    SpecimenNo = textscan(fileID,'%*s %d',1,'delimiter',',');
    SpecimenLabel = textscan(fileID,'%*s %q',1,'delimiter',',');
    Delimiter = {',','"'};
    formatSpec1 = '%*s %f %*s';
    GL = textscan(fileID,formatSpec1,1,'delimiter',Delimiter,...
        'MultipleDelimsAsOne',1,'headerlines',headerlines1);
    formatSpec2 = '%f %f %f %f %f';
    Data = textscan(fileID,formatSpec2,'delimiter',Delimiter,...
        'MultipleDelimsAsOne',1,'headerlines',headerlines2);
    fclose(fileID);

    % Put columns into vectors
```

```
    SpecimenNo = SpecimenNo{1,1};
    SpecimenLabel = SpecimenLabel{1,1};
    GL = GL{1,1};
    Time = Data{:,1};
    AbsPosition = Data{:,2};
    CompPos = Data{:,3};
    CompStrain = Data{:,4};
    Load = Data{:,5};

    % Moving average filter to remove noise on load channel
    windowSize = 3; %Size of moving average window
    b = (1/windowSize)*ones(1,windowSize);
    LoadSmooth = filter(b,1,Load); %Smoothed load data

    % Peak force and strain
    [PkF,indPk] = max(Load(indEstPkF-10:indEstPkF+10)); %indices for strain application
step
    indPk = indPk+indEstPkF-10;
    PkD = CompPos(indPk);
    PkFD = PkF/PkD;
    indRamp = 1:indPk;
    PkStrain = CompStrain(indPk);
    PkTime = Time(indPk);
    % Equilibrium force
    EqF = mean(LoadSmooth(indRelax));
    EqStrain = CompStrain(indRelax(end));
    EqD = CompPos(indRelax(end));
    EqFD = EqF/EqD;
    EqTime = Time(indRelax(end));
    % Initial modulus region
    indIM = find((CompStrain(indRamp) >= IMStart)&(CompStrain(indRamp) < IMEnd)); %indices
for initial mod 2.5-7.5%
    IMFDfit = fit(CompPos(indIM),LoadSmooth(indIM),'poly1'); %Fit linear curve to region
    mIMFDfit = IMFDfit.p1; %retrieve slope
    % Deep modulus region
    indDM = find((CompStrain(indRamp) >= DMStart)&(CompStrain(indRamp) < DMEnd)); %indices
for deep mod 15-20%
    DMFDfit = fit(CompPos(indDM),LoadSmooth(indDM),'poly1'); %Fit linear curve to region
    mDMFDfit = DMFDfit.p1; %retrieve slope

    % Add results to results array: resultsList = {'Filename','Pathname',...
    %    'GaugeLength    [mm]','mIMFDfit    [N/mm]','mDMFDfit    [N/mm]','PkF    [N]','PkFD
[N/mm]','PkStrain','EqF [N]',...
    % 'EqFD [N/mm]','EqStrain'};
    resultsList{l,1} = File;
    resultsList{l,2} = PathName;
    resultsList{l,3} = GL;
    resultsList{l,4} = mIMFDfit;
    resultsList{l,5} = mDMFDfit;
    resultsList{l,6} = PkF;
    resultsList{l,7} = PkFD;
    resultsList{l,8} = PkStrain;
    resultsList{l,9} = EqF;
```

```
    resultsList{l,10} = EqFD;
    resultsList{l,11} = EqStrain;
    l = l+1;

    % Figure output
    scrsz = get(groot,'ScreenSize');
    figure('Name','Press any key to proceed','Position',...
           [1 scrsz(4)*0.4 scrsz(3)*0.9 scrsz(4)*0.5]);
    % Force-time plot for whole test
    ft = subplot(1,3,1);
    plot(Time,Load);
    hold(ft,'on');
    plot(Time,LoadSmooth);
    plot(PkTime,PkF,'mo');
    plot(EqTime,EqF,'co');
    title('Force-time all steps'); grid on;
    xlabel('Time [s]'); ylabel('Force [N]');
    legend('Raw data','Averaged data','Peak pt.','Eq. pt.','location','northeast');
    % Force-displacement plot for strain application step
    fdStrainApp = subplot(1,3,2);
    plot(CompPos(indRamp),Load(indRamp),'c');
    hold(fdStrainApp,'on');
    plot(CompPos(indRamp),LoadSmooth(indRamp),'b');
    plot(PkD,PkF,'mo');
    plot(IMFDfit,'r-',CompPos(indIM),LoadSmooth(indIM),'b');
    plot(DMFDfit,'g-',CompPos(indDM),LoadSmooth(indDM),'b');

%     plot(IMFDfit,CompPos(indIM),LoadSmooth(indIM),'b');
%     hold(fdStrainApp,'on');
%     plot(DMFDfit,'g-',CompPos(indDM),LoadSmooth(indDM),'b');
%     plot(PkD,PkF,'mo');
%     plot(CompPos(indRamp),Load(indRamp),'c');
%     plot(CompPos(indRamp),LoadSmooth(indRamp),'b');
    title('Strain application'); grid on;
    xlabel('Displacement [mm]'); ylabel('Force [N]');
    legend('Raw Data','Averaged Data','Peak','Averaged Data','Initial fit',...
        'Averaged Data','Deep fit','location','southeast');
    % Force-strain plot for strain application step
    fsStrainApp = subplot(1,3,3);
    plot(CompStrain(indRamp),Load(indRamp));
    hold(fsStrainApp,'on');
    plot(CompStrain(indRamp),LoadSmooth(indRamp));
    plot(PkStrain,PkF,'mo');
    title('Strain application'); grid on;
    xlabel('Strain [%]'); ylabel('Force [N]');
    legend('Raw data','Averaged data','Peak','location','southeast');

       runAgain = input('Run again? Y/N [Y]: ', 's');
    if isempty(runAgain)
        runAgain = 'Y';
    end
end
xlsxwrite(XLfilename,resultsList); %Output excel sheet with result list
```

9.2 Appendix Chapter 5.1

Additional data from RNA-seq comparisons between collagen (COL), GelMA (7.5 and 5) and Matrigel (MAT) cultured cells and organoids. Principal Component Analysis (PCA) of all samples shown as well as heatmap of DEGs in coll-MAT, 5-MAT, 7.5-MAT.

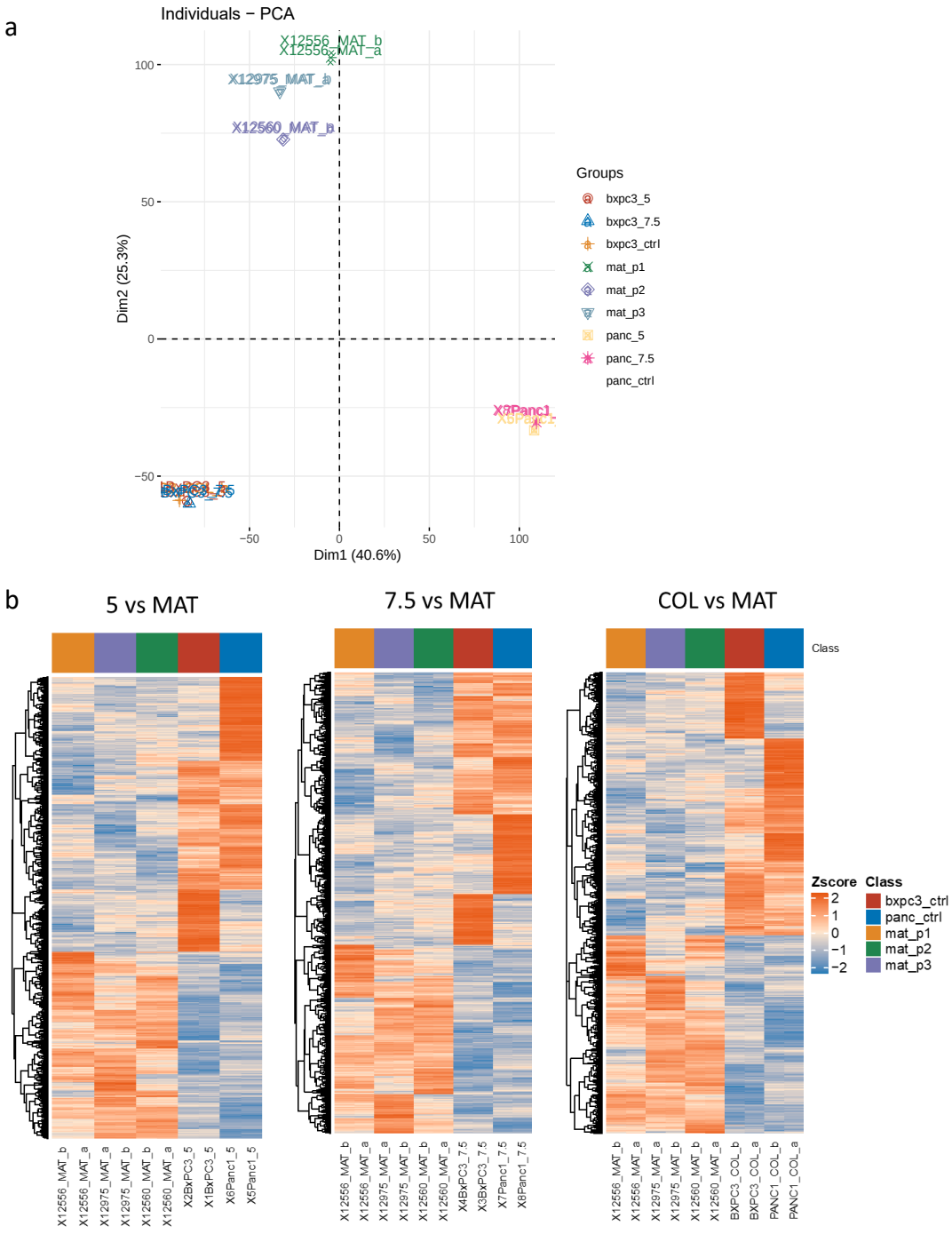

Figure 9.1 Clustering of RNA-seq data from BxPC-3 and PANC-1 cells grown in collagen, 5% and 7.5% GelMA, and PDAC primary organoids in Matrigel (p1=12556, p2=12560, p3=12975), n=2. (a) Unsupervised clustering by principal component analysis (PCA). **(b)** Heatmaps of differentially expressed protein-coding genes FDR < 0.05 and logFC > |1| in the indicated contrasts.

9.3 Appendix Chapter 5.2

For legibility, larger versions of Volcano plots from Figure 5.2 are copied below.

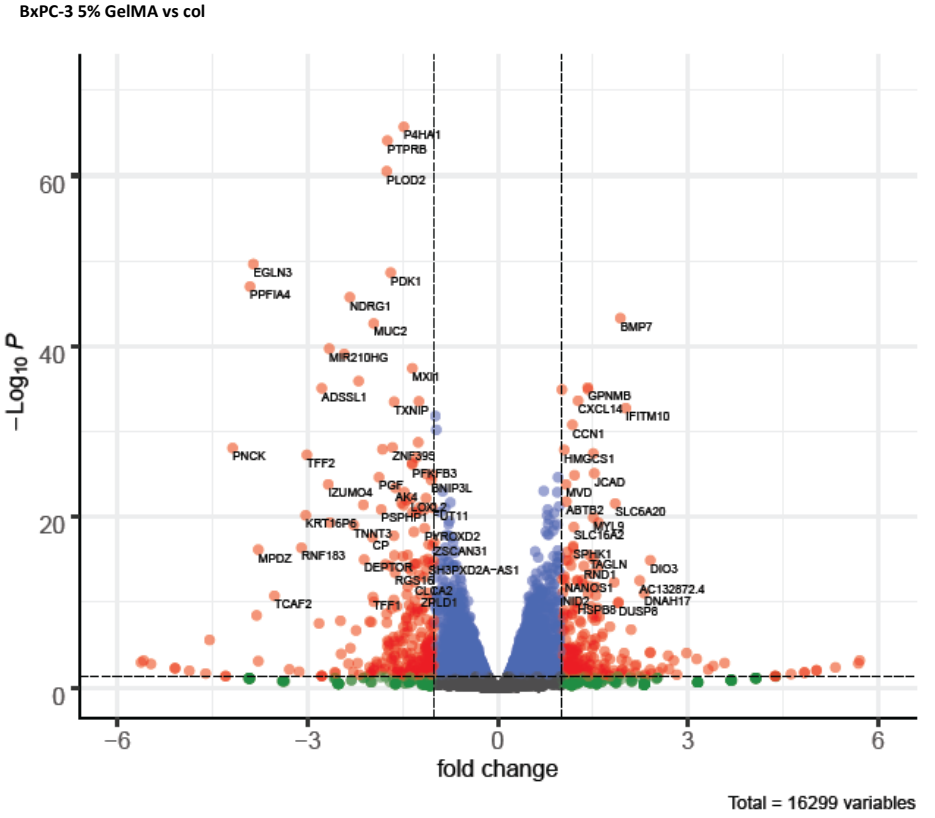

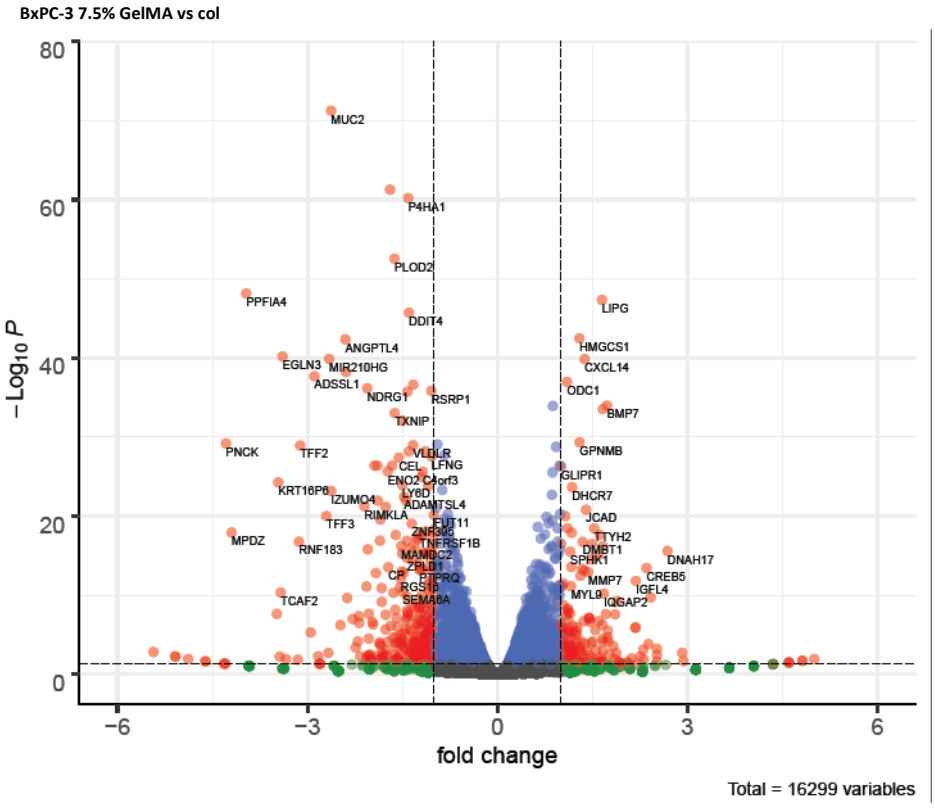

PANC-1 5% GelMA vs col

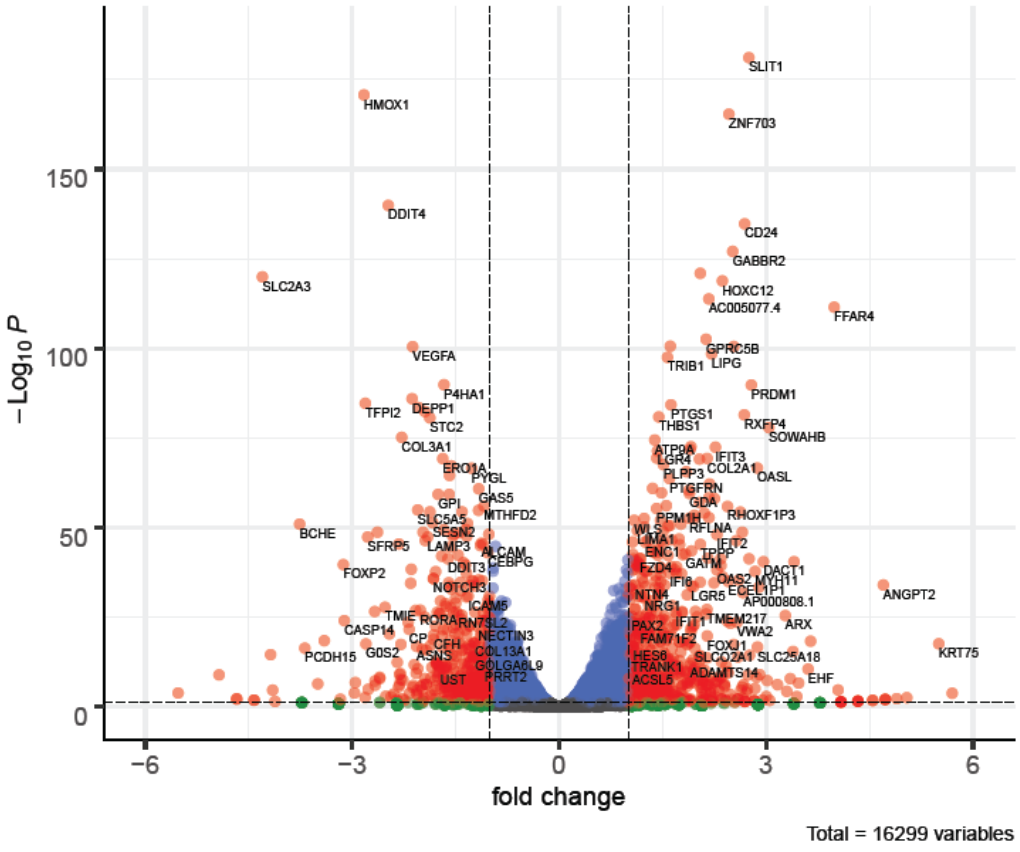

PANC-1 7.5% GelMA vs col

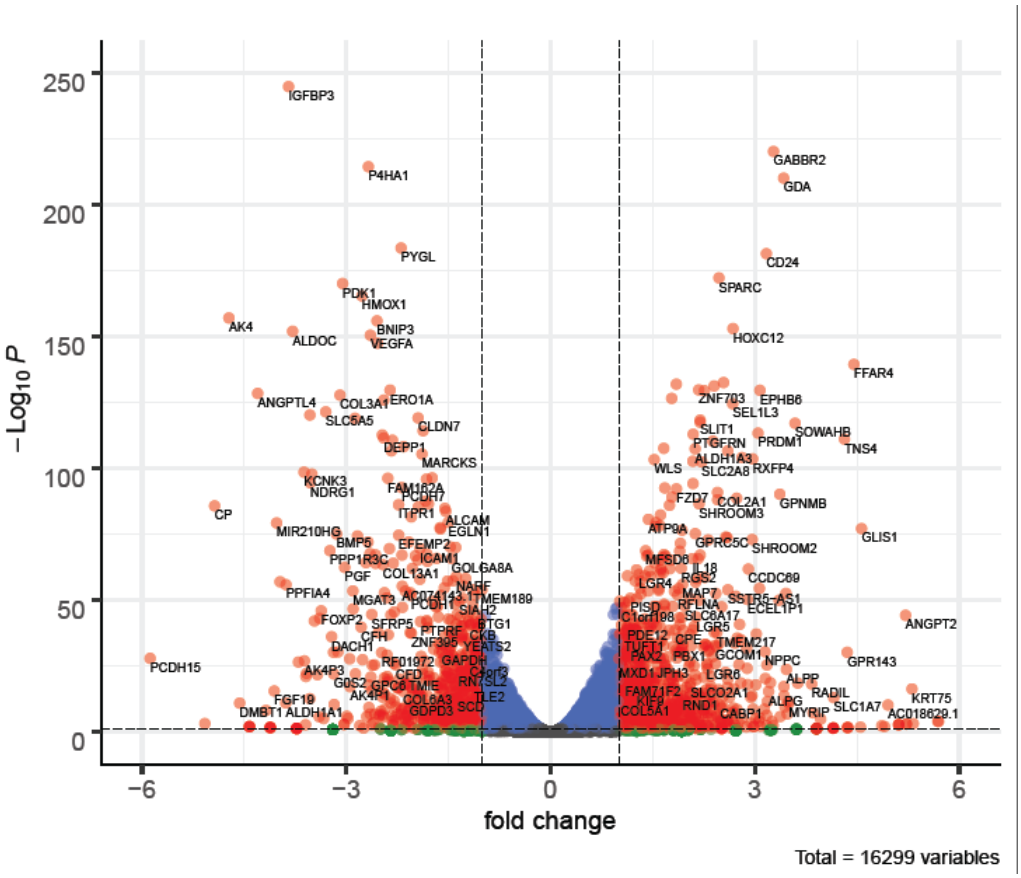

9.4 Appendix Chapter 5.3

Top 20 up- and down- DEGs in BxPC-3 and PANC-1 cells in 7.5% GelMA compared to collagen gels.

Table 9.1 Top 20 DEGs in BxPC-3 and PANC-1 cells between 7.5% GelMA and collagen. FC = fold change.

BxPC-3 cells (7.5% GelMA vs COLL control) DOWN-regulated		
Gene name	**logFC**	**p-value**
CA9	-7.3762797	3.40E-69
AC005696.4	-5.4331949	0.00019093
CASP14	-5.0943162	0.00088939
TSPAN18	-5.0830814	0.0008867
HOPX	-4.8849654	0.00217246
GRID1	-4.6179347	0.00507671
FBLN2	-4.6097629	0.00552874
LSAMP	-4.3233367	0.01247412
HDX	-4.302921	0.0123825
FBN3	-4.2987463	0.01279554
PNCK	-4.288735	1.10E-32
MPDZ	-4.2005246	5.84E-21
PPFIA4	-3.9670125	2.73E-52
PRDM16-DT	-3.9305803	0.02952218
AC015712.1	-3.9299837	0.02949029
CNTFR	-3.9296227	0.03066623
EFNB3	-3.9287502	0.0294248
INSYN1	-3.9230438	0.02951787
ARMC3	-3.9230362	0.02951662
PLEKHG4B	-3.9217553	0.02906473

BxPC-3 cells (7.5% GelMA vs COLL control) UP-regulated		
Gene name	**logFC**	**p-value**
MSI1	5.00138214	0.00227047
GNAZ	4.81518424	0.00386808
RNF165	4.81426351	0.00465174
KCNA2	4.6019717	0.00845417
AC061992.1	4.60128	0.00806245
CACNA1H	4.60117001	0.00736754
ANKRD20A11P	4.35034771	0.01470949
SPON1	4.35013204	0.01439767

GRM4	4.35001479	0.01484002
CCER2	4.34998256	0.01515333
PRCD	4.34883514	0.0167683
PLCH1	4.04639427	0.03030587
HYDIN	4.04635673	0.03018875
CD34	4.04632183	0.03203816
CTNNA2	4.04589369	0.02929333
ZNF788P	4.0458594	0.02872673
NEK5	4.04573588	0.03155845
FAM110B	4.0456444	0.02885425
PHOSPHO1	4.04479709	0.03129284
GJC1	2.93431737	0.00502034

PANC-1 cells (7.5% GelMA vs COLL control) DOWN-regulated		
Gene.name	**logFC**	**p-value**
SLC2A3	-7.8606298	1.31E-186
CASP14	-7.4660556	1.51E-50
CSTA	-6.9961577	1.80E-13
CA9	-6.5820425	5.75E-38
PCDH15	-5.8788139	3.06E-30
SFTA1P	-5.0752258	0.00016834
CP	-4.932496	6.48E-89
AK4	-4.7221174	4.73E-161
DMBT1	-4.5647662	9.28E-13
AL136985.3	-4.4218877	0.00293614
TREM1	-4.4215045	0.00314797
AC244153.1	-4.4210027	0.00284214
AC015660.1	-4.4199906	0.00289018
ANGPTL4	-4.2995351	4.58E-132
LINC01133	-4.1765996	7.80E-10
CIDEB	-4.1162426	0.00748519
PDZK1IP1	-4.1162243	0.00764787
GABRA3	-4.1155982	0.00750927
IFI44L	-4.1150395	0.00747628
ADCY4	-4.1135273	0.00869689

PANC-1 cells (7.5% GelMA vs COLL control) UP-regulated		
Gene.name	**logFC**	**p-value**
TAC3	7.41366642	4.19E-67
AC005747.1	6.09791284	1.12E-06
RNF224	5.69798906	2.38E-05

AL136531.2	5.68697167	1.94E-05
AL024508.2	5.32705293	0.00018214
KRT75	5.30795164	2.49E-18
AADACP1	5.22718009	0.00026297
ENTPD3	5.22600339	0.00027348
ANGPT2	5.2135498	6.41E-47
AC006262.1	5.11314656	0.0004445
IGFL2-AS1	5.11246397	0.00043467
ZBTB7C	5.11037621	0.00051158
AC018629.1	4.9553334	5.32E-12
AC105460.1	4.90460519	0.00286929
SLAMF7	4.86377656	0.00140385
GLIS1	4.56766923	3.21E-80
CLIC5	4.55165664	0.00539563
FFAR4	4.4556871	3.03E-143
AC025569.1	4.36535244	0.00701926
AC083973.1	4.36483908	0.00777902

9.5 Appendix Chapter 6

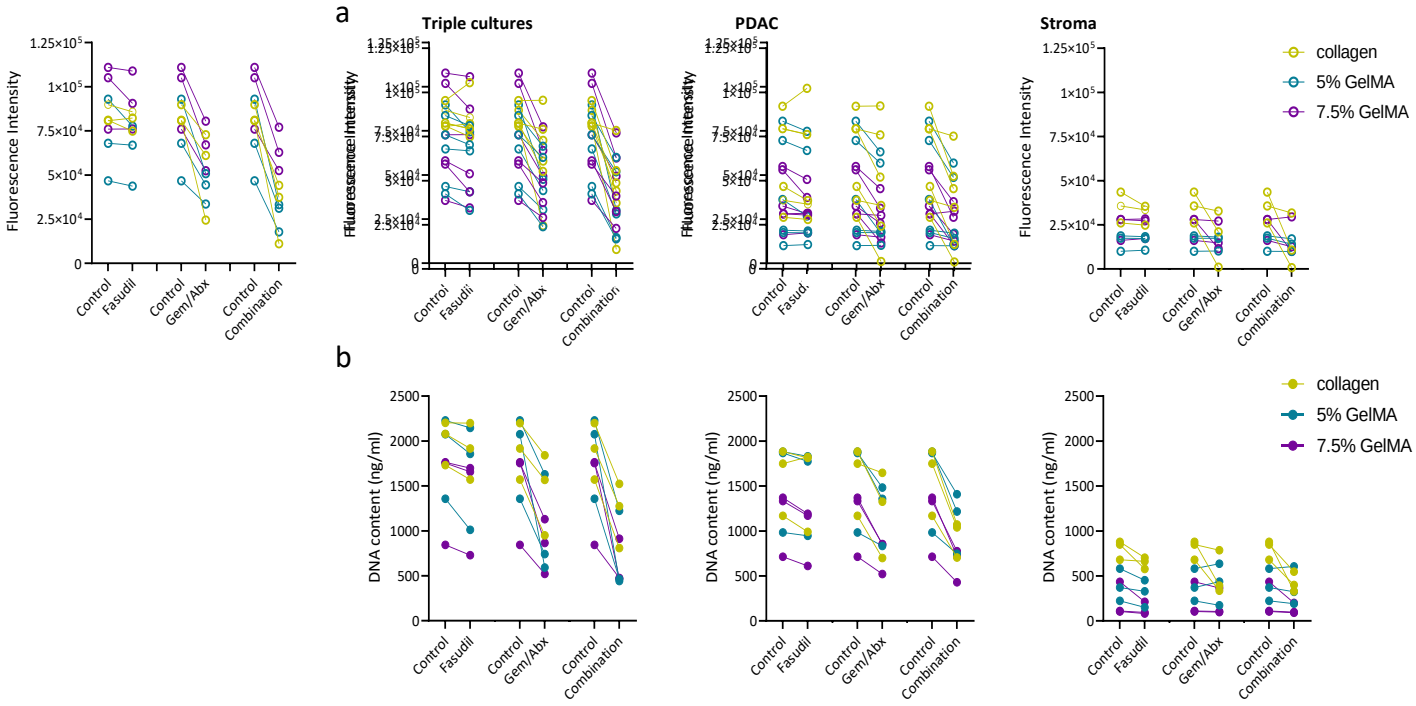

Figure 6.7 Effects of fasudil priming on the efficacy of gemcitabine and abraxane (Gem/Abx) in collagen (yellow), 5% (blue) and 7.5% (purple) GelMA hydrogels as measured via quantification of (a) endogenous cellular reducing ability and (b) DNA content. In this version, each line represents a different patient, for which each assay was repeated for n=4. (a) Alamar Blue quantification of cells' metabolic activity at day 14 of culture. Cultures were treated with 10 µM fasudil on day 7 and 100 nm of each Gem/Abx on day 10. Appropriate untreated and single treatment controls were also set up. Triple cultures consisted of PDAC cells, THP-1 monocytes and patient-derived CAFs in a 1:2:2 ratio. Monoculture control hydrogels (PDAC only and THP-1/CAFs stroma only) were also set up. CAFs were isolated from patients number 2, 3 and 15. **(b)** CyQUANT quantification of DNA content was performed at day 14 of culture.